JAERI-Review
95-014

REACTOR ENGINEERING DEPARTMENT ANNUAL REPORT

(April 1, 1994 – March 31, 1995)

September 1995

Department of Reactor Engineering

日本原子力研究所
Japan Atomic Energy Research Institute

本レポートは，日本原子力研究所が不定期に公刊している研究報告書です。
入手の問合わせは，日本原子力研究所技術情報部情報資料課（〒319-11 茨城県那珂郡東海村）あて，お申しこみください。なお，このほかに財団法人原子力弘済会資料センター（〒319-11 茨城県那珂郡東海村日本原子力研究所内）で複写による実費領布をおこなっております。

This reports are issued irregularly.
Inquiries about availability of the reports should be addressed to Information Division Department of Technical Information, Japan Atomic Energy Research Institute, Tokaimura, Naka-gun, Ibaraki-ken 319-11, Japan.

編集兼発行　日本原子力研究所
印　　刷　ニッセイエブロ株式会社

JAERI-Review 95-014

Reactor Engineering Department Annual Report

(April 1,1994 - March 31,1995)

Department of Reactor Engineering

Tokai Research Establishment
Japan Atomic Energy Research Institute
Tokai-mura, Naka-gun, Ibaraki-ken

(Received August 10, 1995)

This report summarizes the research and development activities in the Department of Reactor Engineering during the fiscal year of 1994 (April 1, 1994 - March 31, 1995).

The major Department's programs promoted in the year are the design activities of advanced reactor system and development of a high intensity proton linear accelerator for the engineering applications including TRU incineration.

Other major tasks of the Department are various basic researches on the nuclear data and group constants, the developments of theoretical methods and codes, the reactor physics experiments and their analyses, fusion neutronics, radiation shielding, reactor instrumentation, reactor control/diagnosis, thermohydraulics and technology developments related to the reactor engineering facilities, the accelerator facilities and the thermal-hydraulic facilities.

The cooperative works to JAERI's major projects such as the high temperature gas cooled reactor or the fusion reactor and to PNC's fast reactor project were also progressed.

The activities of the research committees to which the Department takes a role of secretariat are also summarized in this report.

Keywords: Reactor Engineering Department Annual Report, Advanced Reactor System, Nuclear Data, Proton Linear Accelerator, Reactor Physics, Thermohydraulics, Fusion Neutronics, Radiation Shielding, Reactor Instrumentation, Reactor Control/Diagnosis, Transmutation System

---

平成６年度原子炉工学部年報

日本原子力研究所東海研究所
原 子 炉 工 学 部

（1995年8月10日受理）

本報告は、平成６年度における原子炉工学部の研究活動状況をとりまとめたものである。

当該年度に原子炉工学部において推進された主要な研究活動は、新型炉の概念設計及びTRU消滅処理等への工学的応用を目的とする大強度陽子線形加速器の開発である。

さらに、原子炉工学部では、基礎基盤研究として核データと群定数、炉理論及びコード開発、炉物理実験及び解析、核融合中性子工学、放射線遮蔽、原子炉計測及び計装、原子炉制御及び診断、伝熱流動並びに炉工学施設、加速器施設及び伝熱流動施設の技術開発を行っている。

また、高温ガス炉、核融合等の日本原子力研究所プロジェクト研究及び動力炉・核燃料開発事業団の高速炉研究への協力も推進している。

本報告では、原子炉工学部が運営を担当する各種研究委員会の活動報告もとりまとめられている。

日本原子力研究所東海研究所：〒319-11　茨城県那珂郡東海村白方白根2-4

原子炉工学部年報編集委員会：

土橋敬一郎（委員長）、飯島進（副委員長）、沓掛忠三、竹内末広、柴田恵一、藤村統一郎
山根剛、八木秀之、鍋島邦彦、坂本幸夫、大貫晃、大山幸夫、新谷文将、西田雄彦、草野譲一
永井良治
黒澤潤（事務局）

Contents

Preface

The research activities of the Department of Reactor Engineering, Japan Atomic Energy Research Institute, during the fiscal year 1994 (April 1994 - March 1995) are presented in this report. The activities of the Department cover the broad field: physics of fission reactors, fusion reactor neutronics, shielding, reactor instrumentation diagnosis and control, thermal hydraulics, conceptual design of new type reactors, and accelerator technologies focussing on intense beam.

The total number of permanent staff working in the Department during the year was 159. The Department was funded from JAERI expenditure amounting to 2,110 million yen for FY 1994, excluding nuclear fuel cost and personnel expense. About 671 million yen was provided by the research contracts with external organizations; Science and Technology Agency (STA) for non-destructive measurement technology of trans-uranic elements (TRU) and for the large scale reflood test program and thermal hydraulic demonstration test for high conversion PWR , Power Reactor and Nuclear Fuel Development Corporation (PNC) for reactor physics constants of fast breeder reactor and Advanced Thermal Reactors (ATRs) and Mitsubishi Heavy Industries for development of PWR reactor noise diagnostic system.

The Department has served as secretariat of the Research Committee on Reactor Physics, the Research Committee on Advanced Reactors and the Research Committee on Partitioning and Transmutation and the Research Committee on High Intensity Proton Accelerator. The last one was established in FY 1994.

The research activities have been conducted in the following fourteen laboratories with the support of two divisions.

Nuclear Data Center

This center has two research themes; nuclear data and atomic & molecular data. As to nuclear data, the research activities consist of nuclear data evaluation for JENDL Special Purpose Files and nuclear data measurements. As to atomic & molecular data, main efforts are devoted to compilation and evaluation of atomic and molecular collision data and of atomic spectrum data.

This center has a function of the National Center which disseminates the nuclear and atomic & molecular data to Japanese users, contacts the foreign and international centers and coordinates the international collaboration. This center also serves as a secretariat of Japanese Nuclear Data Committee and of Atomic and Molecular Data Committee.

Reactor System Laboratory

This laboratory has two major research themes. One is feasibility study and pre-conceptual design of new type reactors. Effort is concentrated in design study of innovative FBRs of safe and economic features and also in an advanced fuel cycle with nitride fuel and TRU incineration. Another item is development and improvement of software(data/code) in reactor physics to serve for reactor design and analysis. It aims development of high speed, high accuracy Monte Carlo codes and nodal codes. Effort is now concentrated to develop a comprehensive code system used for reactor core design including thermal hydraulics, core management and kinetics.

Fast Reactor Physics Laboratory

The mock-up experiments have being conducted by using the Fast Critical Facility (FCA) to evaluate the data & method for designing metallic and nitride fuel fast reactors. Experimental studies are carried out on the safety related reactor physics parameters, namely, high temperature Doppler effect, sodium void effect, with the aim to support the development of the demonstration fast reactor. As a part of the OMEGA program, nuclear data and fuel material data of minor actinides are measured under the collaborative work with ORNL.

Thermal Reactor Physics Laboratory

This laboratory carries out three research themes; experimental research of HTGR neutronics, study of compact reactors and experimental research of actinide transmutation by using a proton accelerator. In the first theme, work has been done on reactor physics experiment at a critical assembly VHTRC (Very High Temperature Reactor Critical assembly) for verification of the neutronics design of the HTTR (High Temperature Engineering Test Reactor) under construction at Oarai site. The second theme includes conceptual design of space reactors and an HTGR-MHD combination plant. In the third theme, spallation experiments have been conducted on a lead assembly bombarded by 500 MeV proton beam. A high energy transport code NMTC/J has been verified and modified by using the experimental data.

Sensing Technology Laboratory

This laboratory carries out R&D work in the field of instrumentation and measurement under two themes. One covers general subjects of the nuclear and reactor instrumentation widely, where performed are R&Ds of a new type of neutron detectors, nondestructive measuring technologies to assess the material degradation of reactor components, a neutron emission profile monitor for fusion research, a fuel failure detection system for HTGRs, etc. The other is specified to the nondestructive measurement of TRU waste drums, where both the active and passive neutron assays are applied together with the gamma-ray CTs.

Control and AI Laboratory

This laboratory's research program aims to establish basic technologies for the operational safety and hazardless maintenance activities of nuclear power plants. Researches in both reactor control and diagnosis systems and remote handling technologies have been carried out in order to achieve this final goal. Advanced control and diagnosis system technologies such as highly stable reactor control, early fault diagnosis based on reactor noise and neuro-expert system are being developed to improve the operational safety. Development of the remote handling technologies in hazardous environment, that is, manipulator robotics with redundant degrees of freedom, advanced ultrasonic sensing and image based visual servo robot arm control, is also being conducted.

Shielding Laboratory

The activity of this laboratory is focussed on high energy neutron and photon shielding for the purpose of establishing a technological base of the wide utilization of intense proton accelerators. Four studied are continued: Shielding experiments using a labyrinth, Development of a point-kernel code for high energy neutron shielding design, Development of an energy response calculation code for solid state nuclear track detectors and Health physics study for high energy photons.

Heat Transfer and Fluid Flow Laboratory

In the study of heat transfer and fluid flow, the best-estimate codes for thermal hydraulic analyses of light water reactors (LWRs) have been assessed and developed by focussing on passive safety reactors. The fundamental studies were performed on the two-phase flow structure and critical heat flux. The transient thermal-hydraulic test program was continued aiming at the verification of the core integrity during design basis events of LWRs by 2000.

Fusion Neutronics Laboratory Fusion Neutronics Laboratory

The current research activities undertaken in this laboratory are ; (1) urgent neutronics experiments under ITER/EDA R&D Tasks, (2) long term neutronics studies under the IEA collaboration, (3) integral benchmark experiments and data validation tests for contemporary JENDL-3.2 and FENDL libraries, (4) technical developments for various experimental measurements, in particular, for dosimetry applications, (5) activation cross section measurements at around 14 MeV and also at an energy range from 17.5 to 30 MeV, (6) material irradiation experiments with a high 14 MeV neutron fluence, and (7) developments of new application incorporating D-T fusion neutrons.

Passive Safety Reactor Systems Laboratory

This laboratory has developed new concept of the JAERI passive safety reactor (JPSR) as a next generation light water reactor. In order to develop and evaluate the concept, safety analyses, three-dimensional thermal fluid flow analyses and probabilistic safety assessment (PSA) have been

performed. Experimental studies are under way to investigate the important thermal-hydraulic phenomena including natural circulation, DNB, gravity driven coolant injection, steam condensation, and multi-dimensional flow in pressure vessel. A conceptual design of integral-type passive safety test reactor is in progress. As for an active storage PWR which uses MOX fuel, demonstration tests are being performed using a large scale hydraulic mock-up test facility.

Transmutation System Laboratory

This laboratory has two major research themes; study on transmutation with reactor and study on accelerator-based transmutation. In the first theme, conceptual design studies on burner fast reactors and related fuel fabrication and reprocessing facilities in a partitioning and transmutation (P-T) fuel cycle. This theme includes the system study on P-T and the tasks for national and international collaboration to promote the Long-Term Program for Research and Development on Nuclides Partitioning and Transmutation (OMEGA Program). The second theme consists of conceptual design studies on transmutation systems driven by proton accelerator and development of the design code system, including the high energy cascade simulation.

Accelerator Engineering Laboratory

This laboratory has proposed the Engineering Test Accelerator (ETA) with an energy of 1.5GeV and average current of 10mA for various accelerator-related basic researches with proton induced secondary beams such as neutrons, muon, pion and spallation RI (radio isotope) and for nuclear waste transmutation. As a part of the R&D work for the accelerator development, the 2MeV beam acceleration test with high brightness ion source, RFQ (Radio Frequency Quadruple) and high power rf source was successfully carried out with a beam current of 70mA (peak) and 5% duty. The rf heating and the cooling capability for the drift tube linac (DTL) hot test model was examined.

Free Electron Laser Laboratory

The beam test of the JAERI super-conducting rf linac for FEL was successfully performed to get an electron beam of 14 A of peak current after the main accelerator at around 15 MeV. Measured energy resolution of a fully-accelerated beam is about 0.8% or less of FWHM, maximum transmission of the beam around 80-100%, and maximum electron energy 23 MeV. By utilizing semiconductor detectors and the Stanford-type fast current amplifier, far-infrared (FIR) signals were observed around 25 mm during the spontaneous and stimulated emission measurements. This work is promoted by the specialist committee on laser technology of Nuclear Cross-Over Research and the promotion committee for Nuclear Cross-Over Research, and supported by Science and Technology Agency of Japanese Government.

Reactor Engineering Facility Operation Division

This division has operated four large-scale experiment facilities: FCA (Fast Critical Assembly) , VHTRC (Very High Temperature Reactor Critical assembly), FNS (Fusion Neutron Source) and Heat Transfer and Fluid Flow Test Facilities, in accordance with each experiment program and maintained in the monthly or the annual inspection. Consequently safety operations of these facilities have been achieved and contributed sufficiently to the execution of each experimental study.

Accelerator Division

The accelerator division operates a 20 MV tandem accelerator since 1982, which is designed to provide ions with masses from 1 to 240 amu. The accelerator is used for a wide range of basic research in JAERI and external users. The operation is scheduled under the control of Tandem steering committee and the experimental subjects are selected by the tandem program advisory committee. The tandem collaborative work subcommittee arranges the collaborative work. As a special feature, the division has developed the tandem booster which is a superconducting linac to increase the maximum energy of the heavy ions four times as high as the tandem accelerator provides.

The Department is involved in the following project-oriented programs of JAERI;

(1) Design studies of advanced reactors.
(2) Technology development for OMEGA program
(3) Development of a high intensity proton accelerator.
(4) Development of High Temperature Gas-cooled Reactor.
(5) Engineering research for fusion reactor

The activities of the Department in FY 1994 have contributed to the essential progress in the field of reactor engineering.

Yoshio Murao, Director
Department of Reactor Engineering
August 1, 1995

1. Nuclear Data, and Atomic and Molecular Data

The evaluation for JENDL Special Purpose Files has been continued. A preliminary version of Activation Cross Section File was completed, and sent to IAEA as candidate data for Fusion Evaluated Nuclear Data Library (FENDL). Neutron nuclear data of actinides were evaluated for Actinoid File. A systematic formula for proton-induced fission cross sections was obtained in the intermediate energy region.

Theoretical and evaluation work has been done for covariance data. An anomaly known as Peelle's Pertinent Puzzle was introduced, and general criteria were shown to avoid it. Covariance matrices of neutron cross sections were estimated for some nuclides contained in JENDL-3.2.

Integrated Nuclear Data Evaluation System (INDES) is being developed to keep experiences of JENDL-3, to store basic parameters used in evaluations and to support new evaluations. Mass chain evaluation has been continued within an international framework. The evaluation for A= 122 was completed and published in Nuclear Data Sheets.

As to experimental activities, activation cross sections were measured in the energy regions from 13.5 to 14.9 MeV and from 17.5 to 30 MeV. The tritium and ^{14}C production cross sections of $^{17,18}O$ were measured at 14.7 MeV to estimate water activation.

Benchmark tests of evaluated data libraries have been carried out. Fusion integral measurements were compared with JENDL-3.2 and FENDL-1 calculations. For fast reactors, benchmark calculations were obtained by using ENDF/B-VI, and the results were compared with those of JENDL-3.2.

With respect to atomic and molecular data, data evaluation has been continued for JEAMDL-4. Photon angular distributions from radiative electron capture were calculated. The total cross section was calculated for ionization of excited hydrogen atoms by collisions with bare ions. Analytic cross sections were formulated for collisions of H, H_2, He and Li atoms and ions with atoms and molecules. Spectral data were compiled for Kr^{4+} to Kr^{35+}.

In this chapter, the research activities, 1.1-1.9 and 1.16-1.19, were conducted at the Nuclear Data Center. The measurements, 1.10-1.12, and fusion benchmark tests, 1.13-1.14, were done at the Fusion Neutronics Laboratory. The benchmark test of ENDF/B-VI for fast reactors, 1.15, was carried out at the Reactor System Laboratory.

1.1 JENDL Activation Cross Section File

Y. Nakajima and JNDC Activation Cross Section Data Working Group

A preliminary version of JENDL Activation Cross Section File has been completed in February, 1995. It was sent to IAEA for the use of the international cooperation, especially for candidate data for Fusion Evaluated Nuclear Data Library (FENDL).

This file includes a number of data from JENDL-3.2. If the data of JENDL-3.2 are not consistent with reliable experimental data or other channel cross section data, and/or have unreasonable cross section shape, reevaluation was made independently from JENDL-3.2. The overall consistency with experimental data has been improved. For a number of reactions with no data in JENDL-3.2 their cross sections have been evaluated. Isomeric cross sections have been also evaluated even if the total reaction cross sections have been taken from JENDL-3.2. The evaluation was performed mainly based on the SINCROSS-II system[1]. As an example of the evaluated data the cross sections of ^{209}Bi (n, 2n) ^{208}Bi(5^+, 3.68×10^5 years) and ^{209}Bi (n, 3n) ^{207}Bi($9/2^-$, 32 years) are shown in Fig. 1. 1. 1 along with available experimental data. The evaluated data reproduce measured values very well.

Cross section data of 1,158 reactions for 225 nuclei are compiled in the file with the ENDF-5 format. The review on the data in the file is going on. After the review and validation with integral data the file will be released and will be available without any restriction.

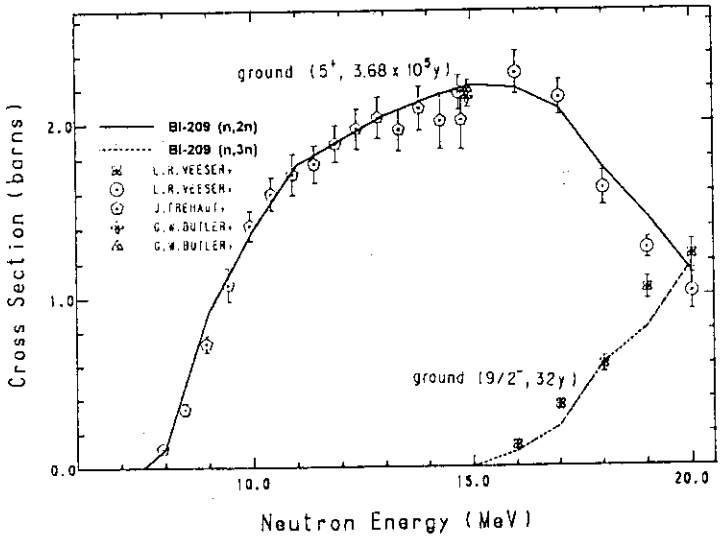

Reference

1) Yamamuro N.: JAERI-M 90-006 (1990).

Fig. 1.1.1 Cross sections of ^{209}Bi (n, 2n)^{208}Bi(5^+, 3.68×10^5 years) and ^{209}Bi (n, 3n)^{207}Bi($9/2^-$, 32 years).

1.2 Consistent Calculations of Fast Neutron Induced Fission, (n,2n) and (n,3n) Cross-Sections for 71 Isotopes of Th, Pa, U, Np, Pu, Am, Cm, Bk and Cf

V.A.Konshin*

In order to evaluate the accumulation of transactinides in spent fuel and to handle nuclear waste, is necessary to have accurate nuclear data of transactinides. In particular their fission, (n,Xn) reactions are important. In this work, the fission, (n,2n) and (n,3n) cross sections of actinides are calculated with theoretical model codes in the incident neutron energy range from 1 to 20 MeV for 71 isotopes; $^{227\text{-}234}$Th, $^{229\text{-}233}$Pa, $^{230\text{-}240}$U, $^{236\text{-}239}$Np, $^{236\text{-}247}$Pu, $^{239\text{-}245}$Am, $^{238\text{-}251}$Cm, $^{245\text{-}249}$Bk, $^{249\text{-}252}$Cf.

In the present work the statistical model code STAPRE[1] was used for the calculation of the cross sections. The neutron transmission coefficients were calculated using the coupled-channel code ECIS[2] with the optical potential parameters obtained by Haouat et al.[3] The matrix element $M^2 = 10/A^3$ MeV^2 determined by Ignatyuk et al.[4] was used for the exciton model. The level densities of residual and fissioning nuclei were calculated with a generalized superfluid phenomenological model proposed by Ignatyuk et al.[5] In the actinide region the superfluid model underestimates the level density at low energies. Therefore the constant temperature model with T=0.385 MeV[6] was adopted for the level density at low energies.

The fission barrier parameters E_f^A and E_f^B were obtained by analyzing the experimental data for fission cross sections. For those nuclei whose experimental data are not existing, the systematics proposed by Kuprijanov et al.[7] and Smirenkin[8] for first plateau region was used. Systematics of E_f^A and E_f^B was also considered. The penetrability parameters were taken from the work of Björnholm and Lynn.[9]

The present results were published as Ref. 10 where the graphs of cross sections obtained in the present works were displayed comparing with available experimental data and evaluated data for all of 71 nuclei. Figure 1.2.1 shows an example of the fission, (n,2n) and (n,3n) cross sections of ^{242}Pu.

References

1) Uhl M. and Stromaier B.: IRK-76/01, Vienna (1976).
2) Raynal J.: SMR-9/8, IAEA, Vienna (1970).
3) Haouat G., et al.: Nucl. Sci. Eng., 81, 491 (1982).

* Research Fellow

4) Ignatyuk A.V., et al.: Sov. J. Nucl. Phys., 47, 224 (1988).
5) Ignatyuk A.V., et al.: Sov. J. Nucl. Phys., 29, 450 (1979).
6) Antsipov G.V., et al.: Nuclear Constants, V.3, p.25 (1985).
7) Kuprijanov V.M., et al.: Sov. J. Nucl. Phys., 39, 176 (1984).
8) Smirenkin G.N.: INDC(CCP)-359G, IAEA, Vienna (1993).
9) Björnholm S. and Lynn J.E.: Rev. Mod. Phys., 52, 725 (1980).
10) Konshin V.A.: JAERI-Research 95-010 (1995).

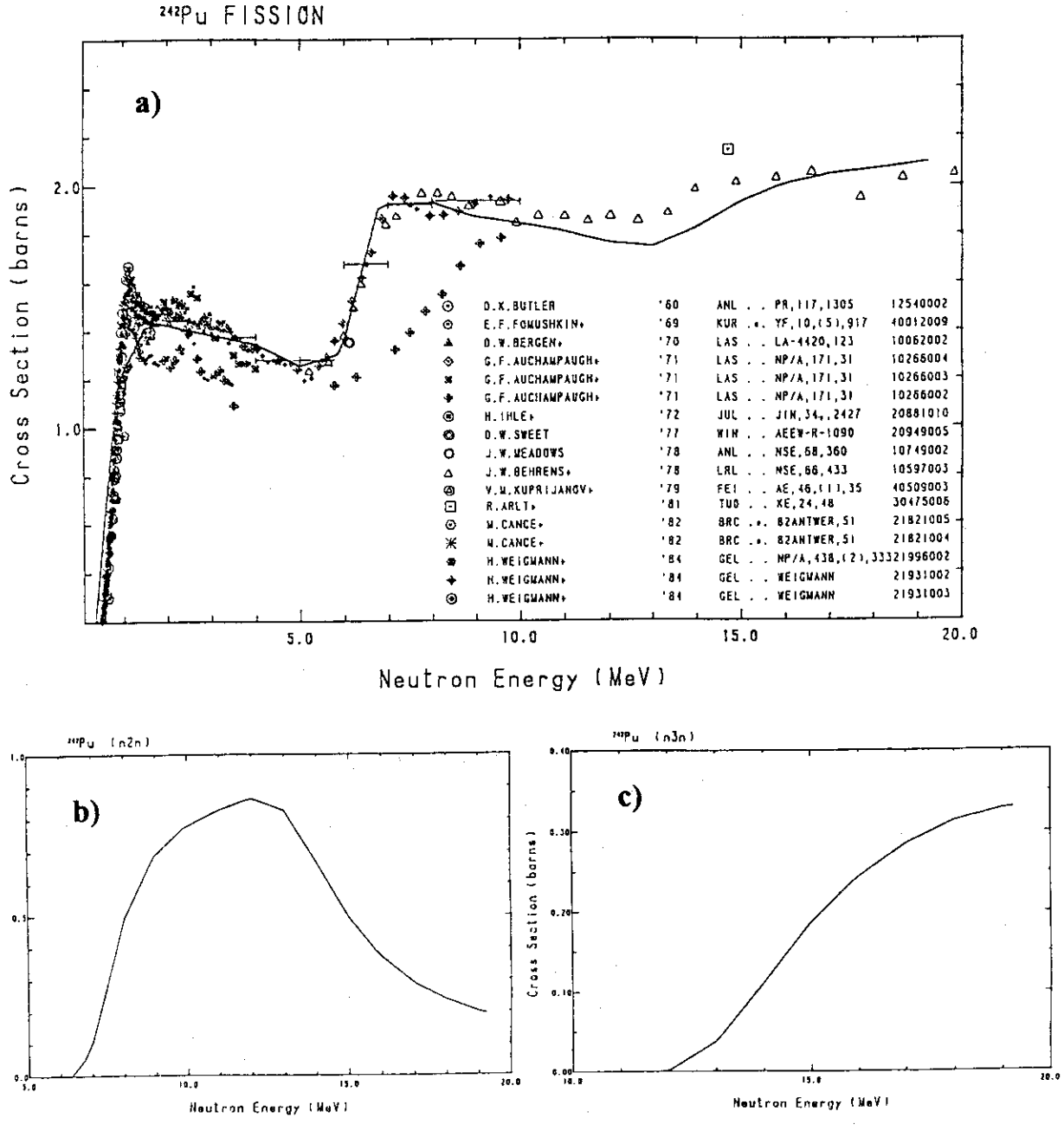

Fig.1.2.1 Cross sections of ^{242}Pu. a: fission, b: (n,2n) and c: (n,3n)

1.3 Evaluation of Neutron Nuclear Data of ^{235}Np and ^{246}Pu

T.Nakagawa and V.A.Konshin*

The evaluation of neutron nuclear data of ^{235}Np and ^{246}Pu was made in the neutron energy range from 10^{-5} eV to 20 MeV. Quantities evaluated are the total, elastic and inelastic scattering, fission, capture, (n,2n) and (n,3n) reaction cross sections, the angular and energy distributions of secondary neutrons, and number of emitted neutrons per fission.

Experimental data are available only to the thermal capture cross section of ^{235}Np. The cross sections in the thermal neutron region are assumed values except for the ^{235}Np capture cross section. No resonance parameters were given for both nuclides. The cross sections in the higher energy region were calculated with CASTHY,[1] ECIS[2] and STAPRE.[3] Figures 1.3.1 and 1.3.2 show the cross sections of both nuclides.

The angular and energy distributions were also calculated with these theoretical calculation codes. The number of neutrons per fission was estimated from systematics reported by Howerton[4] for the prompt neutrons and by Tuttle[5] for the delayed ones.

The present results have been compiled in the ENDF format and will be adopted in JENDL Actinoid File. This work was performed under the contracts between Power Reactor and Nuclear Fuel Development Corporation and Japan Atomic Energy Research Institute.

References

1) Igarasi S. and Fukahori T.: "Program CASTHY - Statistical Model Calculation foe Neutron Cross Sections and Gamma Ray Spectrum -," JAERI 1321 (1991).
2) Raynal J.: Optical Model and Coupled-Channel Calculations in Nuclear Physics, SMR-9/8 (1970).
3) Uhl M. and Stromaier B.: IRK-76/01 (1976).
4) Howerton R.J.: Nucl. Sci. Eng., 62, 438 (1977).
5) Tuttle R.J.: Proc. of Consultants' Meeting on Delayed Neutron Properties, 1979 Vienna, INDC(NDS)-107/G+Special, p.29 (1979).

* Research Fellow

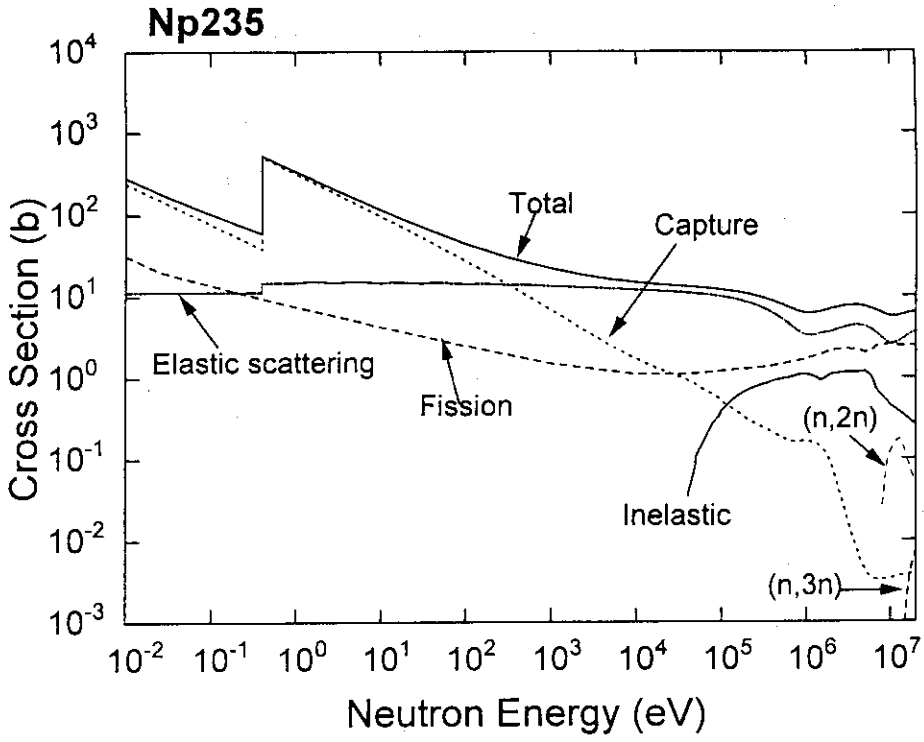

Fig. 1.3.1 Evaluated cross sections of ^{235}Np

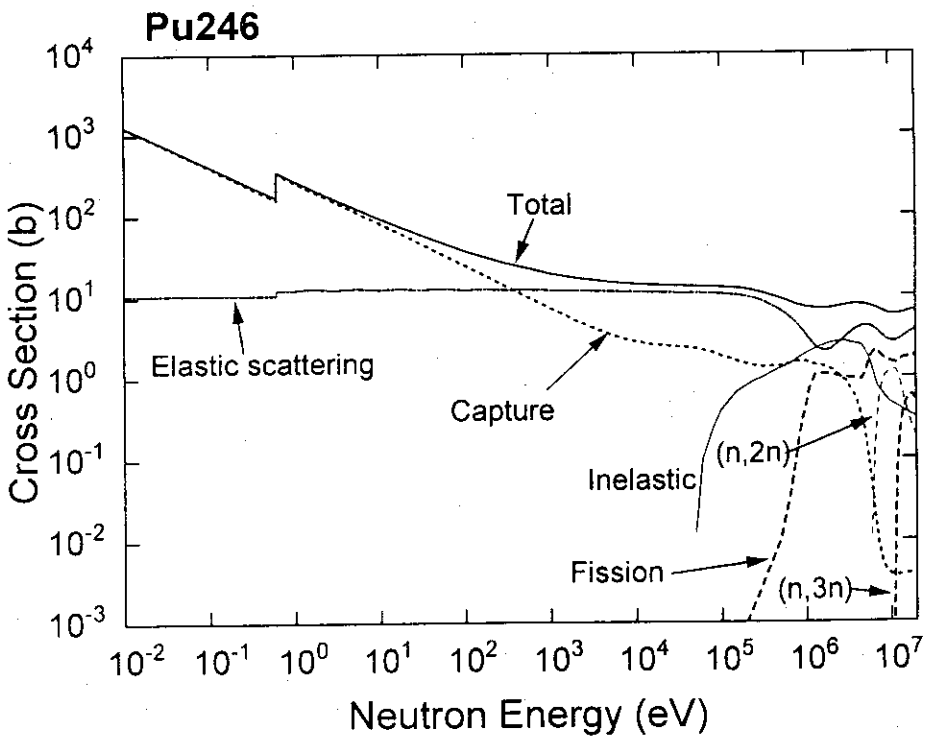

Fig. 1. 3.2 Evaluated cross sections of ^{246}Pu

1.4 Estimation of Covariance Matrices for Important Cross-Section Data

K.Shibata, Y.Nakajima, T.Fukahori, S.Chiba, T.Kawano* and T.Nakagawa

The covariance matrices of cross sections of H and Zr, and the inelastic scattering cross sections of ^{238}U and the resolved resonance parameters of ^{238}U were estimated.

For H, the covariance matrices were given for the total, elastic and capture cross sections on the basis of ENDF/B-V and Horsley's evaluation.[1] In the case of Zr cross sections, the covariance matrices were estimated mainly from experimental data for the capture, (n,2n) reaction and inelastic scattering cross sections. A least-squares fitting code GMA[2] was used for this purpose. Figure 1.4.1 shows the Zr (n,2n) reaction cross section with uncertainties obtained in the present work.

The covariance matrices of the ^{238}U inelastic scattering cross section were estimated by using the method developed by Kawano et al.[3] in Kyushu University. The covariance matrices were calculated from uncertainties of parameters used in the theoretical calculation for JENDL-3.2 and their sensitivities to the cross sections. The uncertainties of parameters were determined by Kawano on the basis of experimental data for the first, second and third levels. For the cross sections of hypothetical levels introduced in JENDL-3.2 evaluation and continuum levels, the error of 20 % was assumed. The covariance matrix of the total inelastic scattering cross section was also estimated from those of partial inelastic scattering.

For the ^{238}U resolved resonance parameters, only errors of the parameters were estimated on the basis of the experimental errors of Olsen et al.[4], Olsen[5] and Moxon et al.[6]

This work was performed under the contracts between Power Reactor and Nuclear Fuel Development Corporation and Japan Atomic Energy Research Institute.

References

1) Horsley A.: Nuclear Data A, 2, 243 (1966).
2) Poenitz W.P.: BNL-NCS-51363, p.249 (1981).
3) Kawano et al.: JAERI-Conf 95-008, p. 246 (1995).
4) Olsen D.K., et al.: Proc. Int. Conf. on Nuclear Cross Sections for Technol., Knoxville, Oct 1979, p.677 (1980).
5) Olsen D.K.: Nucl. Sci. and Eng., 94, 102 (1986).
6) Moxon M.C., et al.: Proc. 1988 Int. Reactor Physics Conference, Jackson Hole, Sep. 1988, I-282 (1988).

* Kyushu University

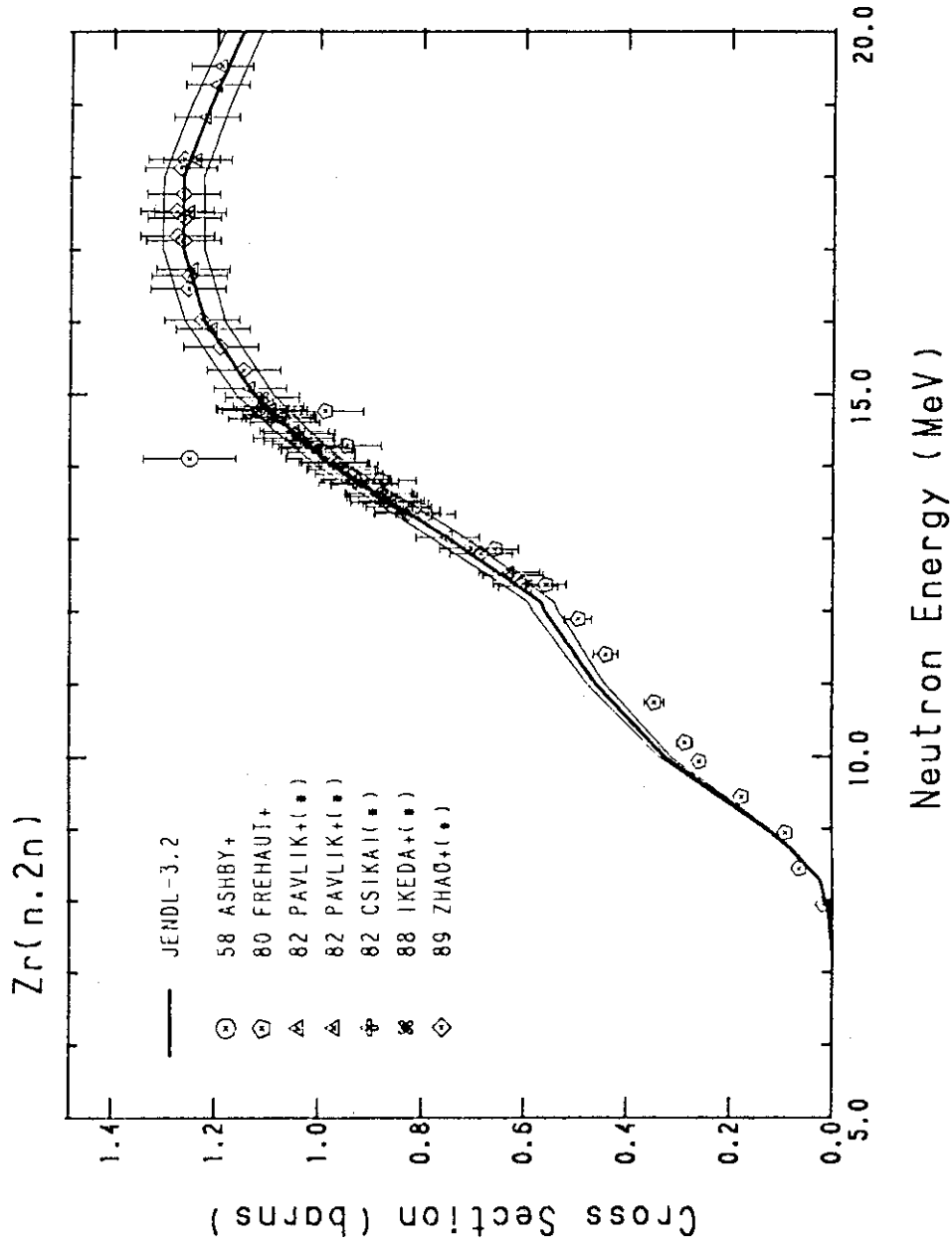

Fig. 1.4.1 Zr (n,2n) reaction cross section
The authors with an asterisk measured the $^{90}Zr(n,2n)$ cross sections. Their data were converted to the Zr(n,2n) cross section in this figure.

1.5 Impacts of Data Transformations on Least-Squares Solutions and Their Significance in Data Analysis and Evaluation

S. Chiba and D.L. Smith*

The least-squares method is commonly employed as a method of statistical inference. This method, however, sometimes yields a result contradictory to our intuition. Let us, for example, try to seek an average of 2 data points, 1 and 1.5, with a condition that there are 3 error components; 10% random error in each data, and 20% "calibration error" which affects both data. The data vector $\mathbf{d}$, its covariance matrix $\mathbf{V_d}$, and the sensitivity matrix $\mathbf{G}$ are summarized as;

$$\mathbf{d} = \begin{pmatrix} 1 \\ 1.5 \end{pmatrix} \tag{1}$$

$$\mathbf{V_d} = \begin{pmatrix} 1\cdot(0.1^2+0.2^2) & 1\cdot 0.2\times 1.5\cdot 0.2 \\ 1\cdot 0.2\times 1.5\cdot 0.2 & 1.5\cdot(0.1^2+0.2^2) \end{pmatrix} = \begin{pmatrix} 0.1125 & 0.06 \\ 0.06 & 0.05 \end{pmatrix} \tag{2}$$

$$\mathbf{G} = \begin{pmatrix} 1 \\ 1 \end{pmatrix} \tag{3}$$

The least-squares solution (LSS) $\mathbf{p}$ and its covariance $\mathbf{V_p}$ is then given by

$$\mathbf{p} = \left(\mathbf{G^t}\cdot\mathbf{V_d^{-1}}\cdot\mathbf{G}\right)^{-1}\mathbf{G^t}\cdot\mathbf{V_d^{-1}}\cdot\mathbf{d} = 0.88 \tag{4}$$

$$\mathbf{V_p} = \left(\mathbf{G^t}\cdot\mathbf{V_d^{-1}}\cdot\mathbf{G}\right)^{-1} = 0.22^2 \tag{5}$$

In this example, therefore, the LSS is lower than both the data. This problem is known as "Peelle's Pertinent Puzzle (PPP)"[1]. The same phenomena happen as a difference of the LSS before and after the data vector is transformed by a set of nonlinear functions; the second definition of PPP[2]. These 2 kinds of anomalies are referred to as the PPP in general[3].

Let us define a term "isomorphic transformation $\mathbf{f}$" as a set of transformations $\mathbf{f}$ $(= (f_1, ..., f_n)^t)$ of a vector $\mathbf{d}$ $(= (d_1, d_2, ..., d_n)^t)$ into another as $\mathbf{d'}=\mathbf{f(d)}=(f_1(\mathbf{d}), f_2(\mathbf{d}), ..., f_n(\mathbf{d}))^t$ without changing the number of data points[4]. Furthermore, the isomorphic transformation must have its inverse $\mathbf{f^{-1}}$ that satisfies $\mathbf{f^{-1}(d')}=\mathbf{d}$.

The LSS in a general form is written down as

$$\mathbf{p} = \mathbf{p_0} + (\mathbf{G^t}\cdot\mathbf{V_d^{-1}}\cdot\mathbf{G})^{-1}\cdot\mathbf{G^t}\cdot\mathbf{V_d^{-1}}\cdot(\mathbf{d} - \mathbf{t(p_0)}) \tag{6}$$

where $\mathbf{t}$ denotes the model (theory) vector containing the parameters to be estimated, while $\mathbf{p_0}$ the initial estimate of the $\mathbf{p}$. The sensitivity matrix $\mathbf{G}$ is generally expressed

*Argonne National Laboratory, U.S.A.

as $G_{ij} = \partial t_i / \partial p_j$. When the data is transformed by an isomorphic transformation **f**, the residual vector (**d** - **t**($\mathbf{p}_0$)), covariance matrix and the sensitivity matrix are transformed as

$$(\mathbf{d} - \mathbf{t}(\mathbf{p}_0)) \rightarrow (\mathbf{d} - \mathbf{t}(\mathbf{p}_0))' = c \cdot (\mathbf{d} - \mathbf{t}(\mathbf{p}_0)) \tag{7}$$

$$\mathbf{V}_d \rightarrow \mathbf{V}'_d = \mathbf{c} \cdot \mathbf{V}_d \cdot \mathbf{c}^t \tag{8}$$

$$\mathbf{G} \rightarrow \mathbf{G}' = \mathbf{c} \cdot \mathbf{G} \tag{9}$$

where the conversion matrix **c** is expressed in various ways in the first Taylor series approximation, namely,

$$c_{ij} = \begin{cases} c_{ij}^{(+)} \equiv \frac{\partial f_i}{\partial t_j} \\ c_{ij}^{(-)} \equiv \frac{\partial f_i}{\partial d_j} \\ c_{ij}^{(0)} \equiv \frac{1}{2} \cdot \left(\frac{\partial f_i}{\partial t_j} + \frac{\partial f_i}{\partial d_j} \right) \end{cases} \tag{10}$$

The LSS is obtained by using the transformed data by putting quantities given in the right-hand side of Eqs. (7), (8) and (9) into Eq. (6). The result becomes identical with Eq. (6) if the **c**-matrices in Eqs. (7), (8) and (9) are replaced simultaneously with $\mathbf{c}^{(+)}$, $\mathbf{c}^{(-)}$ or $\mathbf{c}^{(0)}$. In general, however, the covariance matrix is transformed by using the $\mathbf{c}^{(-)}$ matrix (which is independent of the model **t**), while the sensitivity matrix is transformed by using the $\mathbf{c}^{(+)}$ matrix (which is independent of the data **d**). It was shown that this inconsistency of the transformation was the origin of the second definition of PPP[5]. The origin of the first definition was then shown to be an improper truncation of the data space[5].

It must be also noted that the quantities given in Eqs. (1), (2) and (3) are derived with a linear-isomorphic transformation $\mathbf{F} \equiv \begin{pmatrix} 1.175 & -0.175 \\ 0.713 & 0.287 \end{pmatrix}$ from those data;

$$\mathbf{d} = \begin{pmatrix} 1.311 \\ 0.229 \end{pmatrix}, \quad \mathbf{V_d} = \begin{pmatrix} 0.281^2 & 0 \\ 0 & 0.346^2 \end{pmatrix}, \quad \mathbf{G} = \begin{pmatrix} 1 \\ 1 \end{pmatrix} \tag{11}$$

This transformation does not change the LSS. In this case, the answer of 0.88 is not strange, because it is within the range of the two data 0.229 and 1.311. In this example, the number of error components is actually only 2, while in the first definition of PPP it is recognized to be 3 which implies the existence of a (hidden) 3rd data. Therefore, the correct LSS must be sought with a correct number of data points.

When we apply the least-squares method in actual data evaluation, it is often not possible to comprehend the correct dimension of the problem because experimental results are usually reported after a large amount of information has been truncated. Therefore, the correct method proposed in this work is not feasible. In such a case, the data covariance matrix may be calculated with the "relative" covariance matrix times the

least-squares estimate of the data[6]. This simple prescription often yields much reasonable results than the usual least-squares method that relies on the "absolute" covariance matrix, preserving the important correlation information. This approximate method yields a value of 1.25±0.28 for the first definition of PPP; a result much better than the original answer of 0.88±0.22.

References

1) Peelle R.W.: *Peelle's Pertinent Puzzle*, Informal memorandom dated October 13, 1987, ORNL, USA (1987).

2) Zhao Z. and Perey F.G.: *The covariance matrix of derived quantities and their combination*, ORNL-TM 12106 (1992).

3) Chiba S., and Smith D.L.: *Perspectives on Peelle's pertinent puzzle and its significance in data fitting and evaluation*, Proc. Symp. on Nuclear Data Evaluation Methodology, BNL, Upton, Long Island, New York, USA, Oct. 12 to 16, 1992, p.221(1993), World Scientific.

4) Chiba S.: *Impacts of isomorphic transformation and trucations of data spaces on the least-squares solutions*, Proc. of NEANSC Specialists' Meeting on Evaluation and Processing of Covariance Data, Oak Ridge, Tennessee, USA, Oct. 7 to 9, 1992, p.81, NEA/NSC/DOC(93)3 (1993).

5) Chiba S. and Smith D.L.: J. Nucl. Sci. Technol., **31**, 14(1994).

6) Chiba S. and Smith D.L.: *A suggested procedure for resolving an anomaly in least-squares data analysis known as Peelle's pertinent puzzle and the general implications for nuclear data evaluation*, ANL/NDM-121 (1991).

1.6 Uncertainties of Evaluated Total Cross Sections for 14 Nuclides Contained in JENDL-3.2

M. Nakamura* and K. Shibata

The second revision of JENDL-3 (referred to as JENDL-3.2[1]) was made available in June 1994. It contains evaluated neutron nuclear data for 340 nuclides, and is one of the large libraries in the world. However, it did not include error (variance and covariance) files, which is the largest drawback in JENDL-3.2. One of the difficulties is due to the fact that there is no established procedure to derive variance-covariance data. In general, data evaluation is performed on the basis of available experimental data, but few data give detailed error information to evaluators.

A least-squares program GMA[2] was developed at the Argonne National Laboratory to derive variance and covariance data from a set of experiments with minimal information. With this code, the percentage of the systematic error to the cross-section value is required as input. The correlation matrix for data points in each experiment is calculated from this percentage. The present work has been undertaken to study the applicability of the GMA code to the production of variances and covariances of evaluated data in JENDL-3.2. Estimated were the uncertainties of the total cross sections of 14 nuclides ^{6}Li, ^{7}Li, ^{9}Be, ^{12}C, ^{16}O, ^{23}Na, Ti, Cr, Fe, Ni, ^{235}U, ^{238}U, ^{239}Pu and ^{240}Pu, where the nuclide without a mass number stands for a natural element.

Experimental data are retrieved from a database NESTOR-2, and the data format is converted using a utility program EXPTOGMA. The experimental values from one measurement are extrapolated to specified grid energy points according as the gradient of prior cross sections, and then the weighted average value is calculated at the grid energy. The cross sections in JENDL-3.2 were used for the prior cross sections. This processing is performed by another utility DATGMA.

With the GMA calculation, it is required to identify systematic errors for each measurement in order to generate a covariance matrix. The systematic errors were taken from the references associated with the measurement as much as possible. In some cases,

---

* Kyushu University

where no error information is available, guess-values are assigned. As an example, Fig. 1.6.1 shows estimated variances of the total cross section for ^{6}Li.

References

1) Nakagawa T., et al.: To be published in J. Nucl. Sci. Technol.

2) Poenitz W.P.: "Data Interpretation, Objective Evaluation Procedures and Mathematical Techniques for the Evaluation of Energy-Dependent Ratio, Shape and Cross Section Data", Proc. Conf. Nuclear Data Evaluation Methods and Procedures, BNL-NCS-51363, p. 249 (1981).

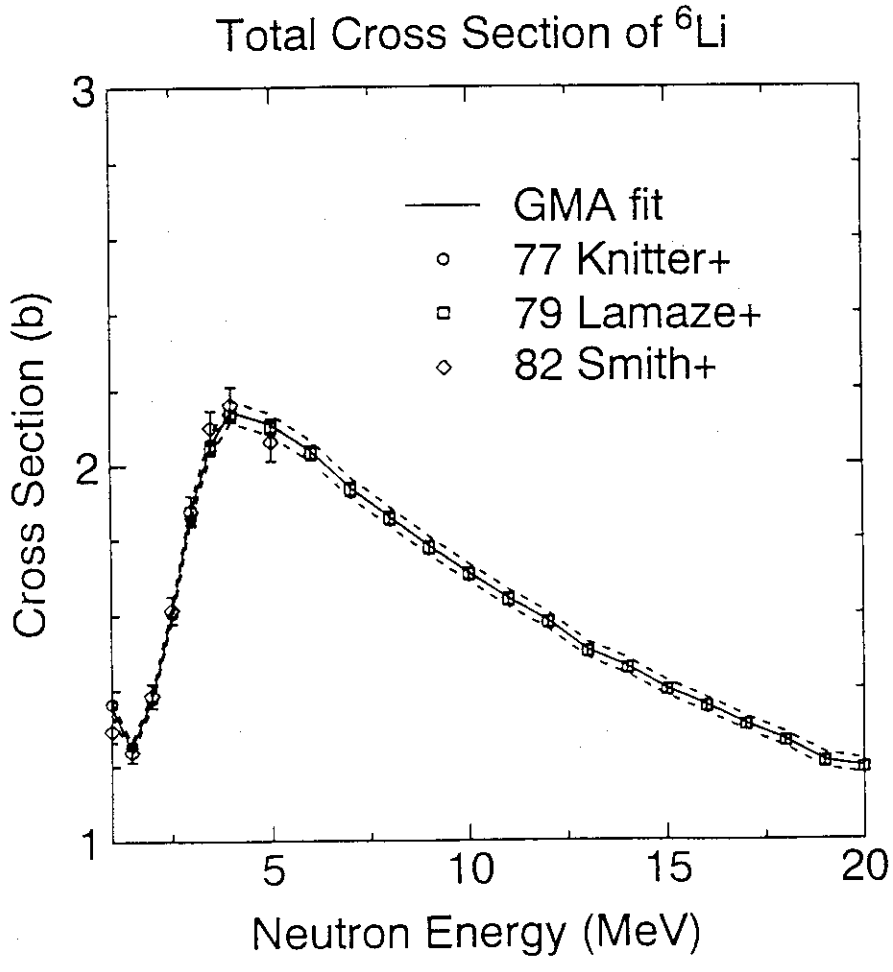

Fig. 1.6.1 Total cross section of ^{6}Li

The solid line is the best estimate, and the dashed lines standard deviations.

1.7 Systematics of Fission Cross Sections in the Intermediate Energy Region

T. Fukahori and S. Chiba

Evaluation of neutron, charged particle and photon nuclear data at the incident energy above 20 MeV is in progress. One of the purposes of developing intermediate energy nuclear data is to supply basic data to waste management system, especially to accelerator-driven waste transmutation system. The fission cross section is an important physical quantity in the transmutation system. At the intermediate energy region, nuclei lighter than the actinides also have considerable fission cross sections. Systematics of fission cross section in the intermediate energy region is under development in JAERI to obtain the values simultaneously for various projectile-target combinations by using accumulated experimental data such as measured at Los Alamos[1] and Gatchina[2]. In this paper, the systematics of proton induced fission cross section is reported as an step of the total systematics study.

The systematics was obtained with fitting experimental data for proton induced fission cross sections of ^{nat}Ag, ^{181}Ta、 ^{197}Au、 ^{206,207,208}Pb、 ^{209}Bi、 ^{232}Th、 ^{233,235,238}U, ^{237}Np and ^{239}Pu above 20 MeV with the following formula.

$$P_{fis}(Z,A,E) = p_1 \cdot [1 - \exp(-p_3(E-p_2))]$$
$$p_i = A^{2/3} \cdot \exp[q_{i,1} + q_{i,2}(Z^2/A) + q_{i,3}(Z^2/A)^2] \qquad (i=1,2,3)$$

where P_{fis} (= σ_{fis} / σ_R) is defined as the fissility, σ_{fis} and σ_R are fission and total reaction (compound formation) cross sections, Z and A are the atomic and mass number of compound nucleus, E is an excitation energy [MeV]、 $q_{i,j}$ is the parameter independent of Z and A. It seems that the p_1, p_2 and p_3 parameters correspond to the saturation fissility, threshold energy and increasing rate, respectively. In the case that the experimental data are only given for the fission cross section, fissility is obtained by using σ_R calculated by Pearlstein's systematics[3]. The low energy cross section of actinoid nuclei is omitted from systematics study, since the cross section has a complicated shape and strongly depends on characteristic of nucleus.

The fitting results of the p parameters and systematics are shown in Fig. 1.7.1. Dots are fitting results, and lines are the obtained systematics. The numerical result of systematics

is summarized in Table 1.7.1. The fission cross section of ^{209}Bi calculated by the systematics is shown Fig. 1.7.2 with the experimental data and fitting result. It is concluded that the systematics reproduces experimental data well.

The systematics of proton induced fission cross section in the intermediate energy region is described. The shape of excited function is obtained for mass range above 180 and energy range from several tens MeV to 10 GeV by the systematics. In the future work, fission cross section induced by neutron, deuteron, alpha, photon, etc. will be included to the systematics. The fragment mass distribution and neutron energy spectrum should be also considered.

References

1) for example, Lisowski, et al.: "Fission Cross Sections in the Intermediate Energy Region", Proc. a Specialists' Meeting on Neutron Cross Section Standards for the Energy Region above 20 MeV, May 21–23, 1991, Uppsala, Sweden, NEANDC–305'U' (1991) p.177.

2) for example, Shcherbakov O.A.: "Experimental Investigations of the (n,f) Reaction", Sov. J. Part. Nucl., 21(2), 177 (1990).

3) Pearlstein S.: "Systematics of Neutron Emission Spectra from High–Energy Proton Bombardment", Nucl. Sci. Eng., 95, 116 (1987).

Table 1.7.1 The result of systematics for proton induced fission cross section

	result	error(%)	Correlation Matrix		
p_1 parameter					
$q_{1,1}$	6.01	4.7	1	-0.99	0.97
$q_{1,2}$	-1.27	1.4	-0.99	1	-0.99
$q_{1,3}$	0.0274	1.1	0.97	-0.99	1
p_2 parameter					
$q_{2,1}$	-11.2	0.8	1	-0.99	0.97
$q_{2,2}$	1.08	0.6	-0.99	1	-0.99
$q_{2,3}$	-0.0219	0.4	0.97	-0.99	1
p_3 parameter					
$q_{3,1}$	11.2	29.4	1	-0.99	0.97
$q_{3,2}$	-1.84	11.0	-0.99	1	-0.99
$q_{3,3}$	0.0382	8.3	0.97	-0.99	1

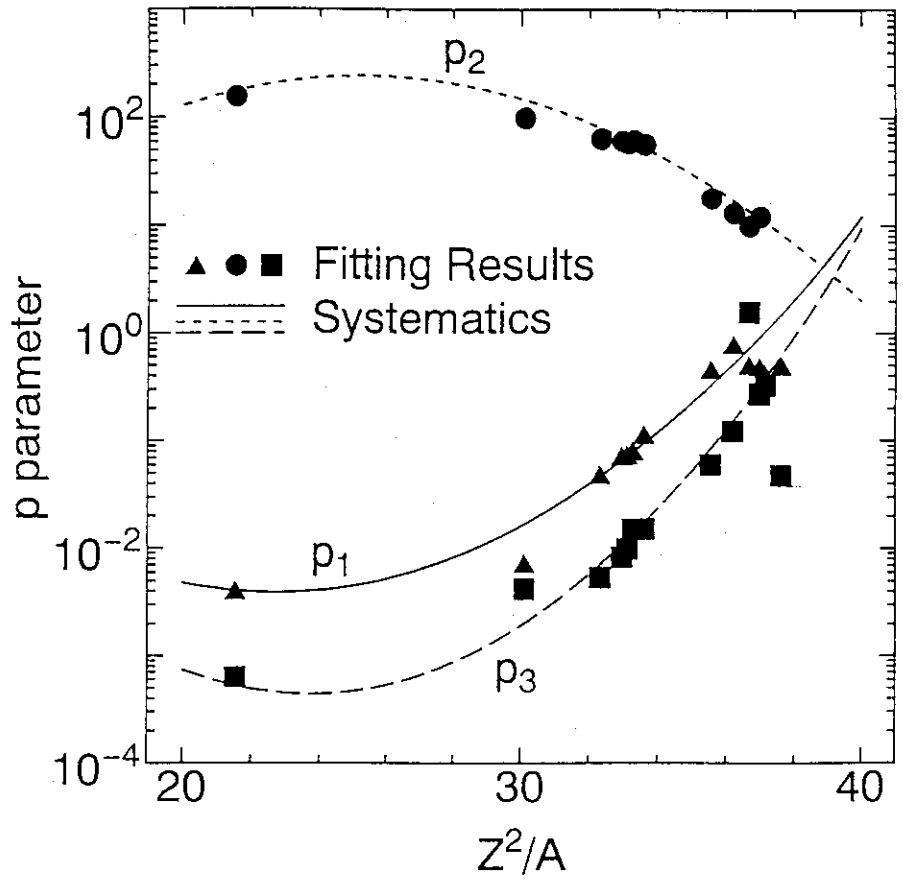

Fig. 1.8.1 Fitting results of p parameters and systematics values

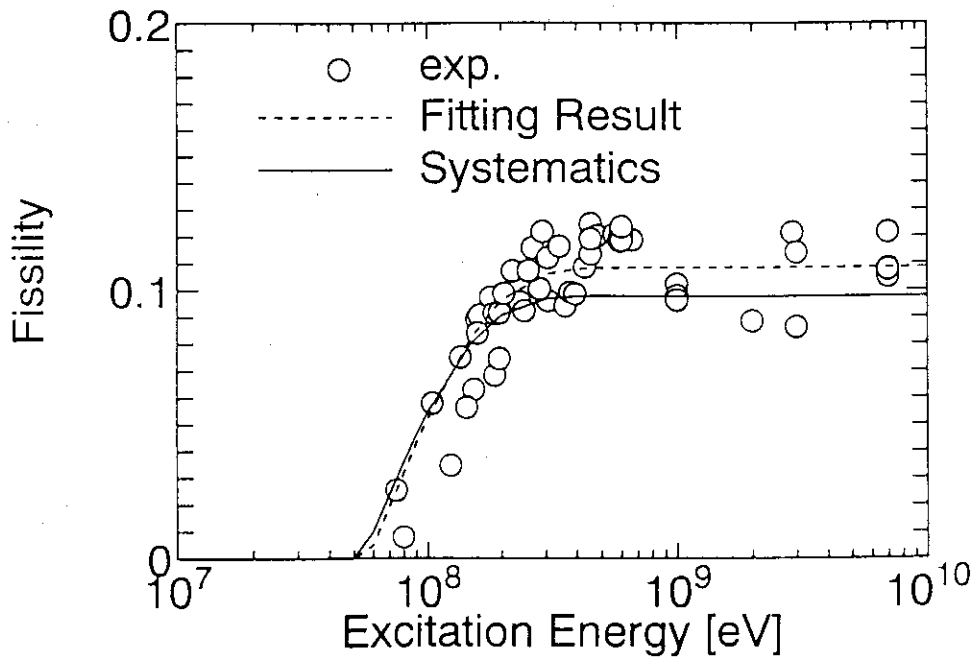

Fig. 1.8.2 Proton induced fissility of ^{209}Bi

1.8 A Code Guidance System for Integrated Nuclear Data Evaluation System

T. Fukahori and T. Nakagawa

Evaluated nuclear data files are necessary to many applications, and nuclear data evaluation is required to obtain the most reliable data sets. The evaluation must be done by using experimental data and by many complicated theoretical calculations with various physical data such as optical potential parameters, level density parameters, and level scheme. Japanese Evaluated Nuclear Data Library, version 3 (JENDL-3)[1] released in 1989 was accomplished by great efforts of many evaluators with a lot of intricate work.

Integrated Nuclear Data Evaluation System (INDES)[2] is being developed to keep their accumulated experiences of JENDL-3, to store basic data of nuclear physics used for the JENDL-3 evaluation, and to support new evaluations. Roughly classified, INDES functions are of three categories; to select the most suitable set of theoretical calculation codes, to retrieve data needed for the theoretical calculation codes from the database in INDES, and to set up input data of theoretical calculation codes automatically. For the first function, a guidance system in INDES, which is called '*Evaluation Tutor* (ET)', has been developed by applying knowledge engineering technology, which is based on the similar method to '*example-base reasoning*'. ET consists of an inference engine, calculating modules of certainty factors, two example-bases, frames, and a rule-base. The theoretical calculation codes for nuclear data evaluation considered in ET are DWUCKY[3], ECIS[4], CASECIS, JUPITOR[5], EGNASH2[3], TNG[6], PEGASUS[7], ALICE-F[8], CASTHY2[9], ELIESE-3[10], RESCAL and HIKARI, and it is easy to add new codes. The information concerning the theoretical calculation codes is stored in frames.

The two example-bases are used to obtain '*certainty factors*' of the theoretical calculation codes from their frequencies of use in the previous nuclear data evaluation. One example-base has been created from the experiences of the JENDL-3 evaluation work. Another is a supplementary example-base which stores results of code selection performed by ET, in order to be used in the next selection and to supply '*learning function*'.

The '*rules*' stored in the rule-base are used in the inference engine to select the theoretical calculation codes. The rules are classified into four types according to nuclear reaction processes; the direct, precquilibrium, compound and other processes. The latest

version of ET has 14 rules.

The scheme of an example run for ^{56}Fe is shown in Fig. 1.8.1. Firstly, the user specifies the basic information such as a target nucleus, a projectile and an incident energy range. Then, certainty factors are calculated for all the registered theoretical calculation codes by counting the number of uses in two example-bases. The rules in the rule-base are executed to make a preliminary decision of code selection. All the codes in the frames are classified into four reaction processes. If a process is judged not to be needed, the codes corresponding to the process are omitted from the selection. The candidate which has the largest certainty factor is selected as the recommended theoretical calculation code for each reaction process. For the codes requiring other auxiliary codes, the auxiliary codes are added to the set of recommended codes.

The rule-base and the theoretical calculation codes contained in ET will be expanded to treat more detailed procedures.

References

1) Shibata K., et al.: "Japanese Evaluated Nuclear Data Library, Version-3, JENDL-3", JAERI-1319 (1990).

2) Nakagawa T. and Fukahori T.: "Integrated Nuclear Data Evaluation System: INDES", Proc. the 1992 Symposium on Nuclear Data, Nov. 26-27, Tokai, Japan, 1992, JAERI-M 93-046 (1993) p.100.

3) Yamamuro N.: JAERI-M 90-006 (1990).

4) Raynal J.: IAEA SMR-9/8 (1972).

5) Tamura T.: ORNL-4152 (1967).

6) Fu C.Y.: ORNL/TM-7042 (1980).

7) Iijima S., et al.: Proc. the 1986 Seminar on Nuclear Data, Nov. 26-27, Tokai, Japan, JAERI-M 87-025 (1987) p.337.

8) Fukahori T.: Proc. Specialists' Meeting on High Energy Nuclear Data, Oct. 3-4, 1991, Tokai, Japan, JAERI-M 92-039 (1992) p.114.

9) Igarasi S. and Fukahori T.: JAERI-1321 (1991).

10) Igarasi S.: JAERI-1224 (1972).

```
READY
et
TIME-14:31:49 CPU-00:00:00 SERVICE-8433 SESSION-00:00:09 MAY 31,1994

ET> INPUT IZ,IA,IZAI,EMIN,EMAX
                IZ      : ATOMIC NUMBER OF TARGET
                IA      : MASS NUMBER OF TARGET
                IZAI    : ZA OF INCIDENT PARTICLE
                EMIN    : MINIMUM INCIDENT ENERGY
                EMAX    : MAXIMUM INCIDENT ENERGY
  26, 56, 1, 1.0e+6, 2.0e+7

ET> DO YOU CONSIDER DIRECT PROCESS (Y/N) ?
y

ET> DIRECT PROCESS IS CONSIDERED.
ET> PLEASE SELECT FOLLOWING THEORY.
ET>             1)      COUPLED CHANNEL
ET>             2)      DWBA
ET>             3)      BOTH 1) AND 2)
2

ET> DWBA THEORY IS SELECTED.
ET> DO YOU USE R-MATRIX THEORY FOR RESONANCE ANALYSIS (Y/N) ?
n

ET> DO YOU CONSIDER DIRECT CAPTURE PROCESS (Y/N) ?
n

ET> DWUCKY          IS SELECTED.
ET> EGNASH IS SELECTED.
ET> DO YOU USE DEFAULT OMP FOR 'EGNASH' CALCULATION (Y/N) ?
n

ET> YOU SHOULD USE 'ELIESE3' FOR CALCULATION OF TRANSMISSION
ET> COEFFICIENTS BEFORE 'EGNASH' IS PERFORMED.
ET> YOU SHOULD INCLUDE 'DWUCKY' RESULTS TO YOUR 'EGNASH'
ET> CALCULATION.
ET> CASTHY  IS SELECTED.


********** RESULTS FOR 26-FE- 56 **********
CODE NAME = DWUCKY              FOR DIRECT PROCESS WITH CF = 0.64664
                COMMENT:
                OUTPUT IS SET IN ENDF-5 FORMAT AND EGNASH INPUT FORMAT
                AUTOMATICALLY.
CODE NAME = EGNASH              FOR PRECOMP PROCESS WITH CF = 0.86021
                COMPILATION CODE = GAMFIL2
CODE NAME = CASTHY              FOR COMPOUND PROCESS WITH CF = 0.97258
                COMPILATION CODE = CTOB
CODE NAME = ELIESE3             FOR #EGNASH PROCESS WITH CF =
                COMMENT:
                CALCULATED QUANTITIES DEPEND ON INCIDENT PARTICLE.  SO,
                MF AND MT NUMBERS CANNOT BE DEFINED AT THIS TIME.
                <DIRECT> ON             #EGNASH

TIME-14:33:27 CPU-00:00:01 SERVICE-20068 SESSION-00:01:47 MAY 31,1994
READY
```

Fig. 1.8.1 Input and output data of the example run

1.9 Evaluation and Compilation of Nuclear Structure and Decay Data for A=122

J. Katakura and JNDC ENSDF Group*

The international nuclear structure and decay data evaluation network aims at a complete and continuous nuclear structure data evaluation of all mass chains. As a member of the network, Japanese group, whose data evaluation center is Nuclear Data Center, Japan Atomic Energy Research Institute, has responsibility for evaluating 12 mass chains with A=118-129. In the year of 1994, the evaluation of A=122 mass chain was completed and published in Nuclear Data Sheets[1]. The evaluated data are also included in ENSDF(Evaluated Nuclear Structure Data File) file which is maintained by National Nuclear Data Center, Brookheaven National Laboratory as a computer readable data file.

In the evaluation of A=122 mass chain, all data available up to December 1, 1992 have been considered for inclusion. The data included in the evaluation are tabulated below.

Nuclide	Data Type	Nuclide	Data Type
^{122}Ag	Adopted Levels	^{122}Sn	^{122}Sn(d,d'),(α,α')
^{122}Cd	Adopted Levels, Gammas		Coulomb Excitation
	^{122}Ag β$^-$ Decay (0.48 s)		^{123}Sb(μ$^-$,νnγ)
^{122}In	Adopted Levels		^{123}Sb(t,α)
	^{122}Cd β$^-$ Decay (5.24 s)		^{124}Sn(p,t)
	^{122}Sn(t,^{3}He)		^{126}Te(d,^{6}Li)
^{122}Sn	Adopted Levels, Gammas	^{122}Sb	Adopted Levels, Gammas
	^{122}In β$^-$ Decay (1.5 s)		^{122}Sb IT Decay (4.191 min)
	^{122}In β$^-$ Decay (10.3 s)		^{121}Sb(n,γ) E=th: Secondary
	^{122}In β$^-$ Decay (10.8 s)		^{121}Sb(n,γ) E=th: Primary
	^{122}Sb ε Decay		^{121}Sb(n,γ) E=res
	^{122}Sn(n,n')		^{121}Sb(d,p)
	^{122}Sn(n,n'γ)		^{122}Sn(p,nγ)
	^{122}Sn(p,p')		^{123}Sb(p,d)
	^{122}Sn(p,p'γ)		^{123}Sb(d,t)

* H. Iimura (JAERI), M. Oshima (JAERI), S. Ohya (Niigata University), K. Ogawa (Chiba University), J. Katakura (JAERI), M. Kambe (Musasi Technology University), K. Kitao (Data Engineering Inc.), T. Tamura (IRM), Y. Tendow (RIKEN), A. Hashizume (JAERO), K. Miyano (Niigata University)

Nuclide	Data Type	Nuclide	Data Type
^{122}Sb	^{120}Sb(α,d)	^{122}Xe	Adopted Levels Gammas
^{122}Te	Adopted Levels, Gammas		^{122}Cs ε Decay (21.0 s)
	^{122}Sb β- Decay		^{122}Cs ε Decay (4.5 min)
	^{122}I ε Decay		^{122}Te(^{3}He,3nγ) ...
	^{119}Sn(α,nγ)	^{122}Cs	Adopted Levels, Gammas
	^{120}Sn(^{3}He,n)		^{122}Cs IT Decay (0.36 s)
	^{121}Sb(^{3}He,d)		^{122}Ba ε Decay
	^{122}Te(γ,γ')		^{112}Sn(^{12}C,pnγ)
	^{122}Te(p,p')	^{122}Ba	Adopted Levels, Gammas
	Coulomb Excitation		^{122}La ε Decay
	^{124}Te(p,t)		^{108}Cd(^{16}O,2nγ)
^{122}I	Adopted Levels, Gammas	^{122}La	Adopted Levels
	^{122}Xe ε Decay	^{122}Ce	Adopted Levels
	(HI,xnγ)		

As an example of the evaluated data the decay scheme of ^{122}Ba β^+/ε decay is shown in Fig. 1.9.1.

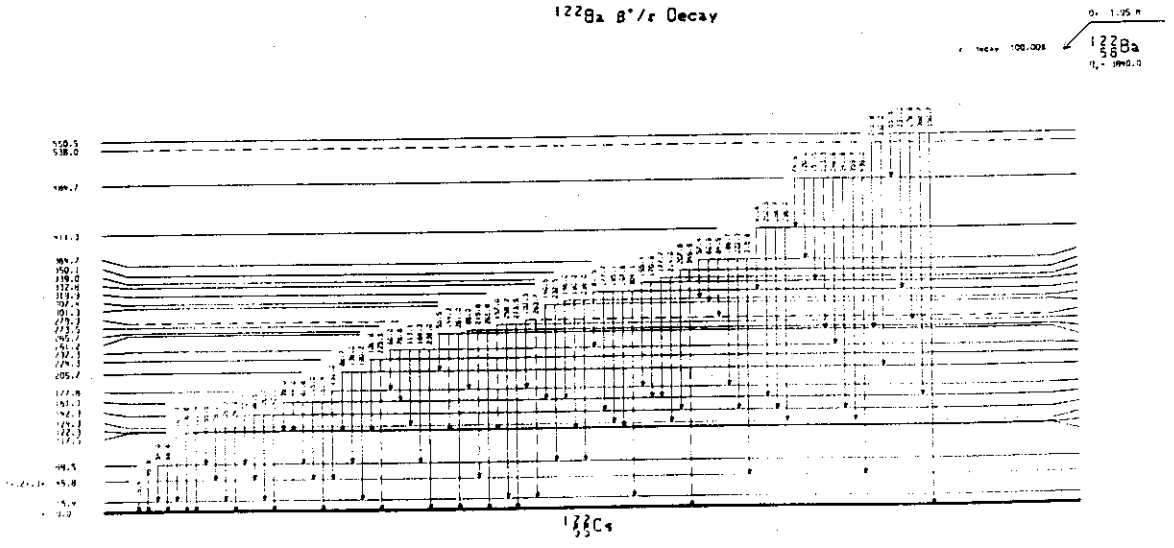

Fig. 1.9.1 Decay scheme of ^{122}Ba β^+/ε decay

The decay scheme is based on the measurement[2] reported in 1987 which is not included in the previous evaluation published in 1986.

Of the other mass chains the newly evaluated data of A=118, 127, 128 and 129 are on the stage of final check and will be published in Nuclear Data sheets. The evaluation of A=120 and 124 are now in progress and are going to be sent to BNL in 1995.

References

1) Tamura T.: Nucl. Data Sheets 71, 461 (1994)
2) Weiss B., et al.: Proc. 5th Int. Conf. Nuclei Far from Stability, Rosseau Lake, Canada, L9 (1987)

1.10 Cross Section Measurements for Short-Lived Radionuclides Production at Neutron Energy Range from 13.5 to 14.9 MeV

Y. Ikeda, A. A. Filatenkov[1] and D. L. Smith[2]

Short-lived radio-activities associated with 14 MeV neutron irradiation play an essential role in estimations of dose and decay heat after shutdown at early stages of the fusion reactor operation. As a total duration of the operation is limited to be short not like in the commercial machine, eventually, the most concern in terms of the radioactivity is placed on the nuclie with short half-lives. Extensive experimental work have been devoted to the measurement of activation cross sections at 14 MeV, resulting in a quite consistent data base for the fusion application. The cross section data for the short-lived radioactivity production, however, have not been well developed. In particular, the data for half-lives with a range from second to minute is recognized to be insufficient in terms of data quantity along with data quality.

With regard to the importance of the experimental data, we have carried out cross section measurements at 14 MeV energy region as the extended scope of the systematic measurement of activation cross sections at FNS. The reactions measured are tabulated in the Table 1.10.1. Since the half-lives were short, a pneumatic sample transfer system was employed between the D-T neutron source and counting room. The one side of six pneumatics tubes were positioned at 10 cm distance and at angles of 0°, 45°, 70°, 95°, 120°, and 155°, with respect to the D-T source. These angels are corresponding to the neutron energies from 13.5 to 14.9 MeV for the D-T neutrons produced with 350 keV incident deuteron beam energy. The neutron flux was derived by the following procedure: (i) An aluminum foil was irradiated at each end of pneumatic tube recording neutron yield with the associated α-particle counts in every 2 seconds. The flux normalized neutron yield was obtained from the reaction rate of the $^{27}Al(n,p)^{27}Mg$ reaction. The cross sections previously measured at FNS were used as the standard reaction. (ii) During irradiation of each objective sample, the neutron yield was monitored in the same manner and the flux was derived with the value obtained in (i).

The irradiation time was set to 2 - 3 times of half-lives of the reaction products. Immediately after irradiation, the sample was returned through the pneumatic tube and was placed on the Ge detector for γ-ray counting. In average, it took around 5 seconds from the end of irradiation to the start of counting. The counting time was also in two half-lives and followed by multiple countings on the same sample to confirm γ-ray line to be the objective

---

1; Khlopin Radium Institute, Russian Federation

2; Argonne National Laboratory, USA.

one. In order to improve insufficient γ-ray counting statistics due to short-lived nature, the measurement was repeated several times. Activation cross sections were finally derived from reaction rates obtained by γ-ray peak counts with necessary corrections, and neutron fluxes derived in (ii). Overall experimental error ranged from ± 4 % to ± 10 %. Larger error was dominated by the γ-ray counting statistics. For the radioactivity of ^{16}N, which is the product of two reactions, $^{16}O(n,p)^{16}N$ and $^{19}F(n,\alpha)^{16}N$, the detector efficiency were determined with use of relative intensities of γ-ray lines due to ^{11}Be, the energy of which ranges from 2.5 MeV to 7.9 MeV. The relative efficiency for the Ge detector was fit to the absolute value. Then, the efficiency for 6.1 MeV γ-ray was determined.

In Figs. 1.10.1 and 1.10.2, the presently measured cross sections for the reactions of $^{28}Si(n,p)^{28}Al$ and $^{16}O(n,p)^{16}N$ are plotted along with cross sections available in the currently evaluated activation files. The agreements between present data and the data previously measured at FNS for the $^{28}Si(n,p)^{28}Al$ demonstrated that a consistency was kept in deriving the cross sections. An attention for the cross section of $^{16}O(n,p)^{16}N$ reaction has been paid in the ITER design from the critical consideration of activated of coolant water with strong ^{16}N activities which concerns additional sources of TF coil nuclear heating and dose rate in the organic insulator. The present data are slightly higher than those of evaluated cross sections.

Table 1.10.1. Reactions investigated and Half-lives, γ-ray energies and branching ratios

	Reaction	$T_{1/2}$ Eγ (Branching)	Sample form
1	$^{11}B(n,p)^{11}Be$	(13.8 s: 2125 keV(33%))	B_4C
2	$^{16}O(n,p)^{16}N$	(7.13 s: 6129 keV(69%))	SiO_2
3	$^{19}F(n,\alpha)^{16}N$	(7.13 s: 6129 keV(69%))	Teflon
4	$^{19}F(n,p)^{19}O$	(26.9 s: 197 keV(91%))	"
5	$^{23}Na(n,p)^{23}Ne$	(37.6 s: 440 keV(33%))	NaF
6	$^{27}Al(n,2n)^{26m}Al$	(6.4 s: 511 keV (200%))	Al
7	$^{28}Si(n,2n)^{27}Si$	(4.13 s: 511 keV (200%))	SiO_2
8	$^{28}Si(n,p)^{28}Al$	(2.24 m: 1779 keV(100%))	SiO_2
9	$^{37}Cl(n,p)^{37}S$	(5 m: 3103 keV(94%))	KCl
10	$^{46}Ti(n,p)^{46m}Sc$	(18.67 s: 143 keV(56%))	"
11	$^{53}Cr(n,p)^{53}V$	(1.61 m: 1006 keV(89.6%))	Cr metal
12	$^{52}Cr(n,p)^{52}V$	(3.75 m: 1434 keV))	"
13	$^{55}Mn(n,\alpha)^{52}V$	(3.75 m: 1434 keV))	MnCu
14	$^{89}Y(n,n')^{89m}Y$	(16 s: 909 keV))	Y metal
15	$^{119}Sn(n,p)^{119m}In$	(2.4 m: 763 keV(99.1%))	Separated Isotope
16	$^{138}Ba(n,p)^{138m}Cs$	(2.9 m: 1436 keV(25%))	Separated Isotope
17	$^{138}Ba(n,2n)^{137m}Ba$	(2.552 m: 661.7 keV(89.9%))	"
18	$^{141}Pr(n,2n)^{140}Pr$	(3.39 m: 511 keV(97.4%))	Pr_6O_{11}
19	$^{186}W(n,2n)^{185m}W$	(1.67 m: 131 keV(4.4%))	W Metal
20	$^{204}Pb(n,2n)^{203m}Pb$	(6.2 s: 825.2 keV(73%))	Separated Isotope

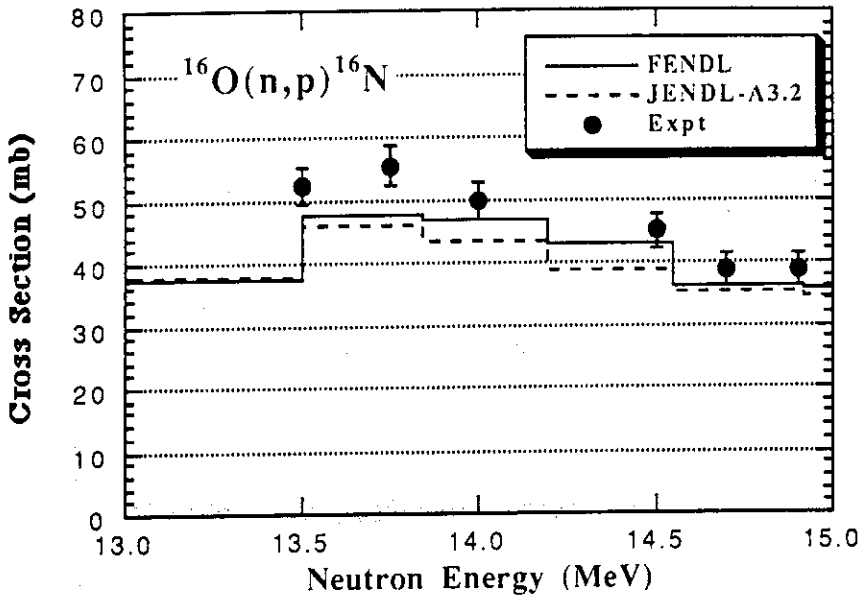

Fig. 1.10.1 Cross sections of the $^{16}O(n,p)^{16}N$ reaction at 14 MeV energy region.

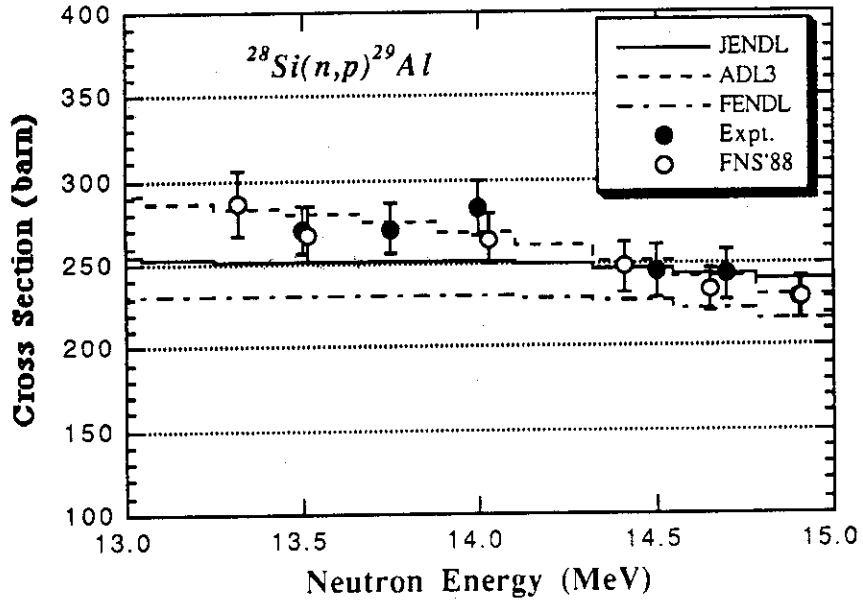

Fig. 1.10.2 Cross sections of $^{28}Si(n,p)^{28}Al$ reaction at 14 MeV energy region.

1.11 Measurements of Activation Cross Sections of Importance for the Neutron Dosimetry at an Energy Range from 17.5 to 30 MeV Using p-Li Monoenergetic Neutron Source at JAERI/TANDEM Facility

Y. Uno, S. Meigo, S. Chiba, T. Fukahori and Y. Ikeda

Since 1993, an experimental program for systematic measurements of activation cross secitons in a neutron energy range from 17.5 to 30 MeV has been underway in order to meet the data requirement from the high energy neutron dosimetry application. The reactions investigated in two years are listed in **Table 1.11.1**. **Tabl 1.11. 2** summarizes the incident proton energies, proton beam current, peak neutron energies, irradiation time and neutron fluxes at the sample positions. The neutron flux was determined by a proton recoil telescope (PRT) counter. The neutron emission spectrum for each proton energy was measured by the time of flight technique incorporating an NE213 scintillation counter. Also, the angular neutron flux distribution for each irradiaiton was measured by moving the NE213 around the neutron target. The total neutron yeild was derived from ^{7}Be activity which is produced via ^{7}L(p,n)^{7}Be reaction in the Li target.

After each irradiation, radioactivities were measured with Ge detectors. From net γ-ray peak counts of interest, the reaction rate was derived after necessary corrections. Cross sections were derived by both the neutron flux and reaction rate. **Figure 1.11.1** shows the neutron spectra corresponding to the incident proton energies of 20, 25 and 32 MeV. In general, there is a considerablly large neutrons in the energy region below the peak. Since the reaction rate is given as the integral product of neutron flux spectrum and cross sections over the whole sensitive energy region. Thus, the contribution of lower nergy neutrons to the total reaction rate was subtracted by using the measured neutron spectrum and estimated cross section as the weighting function. When there is no appropriate evaluated cross section data, the cross sections were calculated with SINCROSS-II[1] code. After several iteration procuder for the low energy neutron contribution estimation, the cross section at each peak neutron energy was determined. The main sources of the experimental error were in the γ-ray counting statistics and in the reference neutron flux determination. They are in a range from ± 5 % to ± several tens %.

In **Fig. 1.11.2**, the cross sections derived in this experimental program were shown for the reactions of ^{59}Co(n,2n)$^{58m+g}$Co and ^{59}Co(n,3n)^{57}Co, along with data in the literature. As the weigting function, the cross section evaluated by Odano[2] was used. The data measued in this work are in good agreement with data reported by Uno[3]. From the view point of data deficiency in the energy region above 20 MeV, a new data obtained in this work are to be of importance in the new cross section evaluation for high energy dosimetry application.

References

1) Yamamurao, N. : "A Nuclear Cross Section Calculation System with Simplified Input-Format Version-II (SINCROS-II)," JAERI-M 90-006 (1990).

2) Odano, N., et al. : "Evaluation of Cross Sections for the Dosimetry Reactions of Niobium," Proc. Int. Conf. on Nucl. Data for Sci., Jeulich (1993) pp.

3) Uno, Y., et al.: to be published in Nucl. Sci and Eng.

Table 1.11.1 Reactions investigated

Sample	Reaction	Half life	Q-Value[MeV]
^{197}Au	^{197}Au(n,2n)^{196m}Au	9.7h	-8.67
	^{197}Au(n,2n)$^{196m+g}$Au	6.183d	-8.07
	^{197}Au(n,3n)^{195}Au	186.09d	-14.72
	^{197}Au(n,4n)^{194}Au	1.646d	-22.79
^{27}Al	^{27}Al(n,α)$^{24m+g}$Na	14.659h	-3.13
^{59}Co	^{59}Co(n,2n)$^{58m+g}$Co	70.916d	-10.45
	^{59}Co(n,3n)^{57}Co	271.77d	-19.03
	^{59}Co(n,p)^{59}Fe	44.496d	-0.78
	^{59}Co(n,α)^{56}Mn	2.5785h	0.33
^{169}Tm	^{169}Tm(n,2n)^{168}Tm	93.1d	-8.03
	^{169}Tm(n,3n)^{167}Tm	9.24d	-14.87
^{89}Y	^{89}Y(n,2n)^{88}Y	106.6d	-11.48
	^{89}Y(n,3n)^{87m}Y	12.9h	-21.21
^{93}Nb	^{93}Nb(n,2n)^{92m}Nb	10.15d	-8.97
^{58}Ni	^{58}Ni(n,2n)^{57}Ni	1.503d	-12.22
	^{58}Ni(n,p)$^{58m+g}$Co	70.916d	0.40
	^{58}Ni(n,np)^{57}Co	271.77d	-8.17
	^{58}Ni(n,2np)^{56}Co	77.7d	-19.55
^{48}Ti	^{48}Ti(n,p)^{48}Sc	1.821d	-3.21
	^{48}Ti(n,np)^{47}Sc	3.341d	-11.44
	^{48}Ti(n,2np)$^{46m+g}$Sc	83.83d	-22.09
nat Cu	nat Cu(n,xn)^{64}Cu	12.701h	-9.91
	nat Cu(n,xn)^{61}Cu	3.408h	-19.74

Table 1.11.2 Incident proton energies, peak neutron energies, neutron yeilds, irradiation time and neutron fluxes at the sample positions

Ep [MeV]	En [MeV]	Neutron Yield [n/Sr/mC]	Irrad. Time [sec]	Flux at the sample position [n/cm^2/sec]
20.0	17.5	6.05E+08	54000	9.613E+05
22.5	20.0	8.93E+08	32445	2.912E+06
25.0	22.5	9.49E+08	29400	1.143E+06
27.5	25.0	1.39E+09	47835	1.163E+06
30.0	28.0	1.37E+09	43901	9.532E+05
32.0	30.0	1.84E+09	42342	9.681E+05

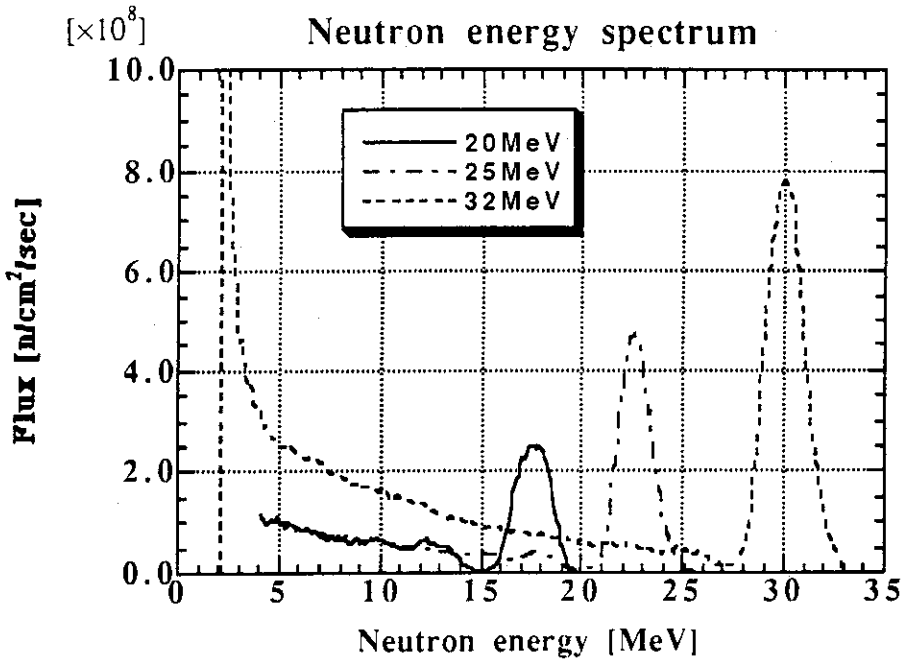

Fig. 1.11.1 Neutron spectra corresponding to incident proton energies of 20, 25 and 32 MeV.

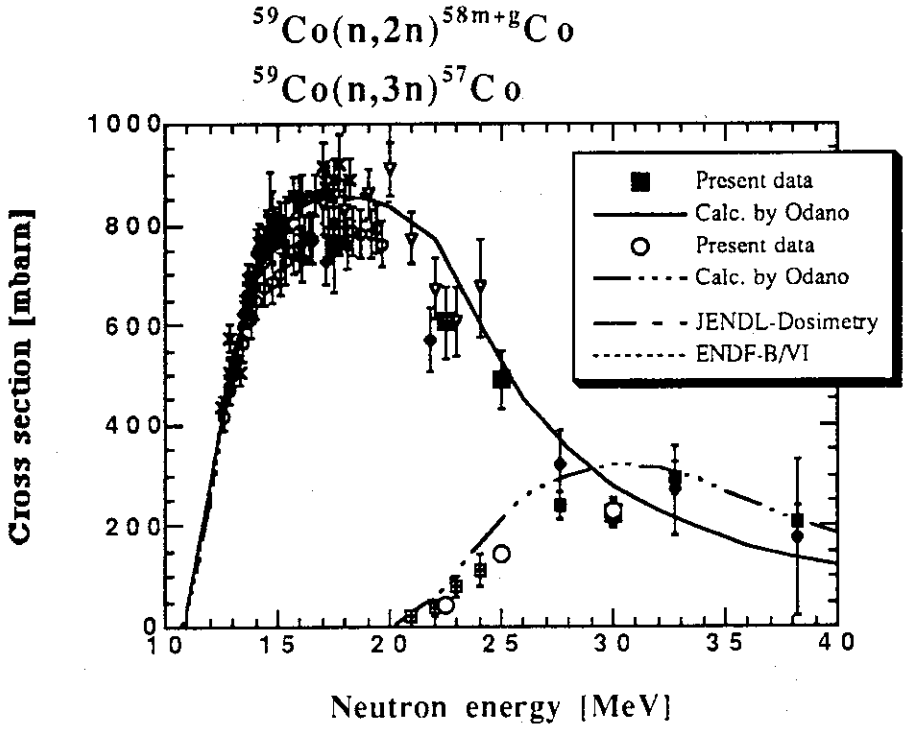

Fig. 1.11.2 Measured cross sections of $^{59}Co(n,2n)^{58m+g}Co$ and $^{59}Co(n,3n)^{57}Co$ along with data in the literature.

1.12 Measurements of Tritium and Carbon-14 Production Cross Sections for 14.7 MeV Neutrons on Oxygen-17 and Oxygen-18

Yu. M. Verzilov, Y. Ikeda, F. Maekawa Y. Oyama and D. L. Smith *

In designs of the first generation (D-T) fusion reactors, water is often used for coolant. Hence radioactivity from water is important from the view point of fusion reactor safety and waste management of long-lived isotopes, ^{14}C, for example. Oxygen in water forms $^{16}O(n,^3He)^{14}C$, $^{17}O(n,\alpha)^{14}C$ and $^{18}O(n,n'\alpha)^{14}C$ reactions whose Q-values are less than 15 MeV of the D-T neutron energy. The $^{17}O(n,\alpha)^{14}C$ and $^{18}O(n,n'\alpha)^{14}C$ reactions are the dominant, since the Q-value of $^{16}O(n,^3He)^{14}C$ reaction is about -14.62 MeV. The reaction $^{17}O(n,\alpha)^{14}C$ (Q-value = + 1.82 MeV) can be induced by fast and low-energy neutrons, and $^{18}O(n,n'\alpha)^{14}C$ (Q-value= - 6.23 MeV) is only by fast neutrons.

Activation cross sections are needed for estimating ^{14}C activity production. The measured cross section data were reported only for $^{17}O(n,\alpha)^{14}C$ reaction from thermal energy to approximately 1 MeV[1,2], and no experimental data for neutrons of energies around 14 MeV. On the other hand, the evaluated data for $^{17}O(n,\alpha)^{14}C$ cross section in the REAC*3 library is around 200 mbarn for 14 MeV neutron region[3] and seem to be large. The status of the $^{17}O(n,\alpha)^{14}C$ and $^{18}O(n,n'\alpha)^{14}C$ cross section data for fusion power plant technology is summarized in the reference[4]. There it is pointed out that cross section data for these reactions are rather uncertain due to lack of experimental information.

In addition to the (n,xα) process which is result in an ^{14}C activity in water the (n,t) reaction is also possible for 14 MeV neutrons. For oxygen isotopes there are three reactions, $^{16}O(n,t)^{14}N$, $^{17}O(n,t)^{15}N$ and $^{18}O(n,t)^{16}N$. Those Q-values are -14.48, -7.79 and -13.34 MeV, respectively. A survey of the measured (n,t) cross section for light nuclei, Z<10, shows that studies have been performed only for nuclei such as $^{6,7}Li$, ^{9}Be, $^{10,11}B$ and ^{19}F so far.

In order to meet the data request for estimation ^{14}C activity in water, the cross sections for $^{17}O(n,\alpha)^{14}C$ and $^{18}O(n,n'\alpha)^{14}C$ reactions have been measured using 14.7 MeV neutrons at FNS. In addition, cross section for $^{17}O(n,t)^{15}N$ and $^{18}O(n,t)^{16}N$ reactions was also measured at the same time. A schematic experimental set-up is shown in Fig. 1.12.1. The samples were made of high purity water having enriched isotopic abundances of hydrogen and oxygen. Deuterium water, D_2O, was added to the set of interested samples in order to estimate tritium activity from interfered $^2H(n,\gamma)^3H$ reaction, since there is deuterium content

---

* Argonne National Laboratory

in each water sample. Two experiments were performed. In the first experiment, three $H_2{}^{16}O$ (^{16}O - 99.97%), three $H_2{}^{17}O$ (^{17}O - 10%) and two D_2O samples were positioned as illustrated in Fig. 1.12.1 and exposed simultaneously for about 150 hours. The $H_2{}^{17}O$ samples were placed at the different distances from the target in order to estimate the ^{14}C contribution from $^{17}O(n,\alpha)^{14}C$ reaction which was induced by low-energy neutrons. In the second experiment, the same sample arrangement was done, except $H_2{}^{17}O$ samples which were changed to the $H_2{}^{18}O$ (^{18}O - 99.8%) samples. The irradiation were performed for about 160 hours.

After neutron irradiation of the water samples, the ^3H and ^{14}C produced in them were measured with a liquid scintillation counting technique. In the present sample processing scheme shown in Fig. 1.12.2, a special care was paid to the carbon-14 losses in $^{14}CO_2$ gas phase during irradiation of the samples and preparation of the scintillation solutions. Two important steps were done prior to the incorporation of the irradiated sample into the liquid scintillator: the fixation of the gas phase and neutralization of the scintillation cocktail.

Since the β-activity measurement gives the total ^3H or ^{14}C activity generated in the sample, it includes all tritium or carbon-14 producing reaction channels. Tritium is produced in water through $^{17}O(n,t)^{15}N$ and $^{18}O(n,t)^{16}N$ reactions because the contributions of the $^2H(n,\gamma)^3H$ and $^{16}O(n,t)^{14}N$ reactions are less than 1%, it was found by direct measurement, and they were neglected. Therefore, in order to distinguish reactions of interest, enriched samples were used. The procedure to deduce the cross sections when two reactions produce the same activity in one sample is described previously[9]. In the similar manner the cross section of $^{17}O(n,\alpha)^{14}C$ and $^{18}O(n,n'\alpha)^{14}C$ reactions were determined. Since the $^{17}O(n,\alpha)^{14}C$ reaction can be induced by D-T and low-energy neutrons, an additional measurement was done in order to estimate ^{14}C activity produced by low-energy neutrons. The contribution of the $^{17}O(n,\alpha)^{14}C$ reaction induced by low energy neutrons was found to be negligible compared to ^{14}C activity produced by D-T neutrons.

The measured cross sections and their maximum errors are given in Table 1.12.1. Each value is based on two independent measurements. The results of an evaluation from JENDL Activation Library are given in the same table for comparison. From the comparison of the data two comments should be made. For ^3H production cross sections the calculated data are underestimated in triton emission process by a factor about 0.4 for both reactions. In contrast, for ^{14}C production cross section the calculated data are overestimated in the cross section value of $^{17}O(n,\alpha)^{14}C$ and $^{18}O(n,n'\alpha)^{14}C$ reactions by the factor 1.3 and 1.8, respectively. The present work yields the first measurement of the cross sections for these four nuclear reactions. The cross section for the $^{17}O(n,\alpha)^{14}C$ reaction obtained in this work is considerably lower than the evaluated value in the REAC*3 library, and it is in overall agreement with the data from JENDL Activation Library.

References

1) Mughabghab S.F., Divadeenam M., and Holden N.E.: Neutron Cross Sections, Vol. 1, Part A, Z=1 - 60, Academic Press (1981).

2) Koehler P.E. and Graff S.M.: Phys. Rev. C, 44, 2788 (1991).

3) Mann F.M.: Proc. Int. Conf. on Nucl. Data for Science and Technology, Julich, Germany, 13-17 May 1991, p. 936, Springer-Verlag (1992).

4) Cheng E.T. and Smith D.L.: "Nuclear Data Needs and Status for Fusion Reactor Technology", ibid., p. 273.

5) Ikeda Y., et al.: JAERI-1312 (1988).

Table 1.12.1 Comparison of measured cross sections with calculated evaluation in JENDL Activation Library.

Reaction	Cross Section (mb)		C/E
	Present results	JENDL	value
$^{17}O(n,t)^{15}N$	18 ± 3	7	0.39
$^{17}O(n,\alpha)^{14}C$	35 ± 7	44	1.26
$^{18}O(n,t)^{16}N$	0.8 ± 0.2	0.3	0.38
$^{18}O(n,n'\alpha)^{14}C$	27 ± 5	48	1.78

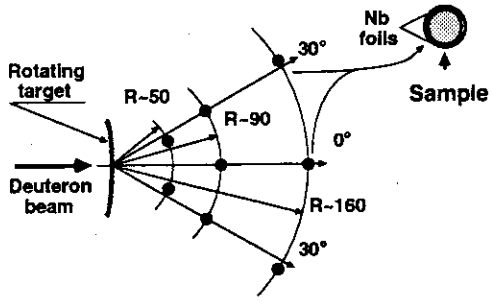

Fig. 1.12.1 Experimental Set-up for the neutron irradiation

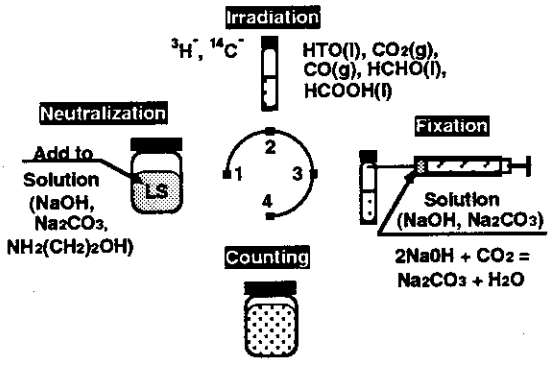

Fig. 1.12.2 Sample processing scheme of the technique

1.13 Integral Data Test of JENDL-3.2 and FENDL-1.0 using FNS Benchmark Experiments

Y. Oyama, F. Maekawa, M. Wada and K. Kosako[1]

Integral data testing of JENDL-3.2[1] and FENDL-1.0[2] is extensively being performed as the activities of both Fusion Neutronics Integral Test Working Group organized under the Reactor Constant Sub-Committee of the Japanese Nuclear Data Committee. The member and the utilized experimental results are summarized in Table 1.13.1. The MCNP calculations for those experiments were performed in the same way as the previous benchmark test for JENDL-3.1. In this time, integral data testing specially for gamma-ray was newly added with new gamma-ray benchmark experiments for Cu, W, Fe performed after completion of JENDL-3.1. On the other hand, The FENDL activity is conducted by IAEA/NDS coordination for making standard libraries so as to use in the International Tokamak Experimental Reactor (ITER) design. For this purpose, the FENDL-1.0 transport library is being tested to feed back the results to FENDL-2.0 compilation. The candidate evaluations for FENDL-2.0 include JENDL-Fusion File with the file-6 form which was partly evaluated for JENDL-3.2.

The integral experiments for data testing of fusion materials were chosen from the recent fusion integral experiments performed at FNS. Most of those experiments were compiled in the report[3] and the latest compilation was made by IAEA/NDS for FENDL benchmarks. Materials included in the selected integral experiments were Li, Be, C, N, O, Fe, Cu, Pb, W and stainless steel for fusion materials. These are of slab geometry and mostly single material to eliminate a modeling uncertainty. One is the time-of-flight experiment for leakage spectrum and another is the in-system parameter experiment such as for spectrum and reaction rates.

The continuous pointwise cross section library FSXLIB-J3R2[4] was prepared from JENDL-3.2 nuclear data file for this purpose. The NJOY83.6 was used for the process of 340 nuclides. For FENDL-1, the processed MCNP library was also provided from IAEA/NDS as FENDL/MC-1.0.

Cross sections of JENDL-3.2 for most of materials are more or less improved from JENDL-3.1. The results of Li_2O, C, N, O, W and Fe showed better agreements than the JENDL-3.1 results. Figure 1.13.1 shows the result of the beryllium TOF experiment that the FENDL-1.0 is better than JENDL-3.1 around 1 MeV. Figure 1.13.2 also shows similar trend for $^{115}In(n,n')$ reaction rate of the result for the in-system beryllium experiment. For the spectrum of the iron in-system experiment shown in Fig. 1.13.3, an improvment from JENDL-3.1 is

---

[1]Sumitomo Atomic Energy Industries Ltd.

obtained by JENDL-3.2, though FENDL-1 is also better than JENDL-3.1. For the lead results of the TOF experiment, the large discrepancy is found in the emission spectrum below 1 MeV as shown in Fig. 1.13.4.

References

1) Nakagawa T.: " JENDL-3 Revision 2," Proc. 1993 Symposium on Nuclear Data, JAERI-M 94-019, pp68-78 (1994)
2) Ganesan S. and Muir D.W.: " FENDL Multigroup Libraries", IAEA-NDS-129, (1992)
3) "Collection of Experimental Data for Fusion Neutronics Benchmark," Eds. Fusion Reactor Physics Subcommittee, JAERI-M 94-014 (1994)
4) Kosako K., et al.: " FSXLIB-J3R2: A Continuos Energy Cross Section Library for MCNP based on JENDL-3.2," to be published in JAERI-Data/Code report (1994)

Table 1.13.1 Integral Experiments and Participants for Testing of JENDL-3.2 (Fusion Neutronics Integral Test WG)

FNS-Slab		
In-system Experiment	n&g Fe, Cu, W	Y. Oyama, F. Maekawa, T. Mori
Leakage Spectrum-TOF	Li2O, Be, C,...	K. Ueki, (Multigroup) K. Hayashi, K. Maki
OKTAVIAN Pulsed Sphere	n&g LiF, CF2, Be, F, Si, Cu, Zr, Pb,...	A. Takahashi, C. Ichihara F. Maekawa(g-ray)
OBNINSK Pulsed Sphere	Fe,...	K. Ueki
KfK Sphere	Be	K. Hayashi
Library Preparation	FSXLIB-J3R2	K. Kosako

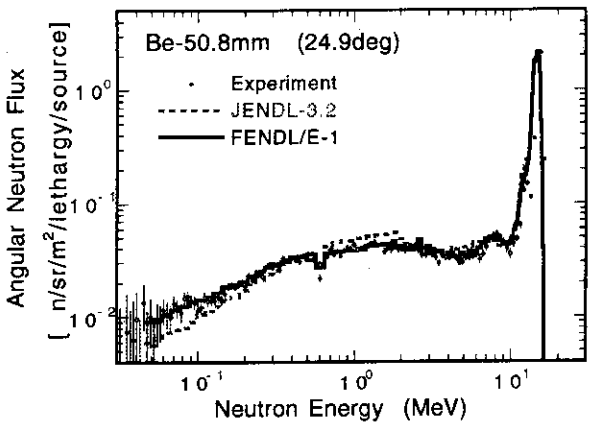

Fig.1.13.1 Result of beryllium TOF experiment

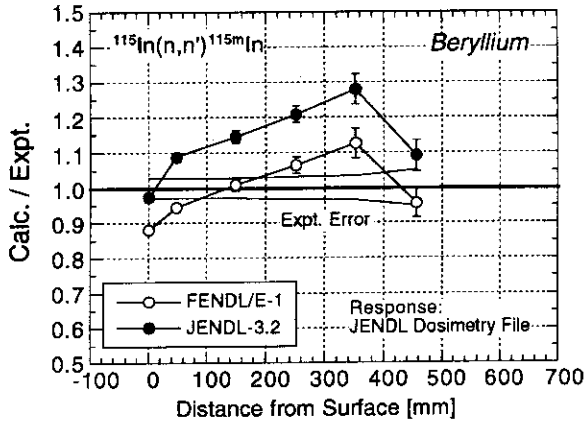

Fig. 1.13.2 Result of beryllium in-sistem experiment

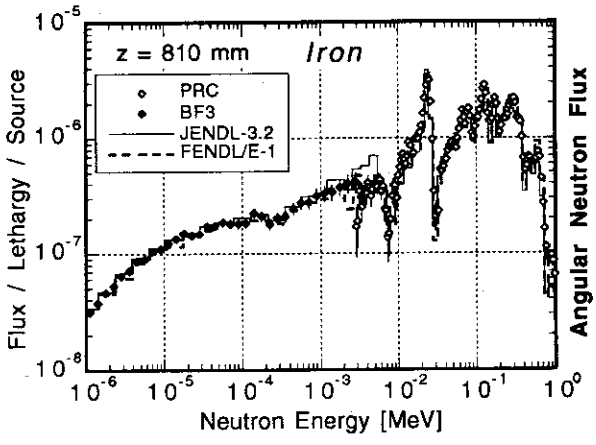

Fig.1.13.3 Result of iron in-system experiment

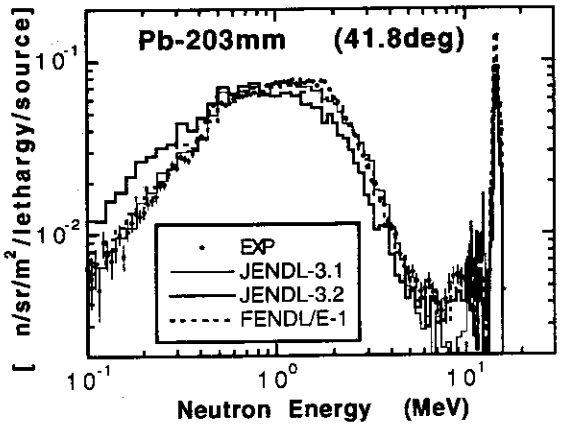

Fig.1.13.4 Result of lead TOF experiment

1.14 Benchmark Test of Secondary Gamma-Ray Data in JENDL-3.2 and FENDL/E-1.0 through Analyses of the FNS and OKTAVIAN Experiments

F. Maekawa, Y. Oyama, M. Wada and H. Maekawa

Secondary gamma-ray data in JENDL-3.2 and FENDL/E-1.0 were tested by benchmark calculations of existing integral experiments. [1,2] Two series of experiment with D-T neutron sources were employed for the benchmark test; (1) FNS/JAERI clean benchmark experiments [3,4] on Fe, Cu, W and type 316 stainless steel (SS316) and (2) OKTAVIAN/Osaka University pulse sphere experiments [5] on LiF, CF_2, Al, Si, Ti, Cr, Mn, Co, Cu, Nb, Mo, W and Pb. The continuous energy Monte Carlo code MCNP-4A with FSXLIB-J3R2 [6] and FENDL/MC-1.0 [7] libraries based on JENDL-3.2 and FENDL/E-1.0, respectively, was used for the calculations.

Figure 1.14.1 shows calculated to experimental values (C/Es) of gamma-ray heating rate in the iron assembly of the FNS experiment. The heating rates by FENDL agree within the experimental error bands of about ± 10 % with the experiment. However those by JENDL are larger than the experiment by 10 - 70 %, especially near the front surface of the assembly where 14 MeV neutrons are dominant for gamma-ray production. Since the gamma-ray heating rate means the deposited energy of gamma-rays to a surrounding medium, the heating rate has strong correlation with total gamma-ray energies released by gamma-ray production reactions around the measuring point. Hence the discrepancy of JENDL implies that energy balance of the gamma-ray production cross section in JENDL is broken or the released gamma-ray energies exceed the theoretical values for incident neutrons around 14 MeV. This point should be improved in the future evaluation. As regard the rest of the materials tested by the FNS experiments, i.e., Cu, W and SS316, although there exists a few problems, it is found that the secondary gamma-ray data in both libraries are almost acceptable.

As for the results of the OKTAVIAN experiment, no significant differences of the calculated spectra from the measured ones are pointed out for all the tested materials. Two examples of comparisons between the measured and the calculated leakage gamma-ray spectra are presented in Figs. 1.14.2 (a) for silicon and (b) for copper. As seen in Fig. 1.14.2 (b), the calculated spectra for copper with both libraries almost perfectly follow the measured spectrum. For the spectrum of silicon in Fig. 1.14.1 (a), JENDL is in good agreement with the experiment while the spectrum by FENDL in the energy range higher than 3 MeV is smaller than the measured one.

In order to quantitatively compare the measured and the calculated spectra for the OKTAVIAN experiments, the spectra were integrated over whole energy ranges. From a viewpoint of engineering, the importance of a gamma-ray is generally in proportion to its

energy, because most of nuclear parameters induced by gamma-rays, such as radiation dose, heating and material damage, have a strong dependence on the total gamma-ray energies deposited to the surrounding medium. Hence the following energy integrals are compared instead of photon numbers.

$$\text{(Total Energy Integral)} = \int \phi(E) \cdot E \cdot dE \qquad (1)$$

The obtained values, namely, total energy integrals, correspond to the energies observed at the detector. Figure 1.14.3 is the C/E ratios of the total energy integrals for all the 13 materials. Since the maximum discrepancies between the experiment and calculations for all the samples do not exceed 27 %, the secondary gamma-ray data of C, F, Al, Si, Ti, Cr, Mn, Co, Cu, Nb, Mo, W and Pb in both JENDL and FENDL/E are mostly validated as far as 14 MeV neutrons are concerned. The C/E ratios for JENDL ranging between 0.81 and 1.14 are closer to unity comparing with those from FENDL lying between 0.73 and 1.16. Hence it is concluded that JENDL provides secondary gamma-ray data for 14 MeV neutrons better than FENDL from an engineering viewpoint.

References

1) Maekawa F. and Oyama Y.: "Benchmark Test of Gamma-Ray Production Data in JENDL-3.2 and FENDL-1," Proc. IAEA/CRP on Measurement, Calculation and Evaluation of Photon Production Data, Bologna, Italy, Nov. 14-17 (1994).
2) Maekawa F. and Oyama Y.: "Benchmark test of 14-MeV Neutron Induced Gamma-Ray Production Data in JENDL-3.2 and FENDL/E-1.0 through Analysis of the OKTAVIAN Experiment," submitted to Nucl. Sci. Eng. (1995).
3) Maekawa F., et al.: "Benchmark Experiment on a Copper Slab Assembly by D-T Neutrons," JAERI-M 94-038 (1994).
4) Konno C., et al.: "Bulk Shielding Experiments on Large SS316 Assemblies Bombarded by D-T Neutrons Volume I: Experiment," JAERI-Research 94-043 (1994).
5) Yamamoto J., et al.: "Gamma-ray Energy Spectra Emitted from Spheres with 14 MeV Neutron Source," JAERI-M 94-14, pp. 32-62 (1994).
6) Kosako K., et al., "FSXLIB-J3R2: A Continuous Energy Cross Section Library for MCNP Based on JENDL-3.2," JAERI-Data/Code 94-020 (1994).
7) R. E. MacFarlane, Private Communication, LANL (1994).

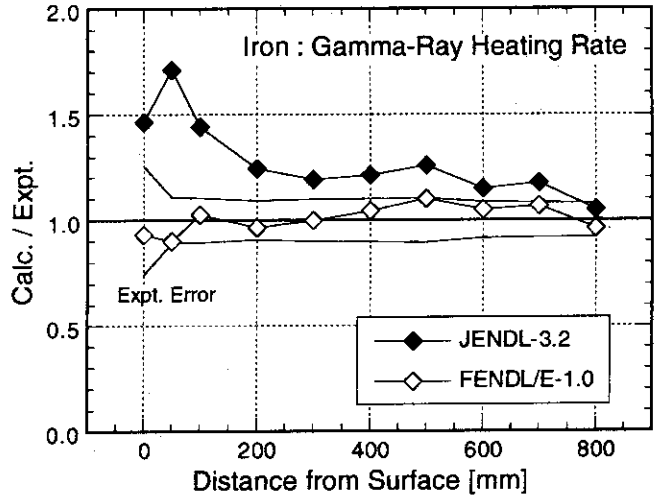

Fig. 1.14.1 Calculated to experimental values of gamma-ray heating rate of iron.

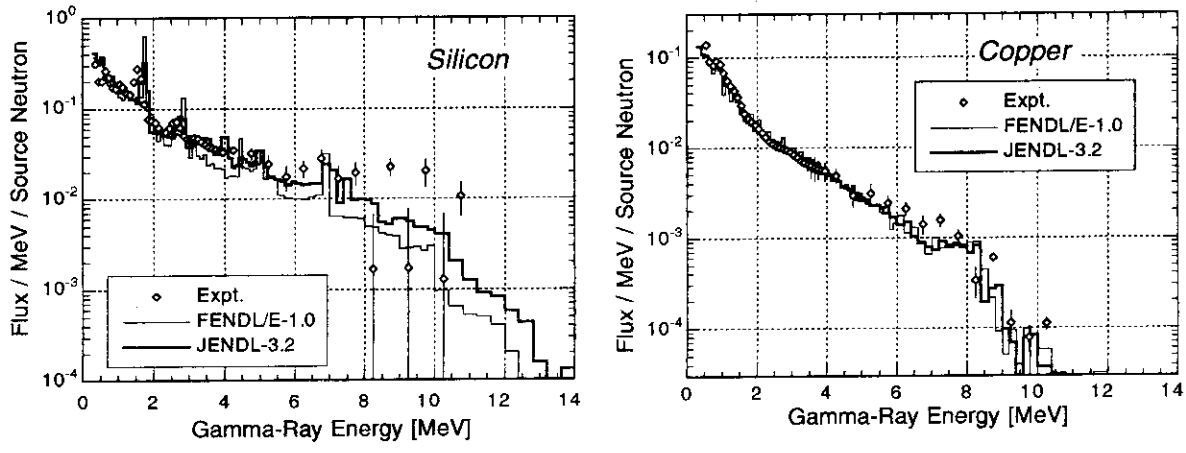

Fig. 1.14.2 Comparisons between measured and calculated leakage gamma-ray spectra.

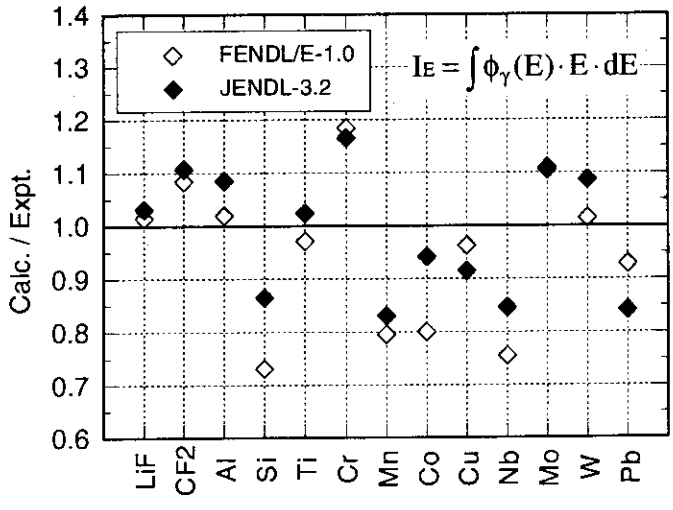

Fig. 1.14.3 Calculated to experimental values of the total energy integrals.

1.15 Fast Reactor Benchmark Calculation for ENDF/B-VI

H. Takano, H. Akie and K. Kaneko*

The newest evaluated nuclear data file JENDL-3 version-2(JENDL-3.2) was compiled and released in June 1994, and benchmark calculations have been made for thermal and fast reactors[1]. In addition, the benchmark calculation has been made for fast reactors by using ENDF/B-VI, the latest version of ENDF nuclear data, and the results are compared with those with JENDL-3.2. The benchmark cores are a large LMFBR mock-up core ZPPR-9 by 3-dimensional calculation, and 1-dimensional benchmark cores of VERA, ZPR, ZEBRA, SNEAK, etc.

Effective multiplication factors(k_{eff}s) and reaction rate ratios calculated for ZPPR-9 with ENDF/B-VI and JENDL-3.2 data are compared in Table 1.15.1. The multiplication factor calculated with ENDF/B-VI is about 1% overestimated, while JENDL-3.2 gives good agreement with experiment. There is only small difference between these nuclear data files in ^{239}Pu fission/^{235}U fission(F9/F5) reaction rate ratio, and are 2~3% differences in reaction rate ratios of ^{238}U capture and fission to ^{239}Pu fission(C8/F9 and F8/F9). These results suggest that the differences between ENDF/B-VI and JENDL-3.2 are caused mainly from ^{238}U cross section. By comparing ^{238}U cross sections between both files, differences are found in inelastic scattering cross section in 2~6MeV energy region and in capture cross section in MeV region.

Table 1.15.1 Calculation/Experiment(C/E) values of effective multiplication factor and reaction rate ratios obtained for ZPPR-9 with ENDF/B-VI and JENDL-3.2

	ENDF/B-VI	JENDL-3.2
k_{eff}	1.011	0.9986
Reaction rate ratio		
F9/F5	0.991	0.997
C8/F9	1.027	1.046
F8/F9	0.985	0.955

F9 : ^{239}Pu fission rate, F5 : ^{235}U fission rate,
C8 : ^{238}U capture rate, F8 : ^{238}U fission rate

* The Japan Research Institute, Ltd., Tokyo

The effective multiplication factors calculated for 1-D benchmark cores are shown in Fig.1.15.1. Similarly to the case in ZPPR-9, ENDF/B-VI gives 1~2% larger k_{eff} than JENDL-3.2, which also overestimates experiment by 1% or more. In this figure are also compared the k_{eff}s calculated with the following nuclear data :

(1) B6+J32(U8in) : ENDF/B-VI but ^{238}U inelastic scattering cross section is replaced by that of JENDL-3.2,

(2) B6+J32(U8in/cap) : ENDF/B-VI but ^{238}U inelastic scattering and capture cross sections are replaced by those of JENDL-3.2,

(3) B6+J32(U8) : ENDF/B-VI but ^{238}U cross section is replaced by that of JENDL-3.2.

From this figure, it is observed that the difference of ^{238}U inelastic scattering cross section leads to the k_{eff} difference of about 1%, by comparing the results of "ENDF/B-VI" and "B6+J32(U8in)". The effect of ^{238}U capture cross section is smaller to be 0.1~0.4% ("B6+J32(U8in)" and "B6+J32(U8in/cap)"). When the ^{238}U cross section in ENDF/B-VI is replaced by JENDL-3.2, the calculated k_{eff} shows good agreement with that calculated by using JENDL-3.2("B6+J32(U8)" and "JENDL-3.2"). It can be concluded that the discrepancy between the k_{eff}s calculated with ENDF/B-VI and JENDL-3.2 is caused from the difference in ^{238}U cross section data, mainly of inelastic scattering for large cores.

In Fig.1.15.2 are compared the calculation/experiment(C/E) values of sodium void reactivities in ZPPR-9 calculated with JENDL-2, JENDL-3 and ENDF/B-VI. The result for ENDF/B-VI overestimates the experimental results and depends considerably on the voided region.

Reference

1) Takano H. : "Benchmark Test of JENDL-3.2 for Thermal and Fast Reactors", Proc. of the 1994 Symposium on Nuclear Data, November 1994, JAERI, Tokai, Japan, JAERI-Conf 95-008, Japan Atomic Energy Research Institute, pp.47-52 (1995).

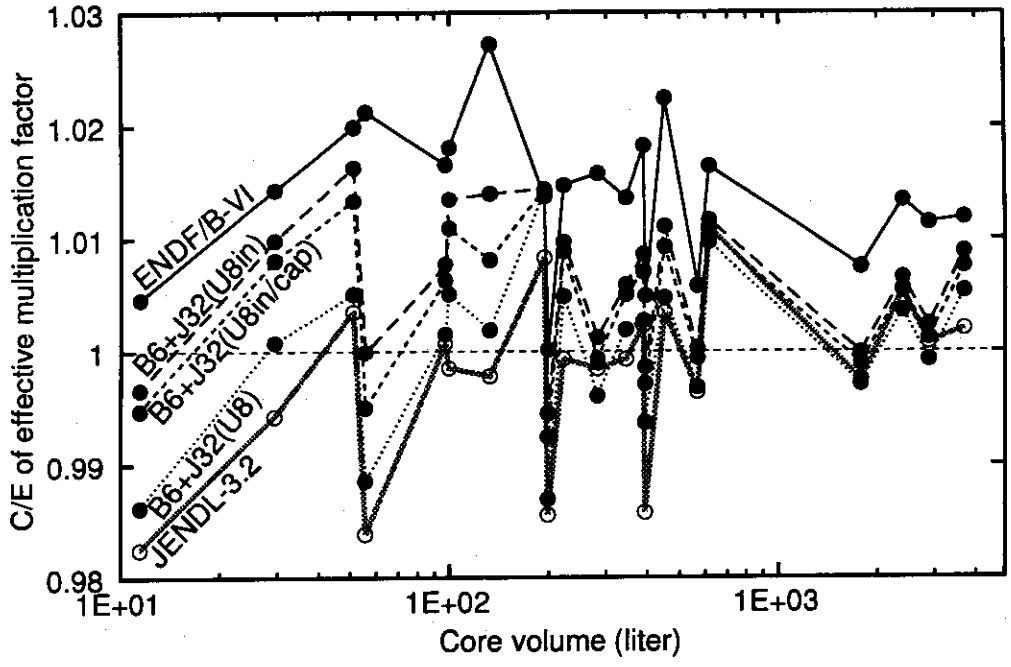

Fig.1.15.1 Calculation/Experiment(C/E) value of effective multiplication factors calculated with different nuclear data libraries for 1-D benchmark fast reactor cores (B6 : ENDF/B-VI, J32 : JENDL-3.2, U8 : U-238 cross section, in : inelastic scattering cross section, cap : capture cross section)

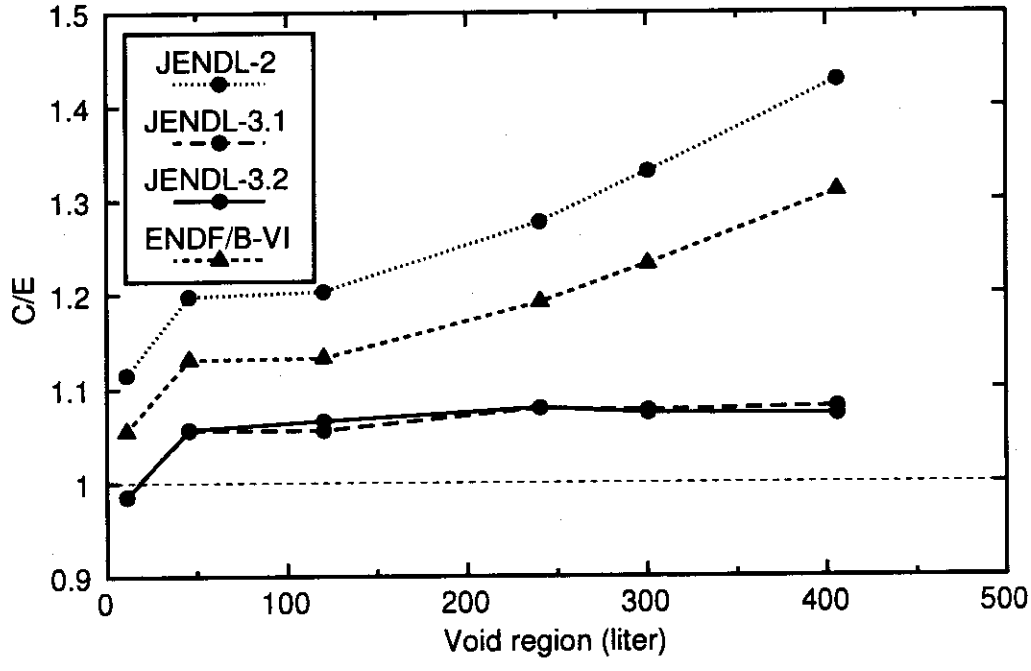

Fig.1.15.2 Sodium void reactivity at the ZPPR-9 core (C/E value)

1.16 Photon Angular Distributions from Radiative Electron Capture In Relativistic Atomic Collisions

J. Eichler*, Ichihara A. and Shirai T.

Radiative electron capture (REC) is one of the dominant processes occurring in collisions of highly or completely stripped relativistic heavy ions with light target atoms. In this reaction, the target electron can be regarded as quasifree, so that REC is essentially equivalent to radiative recombination (RR). Exact relativistic calculations for RR have been carried out in order to estimate differential REC cross sections as a function of the projectile energy and charge number Z.

It is known that the photon angular distribution for REC into the K shell (K–REC) exhibits a $\sin^2\theta$ distribution in the nonrelativistic dipole calculation, where θ is the angle between the beam direction and the photon momentum. Anholt *et al.* measured the K–REC differential cross section for the 197 MeV/u Xe^{54+} + Be collisions[1]. Their result was found to closely follow to the $\sin^2\theta$ distribution. Subsequently, for heavy–ion–atom collisions, it has become customary to assume a $\sin^2\theta$ distribution when total cross section is inferred from measurements at a single photon angle θ. In our relativistic calculation the angular distributions for Z=50 are practically pure $\sin^2\theta$ distributions at all energies considered, in agreement with the experimental result of Anholt *et al.*[1] However, the maximum of the angular distributions is shifted to the forward direction as the projectile charge increases.

Figure 1 shows RR photon angular distributions for capture into the K shell. Fig.1 is composed of 3x3 individual figures for projectile energies 20, 100, and 300 MeV/u ranging from the nonrelativistic to the relativistic regime, and for projectile charges Z=50, 70, and 90 covering the range of primary experimental interest. In this figure the contribution of the spin–flip and non–spin–flip transitions are displayed separately. In the nonrelativistic theory the photon emission at θ=0° and 180° is forbidden by the law of angular momentum conservation. It can be seen that the non–spin–flip cross sections vanish at forward and backward angles. With increasing charge as well as with increasing projectile energies, the relative contributions of spin–flip transitions gain weight and lead to a finite cross section

*Hahn–Meitner–Institut Berlin, Germany

at forward angles. This effect provides a unique signature of magnetic transitions.

The RR photon angular distributions for capture into the L and M shells have also been calculated.[2] For L and M–REC, the angular distribution is affected by the coupling of electron spin to the orbital angular momentum, which gives deviations from the $\sin^2\theta$ distribution. The maximum shifts to the forward direction as the projectile charge and velocity increase. Our result for the 89 MeV/u U^{90+} + C collisions is in good agreement with the experimental result of Stöhlker *et al.*[3]

For planning and evaluating REC experiments, it is useful to have a systematics of photon angular distributions as a function of the projectile energy and charge number. This is necessary in particular if one wants to deduce total cross sections from measurements at a single angle. The present calculation shows that the assumption of a $\sin^2\theta$ distribution is not valid in many cases.

References

1) Anholt R. *et al.*: Phys. Rev. Lett., 53, 234 (1984).

2) Eichler J. *et al.*: Phys. Rev., A51, 3027 (1995).

3) Stöhlker Th. *et al.*: Phys. Rev. Lett., 73, 3520 (1994).

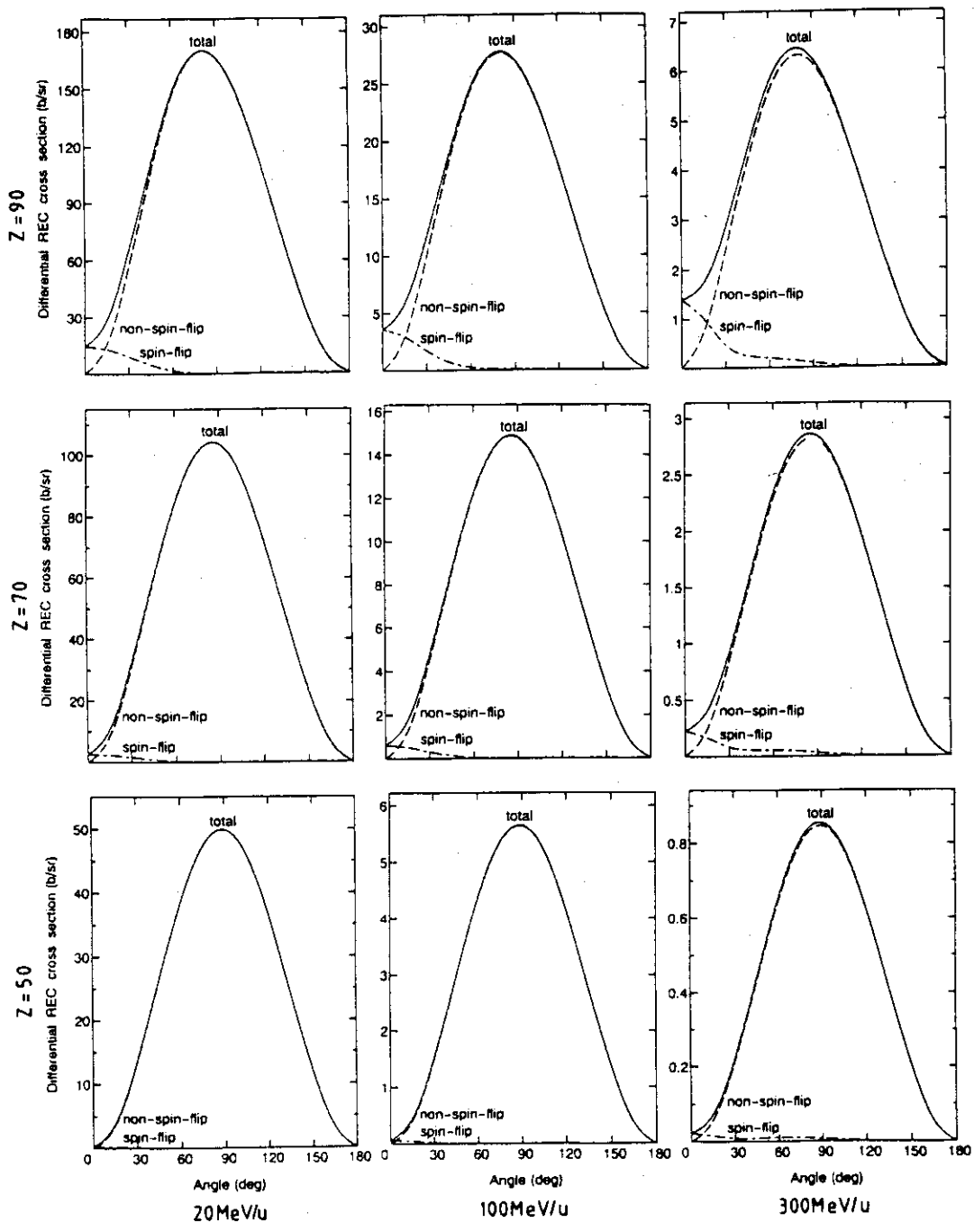

Fig.1.16.1 Angle-differential RR cross sections for capture into the K-shell of projectiles with charge numbers Z=50,70, and 90 and projectile energies of 20, 100, and 300 MeV/u. Spin-flip and non-spin-flip contributions are shown separately.

1.17 Ionization of Excited Hydrogen Atoms by Collisions with Bare Ions

Igarashi A. and Shirai T.

Multistep collision processes involving excited atomic states have been the subject of considerable recent interest in relation to the injection of energetic neutral beams into high-density fusion plasmas[1]. These collision processes have large cross sections and play a crucial role in the stopping of the neutral beam atoms. It is urgently required, therefore, to provide these cross sections for analyzing the performance of neutral beam heating.

Ionization of the ground hydrogen atoms by bare ion impacts at intermediate and high energies has been quite successfully treated by the CDW-EIS approximation proposed by Crothers and McCann in comparison with other predictions[2,3]. Recently, its application has been extended to the ionization of excited hydrogen atoms by Fainstain *et al.*[4] and Olivera *et al.*[5] However, their results show such an *unreasonable* behavior that the CDW-EIS approximation does not conform to the Born approximation even at high energies (Fig. 1 of Ref.5). Besides, discrepancy between the predictions in these two approximations is enhanced as the excited state involved becomes higher.

In order to reexamine their results, we have undertaken an extensive application of the CDW-EIS approximation. In this work, calculation has been carried out for the total cross section for ionization of the excited hydrogen atoms with the principal quantum number $n \leq 5$ by the impacts of bare ions from H^+ to O^{8+} in the range of 1 keV/amu - 10 MeV/amu. Here, total cross section denotes cross section summed over the n^2 degenerate atomic states to be ionized.

The present calculations are compared in Figs. 1.17.1 and 1.17.2 with other calculations presently available for the ionization of the ground and excited states of hydrogen atoms by the H^+ and He^{2+} ion impacts. For the ionization of the ground state, a critical evaluation was reported by Janev and Smith[6], whose recommended data are plotted with triangle mark. We would like to say here only that the CDW-EIS approximation might be more reliable than any other high-energy approximations.

For the ionization of H(n=2) and H(3) atoms, theoretical calculations based on the adiabatic super promotion (ASP) model[7,8], the classical trajectory Monte-Carlo (CTMC) method[9], and the CDW-EIS approximation[4,5] have been reported so far. These results are

plotted in Fig. 1.17.1. The present results disagree with those in Refs. 4 and 5, despite each calculation was made in the CDW-EIS approximation. It should be noted that their results do not tend at all to the Born cross sections at high energies. In addition, the difference between both predictions is enhanced, as the value of n increases.

The total cross section in the CTMC method falls off in proportion to $1/E$ at high energies, while the CDW-EIS approximation leads to a fall-off in proportion to $\ln(E)/E$ where E is the collision energy. The present CDW-EIS and the CTMC cross sections intersect at 100 keV/amu and 50 keV/amu for the ionization of the n=2 and n=3 levels, respectively. It may be concluded, therefore, that a combination of the ASP, CTMC, and CDW-EIS approximations produces a smoothly connected total cross section in a wide range of collision energy. A similar discussion holds true in the case of the He^{2+} ion impacts, too (see Fig. 1.17.2). However, more sophisticated model such as a coupled-channel method is desirable to assess the values of total cross section at the intermediate energies.

References

1) Boly C.D., *et al.*: Phys. Rev. Lett. **52**, 534 (1984); Janev R.K., *et al.*, Nucl. Fusion **29**, 2125 (1989).
2) Crothers D.S.F. and McCann J.F.: J. Phys. B **16**, 3229 (1983).
3) Rivarola R.D., *et al.*: Phys. Scr. **T28**, 101 (1989).
4) Fainstein P.D., *et al.*: J. Phys. B **23**, 1481 (1990).
5) Olivera G.H., *et al.*: in *Abstracts of contributed papers, XVII International Conference on the Physics of Electronic and Atomic Collisions*, Aarhus, 1993, edited by Andersen, T. *et al.* (Aarhus University, Aarhus, 1993), p. 449.
6) Janev J.K. and Smith J.J.: *Atomic and Plasma-Material Interaction Data for Fusion* (Suppl. to Nucl. Fusion) **4**, 68 (1993).
7) Janev R.K. and Krstic P.S.:Phys. Rev. A **46**, 5554 (1992).
8) Krstic P.S. and Janev R.K.: Phys. Rev. A **47**, 3894 (1993).
9) Olson R.E.: J. Phys. B **13**, 483 (1980).

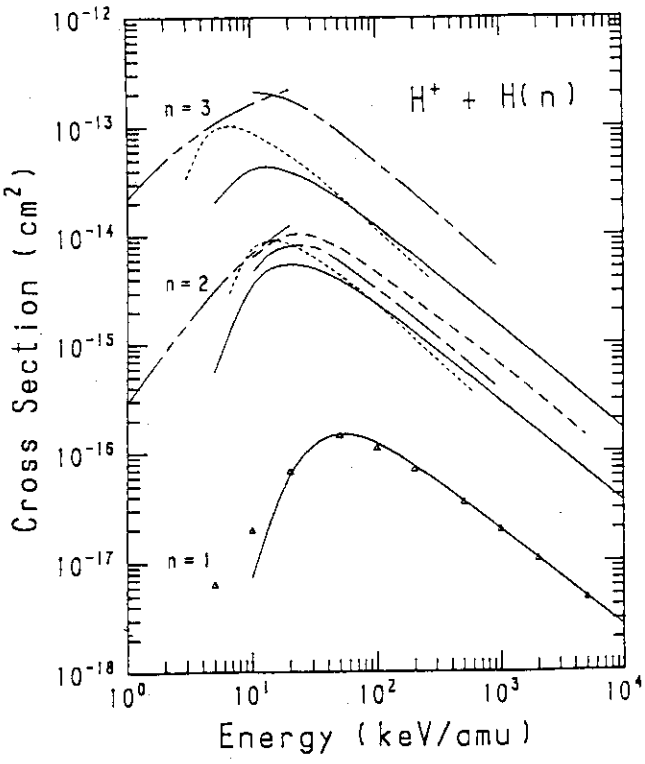

Fig. 1.17.1 Total cross section for ionization in the $H^+ + H(n \leq 3)$ collision system. Solid line: CDW-EIS in the present work; dotted line: CTMC of Olson[9]; dashed line: CDW-EIS of Fainstein *et al.*[4]; dot-dashed line: CDW-EIS of Olivera *et al.*[5]; dot-dot-dashed line: ASP of Janev and Krstic[7]; triangles: recommended data[6].

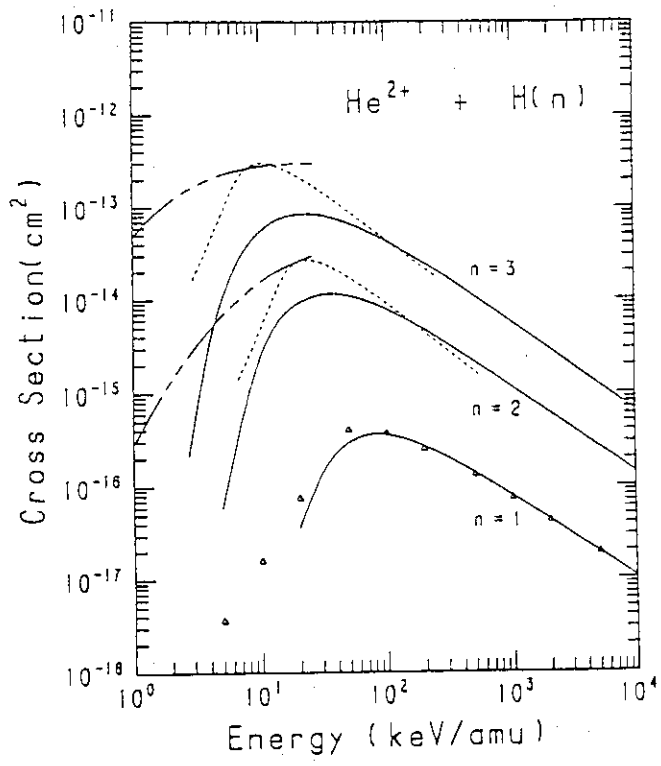

Fig. 1.17.2 Total cross section for ionization in the $He^{2+} + H(n \leq 3)$ collision system. Solid line: CDW-EIS in the present work; dotted line: CTMC of Olson[9]; dot-dot-dashed line: ASP of Krstic and Janev[8]; triangles: recommended data[6].

1.18 Analytic Cross Sections for Collisions of H, H_2, He and Li Atoms and Ions with Atoms and Molecules. III

R. ITO*, T. TABATA*, T. SHIRAI and R.A. PHANEUF**

For diagnostics and modeling of plasmas in thermonuclear-fusion research, data on cross sections for inelastic collisions between atoms, molecules and ions, especially of the lightest elements, are important. Barnett[1] published recommended data on such cross sections for the elements of hydrogen, helium and lithium. To facilitate interpolation, Barnett gave also least-squares Chebyshev polynomial fits to the recommended cross sections as a function of projectile energy. The polynomial fits, however, cannot be used for extrapolation, because they often show physically unreasonable behavior just outside the energy range of the data used. This inconvenience can be removed by using analytic expressions that approximate low-energy and high-energy asymptotic trends.

Green and McNeal[2] proposed semiempirical expressions for inelastic collision cross sections of hydrogen atoms and ions with gaseous atoms and molecules. By using the same functional forms as the Green-McNeal expressions and some modified forms, Nakai *et al.*[3] published a number of analytic cross sections for charge transfer of hydrogen atoms ions colliding with gaseous atoms and molecules. Analytic cross sections are also available for the following reactions: charge transfer of hydrogen atoms and ions colliding with metal vapors,[4] single-electron capture of hydrogen ions leading to specified excited states of hydrogen,[5] charge transfer of helium atoms and ions colliding with gaseous atoms and molecules,[6] single-electron capture by multiply-charged ions colliding with H, H_2, and He,[7] and ionization of H, H_2, and He by multiply-charged ions.[8]

Presently a project of formulating analytic expressions fitted to Barnett's recommended data is in progress. In previous report,[9,10] analytic expressions for the cross sections of the following reactions were given:

(1) Electron capture by H, H^+, H_2^+, He^+, and He^{2+} colliding with atoms, molecules, and ions (H, He, Li; H_2; H^-, He^+).

---

* University of Osaka Prefecture

** Oak Ridge National Laboratory

(2) Electron capture into excited states by H^+, He^+, and He^{2+}, colliding with atoms and molecules (H, He, Li; H_2).

(3) Excitation and spectral line emission by H^+, He^+, and He^{2+}, colliding with atoms and molecules (H, He, Li; H_2).

The present report is a sequel to the previous reports, and treats the following types of collisions: ionization collisions, charge-production collisions, electron-loss and electron-detachment collisions. The possible error of analytic expressions when they are used for the extrapolation of the recommended data was discussed in one of the previous report[9].

References

1) Barnett C.F., *Atomic Data for Fusion Volume 1:Collisions of H, H_2, He and Li Atoms and Ions with and Molecules,* ed. Hunter H.T., *et al.*, ORNL-6086/V1 (1990).

2) Green A.E.S. and McNeal R.J.: J. Geophys. Res. **76**, 133 (1971).

3) Nakai Y., *et al.*: At. Data & Nucl. Data Tables **37**, 69 (1987).

4) Tabata T., *et al.*: Nucl. Instrum. & Methods B**31**, 375 (1988).

5) Tabata T., *et al.*: *Partial Cross-Sections for Single-Electron Capture of Hydrogen Ions Colliding with Gaseous Atoms and Molecules*, Osaka Prefect. Radiat Res. Inst. Tech.Rep.**11** (1990).

6) Tabata T.,*et al.*: *Cross Sections for Charge Transfer of Helium Atoms and Ions Colliding with Gaseous Atoms and Molecules*, Radiat. Center Osaka Prefect. Tech. Rep. **7** (1987).

7) Nakai Y., *et al.*: Phys. Scr. T**28**, 77 (1989).

8) Tabata T., *et al.*: At. Plasma-Mater. Interact. Data for Fusion **2**, 91 (1992).

9) Ito R., *et al.*: *Analytic Cross Sections for Collisions of H, H_2, He and Li Atoms and Ions Colliding with Atoms and Molecules. I,* JAERI-M 93-117 (1993).

10) Ito R., *et al.*: *Analytic Cross Sections for Collisions of H, H_2, He and Li Atoms and Ions Colliding with Atoms and Molecules. II,* JAERI-Data/Code 94-005 (1994).

1.19 Spectral Data and Grotrian Diagrams for Highly Ionized Krypton, Kr V - Kr XXXVI

T. Shirai, K. Okazaki* and J. Sugar**

We have undertaken publication of a series of compilations of spectra of highly ionized atoms of particular interest to the fusion energy community. These selected elements occur as impurities in wall materials of fusion machines or are specifically injected into the hot plasmas for diagnostics. Much work on these spectra has appeared in recent years. We have critically compiled these data into single monographs for each element, including wavelengths, classifications, intensities, transition probabilities, and a short review of the literature for each ion. We cite the uncertainties of the data as given by the authors. These rarely include the confidence level, so we assume that they represent one standard deviation of the measurements. Monographs[1-9] are already published for Ti, V, Cr, Mn, Fe, Co, Ni, Cu, and Mo. The present compilation contains data for Kr V to Kr XXXVI.

All relevant papers on wavelengths and energy levels published through December 1993 were collected and surveyed, and the best measurements, in our judgement, were included in the tables. We consulted the following comprehensive compilations: for wavelengths, the tables by Kelly[10] , for forbidden lines arising within ground configurations of the type ns^2np^k (n=2 and 3, k=1 to 5), the paper by Kaufman and Sugar[11] and a review article by Fawcett.[12]

Sugar and Musgrove[13] have published a comprehensive critical compilation of energy levels for all stages of ionization. Their values are adopted for this compilation, except where superseded by more recent data. For the He- and H-sequences, only theoretical results are given since they are considered to be more accurate than the experimental values. The latter are cited in the brief review.

We caution that the intensity estimates in experimental work are usually visual estimates of relative plate blackening. There is generally no correlation between intensity

---

* Institute of Physical and Chemical Research, Wako
** National Institute of Standards and Technology, Gaithersburg

estimates by different authors, or by the same author for widely different wavelength ranges.

References

1) Mori K., *et al.*: Atom. Data and Nucl. Data Tables **34**, 79 (1986).
2) Shirai T., *et al.*: J. Phys. Chem. Ref. Data **21**, 273 (1992).
3) Shirai T., *et al.*: J. Phys. Chem. Ref. Data **22**, 1279 (1993).
4) Shirai T., *et al.*: J. Phys. Chem. Ref. Data **23**, 179 (1994).
5) Shirai T., *et al.*: J. Phys. Chem. Ref. Data **19**, 127 (1990).
6) Shirai T., *et al.*: J. Phys. Chem. Ref. Data **21**, 23 (1992).
7) Shirai T., *et al.*: Atom. Data and Nucl. Data Tables **37**, 235 (1987).
8) Shirai T., *et al.*: J. Phys. Chem. Ref. Data **20**, 1 (1991).
9) Shirai T., *et al.*: J. Phys. Chem. Ref. Data **16**, 327 (1987).
10) Kelly R.L.: J. Phys. Chem. Ref. Data **16**, Suppl. 1 (1987).
11) Kaufman V. and Sugar J.: J. Phys. Chem. Ref. Data **15**, 321 (1986).
12) Fawcett B.C.: J. Opt. Soc. Am. B **1**, 195 (1984).
13) Sugar J. and Musgrove A.: J. Phys. Chem. Ref. Data **20**, 859 (1985).

2. Theoretical Method and Code Development

A 3-D neutronics-thermohydraulics coupled kinetics code is under development. The code is a modular type and the Datapool system developed in JAERI is adopted for data transfer between modules. Neutronics and thermohydraulics calculation routines of the SPACE2 and FX2-TH codes are implemented. Users can arbitrary select calculation models for neutronics, thermohydraulics and kinetics calculations among the models available in both codes. The structure of code is very flexible, and the modification is easy.

An analysis of uncontrolled withdrawal of control rods was made for a PWR core at zero power by using the THYDE-NEU code. The transient is initiated by the withdrawal of control rod banks from the core bottom at the speed of 2.0 cm/s. The calculation results show that the power rapidly increases at around 110 sec and scrams at 111 sec. After the scram, the power exponentially decreases but the peak fuel temperature levels off about 3 sec.

A new method based on a statistical geometry model has been established to treat a great number of randomly distributed spherical fuels in continuous energy Monte Carlo calculations. A location of a spherical fuel is sampled probabilistically along a particle flight path from the spatial probability distribution of spherical fuels. The MCRDF and MCNP-CFP codes have been developed for the analysis of a practical reactor. Based on this method, the heterogeneity effect of VHTRC-1-4 core at JAERI was calculated.

Neural networks were applied in order to search a multi-dimensional design window in the reactor conceptual design stage. The network consists of input, hidden and output layers. The present method could reduce much computation time. This method was implemented in IRDS and tested for a thermohydraulics design of a high conversion LWR. With this function, designers can easily find the feasible region of design parameters on an engineering workstation.

The activities described in this chapter are contributed by Reactor System Laboratory.

2.1 Development of a Modular System for 3-D Neutronics-Thermohydraulics Coupled Kinetics

Y. Nagaya and K. Tsuchihashi

A 3-D neutronics-thermohydraulics coupled kinetics code is very complicated because the code must treat both neutronics and thermohydraulics each of which is categorized into very different field. Additionally, the reactor type and calculation models that can be used depend on the component module. Therefore, we are developing a kinetics code system in which the information exchange between neutronics and thermohydraulics is transparent and the optional module can be easily added.

In the previous year, we separated the SPACE2 code [1] into modules and reconstructed a system which was consisted of a neutronics module, a thermohydraulics module, a kinetics module and a data base to connect neutronics and thermohydraulics calculations. The neutronics module based on a steady state diffusion code CITATION[2] reads the fuel temperature (coolant density, control rod data, etc.) stored in the data base, performs a neutronics calculation and writes a power distribution and reactivity feedback coefficients into the data base. The thermohydraulics module based on a code EUREKA2[3] reads a power level and a power distribution from the data base, performs the thermohydraulics calculation and writes fuel temperature (coolant density, etc.) into the data base. The homogenized model based on the RELAP4[4] code is used for hydraulics calculation in this module. The kinetics module solves a point kinetics equation with reactivity feedback. This module reads reactivity feedback coefficients from the data base, makes calculations and write a power level into the data base. The Datapool system[5] developed in JAERI was used for the data storage between these modules. The Datapool system made the data transfer between different fields transparent and easy and enabled the options to be added easily.

The adiabatic approximation[6] is used to solve a time-dependent diffusion equation in SPACE2 and the reactivity in a point kinetics equation is given by the table look up method with the approximation that reactivity coefficients are constant in the core, so the applicable range is restricted. Thus, we separate the FX2-TH[7] code into modules and put these modules into the

system above. Although the thermohydraulics model in FX2-TH is used for fast breeder reactors and diffusion of neutrons is treated in the two-dimensional geometry, the equation for the shape function is solved with the improved quasi-static approximation[8] and includes the effect of precursors and the time-dependence of the shape function. Also, the time-dependence of the reactivity is taken into account, so the reactivity is rather realistic compared with the one calculated in SPACE2 . Therefore, a new system will perform the calculations more accurately than SPACE2.

We decomposed the two kinetics codes into modules and put these modules into the new system. Accordingly, we have two modules in each function and can use the modules selectively with the common data in the data base. Fig 2.1.1 shows a structure of the present modular system. In this new system we can analyze a fast breeder reactor with three-dimensional geometry and perform a transient calculation with the RELAP4 thermohydraulics model and the improved quasi-static approximation.

References

1) Inabe T. : Private communication (1993)
2) Fowler T. B., et al. : "Nuclear Reactor Core Analysis Code; CITATION", ORNL-TM-2496 (1969)
3) Ohnishi N., et al. : "EUREKA-2: A Computer Code for the Reactivity Accident Analysis in a Water Cooled Reactor", JAERI-M 84-074 (1984) (in Japanese)
4) Fisher S. R., et al. : "RELAP4/MOD6 - A Computer Program for Transient Thermal-Hydraulic Analysis of Nuclear Reactors and Related Systems - User's Manual", CDAP-TR-003, EG&G IDAHO Inc. (1978)
5) Tomiyama M., et al. : "Datapool; Its Concept and Facilities", JAERI-M 8715 (1980) (in Japanese)
6) Henry A. F., et al. : Nucl. Sci. and Eng., **4**, 727 (1958)
7) Shober R. A., et al. : "FX2-TH: A Two- Dimensional Nuclear Reactor Code with Thermal-Hydraulic Feedback", ANL-78-97 (1978)
8) Ott K. O., et al. : Nucl. Sci. and Eng., **36**, 402 (1969)

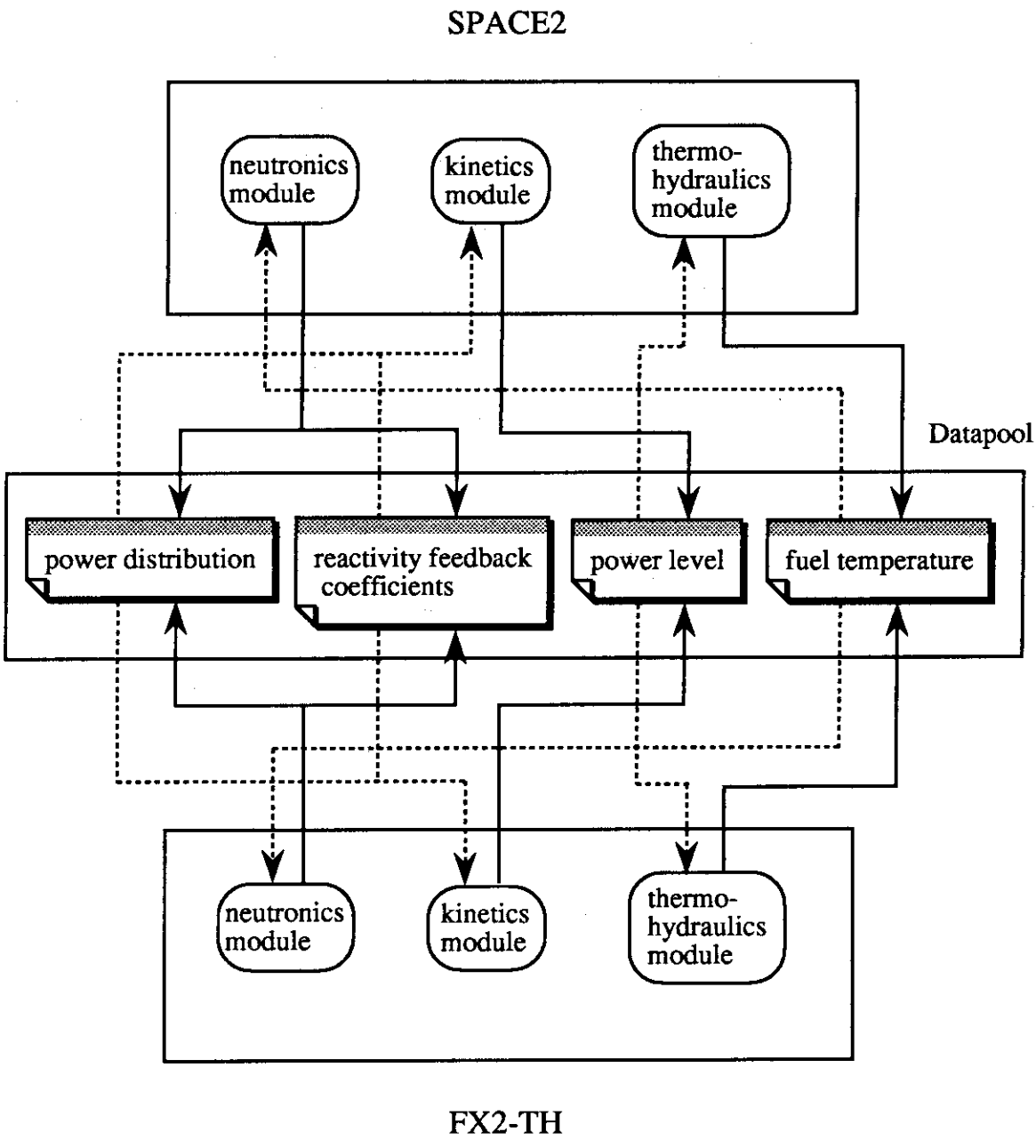

Fig. 2. 1. 1 Structure of the new kinetics code system

2.2 Three-Dimensional Analysis of Uncontrolled Withdrawal of Control Rods from a PWR Core at Zero Power

Y. Asahi

A calculation with the THYDE-NEU code, which is an upgraded version of THYDE-W[1], was performed for uncontrolled withdrawal of control rods at zero power. It is one of the accident situations postulated in licensing calculations for PWRs.

Suppose that (a) all control rods banks are fully inserted in the core, (b) the reactor is initially at hot zero power, that is, 10^{-13} times nominal power (0.2775 mW), (c) the core is initially at criticality and (d) the core is at the beginning of cycle 1 so that there is no xenon or iodine and no fuel depletion. The transient is generated by the withdrawal of control rod banks from the core bottom at 1.9928 cm/sec (72 steps/minutes). Scram rods begin to fall 0.6 seconds after fission power reaches 35 % of nominal with a constant speed of 2.2 seconds for complete insertion (228 steps).

The constant G-source boundary condition is applied for the inlet and outlet of the core. The conductance in the fuel gap is assumed to be $h_{gap} = 10^4$ W/m^2/^{O}K. The group constants and their derivatives used in the calculation are the same as those described in Ref. 2. An effective neutron multiplication of one is achieved from a search calculation of the critical boron concentration, which was found to be 850 ppm. Relief valves are placed at the core top, which are assumed to open and close at 16.5 MPa and 15.5 MPa, respectively. It is the IDI (implicit direct integration) method[3] that is used in THYDE-NEU to solve the transient multi-group diffusion equation with delayed neutron behavior. It ensures conservation of number of neutrons.

The calculated temporal behavior of the reactor power and the peak fuel temperature is shown in Figs. 2.2.1 and 2.2.2, respectively. The reactor power gradually increases as the controls rods are withdrawn. At around 110 sec, a rapid increace of the reactor power (prompt criticality) occurs, resulting in scram at 111 sec. The behavior of the power after scram is described asymptotically by $\exp(-\lambda t)$, where λ is the smallest (0.0128 sec^{-1}) of the decay constants of the delayed neutron precursors. The peak fuel temperature remains almost consstant (300 ^{O}C) until around 110 sec when the reactor power rapidly increases. After

1) Asahi, Y. et. al., : "THYDE-W : RCS(Reactor Coolant System) Analysis Code", JAERI-M90-172 (1990)

2) Finnemann, H. and Galati, A., : "NEACRP 3-D LWR Core Transient Benchmark (Final Specification)", NEACRP-L-335 (Revision 1), OECD Nuclear Energy Agency (1992)

3) Asahi,Y., : "Direct Numerical Integration of Transient 3-D Neutron Diffusion Equation", Section 2.8, Reactor Engineering Dept. Annual Report, JAERI-M 92-125 (1992)

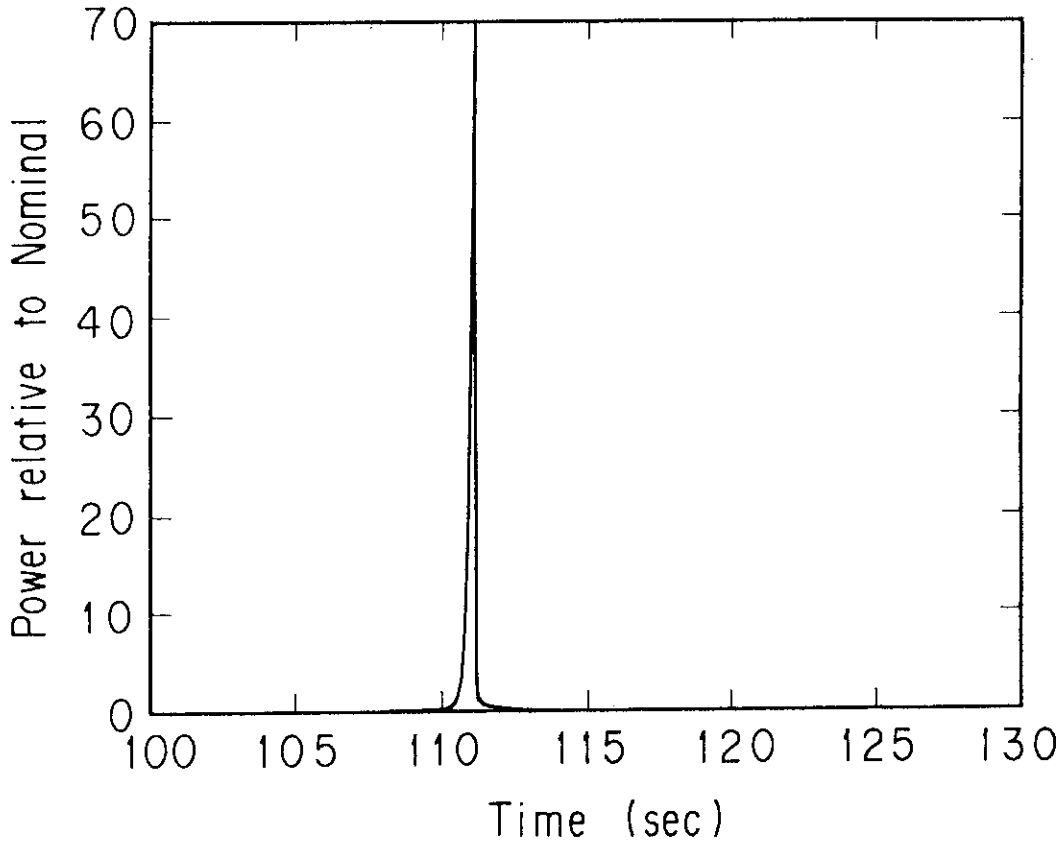

Fig. 2.2.1 Reactor power

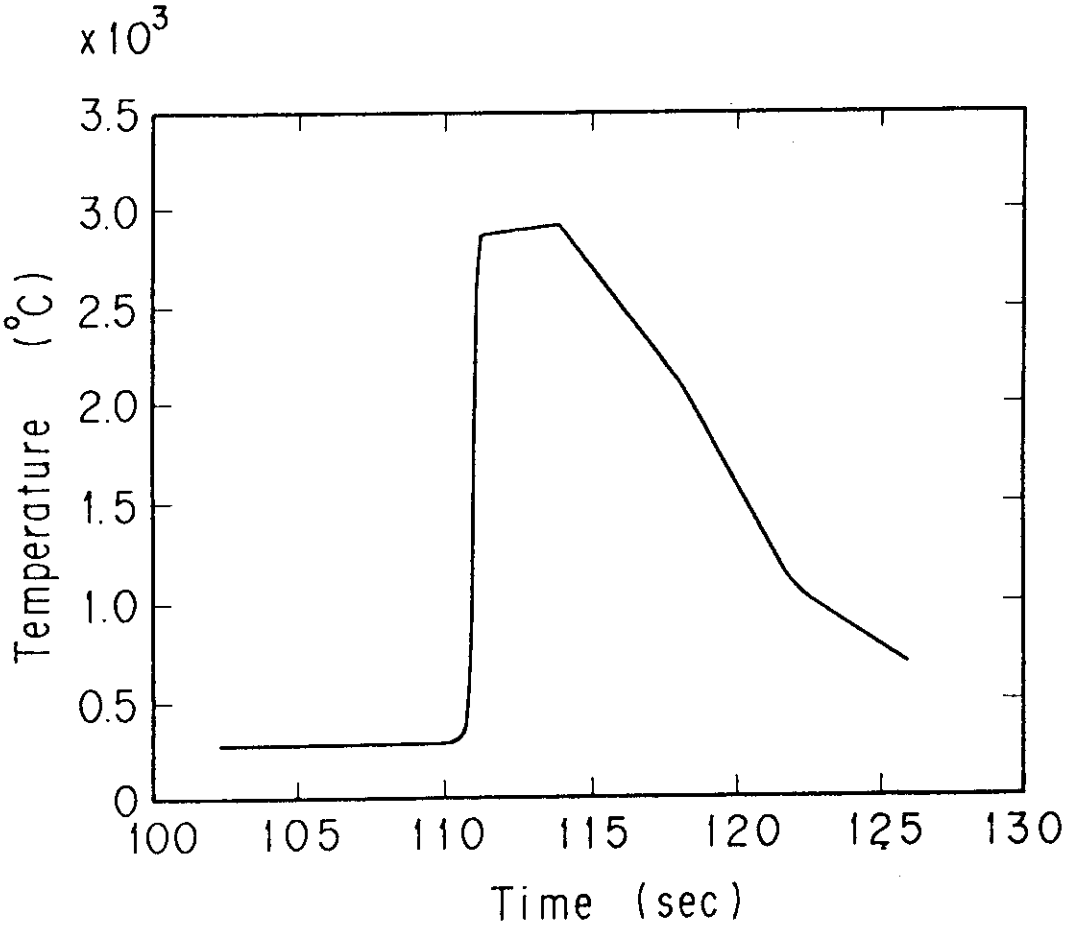

Fig. 2. 2. 2 Peak fuel temperature

2.3 Continuous Energy Monte Carlo Calculations of Randomly Distributed Spherical Fuels in HTTR Based on Statistical Geometry Model

I. Murata*, T. Mori and M. Nakagawa

A new method based on a statistical geometry model[1] has been established to treat a great number of randomly distributed spherical fuels in continuous energy Monte Carlo calculations. In the present method, location of a spherical fuel is sampled probabilistically along a particle flight path from the spatial probability distribution of spherical fuels which is called a nearest neighbor distribution, NND. By using the present statistical geometry model, the heterogeneity effect can be taken into account without any loss of the advantage of the continuous energy method.

In order to evaluate the NNDs for the statistical geometry model, a Monte Carlo hard sphere packing simulation code MCRDF has been newly developed by using the random vector synthesis method to reduce overlaps of spheres. The obtained NNDs were validated by comparison with a cross section photograph of real fuel compacts used in HTTR of JAERI[2] and an X-ray diffraction experimental result of Ni-P alloys[3], as shown in Fig.2.3.1.

The present method has been implemented in a continuous energy Monte Carlo code MCNP[4] to develop a modified version MCNP-CFP. The accuracy of the NNDs and the validity of algorithm to sample spherical fuels were confirmed through an inventory check of spherical fuels in a fuel compact and criticality calculations with ordered packed geometry. Table 2.3.1 summarizes the results of the inventory check carried out by using both the track length estimator and the direct evaluation method for several types of compact geometry. The results of criticality calculations with ordered packed geometry (BCC and FCC) are tabulated in Table 2.3.2

Moreover, the critical experiment by VHTRC at JAERI (VHTRC-1-4 core)[5] was analyzed by the MCNP-CFP code to study the applicability to practical reactor calculations. The reactivity effect of double heterogeneity by CFPs (coated fuel particles) and a fuel compact was evaluated from the difference to the calculated value with a CFP smeared model, and the result is shown in Table 2.3.3, together with the results by the conventional multi-group method. As a result, it was confirmed that the present method was applicable to the practical reactor analysis. Considering speed-up of computations due to vectorization or parallelization in the future, it is expected to be widely used in the nuclear and shielding design especially in HTGR cores.

---

* Department of HTTR Project, Oarai Research Establishment, JAERI

Present address: Department of Nuclear Engineering, Osaka University

References

1) Murata I., Mori T. and Nagagawa M.:"Continuous Energy Monte Carlo Calculations of Randomly Distributed Spherical Fuels in HTGRs Based on Statistical Geometry Model", to be submitted in Nucl.Sci. Eng. (1995).
2) Fukuda K.:Private communication. See also JAERI-M 86-092(1986).
3) Cargill G.S.III:J. Appl. Phys., 41, 2248 (1970).
4) Briesmeister J.:"MCNP-3B Newsletter", Los Alamos National Laboratory, July (1988).
5) Akino F. et al.:Proc. Int. Conf. on Physics of Reactors: Operation, Design and Computation, 593, Marseille (1990).
6) Tsuchihashi K., Ishiguro Y. and Kaneko K.:J. Nucl. Sci. Technol., 22(1), 16 (1985).
7) Akino F.:Private Communication (1994).

Table 2.3.1 Results of CFP(coated fuel particle) inventory check calculations

Surface type	Packing fraction		Relative difference (%)	Geometry (the radius of CFP=5 cm)
	Exact value[a]	Calculation		
Plane	0.2187	0.2185±0.0003[b]	-0.09	100×100×100(cm)
		0.2185±0.0003[c]	-0.09	
Sphere	0.2187	0.2186±0.0004[b]	-0.05	r=50 cm
Cylinder	0.2187	0.2185±0.0004[b]	-0.09	r=50 cm by 100cm-long
Cone	0.1215	0.1216±0.0004[b]	+0.08	r=32 cm by 50cm-long

a:The value is equal to 0.3×f, where f is a correction factor for the wall interference effect.
b:The NND was calculated for the packing after decreasing the radius of CFPs packed in random close packing state.
c:The NND was calculated for the packing of CFPs packed in 30%.

Table 2.3.2 Effective multiplication factors for ordered packing lattices

Lattice[a]	Unit cell size (cm)	Matrix material	Effective multiplication factor		Difference (Δk)
			Original code	MCNP-CFP	
Bodycenter cubic (BCC)	6	Graphite	1.146±0.002	1.148±0.002	+0.002
		-	1.105±0.001	1.107±0.002	+0.002
Face center cubic (FCC)	8.48	Graphite	1.140±0.002	1.141±0.002	+0.001
		-	1.102±0.002	1.105±0.003	+0.003

a:Calculation conditions are as follows:
1) The packing fraction is adjusted to 0.3 by reducing the radii of spherical fuels packed in a BCC or FCC lattice.
2)The fuel contains 10% enriched UO_2.

Table 2.3.3 Double heterogeneity effect of CFPs in a fuel compact

Case	Double heterogeneity effect (%Δk/k)	Condition
Present work	1.0	Calculated by MCNP-CFP
Infinite cell calculation[6]	0.84 ~1.08	Predicted by 4 approximation methods
Core calculation[7]	0.90	Calculated by SRAC

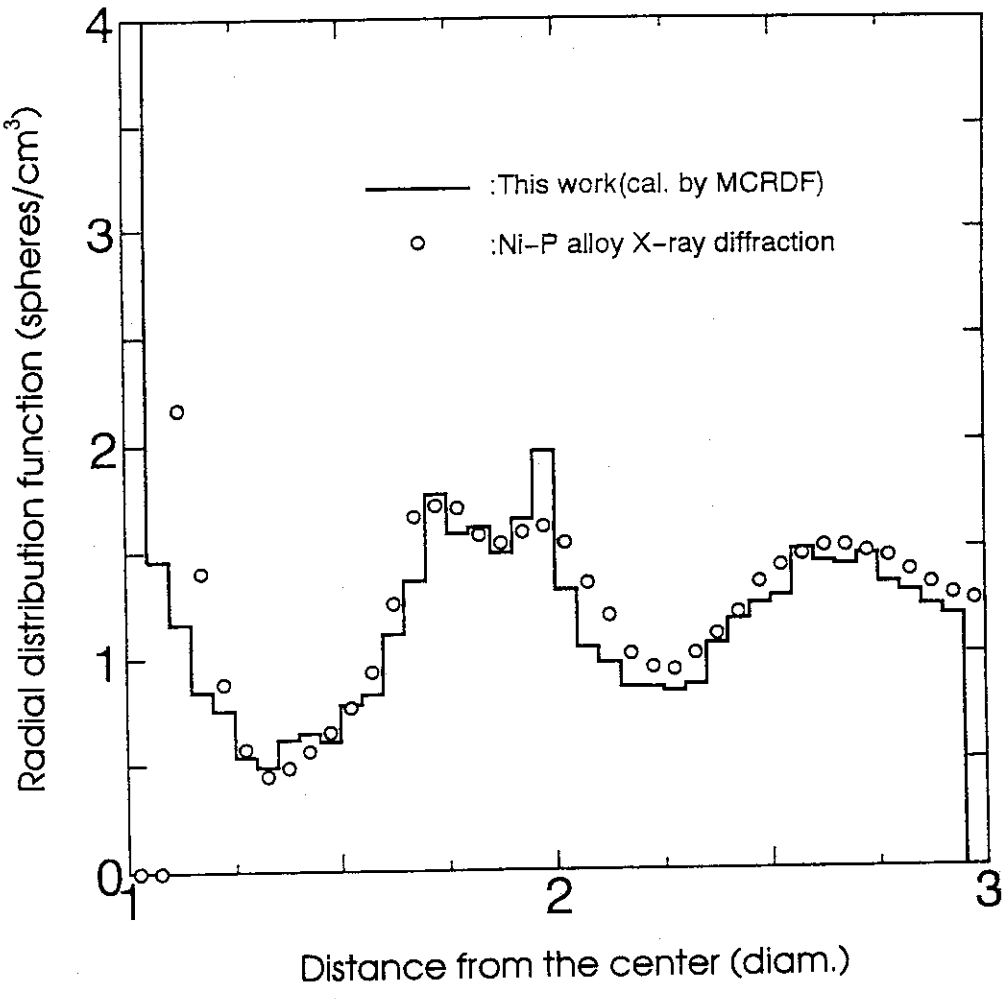

Fig.2.3.1 Comparison of evaluated radial distribution function with the experiment

2.4 Multi-Dimensional Design Window Search Using Neural Networks

T. Kugo, M. Nakagawa and S. Fujii*

The main purpose of the conceptual design is to search a design window which is a feasible range of basic design parameters and then to decide an optimal set of them. It is useful to draw a design window and distributions of core characteristics inside it. For this purpose, many parametric survey calculations should be carried out in the conventional way. And a considerable amount of computation cost must be needed. In our previous study[1], we investigated the boundary search procedure to search automatically a window in two-dimensional space, that is, for two design parameters. This procedure does not need so much time as calculating all possible combinations of parameters. But this procedure can not be applied to more than three-dimensional design window search, because execution time increases exponentially with increment of dimensions. At the present work, we applied neural networks(NNW) to multi-dimensional design window search in order to reduce computation time. We intend to use NNW for checking whether a searching point is feasible or not, and for calculating core characteristics if a searching point is feasible. This search method and the application to thermal hydraulic design are described below.

Our NNW adopts a three-layered feedforward structure as shown in Fig.2.4.1. Design parameters and core characteristics are set to neurons of an input and output layer, respectively. Here, design parameters are pin diameter, pin pitch, hot channel factor, averaged linear heat rate and core height. As for core characteristics, we consider DNBR, maximum fuel temperature, maximum cladding temperature, coolant outlet temperature and so on. As an activation function of neurons, the sigmoid function is employed. The design window search procedure using NNW is shown in Fig.2.4.2. At first, teaching data sets are prepared by the execution of analysis codes at coarse grid points. Then, the NNW is trained by the error back propagation with momentum term using the teaching data. The trained NNW is used for smoothing a design window and distributions of core characteristics by interpolating them into fine grid points. This method has been implemented in Intelligent Reactor Design System(IRDS)[2]. Display of a three-dimensional

*Kawasaki Heavy Industries, Tokyo

design window and a contour map of an interesting core characteristics are available on an engineering workstation.

As an example to demonstrate performances of the present method, we obtained a three-dimensional design window for pin diameter, pin pitch and hot channel factor of a high conversion LWR. The other design parameters are fixed as follows;

linear heat rate = 16 kW/m, core height = 2m.

As a spacer, a spiral rib was assumed. The thermal hydraulic calculations to prepare teaching data sets were performed by the GAPCON-THERMAL2-HC code[3]. The design limit in this case was considered by the criteria; 1.3 for DNBR, the melting point for fuel temperature, the saturated temperature for coolant and so on. The obtained design window is shown in Fig.2.4.3. Since the number of the execution of analysis code is considerably reduced by the present method compared with the boundary search procedure, the computation time consumed in the present method becomes reasonable. Thus, designers can easily and quickly find the feasible region in multi-dimensional space with the help of the present method. And the present method provides valuable information to decide design parameter values.

References

1) Nakagawa M. et al. :"Design Window Search Based on A.I. Technique," J. Nucl. Sci. Technol.,29,p1116,(1992).

2) Kugo T. et al. :"Development of Intelligent Reactor Design System IRDS," M&C+SNA'93, Vol.2,p199-209 (1993).

3) Mori T., Nakagawa M. and Fujii S.:"Parametric Study on Thermal-Hydraulic Characteristics of High Conversion Light Water Reactor," JAERI-M 88-224(1988) (in Japanese).

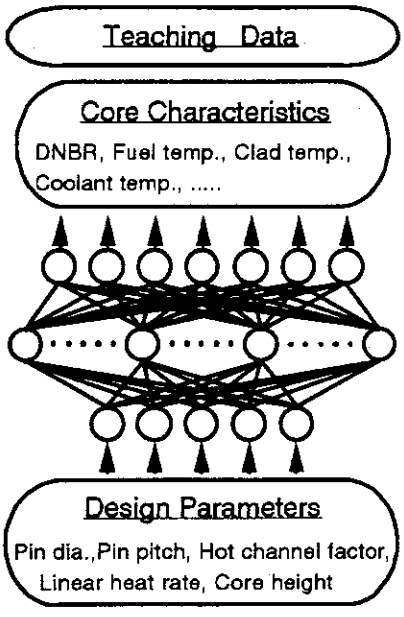

Fig.2.4.1 Structure of neural network

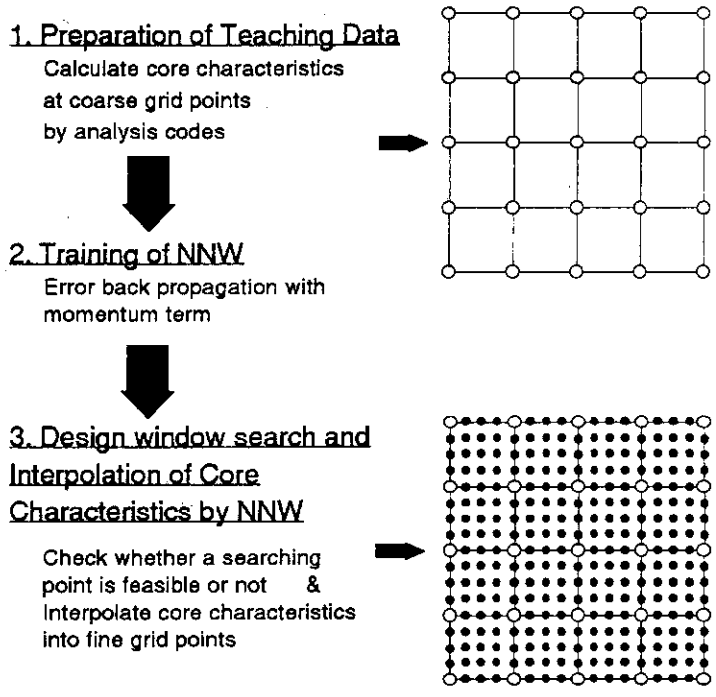

Fig.2.4.2 Design window search procedure using neural network

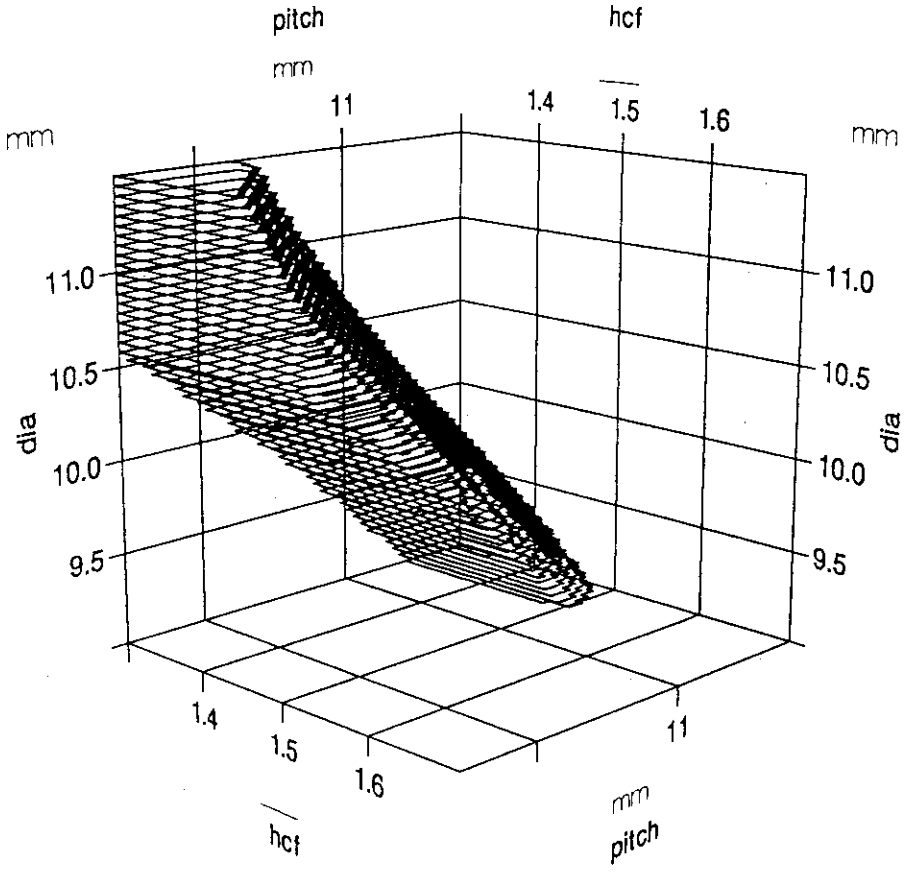

Fig.2.4.3 An example of three-dimensional design window obtained by the present method

3. Reactor Physics Experiment and Analysis

The Pu-240 effect on the sodium void worth was measured on the MOX fueled mockup core at the Fast Critical Facility (FCA). The positive sodium void worth increased when the Pu-240 content in the central region of the assembly was increased. The calculation based on JENDL-3 predicted well the experimental values.

The previously measured ^{238}U Doppler effect on the various FCA assemblies were analyzed using JENDL-3. 1 and JENDL-3.2 data. In the analysis, the ultra-fine group collision probability code PEACO-X was used. For MOX fuel mockup cores, the JENDL-3.2 calculation agrees well with experiments. For Pu/U-235 cores, however, the calc./expt. values deviate between 0.8 and 1.2. The further investigation is needed for the analysis of Doppler effect in Pu/U-235 cores at FCA.

The shielding effect in the reaction rate measurements were evaluated by the PEACO-X code. For the capture rates of ^{238}U foil placed between depleted oxide U plates and placed between stainless steel plates, the PEACO-X calculation agrees well with the experiments.

The foil activation technique developed at FCA for ^{238}U fission rate and 238U capture rate measurement was validated by the experiments at the well thermalized neutron field. The agreement between the measured reaction rates and the reference reaction rates which were calculated using well-established data agreed within experimental errors.

FCA team, together with French, USA and Russia teams, participated in the international, β eff benchmark experiments at the French fast critical facility MASURCA which was organized by the OECD/NEA/Nuclear Science Committee. The measurements were conducted on the 30% enriched U core and the 25% fertile Pu core.

The integral data measured on the FCA mockup cores of the JOYO Mark-II core were

analyzed by the continuous energy Monte Carlo code MVP and JENDL-3. 1 and -3.2 data.

An advanced fast reactor concept was investigated to enhance safety margins of a metal fuel fast reactor by adding small amount of moderator material as core material. To evaluate the data & method of nuclear calculation for this concept, a series of mockup experiments on FCA were planned.

As a part of the examination of the neutronics calculation of HTTR (High Temperature Test Reactor, under construction), the criticality and the axial neutron flux distribution were measured on the mockup core with a control rod partially inserted at the Very High Temperature Reactor Critical Facility (VHTRC). The accuracy of the criticality calculation was much better than the required one. As for the calculation of the strongly distorted neutron flux by the partially inserted control rod, the further improvement is needed.

3.1 Mock-up Experiment for Moderator Added Fast Reactor (I)
--- Mock-up Core Characteristics ---

T. Osugi, K. Tsujimoto[1] and S. Okajima

New reactor concepts have been investigated to enhance safety margins for a metal or nitride fast reactor by adding small amount of moderator material into the core.[1),2)] With softened neutron spectrum of these cores, Na void effect can be reduced and Doppler effect be increased.

A series of mock-up experiments for moderator added metal fueled fast reactor was planned at FCA (Fast Critical Assembly) to obtain the experimental data on reactivity effects and spectrum indexes. Mock-up cores (FCA XVIII cores) consist of a test region, a buffer region and a driver region; a test region simulates a moderator added core, a driver region maintain criticality of the mock-up core, and a buffer region alleviates neutron spectrum disturbance from driver region to test region.

Figure 3.1.1 shows a plate configuration in the test region cell. Moderator material (ZrH) is simulated by polystyrene (CH) plate and zirconium (Zr) plate mounted at central part of the cell. Atomic number density ratios of hydrogen to heavy nuclide (H/HM) of the cell are set to be 0.02, 0.05, and 0.13 using three kind of CH plates with different densities (CH95V, CH80V, and CH45V). The plate configuration in buffer region cell is similar to that in the test region cell except with fixed polystyrene density; CH80V. Driver region cells are same as those of FCA XVII cores.

Cell averaged neutron spectrum and adjoint neutron flux of the mock-up cores are shown in Figs. 3.1.2 and 3.1.3, respectively. Softened neutron spectrum with increase of H/HM value increases Doppler effect, and flatter adjoint neutron spectrum decreases Na void effect (see Fig.3.1.4). Here, Doppler effects are represented by central reactivity worths of Doppler sample, and Na void effects by central Na void effects of FCA XVIII cores.

From these figures, it was concluded that moderator added metal fast reactor can be well simulated by FCA XVIII mock-up cores, and that FCA XVIII cores can be regarded as benchmark core from the view point of their systematic variation of neutron spectrum.

---

[1]Tohoku University

References

1) H. Takano et al. : "A CONCEPT OF ADVANCED FAST BREEDER REACTOR WITH INSTANTANEOUS NEGATIVE TEMPERATURE COEFFICIENT," in Proc. of International Conference on Fast Reactor and Related Fuel Cycles, October 28 - November 1, 1991, Kyoto, Japan, p.16.1 (1991).

2) K. Tsujimoto et al. : " IMPROVEMENT OF REACTIVITY COEFFICIENT OF METALLIC FUEL LMFBR," in Proc. of International Conference on Reactor Physics and Reactor Computations, Tel-Aviv, Israel, January 23 - 26, 1994, p. 397 (1994)

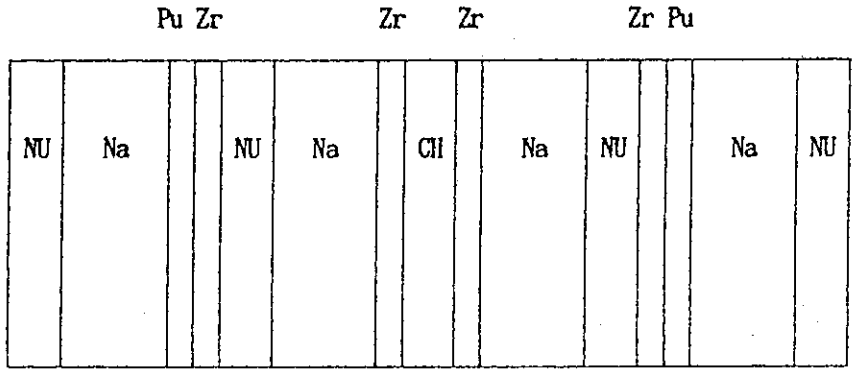

Fig.3.1.1 Plate configuration in the test region cell of the FCA XVIII core

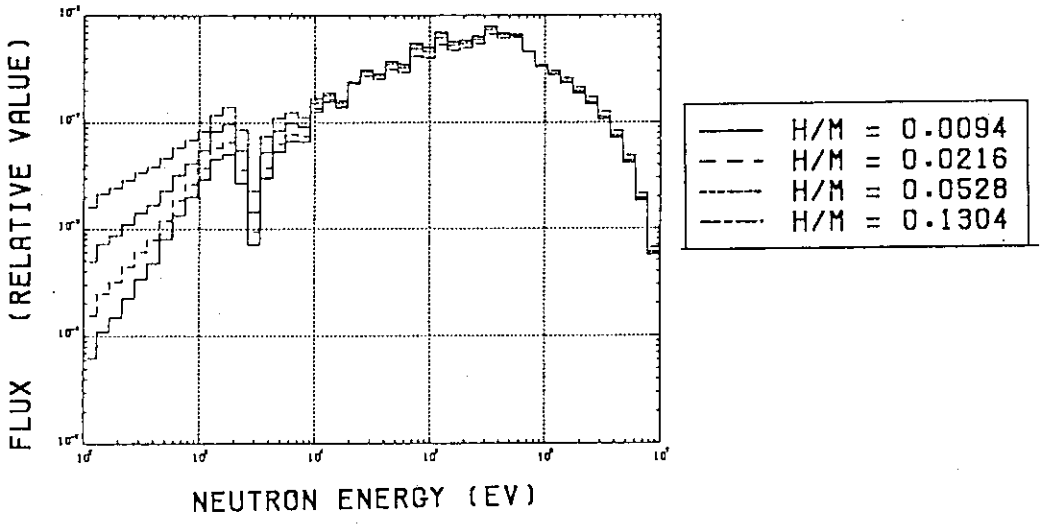

Fig.3.1.2 Cell averaged neutron spectrum of the FCA XVIII core

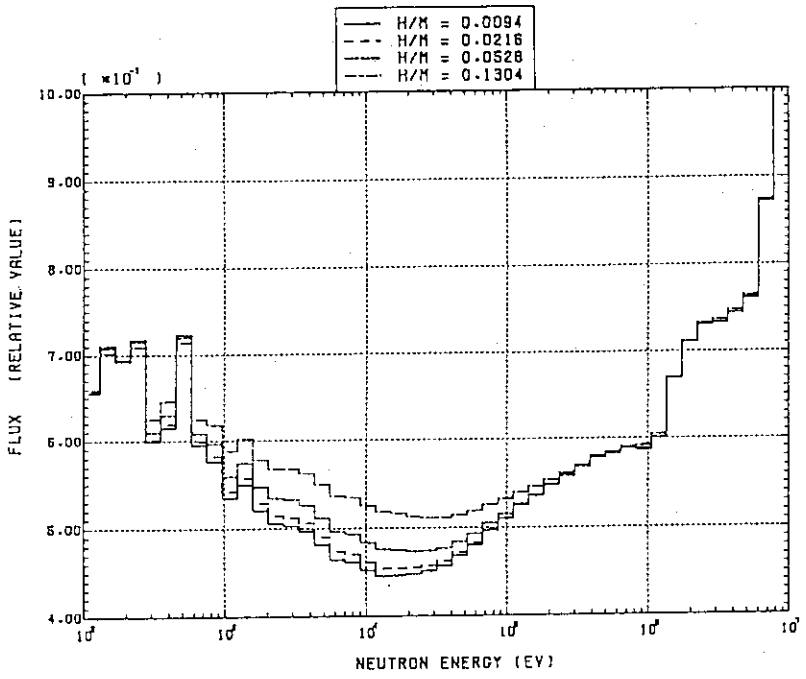

Fig.3.1.3 Cell averaged adjoint neutron flux of the FCA XVIII core

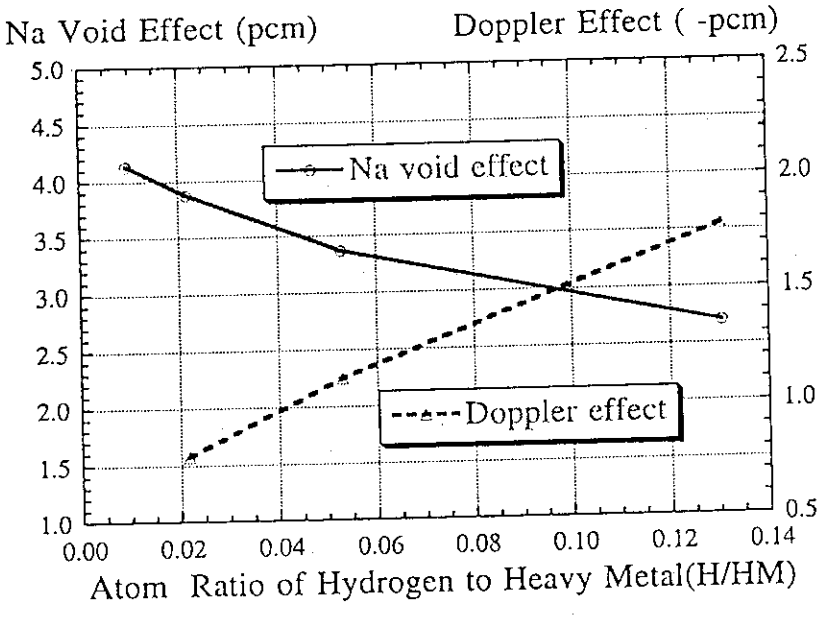

Fig.3.1.4 Calculated Na void effect and Doppler effect in FCA XVIII core

3.2 OECD/NEA/NSC β eff Benchmark Experiment at MASURCA/Cadarache

T. Sakurai and T. Nemoto

JAERI participated in the international benchmark experiment of effective delayed neutron fraction rate(β eff)[1] hosted by CEA(France) at MASURCA fast critical facility of Cadarache with ENEA(Italy), AEA-technology(U.K.), IPPE(Russian) and LANL(U.S.A.). Measurements for β eff at two assemblies of R2(30%enriched uranium core) and Zona2(25% enriched plutonium core)[1] have been accomplished. Techniques of β eff determination by each participant is summarized in Table 1. JAERI-team performed fission rate measurements

Table 1 Techniques of β eff determination

Participant	Technique	Measured items
MASURCA (CEA and ENEA)	Reactor noise analysis [1] Cf source [1]	Power spectral density of neutron fluctuations Fission rate* Pseudo-reactivity worth of ^{252}Cf source
JAERI	Cf source [2]	Fission rate*, Pseudo-reactivity worth of ^{252}Cf source
IPPE	Rossi- α	Fission rate*, Rossi- α **
LANL	Nelson number [3]	Rossi- α **

* Absolute fission rate of ^{235}U(R2) or ^{239}Pu(Zona2) and ratios of ^{238}U fission to ^{235}U fission(R2) or ^{238}U fission to ^{239}Pu fission(Zona2) at the core center

** Rossi- α measurements were made only at assembly R2.

with absolute fission chambers of ^{235}U, ^{238}U and ^{239}Pu calibrated with uncertainty less than 1% and measurements of pseudo-reactivity worth of ^{252}Cf source neutrons with a ^{252}Cf source calibrated with uncertainty less than 1% to determine β eff by means of Cf source technique.

JAERI-team, MASURCA-team and IPPE-team have already reported their results of β eff which were compared to check their accuracy. Fission rate is the most important parameter for the experimental determination of β eff by the three teams. Absolute fission rate at the core center based on JAERI's fission chamber measurements were compared to those based

on fission chamber measurements by MASURCA-team and IPPE-team as shown in table 2, where the uncertainties of ~1%, 1.5~2% and ~1.8% at 1 σ are assigned to the results of JAERI-team, IPPE-team and MASURCA-team respectively. The agreements are

Table 2 Comparison of absolute fission rates at the core center

Assembly	Fission rate	Relative difference from JAERI result		
		JAERI	IPPE	MASURCA
R2	^{235}U	0.0% (reference)	-2.2%	-1.6%
Zona2	^{239}Pu	0.0% (reference)	-0.2%	-1.4%

of the order of the uncertainties of the results by each team. The target accuracy of 1.5% [4] for the absolute fission rates at the core center has been achieved by taking the average of the three team's results.

Values of β eff by JAERI-team were compared to those by MASURCA-team and IPPE-team as shown in table 3, where the uncertainty of the each result is 2~3% at 1 σ.

Table 3 Comparison of β eff*

Assembly	Relative difference from JAERI result			
	JAERI Cf technique**	MASURCA Cf technique***	MASURCA Reactor noise analysis	IPPE Rossi- α
R2	0.0% (reference)	1.5%	-1.3%	4.3%
Zona2	0.0% (reference)	-0.3%	-4.8%	------

* β eff value deduced by using calculated fission integral supplied by CEA

** Results by using JAERI ^{252}Cf source

*** Results by using MASURCA ^{252}Cf source

Good agreement within 1.5 % was achieved for the β eff values by ^{252}Cf source technique between JAERI source and MASURCA source both at assemblies R2 and Zona2. On the other hand, a discrepancy of more than 4% was found on β eff value between ^{252}Cf source technique with JAERI source and Rossi-α technique at assembly R2. A discrepancy of more than 4% was also found on β eff value between ^{252}Cf source technique and reactor noise analysis technique at assembly Zona2.

In conclusion, accuracy of the absolute fission rates of ^{235}U and ^{239}Pu ($\sim$1% at 1 σ) based on JAERI fission chambers have been confirmed through good agreements as shown in table 2. On the other hand, discrepancies on β eff value of more than experimental error have been observed between Cf source technique with JAERI source and Rossi-α technique or reactor noise analysis technique.

References

1) Martini M. et al., NEACRP-A-1064 (1990)
2) Fisher E. A., Nucl. Sci. Eng. 62 , 105 (1977)
3) Spriggs G. D., Nucl. Sci. Eng. 113 , 161 (1993)
4) Martini M. et al., NEACRP-A-1120 (1991)

3.3 Analysis of Doppler Effect Measurement in FCA Cores Using JENDL-3.2 Library

S. Okajima

The JENDL-3.2[1] was released in June of 1994. In JENDL-3.2, the unresolved resonance region of ^{238}U was extended from 50 keV up to 150 keV since the Doppler effect is important in this energy region. To evaluate the calculation accuracy of the ^{238}U Doppler effect using JENDL-3.2, the Doppler effect measured in FCA cores were analyzed.

The Doppler effect measurements for ^{238}U have been carried out in various FCA assemblies which covered a wide range of the neutron spectra from a small experimental fast reactor to a large commercial fast reactor[2,3]. The details of the Doppler effect measurement at FCA are described elsewhere[2,3]. Here the measurement technique is briefly described. A natural UO_2 Doppler sample (25 mm diameter x 150 mm long, 605 g of uranium) is placed in the core center and kept at a desired high temperature for a certain period. The Doppler reactivity worth is derived from the difference between the reactivities measured for the unheated and heated Doppler sample. The reactivity is measured using a fine control rod which keeps the reactor at a constant power level. The measurement was carried out at sample temperatures of 20°C, 550°C and 800°C.

The calculation flow is shown in Fig. 3.3.1. A 70 group cross section set JFS-3-J3[4], processed from JENDL-3.2, was used in the core calculation. The conventional collision probability code SLAROM[5] was used to calculate the effective cross sections of core regions and blanket regions. The Doppler reactivity worth was calculated by the first-order perturbation theory. The perturbation is caused by the change of the effective cross section of the sample due to the change in the sample temperature. The unperturbed real and adjoint fluxes with a 70 group structure were obtained from the two-dimensional diffusion calculation in R-Z geometry. The Doppler sample and the homogenized experimental device regions are placed at the position corresponding to the measurement. A collision probability code with an ultra-fine group structure, PEACO-X[6], was used to calculate the effective cross section of the Doppler sample in a pin cell model. The cell consists of three regions: (a) the Doppler sample at the center, (b) the region surrounded in turn by the homogenized experimental device region and (c) the region surrounded by a homogenized test region of the core. The PEACO-X code can handle the resonance interaction effect between the hot sample and the adjacent cold core[2,6], and the overlapping effect between the sample and the structural material in the experimental devices.

The calculated results were compared between JENDL-3.1 and JENDL-3.2. The

ratio between calculated and experimental values (C/E) are shown in Fig. 3.3.2, as a function of spectrum-related indicator SPI which is a proportion of neutrons between 40.9 keV and 101 eV to total neutron. The JENDL-3.2 calculation in MOX fuel mockup cores gives 3 - 5 % larger Doppler reactivity worths than the JENDL-3.1 calculation because of the extension of the unresolved resonance region of ^{238}U. The JENDL-3.2 calculation agrees well with the experimental values within 5%. In Pu/U-235 cores the JENDL-3.2 calculation gives 3 - 15 % larger than the JENDL-3.1 calculation. The calculation in the Pu/U-235 cores shows larger increase than that in MOX fuel mockup cores. This larger increase is caused by the softer neutron spectrum below 10 keV in addition to the extension of the unresolved resonance region of ^{238}U. The former effect is given by the smaller capture cross section of ^{235}U in JENDL-3.2. When the cross section data of ^{235}U was changed from JENDL-3.2 to JENDL-3.1 in the flux calculation, the calculation shows 3 - 5 % smaller Doppler reactivity worth than the JENDL-3.2 calculation. The C/E values in Pu/U-235 cores range from 0.8 to 1.2. Further investigation is required to analyze the Doppler effect measurements in Pu/U-235 cores at FCA.

References

1) Nakagawa T., et al. : J. Nucl. Sci. and Technol., (to be published).
2) Okajima S., Oigawa H. and Mukaiyama T. : ibid., **31**, (1994) 1097.
3) Mukaiyama T. and Okajima S. : ibid., **22**, (1985) 243.
4) Takano H. and Kaneko K. : "Benchmark Test of JENDL-3T and 3T/Rev.1," JAERI-M 89-147 (1989) (in Japanese).
5) Nakagawa M. and Tsuchihashi K. : "SLAROM: A code for cell Homogenization Calculation of Fast Reactor," JAERI 1294 (1984).
6) Okajima S., Oigawa H. and Mukaiyama T. : "Measurement of Doppler Effect up to 2000 °C at FCA (3) -Development of a Cell Code, PEACO-X, with Ultra-fine Group Structure-", JAERI-M 92-185 (1992) (in Japanese).

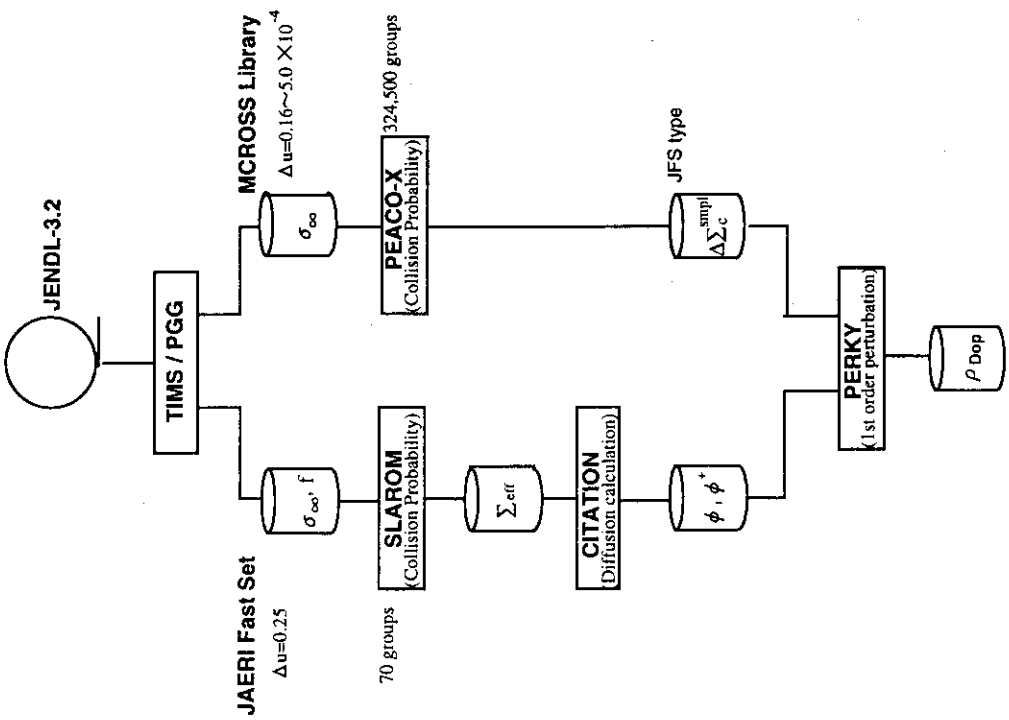

Fig. 3.3.1 Calculation flow for the analysis of Doppler reactivity worth

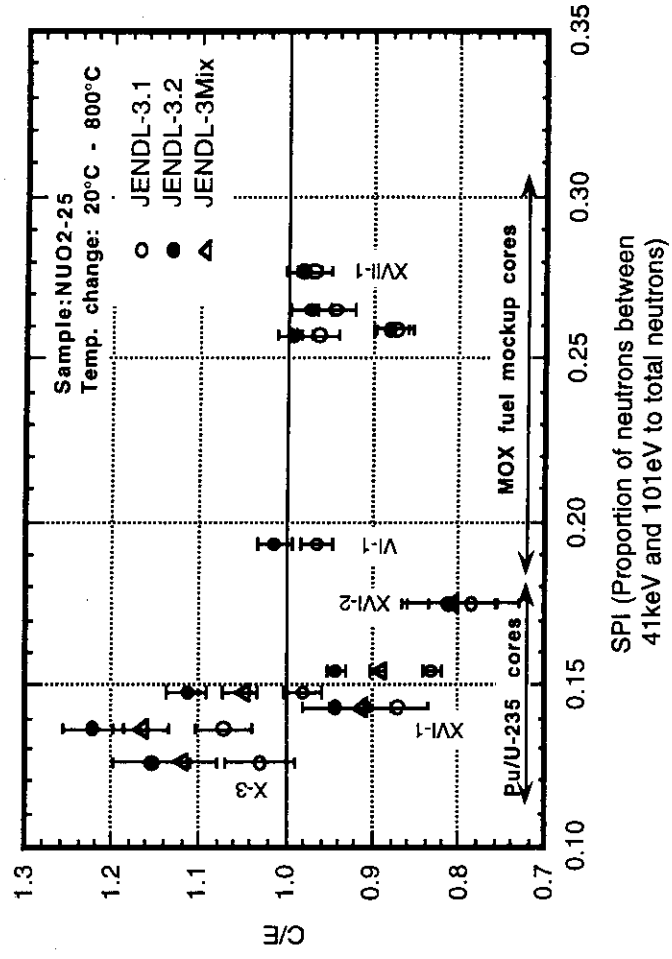

Fig. 3.3.2 Comaprison of C/E values of Doppler reactivity worth between JENDL-3.1 and JENDL-3.2 (JENDL-3Mix consists of the JENDL-3.1 cross section data for U-235 and the JENDL-3.2 cross section data for the other nuclides)

3.4 Evaluation of Shielding Effect for Reaction Rate Measurement using Activation Foil

T. Osugi and S. Okajima

A reaction rate in a medium is usually measured by using a activation foil inserted in the medium. Count rates of the foil are heavily affected by surrounding medium; i.e. foil shielding effect. Therefore, it is quite important to evaluate the shielding effect of the foil in deducing the reaction rate from the count rate of the foil. Here, we evaluate the shielding effect of U-238 foil using a conventional small group and a ultra-fine group cell calculation code, and compare the results with experimental values.

Calculation

Figure 3.4.1 shows a cell calculation model for effective capture cross section of foil region in DUO_2 or SS plate for core or blanket cell. Two cell calculation codes are used; SLAROM[1] for conventional small group method, and PEACO-X[2] for ultra-fine group method as reference calculation. The calculated results show that;

(1) SLAROM fails to take into account the shielding effect of U-238 from surrounding medium to foil, and overestimates U-238 capture reaction rate in SS plate comparing with PEACO-X results.

(2) Self-shielding effects defined as the ratio of capture reaction rate in U-238 foil to that in medium are calculated to be of 1.2% (core cell) to 1.5% (blanket cell) in DUO_2 plate, and of 8.8% (core cell) to 16.5% (blanket cell) in SS plate by PEACO-X calculation. SLAROM calculation with isolated lump resonance approximation for foil region shows fairly good agreement with the reference (PEACO-X) calculation in SS plate, but overestimates it in DUO_2 plate as shown in Table 3.4.1.

Comparison between calculated and experimental effects

U-238 capture rates were measured with foils placed between the DUO_2 or SS plates in the core and blanket cells of the FCA XVII core (simulating a prototype MOX FBR). Comparison was made for the SS effect defined as ratio of reaction rate in SS plate to that in DUO_2 plate, and shown in Table 3.4.2. The PEACO-X calculation shows good agreement with the experiments for both of the core and blanket cells. The SLAROM calculation, in which the lump resonance approximation is applied only for foils in SS plate, shows good agreement with the measured effect for core cell, but overestimates the measured one about 9% for blanket cell which has softer neutron spectrum than core cell does.

References

1) M. Nakagawa et al. : JAERI 1294 (1984).
2) S. Okajima et al. : JAERI-M 92-185 (1992).

Table 3.4.1 Shielding effect* of U-238 capture reaction rate in DUO2 plate and SS plate

	Core Cell		Blanket Cell	
Medium	PEACO-X	SLAROM	PEACO-X	SLAROM
DUO_2	0.988	0.888	0.985	0.856
SS	0.912	0.883	0.835	0.792

* : the ratio of capture reaction rate in U-238 foil to that in medium.

Table 3.4.2 Comparison of SS effect* between calculation and experiment

	Experiment	C/E Value	
Cell		by SLAROM	by PEACO-X
Core	1.221±2%	1.002	0.973
Blanket	1.332±2%	1.085	1.007

* : the ratio of U-238 capture rate in SS plate to that in DUO_2 plate.

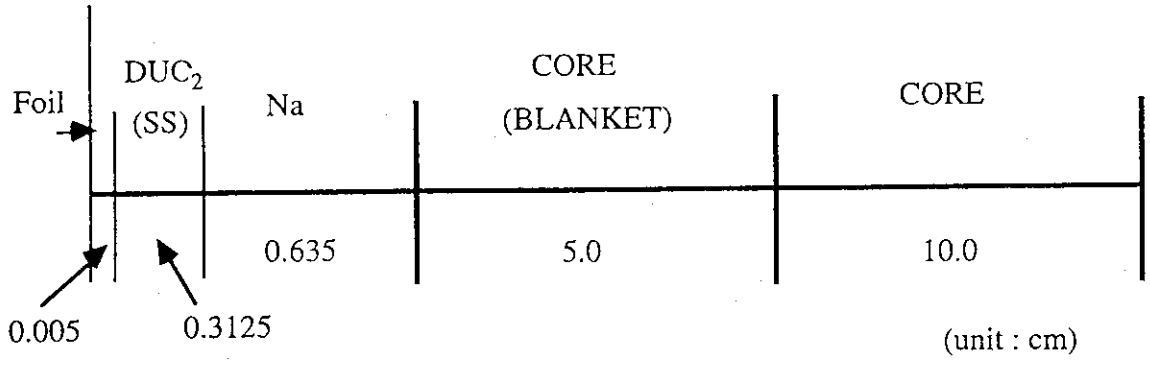

Fig. 3.4.1 Cell calculation model for evaluation of shielding effect of U-238 capture reaction rate

3.5 Validation of Reaction Rate Measurement Technique at FCA by using a Thermal Neutron Standard Field

T. Sakurai, T. Nemoto, K. Kobayashi* and H. Unesaki*

Measurements of ^{235}U fission rate(F5) and ^{238}U capture rate(C8) were made in a thermal neutron standard field of Kyoto University Research Reactor Heavy Water Facility[1]. The reaction rates were measured by foil activation techniques of FCA[2] with thin metallic foils of depleted uranium and enriched uranium. The results were compared with the 'reference' reaction rates which are obtained with well-known thermal neutron cross sections and thermal neutron flux to confirm reliability of the present foil activation technique.

Foils of enriched uranium and depleted uranium were irradiated with gold foils as neutron flux monitor on a rotating wheel which is placed in an irradiaton room of the Heavy Water Facility as shown in Fig.1. The irradiation was made for three hours at reactor power of 200kW.

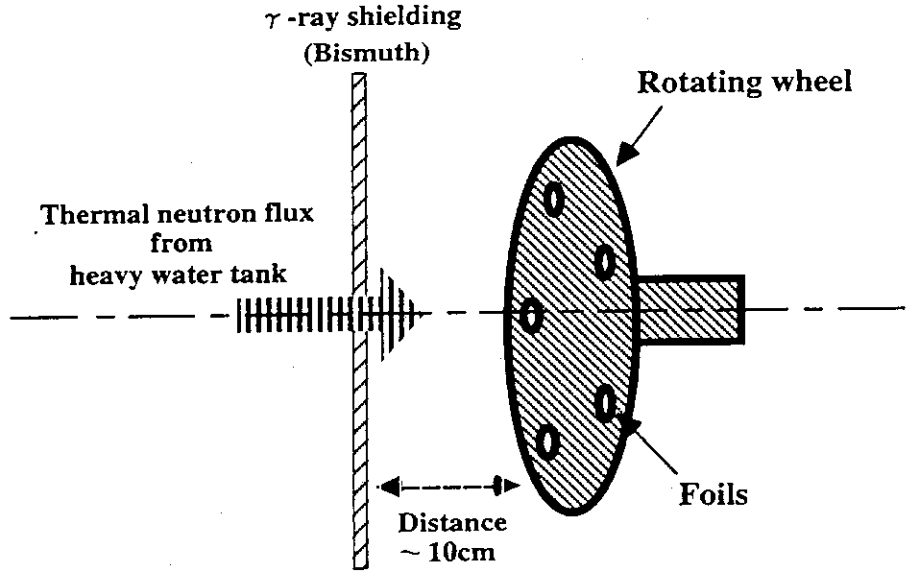

Fig.1 Foil irradiation arrangement in the irradiation room of KUR Heavy Water Facility

The irradiated uranium foils were transported to JAERI. The reaction rates were determined with activity of the uranium foils measured by a γ -ray spectroscopy system of FCA[3] which was calibrated by using an absolute fission chamber of ^{235}U[4] for F5 and ^{243}Am-^{239}Np sources[5] for C8. Irradiation of the absolute fission chamber and an enriched

* Research Reactor Institute, Kyoto University

uranium foil for the calibration of the γ -ray spectroscopy system was also made at the Heavy Water Facility.

The reference reaction rates were obtained with thermal neutron cross sections[6] of ^{235}U fission and ^{238}U capture, Westcott g-factor of the reactions[7] and neutron flux during irradiation. The neutron flux was determined from activity of the irradiated gold foil which was measured by $4\pi\ \beta-\gamma$ coincidence technique.

Comparisons between measured and reference reaction rates are summarized in Table 1.

Table 1 Comparison between reference and measured reaction rates at KUR thermal neutron standard field

Reaction	Reference value*	Foil measurement*	Foil / Ref.
^{238}U capture	1.773×10^{-16} $\pm0.8\%$**	1.758×10^{-16} $\pm1.0\%$	0.992
^{235}U fission	3.717×10^{-14} $\pm0.4\%$	3.685×10^{-14} $\pm1.1\%$	0.991
^{238}U capture / ^{235}U fission	4.77×10^{-3} $\pm0.8\%$	4.78×10^{-3} $\pm1.5\%$	1.002

* Reaction rate per atom at 200 kW operation of KUR ** Uncertainty at 1 σ

Uncertainties in the foil measurements were estimated from statistical errors of γ -ray counting of foils and uncertainties in calibration of γ -ray spectroscopy system, foil weight, correction for decay of ^{239}Np(for C8) and correction for γ -ray self attenuation in the depleted uranium foil(for C8). Uncertainties in reference reaction rates were estimated from uncertainties in evaluated thermal cross sections[6] and statistical error of gold foil activity measurement.

Good agreement within experimental error was obtained between the measured and the reference reaction rates. The reliability of the present foil activation technique was confirmed through these agreements. This work was performed under the Visiting Researcher's Program of the Research Reactor Institute, Kyoto University.

References

1) Kanda K., et al., Nucl. Instrum. Methods. 148, 535 (1978).
2) Sakurai T., et al., to be published in JAERI-research (in Japanese).
3) Nemoto T., et al., JAERI-M 84-147 (1984) (in Japanese).
4) Ūbu M., JAERI-M 9757(1981) (in Japanese).
5) Kono N., et al., Private Communication, Japan Atomic Energy Research Institute, (1987).
6) Mughabghab S.F., et al., Academic Press (1981).
7) Westcott C.H., AECL-1101 (1960).

3.6 Measurement of Na Void Worth in Various Pu Isotope Composition

S. IIJIMA and H. Oigawa

The increase of Pu-240 in the LMFBR fuel brings a growth of positive sodium void worth, though there is few experimental data for the effects of plutonium composition on the sodium void worth. A series of sodium void worth experiment was made at FCA Assembly XVII-1, which was the mockup core of oxide-fueled LMFBR, and the reactivity effects for the increase of Pu-240 were measured.

The Pu-240 fuel was added at the center region of the assembly XVII-1 on two steps and the ratios of Pu-240 in the plutonium fuel were increased to 18% and 22% from 8% in the reference core. The equivalence diameter of the center region is 31 cm and the height is 30 cm. A cross-section view of assembly XVII-1 is shown in Fig. 3.6.1. The sodium void worth was measured at the center region of the reference core and the two modified cores.

The sodium void worths were sensitive to the increase of Pu-240 and were 13% and 25% larger than the reference core. The experimental results are shown in Fig. 3.6.1. A sodium void worth consists of positive non-leakage reactivity and negative leakage reactivity. The increase of Pu-240 changes an energy distribution of adjoint flux and brings a growth of non-leakage reactivity on the sodium void worth.

Sodium void worths are analyzed using the cross-section library JENDL-3 and JAERI's standard calculation system for fast reactor neutronics. The JFS-3 group constant set with a 70 energy group structure is generated from JENDL-3. A diffusion calculation is made in R-Z geometry and 70 energy groups. The sodium void worths were calculated by first order perturbation method based on diffusion theory.

The calculated-to- experiment (C/E) values are given in Table 3.6.1. The calculated values show a good agreement with the measured values.

Table 6.3.1 C/E values of sodium void worth

	C/E
Reference	0.979
18% Core	0.994
22% Core	0.984

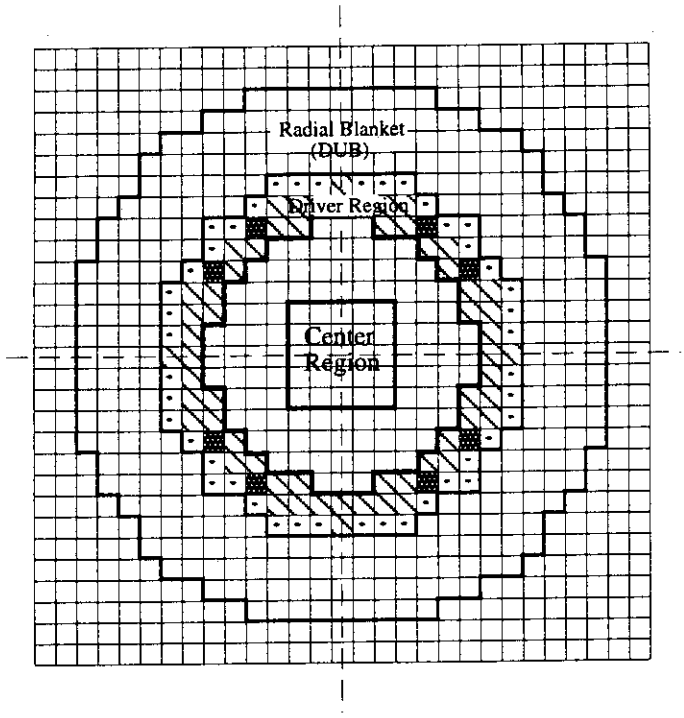

Fig. 6.3.1 Vertical cross section of FCA XVII-1

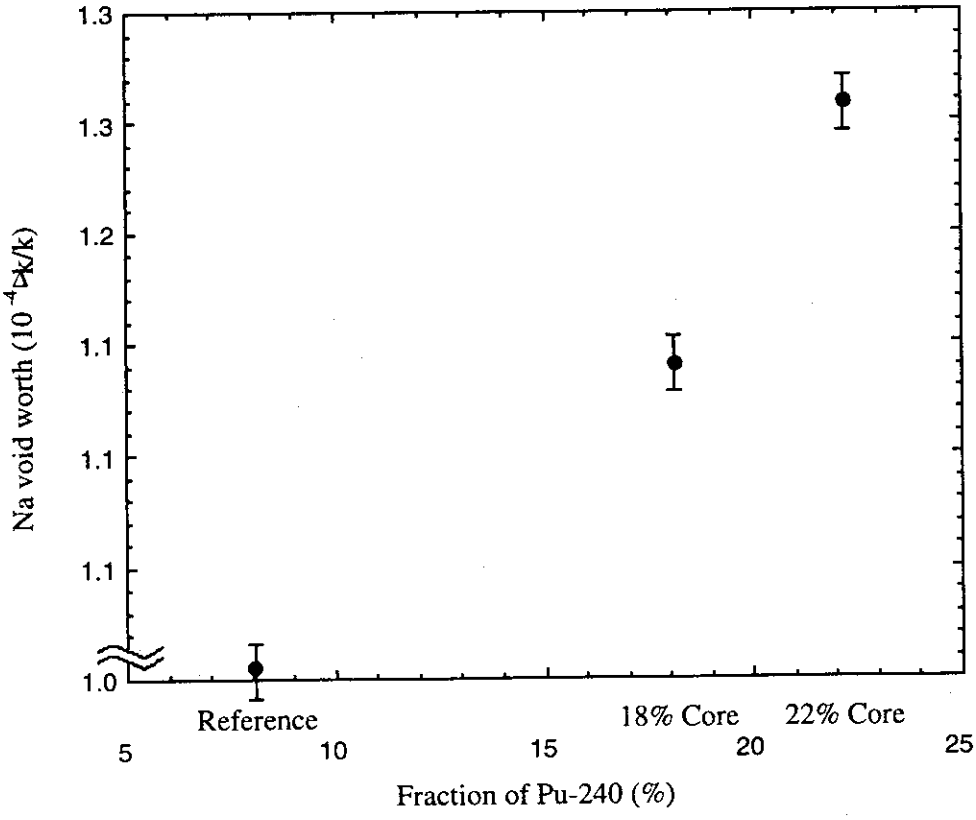

Fig. 6.3.2 Pu-240 effects of sodium void worth measured in FCA assembly XVII-1

3.7 Measurements of Axial Distribution of $^{63}Cu(n,\gamma)$ Reaction Rate in VHTRC-7 Core

T. Yamane, T. Ono, M. Takeuchi and F. Akino

In normal operation of reactors, neutron flux and power distributions are affected by control rods which are partially inserted in core and/or reflector regions. In order to examine and improve the calculation accuracy of power distribution distorted by the partially inserted control rods, axial neutron flux distribution was measured in the VHTRC-7 core by the activation technique.

The VHTRC-7 core, which is loaded with 2,4 and 6 wt%-enriched coated particle fuel in an axially zoning pattern, has an HTTR-mock-up control rod that is partially inserted in the central column of the movable half assembly, as shown in Fig.3.7.1. The HTTR-mock-up control rod (BW-40) consists of a stack of neutron absorbing pellets (a mixture of B_4C and graphite powder), of which boron content is 38.3wt% and diameter 89.6mm. The pellets are housed by a stainless steel tube and the stack length is adjusted to 1150mm. Copper wires of 2mm in diameter and 10mm long were used as activation samples, which were irradiated along the graphite rods at five different radial positions indicated by A, B, C, D and E in the same figure. A traverse at the position A was made only in the fixed half assembly. The radioactivity of irradiated samples induced by $^{63}Cu(n,\gamma)^{64}Cu$ reaction was measured by counting γ-rays mainly coming from β^+ annihilation with a well-type NaI(Tl) detector.

Analysis was performed with the SRAC code system using nuclear data based on the ENDF/B-IV, except the data for Cu isotopes which were taken from the JENDL-2. The cell calculation for a fuel block was made by the collision probability method in which a fuel block was accurately modeled in geometry and the doubly heterogeneous effect was taken into account. In the cell calculation for the central block, a one-dimensional Sn method was employed with an approximation of infinite cylinder where the BW-40 was centralized and the graphite block was surrounded by a homogenized fuel region. The core calculation was carried out with a diffusion code CITATION using a three-dimensional Triangular-Z model to obtain neutron flux distribution.

The relative distribution of $^{63}Cu(n,\gamma)^{64}Cu$ reaction rate, which was directly measurable quantity, were compared between the results of calculation and experiment. Figure 3.7.2 shows the typical results, in which a normalization is made for the average of reaction rates in the core region. A very strong distortion by the partially inserted BW-40 is observed in the movable half assembly. The calculation results in overestimation near the top of BW-40 and underestimation along BW-40 in the movable half. This fact will be ascribed to the limitations

of the geometrical model and of the diffusion approximation near the strong absorber. When the comparison is limited to the distribution in fuel region (at the positions C, D and E), the calculation results agree with the experimental ones within 4% on the average and 7% at the maximum.

The accuracy of the present calculation method can be estimated about 10% for predicting the three-dimensional neutron flux distribution in fuel region, taking account of about 2% experimental uncertainty. More detailed analysis on this experiment will be continued to improve the accuracy of nuclear design calculation.

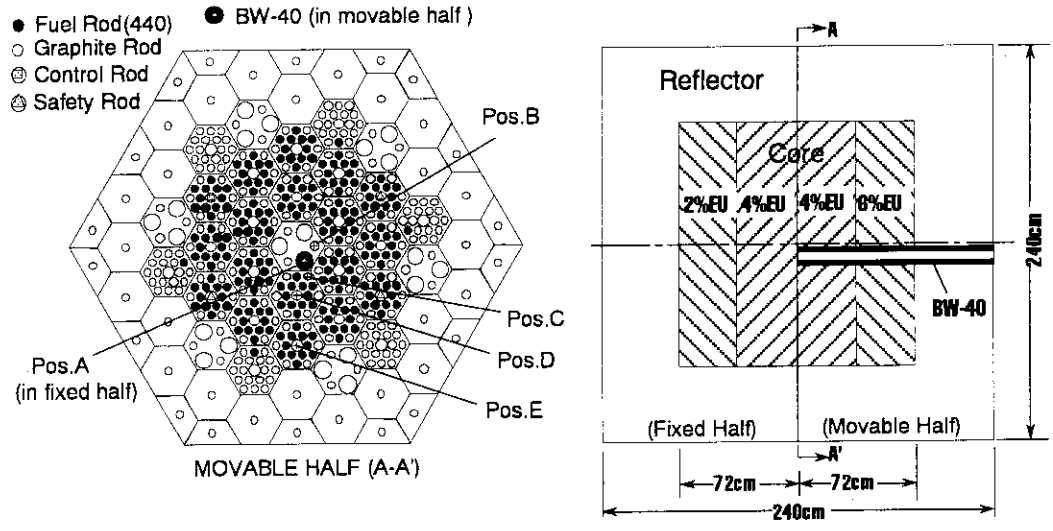

Fig.3.7.1 Cross-sectional view of VHTRC-7 core

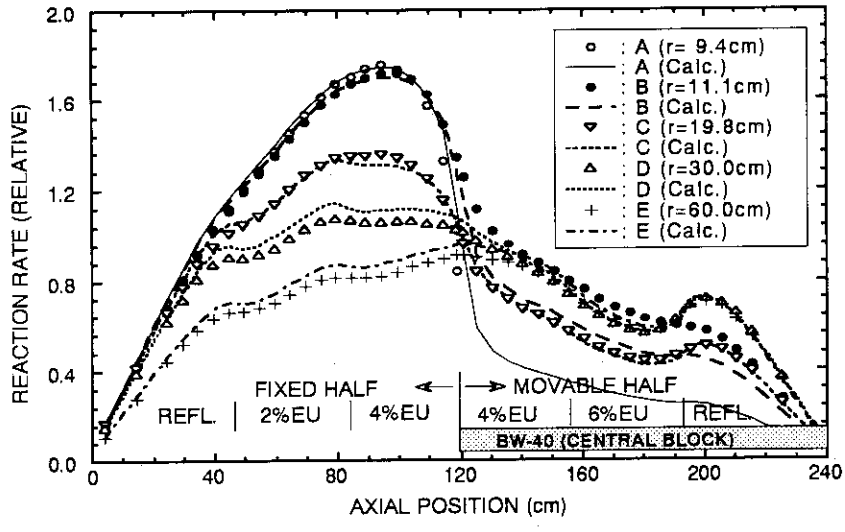

Fig.3.7.2 Typical results of $^{63}Cu(n,\gamma)^{64}Cu$ reaction rate distribution in VHTRC-7 core

3.8 Measurement of Critical Mass of VHTRC-7 Core

F. Akino, T.Yamane, M.Takeuchi, T.Ono and S.Fujisaki

In order to verify the calculation accuracy related to the nuclear design of HTTR (High Temperature Engineering Test Reactor)[1], the critical experiments have been conducted using the critical assembly VHTRC (Very High Temperature Reactor Critical Assembly)[2].

The VHTRC-7 core was assembled at VHTRC for simulation of partially inserted control rods of HTTR. The VHTRC-7 core is loaded with 2-4-6wt% enriched fuel in an axially zoning pattern and with an HTTR-mock-up control rod at the central column of movable half of VHTRC. The fuel rod of the fixed half assembly contains 2wt% and 4wt% enriched fuel compacts (10 compacts for each enrichment). On the other side, the fuel rod of the movable half assembly contains 4wt% and 6wt% enriched fuel compacts (10 compacts for each enrichment). The HTTR-mock-up control rod consists of a stack of neutron absorbing pellets (outer diameter:89.6mm, inner diameter:60.0mm, height:25.2mm, boron content: 38.3wt%, stack length:1150mm) inserted into a stainless steel tube. The core reached criticality with about 18 fuel columns at a room temperature. The fuel rod loading pattern was shown in Fig.3.8.1. The measured critical mass was corrected for the excess reactivity and for the reactivity worth of inserted materials in the core, such as insertion holes of control and safety rods, thermocouples and a guide tube of neutron source and a gap between two half assemblies. The measured ^{235}U critical mass of VHTRC-7 core was 7.271 $\pm$0.003kg.

Calculations were carried out by the SRAC code system[3] with the ENDF/B-IV nuclear data library. The double heterogeneity of fuel rods in a graphite block and coated particles in a fuel compact was taken into account in the cell calculation for a fuel block. The cell calculation for the central block having the HTTR-mock-up control rod was carried out by the Sn method using the TWOTRAN code (X-Y geometry, S_4 approximation). Thermal neutrons in the energy range from 0.0eV to 1.125eV were divided into 39 groups and fast neutrons in the energy range from 1.125eV to 10MeV were divided into 22 groups. Using the neutron spectra obtained by the cell calculations, the cross sections of 61 groups were condensed into 24 groups for the core calculation. The group constants for reflector were condensed by means of an asymptotic spectrum. The calculation of critical mass was carried out using these group constants by three-dimensional diffusion approximation in the core calculation. The calculated value of ^{235}U critical mass was 7.133kg.

The discrepancy of ^{235}U critical mass between calculation and experiment is 2% which is 0.3% Δk discrepancy in the effective multiplication factor. The result satisfies the accuracy requirement within 1% Δk for the nuclear design of HTTR.

References

1) Sanokawa K. and Saito S. : J.At. Energy Soc. Japan, 29,603 (1987)
2) Yasuda H., et al. : "Construction of VHTRC (Very High Temperature Reactor Critical Assembly)", JAERI 1305 (1987)
3) Tsuchihasi K. et al. : "Revised SRAC Code System", JAERI 1302 (1987)

Table 3.8.1 Reactivity worth of a fuel rod and corrections for critical mass

Item	Reactivity worth (¢)
Fuel rod	13.4 ± 0.2
Critical mass correction values	
(1) Control rod, safety rod insertion holes	68.2 ± 1.9
(2) Control rod, safety rod tips in the core	14.8 ± 0.2
(3) Thermocouples and a guide tube of neutron source	2.1 ± 0.3
(4) Gap between the two half assemblies	12.8 ± 4.2

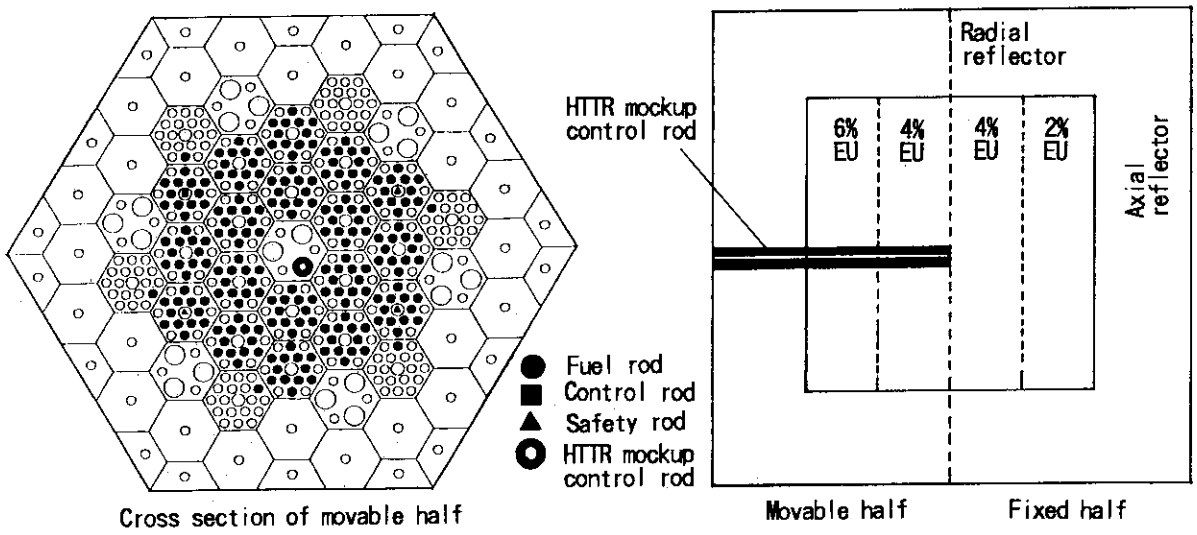

Fig. 3.8.1 Fuel rod loading pattern of the VHTRC-7 core.

3.9 Analysis of Experiments at FCA X-1 and X-2 Assemblies by Using the MVP Monte Carlo Code

M. Nakagawa

The FCA assemblies X-1 and X-2[1] were constructed for the mockup experiments of the Fast Experimental Reactor "JOYO" MK-II core. Both assemblies have the core regions simulating MK-II but the reflector regions were replaced by depleted uranium in the axial and natural uranium in the radial directions, respectively, for the X-1 core. On the other hand, these were composed of sodium and SUS in the X-2 core. There is no control rod position. The axial core height is 50.4cm and thickness of axial reflector is 35.56cm . Measurements were made for criticality, central fission rate ratio, fission rate distribution, sample worth and control rod worth.

Calculation model

The calculations have been performed by the MVP code[2]. The core geometry is modeled as precisely as possible by using multiple lattice geometry. The whole cores can be presented by square lattice of which each cell corresponds to unit matrix with 5.52cm×5.52cm×height (first level lattice). In each matrix, a drawer is inserted, in which fuel and other material plates are repeatedly arranged (second level lattice). Unit of material arrangement has dimension of 5.08×5.08×5.08cm. In the calculation model, matrix, drawer, void and plate arrangement are precisely described. All the calculations have been performed by using JENDL3.1. Some calculations were made using JENDL3.2 and the differences of calculated results were small between those nuclear data. The total numbers of neutron histories were 600 000 and 800 000 for the X-1 and X-2 cores, respectively.

Calculation results

The calculated results of criticality and control rod worth are compared with the measured values in Table 3.9.1. Prediction accuracy is very good for the X-2 core though the calculation underestimates k_{eff} by 0.8% for the X-1 core. In this core, leakage neutrons from the core strongly absorbed by ^{238}U in the blanket of which composition consists of mostly depleted or natural uranium. Accordingly the cause of discrepancy in k_{eff} of the X-1 core may be due to large capture cross section of ^{238}U. The prediction accuracy of control rod worth in the X-2 core is good for 90% enriched B_4C while the worth is underestimated for natural B_4C. The reason of such inconsistency is not clear at present. The central fission ratios, $^{238}F/^{235}F$, $^{239}F/^{235}F$ and $^{237}F/^{235}F$, which were

measured in the X-2 core by fission counters were calculated (averaged values in the central drawer) and compared in Table 3.9.2. The calculations agree very well with the measurements for $^{239}F/^{235}F$ and $^{237}F/^{235}F$. Although the ratio $^{238}F/^{235}F$ is fairly overestimated, the uncertainty involved in the C/E value is not small. Table 3.9.3 shows the C/E values for the radial fission rate distribution. The agreement is satisfactory. Neutron spectra of both cores are compared in Fig.3.9.1. The X-1 core has harder spectrum than the X-2 one because the depleted uranium blanket of the former core strongly absorbed neutrons in the resonance region. Hence, reflected component is small.

References

1) Nakano M.:private communication

2) Mori T. and Nakagawa M.:"MVP/GMVP: General Purpose Monte Carlo Codes", JAERI-Data/Code 94-007(1994)

Table 3.9.1 Comparison of k_{eff} and control rod worth

Core		k_{eff}	Control rod worth Natural B_4C	90%enriched B_4C
	Experiment	1.0038	---	---
X-1	Calculation	0.9962±0.0007	---	---
	C/E	0.992±0.001	---	---
	Experiment	0.9992	0.0246	0.0484
X-2	Calculation	0.9998±0.0008	0.0226±4.9(%)	0.0470±2.6(%)
	C/E	1.001±0.001	0.920±0.045	0.972±0.025

Table 3.9.2 Central fission ratios at FCA X-2 core

	$^{238}F/^{235}F$	$^{239}F/^{235}F$	$^{237}F/^{235}F$
Experiment	0.0501±3.5%	1.093±3.2%	0.353±4.7%
Calculation	0.0545±2.8%	1.093±1.5%	0.354±2.0%
C/E	1.088±4.5%	1.010±3.5%	1.003±5.1%

Table 3.9.3 C/E of radial fission rate distributions in X-2 core [a)]

Distance from center(cm)		^{235}F	^{238}F	^{239}F	^{237}F
	0	1.0	1.0	1.0	1.0
	5.52	0.996	1.002	0.998	1.004
	11.04	0.998	1.001	0.999	1.008
Core	16.56	0.986	1.010	0.988	0.999
	22.08	0.990	1.019	0.995	1.009
	27.60	0.968	1.023	0.971	0.997
	33.12	1.004	0.956	0.971	0.960
Refl.	38.64	1.039	1.011	0.990	0.966
	44.16	1.047	0.995	1.089[b)]	0.943

a) Normalized at core center

b) 1 σ =6.7%

Total number of histories=800 000

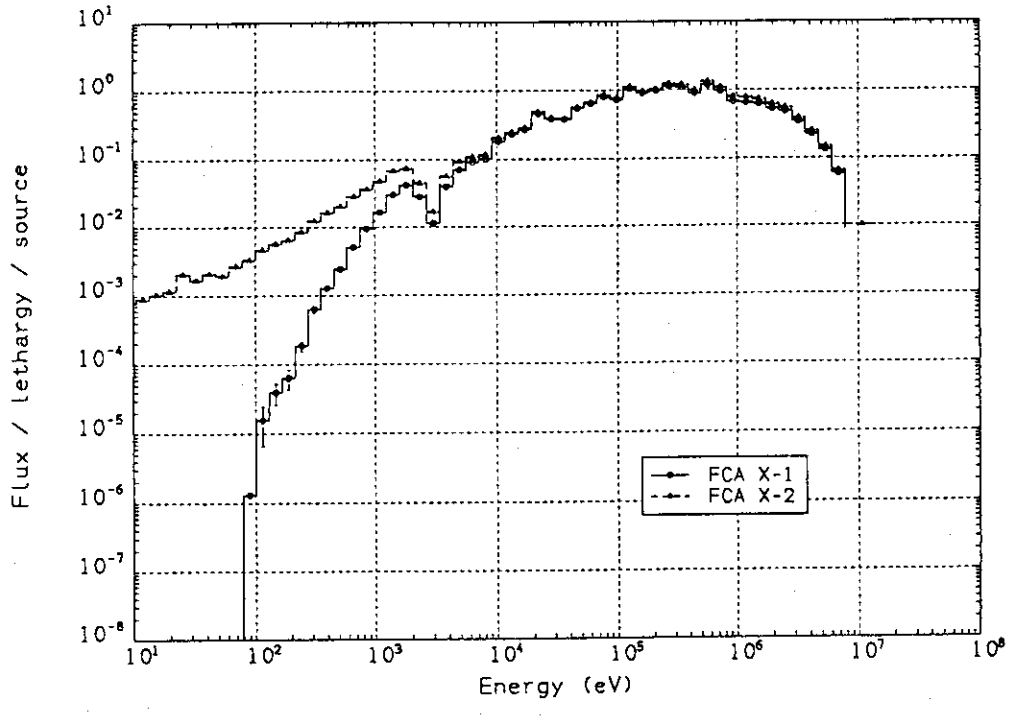

Fig.3.9.1 Comparison of neutron spectra between FCA X-1 and X-2 cores

4 Advanced Reactor System Design Studies

Innovative concepts of advanced reactor systems such as a passive safety light water reactor and a lead-cooled fast reactor (LCFR) have been developed to meet various needs for nuclear energy in next century.

A concept of JAERI Passive Safety Reactor (JPSR) is being developed. The JPSR has two major features: 1) an inherent matching nature of core heat generation rate and heat removal rate in secondary side and 2) simplification of reactor system by using passive safety systems. In order to develop and improve the reactor design, experimental and analytical studies have been performed.

Steam condensation phenomenon was visualized by neutron radiography technique and it was clarified that the steam-air mixture discharged into a water pool is condensed rapidly when the pool water temperature is lower than 70°C. Core make-up tank (CMT) experiment was performed to investigate the effects of water subcooling in a pressure line and a partition structure in CMT. It was however found that the passive valve actuated by pressure difference is not reliable.

Large and small break LOCA analyses indicated the effectiveness of the passive residual heat removal (RHR) system and passive coolant injection system. Three-dimensional thermal fluid flow analyses in the downcomer were performed to evaluate the natural circulation driving force during the actuation period of passive RHR system.

Based on the experimental findings, analytical results and probabilistic safety assessment (PSA) results, the passive safety systems were modified as follows: 1) the CMT system was removed and advanced accumulators were adopted, 2) an additional RHR loop for non-LOCA events was installed. Then the PSA procedure was repeated for the modified design. The results indicated that the core damage frequency for the modified JPSR is sufficiently low compared with that for a conventional PWR.

ATWS analyses were performed for the LCFR covering the events of unprotected loss of flow (ULOF), unprotected transient overpower (UTOP) and unprotected loss of heat sink (ULOHS). It was confirmed that the LCFR has enough safety margin in ULOF and ULOHS accidents. However, the core design should be improved to cope with the UTOP event because the fuel temperature exceeds the melting point in the present analysis.

In this chapter, followings are in charge of sections in parenthesis: passive safety reactor systems laboratory (4.1 through 4.6) and reactor system laboratory (4.7).

Passive Safety Reactor Systems Laboratory

This laboratory developed new concept of JAERI passive safety reactor (JPSR) for a next generation light water reactor. In order to develop and evaluate the concept, safety analyses, three-dimensional thermal fluid flow analyses and probabilistic safety assessment (PSA) have been performed. Experimental studies are under way to investigate the important thermal-hydraulic phenomena including natural circulation, DNB, gravity driven coolant injection, steam condensation, and multi-dimensional flow in pressure vessel. A conceptual design of integral-type passive safety test reactor is in progress. As for an active storage PWR which uses MOX fuel, demonstration tests are being performed using a large scale hydraulic mock-up test facility.

4.1 Visualization of Steam Condensation in a Water Pool by means of Neutron Radiography

H. Yoshida, F. Araya and T. Iwamura

In a conceptual design of the passive safety reactor, to avoid the pressure increase in the containment vessel caused by steam release in an accident, the released steam is led to a water pool, and condensed. However, the condensation process of the steam contains non condensate gas in water is very complicated, and prediction procedures are not tested. Then those procedures must be checked. In this study, as the first stage of these verifications process, visualization of steam condensation in a water pool by means of neutron radiography (NRG) was done.

Figure. 4.1.1 shows schematic diagrams of experimental apparatus. Steam generated in the steam generator is injected to the test section that constructed in the JRR-3M NRG room. Air is mixed to steam before injected to the test section. When experiments were performed, water temperature in the test section increased, and effects of water temperature to the steam condensation were observed. Steam supply pressure decreased from 0.45 MPa to 0.2 MPa because of a small heater capacity in the steam generator.

In Fig. 4.1.2, the test section is shown. Pool height, width and depth are 396 mm, 300 mm and 15 mm respectively. Steam-air mixture injection nozzles are constructed at lower and side panel of the test section. Diameters of lower and side inlet nozzles are 10 mm and 8 mm respectively. In the test section, 12 thermocouples are set up to measure a temperature distribution in the test section. However, remarkable differences could not be observed.

In the experimental procedures, three types gases are used, namely steam only, air only and steam-air mixture. Figure. 4.1.3 shows examples of void fraction maps. Three type gases were injected at the lower nozzle, and water temperature in the test section was set to about 30°C. The case of steam only, air only and steam-air mixture are corresponding to (a), (b) and (c) in Fig. 4.1.3. Volume flow rates of steam and air were fixed at about 120 l/min. and 4.63 l/min. respectively.

At the case (a), no void was observed. At water temperature (T) lower than 70°C,

void could not be watched, and all injected steam was quickly condensed at the inlet nozzle. In the figure (b), voids moved to upward in the water were clearly observed. In the case of steam-air mixture was injected, an overall void fraction is smaller than that in the case (b) which uses air only.

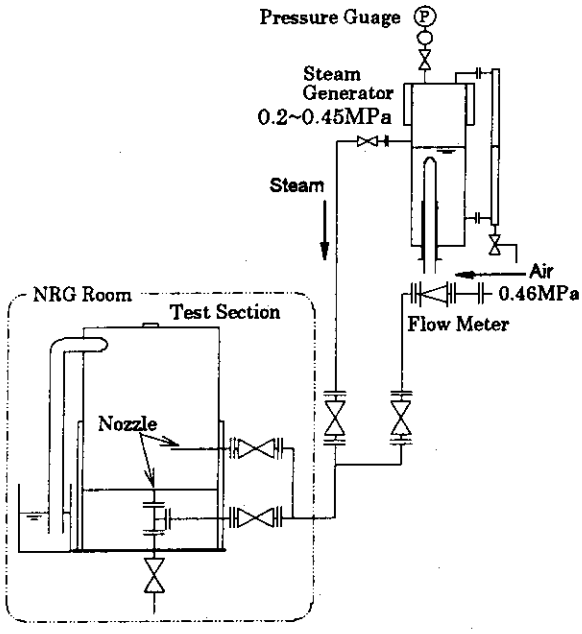

Fig. 4.1.1 Experimental apparatus

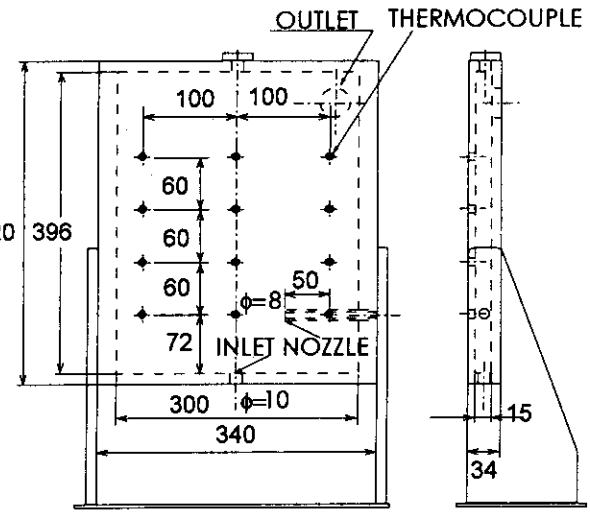

Fig. 4.1.2 Test section

Steam flow rate	127.8 l/min.
air flow rate	0 l/min.

Steam flow rate	0 l/min.
air flow rate	4.63 l/min.

Steam flow rate	116.0 l/min.
air flow rate	4.63 l/min.

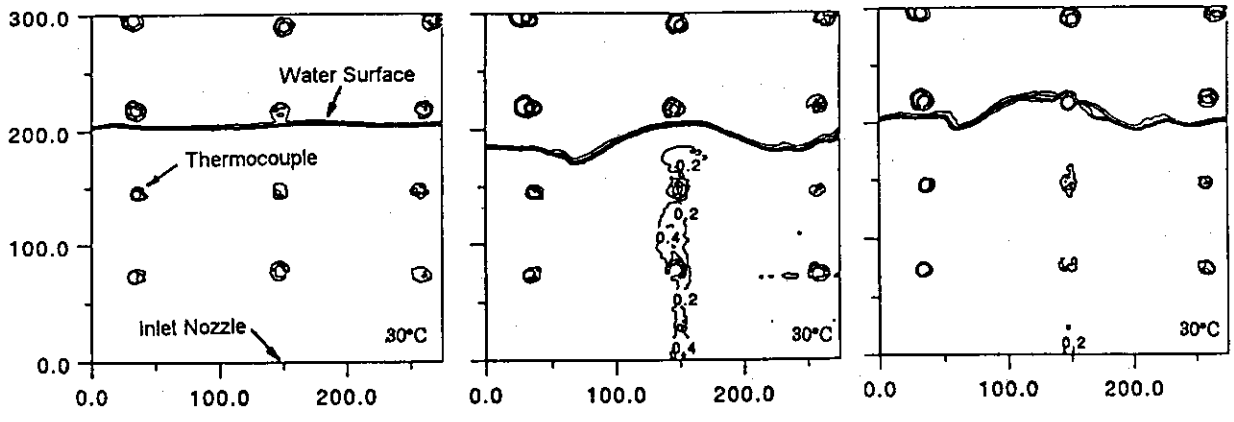

(a)Steam (b)Air (c)Steam-air mixture

Fig 4.1.3 Examples of observed void fraction maps (T=30℃)

4.2 Thermal-Hydraulic Experiment on Core Make-up Tank

F. Araya, T. Satoh, H. Watanabe, Y. Murao and T. Iwamura

A concept of JAERI Passive safety reactor (JPSR) has been developed to reduce man power in operation and maintenance and influence of human errors on reactor safety. As a passive coolant injection system, JPSR adopts core make-up tanks (CMTs) for maintain core coolability in loss-of-coolant accidents (LOCAs). A similar passive coolant injection system called a pressure balanced coolant injection system (PBIS) consisted of the CMT is also adopted to other passive safety reactor systems, such as SPWR[1] and AP-600[2]. Since the PBIS is not used in the current PWRs, thermal-hydraulic characteristics of the system are not well understood. Under the such situation of knowledge on the system consisting the CMT, an experiment was conducted to get understand thermal-hydraulic injection behaviors of coolant supplied from the CMT under LOCA conditions and to investigate adoption of the system to JPSR.

JPSR Design JPSR adopts a core make-up tank as the PBIS in the original design[3]. The CMT is designed to be connected to the upper plenum of the reactor pressure vessel through a pressure balance line and injection line. The system is designed to be actuated by opening valves installed parallel in the injection line by passive or active ways. One valve is a valve opened passively due to pressure imbalance caused by steam inflow of the pressure balance line after the inlet nozzle of the line is exposed in the steam by a water level reduction in the upper plenum due to LOCA. The other is manually opening valve. The CMT contains cold borated water to cool and shutdown the reactor core.

Experimental facility and experimental procedure A schematic view graph of the experimental facility is shown in Fig.4.2.1. The facility consists of mainly the CMT, the upper plenum simulator and the water discharge line. The CMT is connected to the upper plenum simulator through a pressure balance line and a injection line in which a differential pressure valve and a manually operated valve are installed parallel. In order to observe flow behaviors, view windows are installed in the upper plenum simulator, the pressure balance line and the top of the CMT. As for preparation of experiments, water is filled the CMT and upper plenum simulator in which water partially filled so as to cover an inlet nozzle of the pressure balance line. The maximum operating pressure is 4MPa. The facility is heated up by a heater with 22kW capacity before experiment. Experiments are started by discharging water through the water discharge line so as to simulate LOCA conditions. After steam flows into the pressure balance line caused by reduction of water level in the upper plenum simulator due to loss of water, differential pressure through the valves in

the injection line increases. The differential pressure valve is designed to be opened automatically when the differential pressure reaches to 2 mH_2O. The cold water contained in the CMT is injected into the upper plenum simulator. In most of experiments, the manually operated valve is used and is kept to open until end of experiment after opening and the differential pressure valve is not used. In case that the differential pressure valve is used, manual operation is not performed and the manually operated valve is not used.

Experimental results The following three series of experiments were carried out.

(1) Water subcooling in pressure balance line

In this series of experiments, subcooling of water in the pressure balance line was changed in each run. One representative results of the experiments are shown in Fig. 4.2.2. This figure shows transients of water level in the upper plenum simulator and static head in the pressure balance line which gives pressure difference through the valves in the injection line. The set point of the valve actuation is 1.8 mH_2O. This figure shows that, in the high subcooling case which are shown in thick lines, a time reaches to the set point is delayed than that in the low subcooled case.

(2) Partition structure in CMT

In this series of experiments, effects of the partitioning structure were observed. Namely, experiments were performed with and without the structure and results were compared. Figure 4.2.3 shows temperature distributions under the water level at the same time after initiation of injection of water from the CMT. This figure shows that high temperature region is thick in the case without the structure shown in a dotted line and the structure has effect to reduce steam condensation on the water surface.

(3) Differential pressure opening valve

A valve was developed based on a check valve so as to open at a pressure difference of 2 mH_2O and used in the experiment. The developed valve did not behave as expected. Namely, the valve was not opened and closed at the set point in the experiment. This shows that the differential pressure valve can not be applied to the JPSR design.

References

1) Sako K., et al., "Concept of highly passive safe reactor SPWR", presented at International specialist meeting on potential of small nuclear reactors for future clean and safe energy source, TIT, Tokyo, Japan, Oct. 23-25,1991.

2) McIntyre B.A. and Beck R.K., "Westinghouse advanced passive 600 plant", Nuclear Safety, Vol. 33, No. 1, 1992.

3) Murao Y., et al., "Transient characteristics of JAERI passive safety light water reactor system", presented at ARS'94, Pittsburgh, USA, April 17-21, 1994.

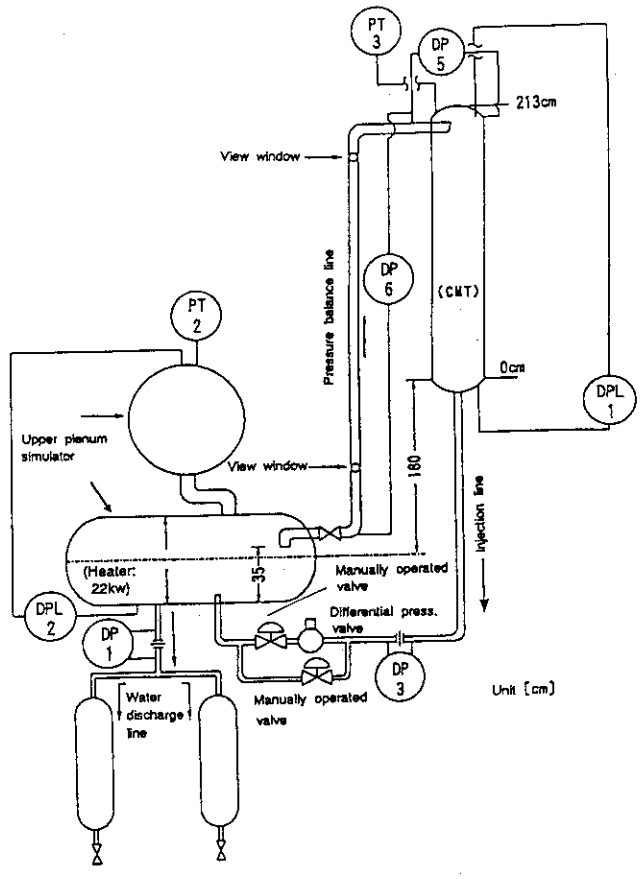

Fig.4.2.1 Schematic view of CMT experimental facility

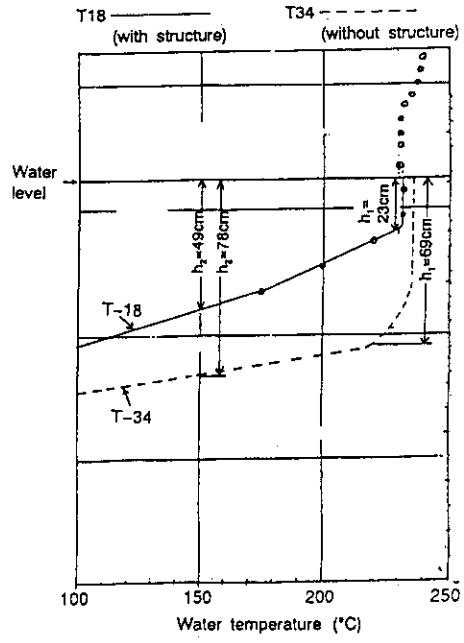

Fig.4.2.3 Effects of partitioning structure on temperature distribution under water level

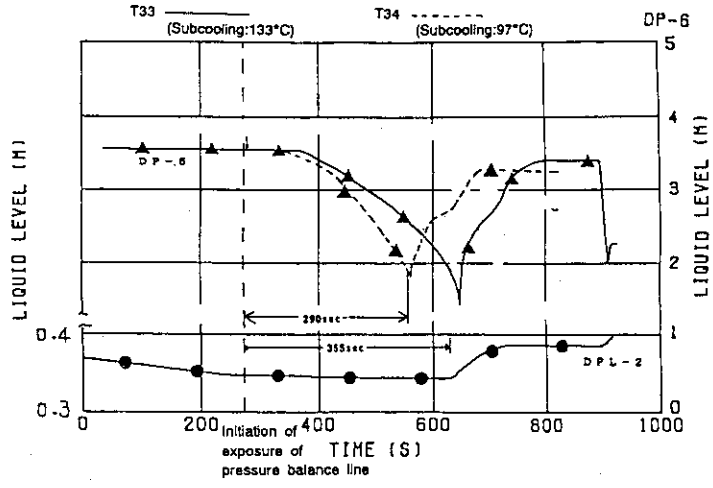

Fig.4.2.2 Effects water subcooling in pressure balance line

4.3 Transient Thermal-Hydraulic Analyses for Design of JPSR

F. Araya, Y. Murao and T. Iwamura

A concept of JAERI Passive safety reactor (JPSR) has been studied confirming its safety by performing transient thermal-hydraulic analyses. The possibility of a pressurized water reactor concept with highly inherent matching nature of the core power to the heat removal rate has been confirmed. In order to confirm feasibility of the concept in accident conditions, transient analyses were performed. In this section, calculated results of large and small break loss of coolant accident (LOCA) analyses with the RETRAN-02/Mod3 code are presented. The passive safety systems of the JPSR design relating to LOCAs are residual heat removal system, accumulators, gravity coolant injection systems. More detailed explanation is given in the reference 1).

Large break LOCA

In order to understand JPSR behaviors without safety systems in a large break LOCA (LBLOCA), transient analyses were performed. Calculated results in a LBLOCA case with a break area of 200% of the cross sectional area of the cold leg piping are shown in Fig.4.3.1. As shown here, cladding temperature increases just after initiation of LOCA. The maximum temperature is about 550 deg. C at around 5 seconds. This value is low enough than the safety limit of 2200 deg. C. After reaching the maximum temperature, the temperature decreases due to release of stored energy and reduction of core power. At around 20 seconds the cladding temperature is steeply decreased due to heat transfer mode change caused by large core flow. After this time, the cladding temperature is kept at low value until about 48 seconds. After this time, the cladding temperature begins to increase because any safety injection system is not considered to be actuated in the calculation. However around this time, a pressure in the primary coolant system decreases enough and is almost the same as that of the containment. This fact shows that any safety coolant injection system such as an accumulator, a gravity driven coolant injection system adopted in JPSR can feed coolant into the primary system before start of the cladding temperature increase with enough margin. Similar results were given by sensitivity calculations with changing the break area size to 50% of the cross sectional area of the cold leg. This also implies that the core make-up tank originally adopted inJPSR as a passive coolant injection system is not needed for JPSR in LBLOCAs.

Small break LOCA

Two heat exchangers of the residual heat removal (RHR) system are adopted between the hot and cold legs in each loop. Main purpose of the system is remove residual heat and decay heat

in a shutdown condition. On the other hand, in a small break LOCA, the system is used to enhance depressurization of the primary coolant system by cooling the system. The present analysis was performed with a objective to confirm effectiveness of the RHR system on depressurization of the primary coolant system.

Figure 4.3.2 shows the pressure transients of cases with and without actuation of RHR under a 5% split break LOCA at the cold leg. The RHR flow rate is also shown in the figure. The flow transient shows that a natural circulation is established until 100 s after initiation of LOCA. Therefore the pressure in the case with RHR actuation is rapidly decreased to a pressure level of actuation set point of the accumulator. During this time period, the core is covered by coolant and cooled enough. On the other hand, in the case without RHR actuation, the system pressure is not decreased so much during the time period of the calculations. These results shows that the RHR is effective to depressurize the primary coolant system during SBLOCAs.

Discussions

In the pervious paragraphs, it is shown that, in large break LOCAs from 200% to 50% break area, the primary coolant system can be depressurized to the containment pressure level without heatup of the fuel cladding temperature. This implies that the safety of the core can be maintained until and also after actuation of the accumulators and the gravity driven coolant injection systems. In small break LOCAs, the primary coolant system is depressurized by actuation of RHRs and the coolant can be added from the accumurators. This shows that the core can be cooled by injection of cold coolant and cooling capability of the RHR. As backup of the depressurization system, depressurization valves are also available in JPSR. These facts show that the present safety system can cool the core without damage in whole range LOCA.

References

1) Murao Y., Araya F. and Iwamura T., " A concept of passive safety light water reactor system (JPSR)", presented at ICONE-3, Kyoto, Japan, (April 23-27,1995).

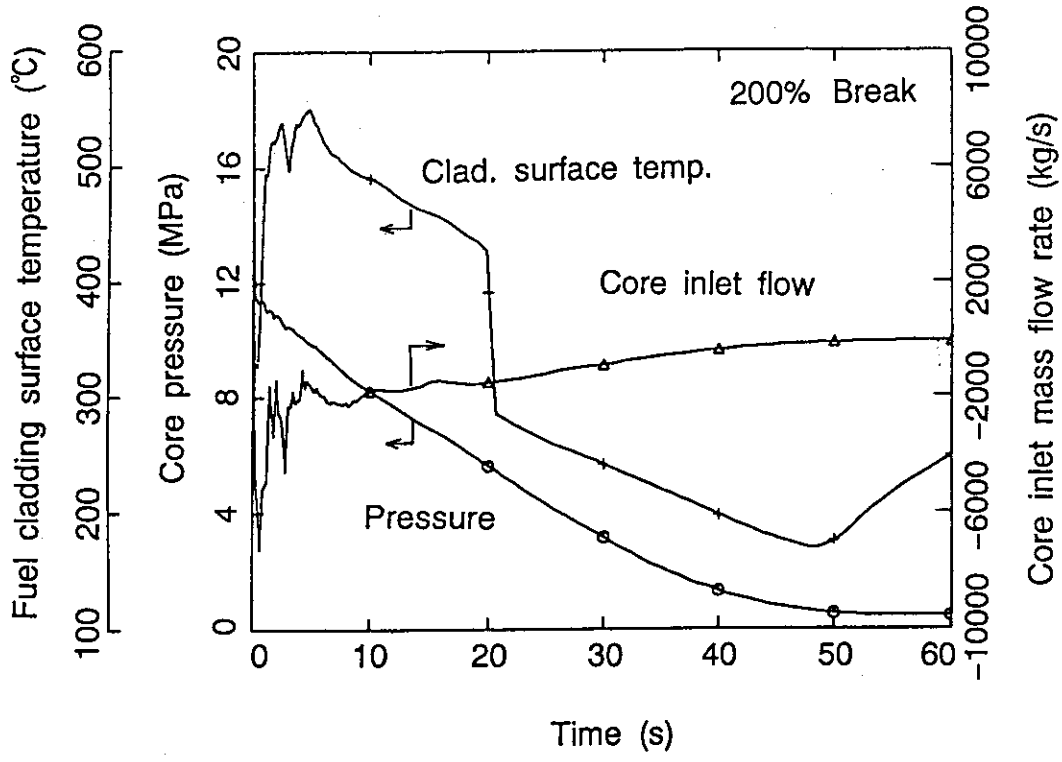

Fig.4.3.1 JPSR behaviors in 200% large break LOCA

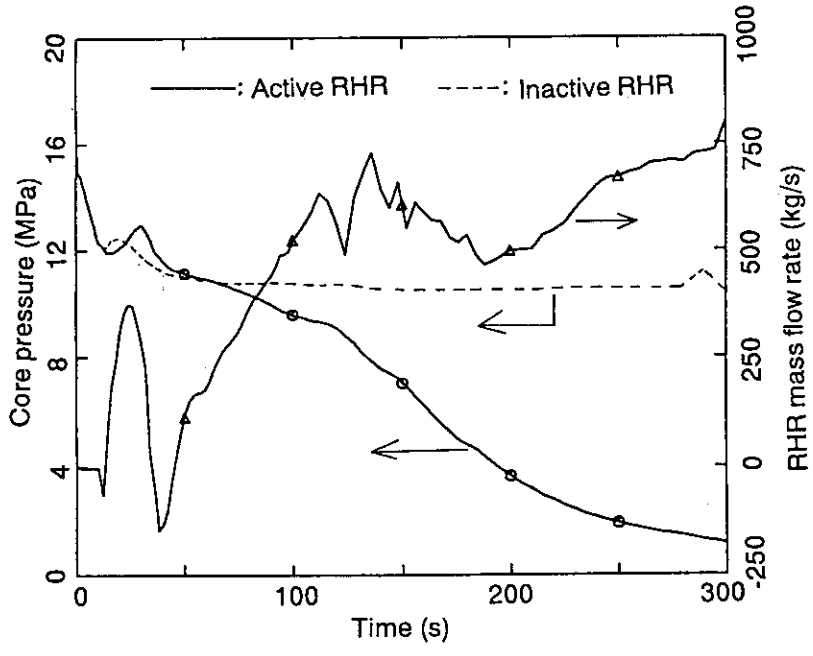

Fig.4.3.2 Effect of RHR on pressure in 5% small break LOCA

4.4 Thermal Fluid Flow Analysis in Downcomer on Residual Heat Removal Stage of JPSR

K. Kunii

The residual heat removal for the JPSR is passively performed by a natural circulation. It is important for the residual heat removal system to estimate the effect of the three-dimensional thermal fluid flow in annulus downcomer on the density difference to drive the natural circulation. The numerical analysis has been performed taking account of the downcomer being a three-dimensional annulus flow pass different from one-dimensional one. The purposes of the present analysis are to confirm: (i) the applicability of one-dimensional approximation to three-dimensional thermal fluid flow in downcomer assumed on the preliminary design of the passive residual heat removal system[1], (ii) the ability in achievement of an enough driving-force of the natural circulation to remove the residual heat.

The three-dimensional numerical calculation code, STREAM, was adopted to analyze the flow pattern and temperature distribution in downcomer. Boundary conditions were set as follows: free slip and adiabatic change on wall, free outlet, additional flow pass and perforated plate corresponding to the lower plenum with drag to flow.

Figures 4.4.1(a) and (b) show flow field and temperature distribution in case of inlet flow velocity V_{in}=1.0 m/s at a quasi-steady time after inlet starts into downcomer t=168 s. The flow pattern shows multi-dimensionality because axial-symmetric vortexes in heights of the downcomer arise. The temperature distribution becomes almost uniform though the temperatures in the both sides are slightly colder than in the middle. Figure 4.4.2 shows variation of driving-force ratio (R_d) with time in any cases of V_{in}. The R_d is introduced to estimate the density difference in downcomer, i.e.,

$$R_d = \frac{1}{V}\int_V \left(\frac{\rho'}{\rho'_{max}}\right) dV$$

where, ρ' ; density difference between present and initial states

ρ'_{max}; density difference between inlet and initial states

V ; volume of downcomer effective to generate density difference

The R_d in any case of V_{in} increases up to about 0.9 where quasi-steady state is almost achieved shown in Fig.4.4.2. It could take about 1 min to achieve the required driving-force in case of V_{in}=2.5 m/s and about 6 min in case of V_{in}=0.5 m/s. Figure 4.4.3 shows the R_d with non-dimensional time tV_D/L_D, where V_D ; average velocity in horizontal cross-section of downcomer (=$0.156V_{in}$), L_D ; heights from inlet to the near-edge of downcomer effective to generate the density difference, i.e., tV_D/L_D is referred as a variable in proportion to time-integrated coolant amount. It is found that the R_d in any cases of V_{in} can be expressed as a functional curve (broken line) with time-integrated coolant amount not dependent only on V_{in} and that the difference exists between the functional curve and bold line referred as the case assuming inlet coolant flows down in stratified state in downcomer close to the case of the preliminary design[1].

The following conclusions were obtained by the three-dimensional numerical analysis in downcomer under the conditions with various inlet flow rates: (1) Flow pattern in downcomer shows remarkable multi-dimensionality especially in case of lower inlet flow rate while the temperature distribution does not deviate from uniform one so much. Therefore the approximation of the one-dimensional is possible only for temperature distribution. (2) It can be expected to obtain the enough driving-force at a steady state in any case of inlet flow rate as assumed in the preliminary design[1]. (3) The driving-force in any case of inlet flow rate can be estimated as the functional curve with the time-integrated coolant amount.

Reference

1) Iwamura T. and Murao Y.: JAERI-Review 94-009 (1994).

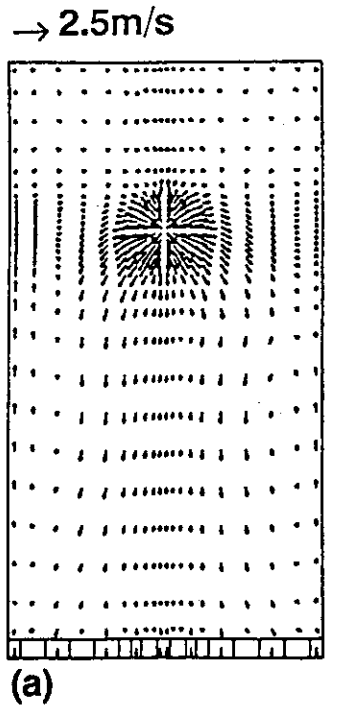

Fig.4.4.1 Fow field and temperature distribution in case of V_{in}=1.0m/s, t=168sec, △T=−9.5K

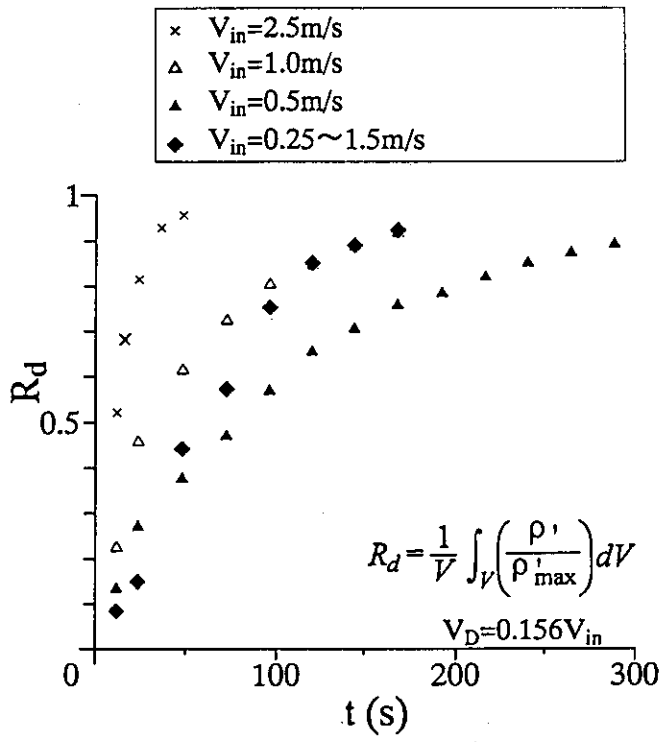

Fig.4.4.2 Variation of driving-force ratio with time in case of V_{in}=0.25~2.5m/s

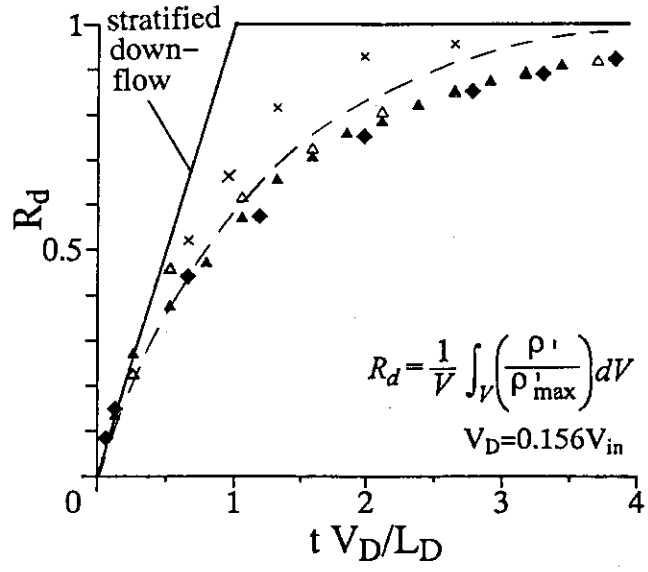

Fig.4.4.3 Variation of driving-force ratio with non-dimensional time in case of V_{in}=0.25~2.5m/s

4.5 Study on Passive Safety Systems

Y. Murao, F. Araya and T. Iwamura

A concept of JAERI Passive Safety Reactor (JPSR) system has been developed for reducing manpower in operation and maintenance and influence of human errors on reactor safety. More detailed information on the JPSR design was reported in reference 1). The view graph of major systems consisting JPSR around the reactor containment is shown in Fig.4.5.1. Based on analysis results carried out until now, a passive heat removal system and a passive coolant injection system were improved as described below. A concept of improved passive safety systems is shown in Fig. 4.5.2.

Passive Heat Removal Systems

Analysis result with the Probabilistic Safety Assessment (PSA) methodology on JPSR showed that the core damage frequency was not low enough for loss-of-offsite power accidents. Based on the result, the passive safety systems were improved as follows. A residual heat removal system (RHR) D shown in Fig. 4.5.2 is newly added to JPSR. An inlet side of the primary side of RHR D is connected to the pressurizer at a certain level. An outlet side is connected to a hot leg C which is not connected to the pressurizer. Since a water level in the pressurizer increases in a transient that heat removal rate is not enough, a natural circulation flow circuit E-B-A-D-C-E is formed when the water level reaches to and over the level of inlet pipe of RHR D. The natural circulation causes heat removal from the primary system and depressurization of the primary coolant loop. The reactor core is cooled by heat exchange between the core region and the upper plenum. Each of the RHR heat exchangers F and G, which are already adopted in the pervious design and installed between the hot legs of B and C and the cold legs H and I, was changed to be actuated by an active valve J only. These RHR heat exchangers also have roles of a backup system of the RHR D, as a system for enhancing depressurization of the primary system in small break LOCA conditions and a RHR in shutdown conditions. The secondary side of each heat exchanger F and G is connected to and cooled by each of gravity driven coolant injection pools K and L, respectively. An inlet and outlet of secondary side on the RHR D are connected to the gravity driven pools K and L, respectively. Therefore the heat generated in the core is transferred to the pools. The heat stored in the pool is removed by pool water cooling systems with natural circulation of water and transferred to the atmosphere outside of the containment by air coolers. The cooling capability is enhanced by stacks of air cooler set outside the containment.

Passive Coolant Injection Systems

In the pervious design, the core make-up tank was installed for maintaining water level in the core in late phase of a blowdown phase in LOCAs. As reported in Section 4.2, it was found that initiation of coolant injection was delayed due to subcooling of coolant in the pressure balance line and a passively actuated vale developed for the experiments did not give reliable actuation in the experiments performed. On the other hand, in the LOCA analysis described in Section 4.3, it was found that the core was cooled enough until late of the blowdown phase in large break LOCAs due to large mass inventory in the JPSR pressure vessel. Based on the experimental and analytical results, the core make-up tank was deleted from the JPSR design. In order to enhance refilling of water in the core after the blowdown, the flow controlled accumulator which was developed for MS-600[2] was adopted to JPSR. The accumulator can make the system to move to a coolant injection condition at a low flow rate without injection of Nitrogen gas to the system. After depressurization of the primary system to a containment pressure, core cooling is available by a coolant injection driven by gravity feed from the gravity coolant injection pools. When the depressurization of the primary system is not enough, a depressurization system is available to enhance the depressurization. As for small leakage from the primary system, charging pumps adopted as a non-safety system can supply coolant to the primary system.

References

1) Murao Y., Araya F. and Iwamura T., "A Concept of Passive Safety Light Water Reactor System (JPSR)", presented at ICONE-3, Kyoto, Japan (April 23-27, 1995).

2) Shiraishi T., et al., "Characteristics of the Flow-Controlled Accumulator", J of Nucl. Tech., Vol. 108, No. 2, Nov. 1994.

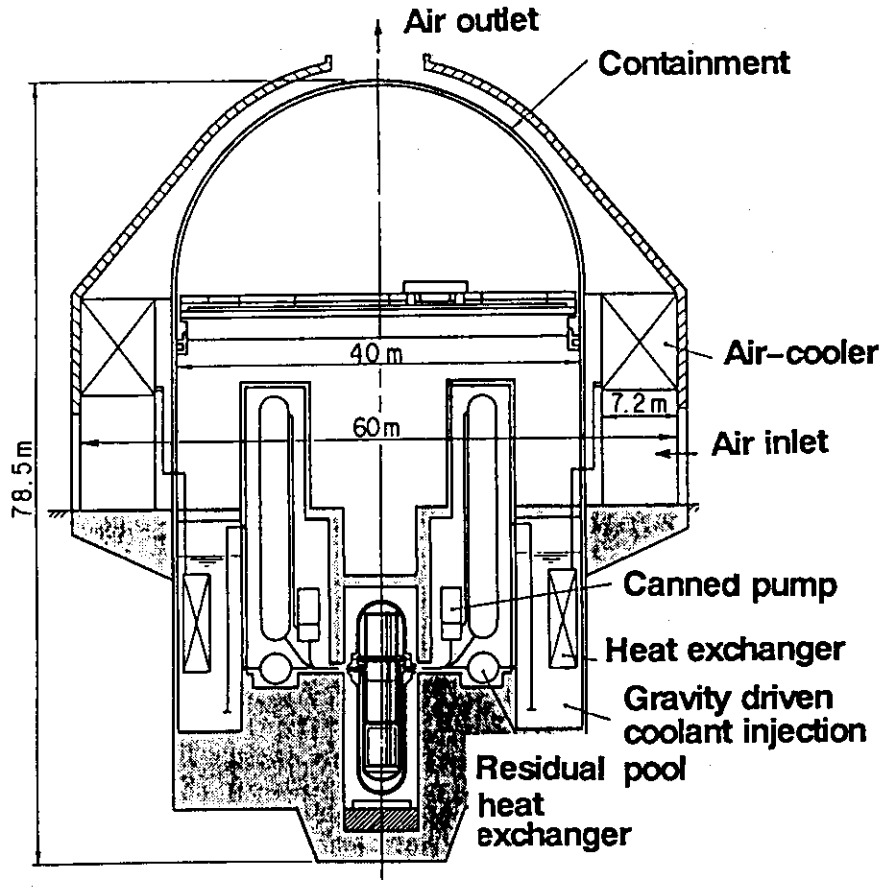

Fig.4.5.1 Plant image of JPSR

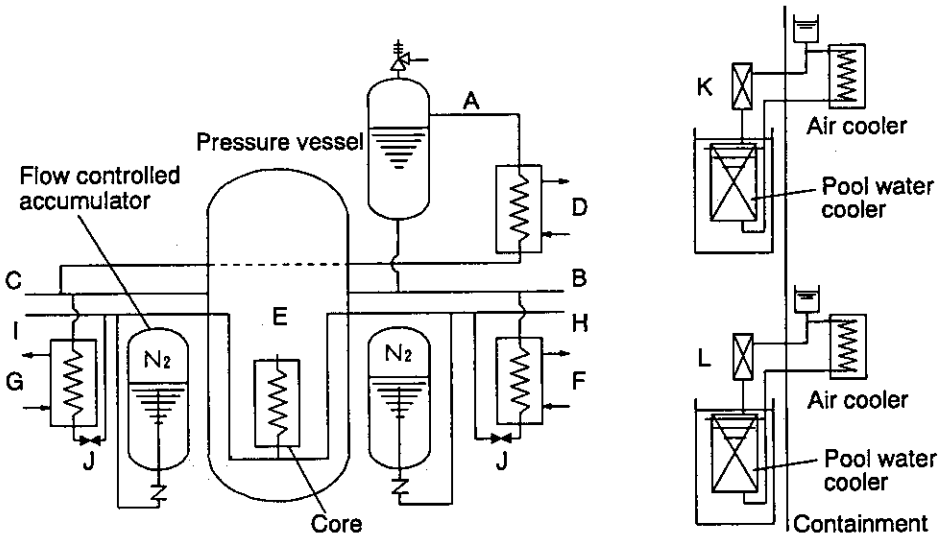

Legend	
A : Pressurizer	D : RHR heat exchanger newly adopted
B,C : Hot leg	F,G : RHR heat exchanger originally adopted
H,I : Cold leg	J : Actively opening valve
E : Upper plenum	K,L : Gravity driven injection pool

Fig.4.5.2 Flow diagram of passive engineered-safety-featured-system

4.6 Review of Improved Design of JPSR with PSA Methodology

T. Iwamura, F. Araya and Y. Murao

A simplified probabilistic safety assessment (PSA) method was used to assist in the design improvement of the JAERI passive safety reactor (JPSR)[1]. The first phase PSA was performed to clarify safety features and identify vulnerabilities of the original JPSR design.

Based on the first phase PSA results, it was clarified that the improvement of passive residual heat removal (RHR) system is the most efficient way to reduce the total core damage frequency (CDF). Then the designs of safety systems have been revised to improve plant safety by resolving the identified vulnerabilities as follows: 1) The core makeup tank system was removed from the safety injection systems. This simplification was also justified by the thermal-hydraulic analyses[2] for large break LOCA events and experiment[3] for the core makeup tank system. 2) An additional RHR loop for non-LOCA event was installed between the pressurizer and the hot leg which is not connected to the pressurizer. The new RHR loop has no valves and the natural circulation cooling is actuated by increasing the water level in the pressurizer due to the increase of primary water temperature. The secondary side of the RHR heat exchanger is cooled by the natural circulation of water in the gravity coolant injection pool. 3) The passive valves are excluded from the lower RHR loops for simplification. Instead, a motor-operated valve and an air-operated valve are installed in parallel to avoid common cause failure. Figure 4.6.1 shows the modified flow diagram of primary system and passive safety systems.

The second phase PSA was performed for the modified design by the following procedure: 1) The safety design features were classified. 2) Initiating events were selected by using failure mode and effect analysis (FMEA) and considering past PSA results. The selected initiating events are: large break LOCA, medium break LOCA, small break LOCA, steam generator tube rupture (SGTR), main steam line break, loss of offsite power, loss of feed water, and other transients. 3) Accident mitigation systems were identified and core damage sequences were constructed. 4) Success criteria were determined. 5) System unavailabilities were estimated by fault tree analyses considering the features of passive safety components. Component failure data used for the fault trees are determined by referring conventional plant data. Common cause failures are taken into account with the beta-factor method. 6) Event trees were constructed and quantified for each initiating

event.

This process has been taken repeatedly to meet the safety goal which gives enough low CDF in comparison to a current PWR. The CDFs for the improved design are compared with the original values in Fig.4.6.2. The annual frequencies of initiating events are also shown in this figure. The total CDF for the improved design was evaluated to be 4.2 X 10^{-8} /RY (reactor year) which was decreased by three orders of magnitude from the original design. The dominant initiating event that could lead to core damage was the small break LOCA and the dominant sequence was the failure of passive RHR system. The effect of design changes on the CDFs initiated by the LOCA events is very small because the elimination of core makeup system has little effect on the CDF. On the other hand, the CDFs induced by the SGTR and non-LOCA events are significantly reduced from the original design. This is due to the fact that the failure probability of RHR system becomes four orders in magnitude smaller than the original value by adding the upper RHR loop to the original RHR system. It should be noted that the contribution of high frequency events such as various transients including loss of offsite power to CDF could be significantly reduced by the design modification.

Sensitivity studies were performed to evaluate the effects of uncertainty in the safety system unavailability data and in the beta factor used in common mode failure evaluation. The effect of design alternatives, in which passive systems were replaced by corresponding active systems, was also evaluated. The results indicated that the modified JPSR design has enough safety margin. It was also concluded that the total CDF for the modified JPSR is less than that for a conventional PWR (1.6 X 10^{-7}/RY)[4].

References

1) Murao,Y., et al.: A Concept of JAERI Passive Safety Light Water Reactor System (JPSR), ICONE-3, Kyoto pp.723-728 (1995).

2) Araya,F., et al.:Transient Thermal-Hydraulic Analyses for Design of JAERI Passive Safety Reactor (JPSR), ICONE-3, Kyoto pp.1011-1016 (1995).

3) Araya,F.,et al.: Study on Concept of JAERI Passive Safety Reactor (JPSR) (15) - Thermal Hydraulic Experiment on Core Make-up Tank-, Annual Meeting of Atomic Energy Society of Japan, Tokyo, D32 (1995).

4) Hirano, M., et al.: Recent Results of Level 1 PSA for Nuclear Power Plant in Japan, CSNI Workshop on PSA Application and Limitation, NUREG/CP-0115 (1991).

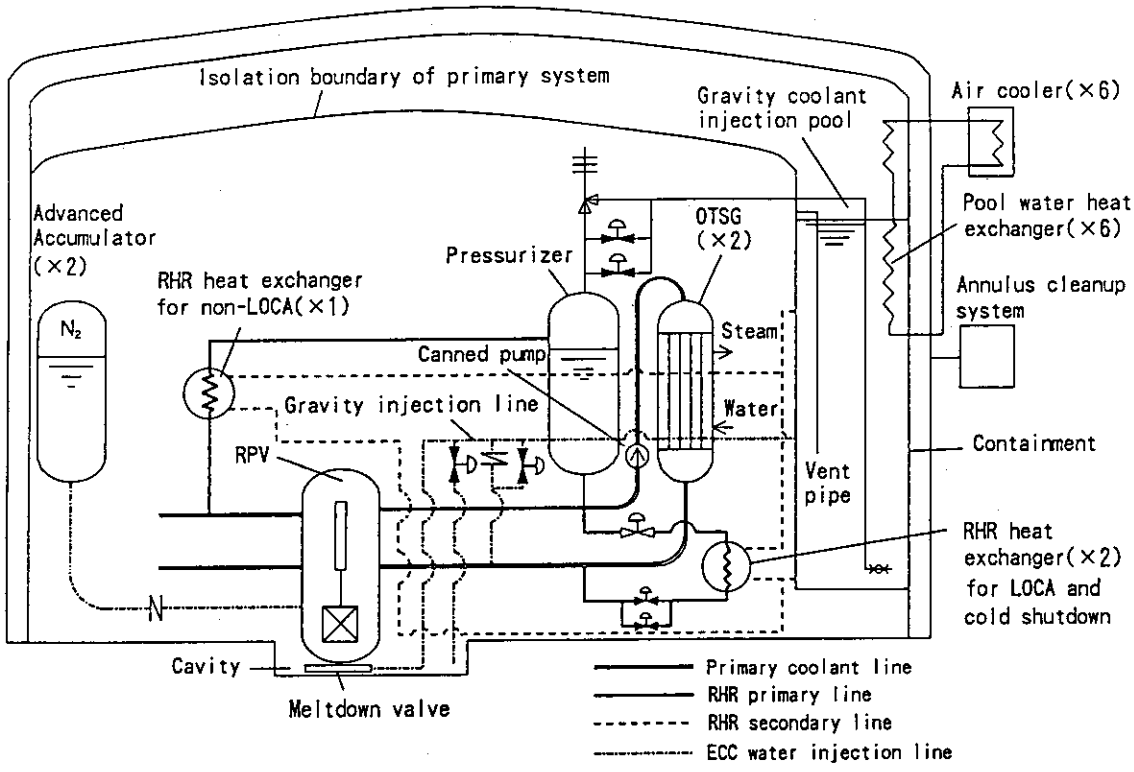

Fig.4.6.1 Flow diagram of primary system and passive safety system for improved JPSR

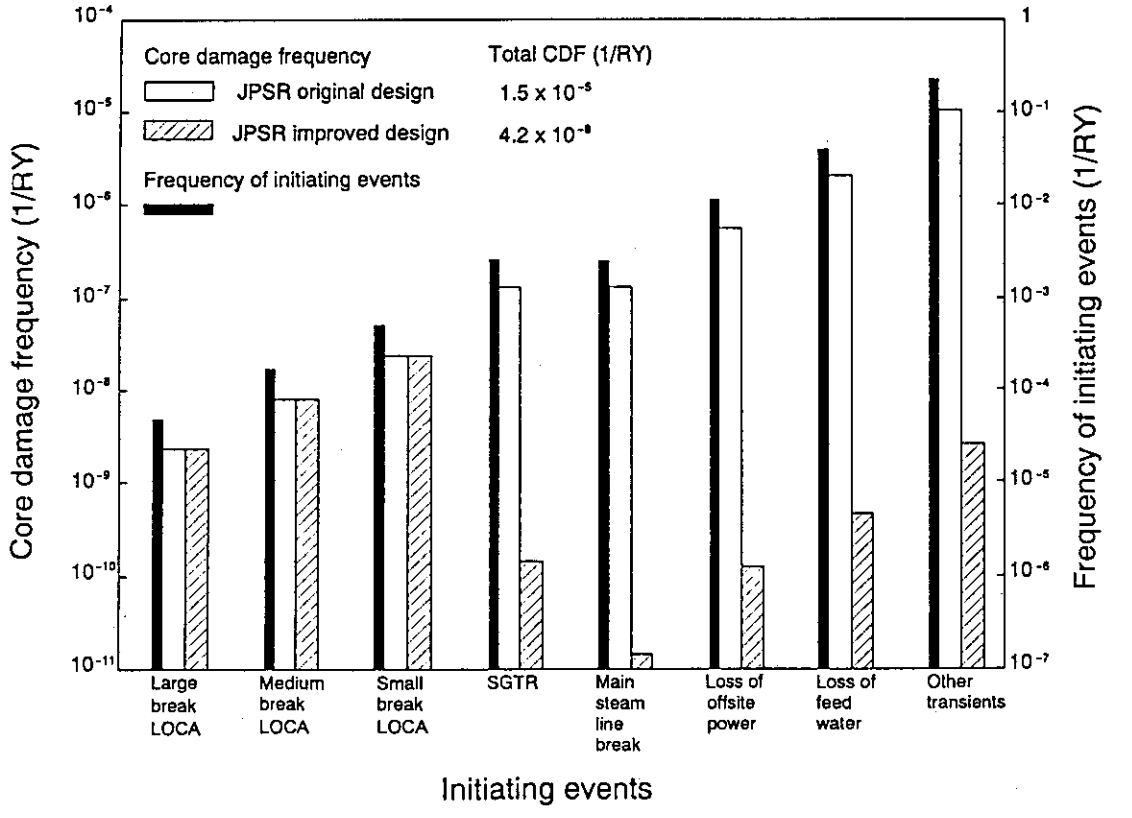

Fig.4.6.2 Comparison of core damage frequencies between original and improved JPSR designs and annual frequencies of initiating events

4.7 Analysis of ATWS Sequences in Lead Cooled Fast Reactor

H. Akie, H. Takano, Y.Tanaka* and K. Kaneko**

A fast reactor concept with lead coolant and nitride fuel has been studied to improve reactor safety, plant cost, uranium resource utilization and fuel cycle cost in sodium cooled MOX fuel fast reactors. We proposed a reactor design with small void and burnup reactivities, and integrated tank-type system[1]. Analyses of ATWS events of this reactor were made.

The analyzed ATWS events are unprotected loss of flow(ULOF), unprotected transient over power(UTOP) and unprotected loss of heat sink(ULOHS). In these analyses, fuel, cladding and coolant temperatures were calculated for peak power channel in the core, and compared with the limits of nitride fuel melting point(~2900°C), nitride fuel thermal decomposition temperature(~1900°C), steel cladding melting point(~1400°C) and lead coolant boiling point(~1700°C).

The results of ULOF analysis are summarized in Table 4.7.1. In this analysis, coolant flow rate was assumed to decrease to 10 or 15% of nominal with the flow coastdown time of 10~50 seconds. As shown in the table, coolant temperatures are 900~1100°C and they are below enough the boiling point in all cases. The peak fuel temperatures are also less than the melting point.

Table 4.7.1 Coolant and fuel peak temperatures calculated for different coolant flow rates and flow coastdown time of ULOF event

Flow rate (%)	Coastdown time (sec)	Coolant peak temperature (°C)	Fuel peak temperature (°C)
15	10	1024	1106
15	20	966	1043
15	30	934	1008
15	50	901	971
10	10	1107	1146

* Advanced Reactor Technology Co., Ltd., Tokyo

** The Japan Research Institute, Ltd., Tokyo

In the UTOP event, there was a larger temperature increase. Table 4.7.2 shows the reactor power levels and fuel peak temperatures obtained for different reactivities inserted and reactivity feedbacks caused by control rod thermal expansion. It is shown in the table that the fuel temperature exceeds the melting point without the control rod reactivity feedback. Even with the standard reactivity feedback, which was estimated referring to sodium cooled reactors' design, the reactor power level increases more than 200% of operation condition. However, the fuel peak temperature is lower than the melting point and there is enough margin. In the ULOHS analysis, though the coolant temperature increases up to about 730°C after 30 minutes, it is far lower than the coolant boiling temperature.

Table 4.7.2 Core power level and fuel peak temperature in UTOP event and dependence on inserted reactivity and reactivity feedback by control rod thermal expansion

Reactivity insertion (¢)*	Reactivity feedback by control rod thermal expansion	Power (%)	Fuel peak temperature (°C)
70	none	~400	> melting point
35	none	~250	> melting point
35	standard**	~216	1340
35	×10	~192	1250
35	×60	~140	1080

* : 3¢/sec. insertion rate,
** : standard reactivity feedback evaluated referring to Na cooled reactors' design

From these analyses, it is confirmed that the lead cooled nitride fuel fast reactor has enough safety in ULOF and ULOHS transient accidents. In the view point of longer term, however, there would be cladding damage under high temperature, and hence an operator's action will be necessary to avoid the damage. In the UTOP event, it seems to need an mechanism which introduces more than 10 times of negative reactivity feedback of standard control rod thermal expansion. Another solution for UTOP event behavior is to reduce the reactivity insertion. In the present design of the reactor core(Fig. 4.7.1), the central control rod has a worth of more than 30¢. If the worth of the rod is distributed to another six rods, each rod worth becomes only about 5¢. Therefore, it is possible to reduce the reactivity insertion by one rod to about 10¢, even taking into account interference effect between control rods. As for the UTOP event behavior, the core design should be improved so as to have small control rod worth and negative void reactivity.

Reference

1) Takano H., et al. : "A Design Study for Inherent Safety Core, Aseismicity and Heat Transfer System in Lead-Cooled Nitride-Fuel Fast Reactor", Proc. Int. Topical Mtg. on Advanced Reactors Safety (ARS'94), April 1994, Pittsburgh, U.S.A., pp.549-566 (1994).

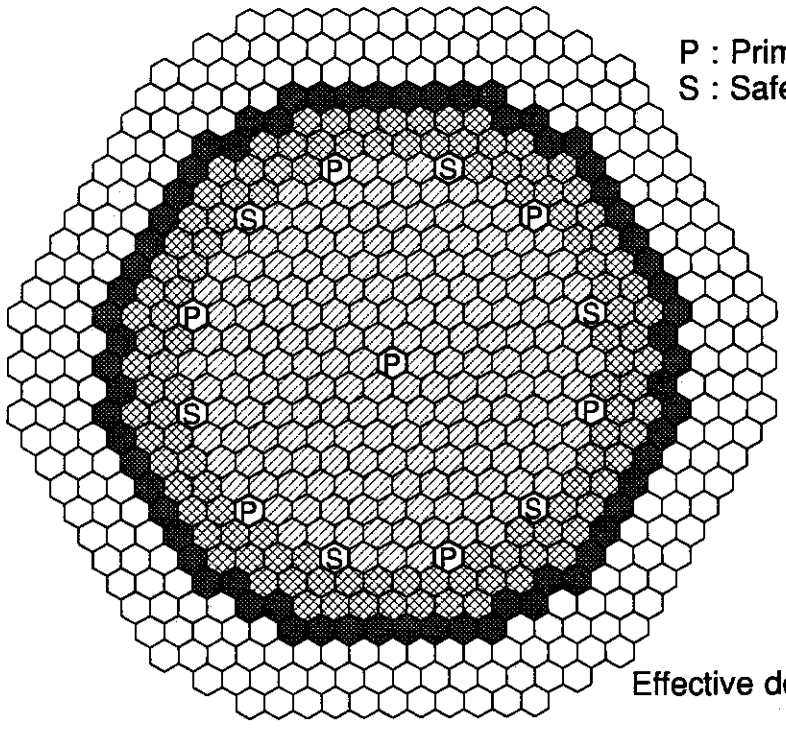

Effective delayed neutron fraction (%)	0.438
Burnup reactivity (%dk/kk')	0.137
Reactivity controlled by central rod (¢)	31.3
1/6 reactivity of central rod (¢) with interference effect	5.2 10.4

Fig. 4.7.1 Control rod arrangement in the lead cooled reactor core and control rod worth

5. Fusion Neutronics

Bulk shielding experiments and analyses on the SS316/H_2O configuration were conducted as the major part of T-16 Task under ITER/EDA R&D framework. Special attention was paid on the reduction of background at deep location of the experimental assembly, which was due to the room returned neutrons. Adding a shield with polyethylene /water on the rear part of assembly, further experimental measurements were carried out for the responses which are sensitive to the low energy neutrons. The validity of experimental data was demonstrated with ± 10 % accuracy up to 950 mm depth. The development of experimental technique was also carried out on the nuclear heating and induced radioactivity measurements as sub-Tasks of T-16. In particular, the algorithm for the induced radioactivity calculation under a pulsed mode operation was experimentally verified by the present experiment. The review meeting of T-218 Task for '95 and '96 ITER R&D was held at ENEA Frascati, Italy. According to the agreement, a series of streaming experiments is to be conducted at JAERI.

Endeavor for establishing FENDL library was continued in conjunction with JENDL-3.2 data validation. Both results for neutron and γ-ray integral tests based on the experimental data taken at FNS were the major contributor in the data validation. A new benchmark experiment was performed on iron and tungsten materials with particular emphasis on the low energy neutron spectrum and associated secondary γ-ray spectrum. On the FENDL activation library, also extensive data validation was performed with use of integral experimental data provided by FNS group. As the new international collaboration on the Fusion Neutronics under IEA, four research items were identified among Japan, US, EU and Russia and agreed to initiate all activities in 1995. The γ-ray spectrum measurement technique was established by using a C_6D_6 liquid scintilator. A novel method for the low level tritium counting with the liquid scintilator was developed by optimization of the solvent fraction with the best figure of merit in terms of effective counting efficiency. In conjunction to the low level counting scheme development, a Cherenkov counting system for the ^{31}P activities was proposed and demonstrated its feasibility in the neutron dosimetry featuring high counting efficiency.

Benchmark experiments on the characteristics of ^{16}N radioactivity production in the flowing water exposed to 14 MeV neutrons and high energy γ-ray transmission measurements for SS304 and Cu associated with ^{16}N decay were carried out. The results gave rise to a serious concern on the additional radiation source to dose around TF coils in ITER. It was suggested that a further examination should be addressed. The activated water, however, was found to provide potential applications in terms of a radiography with high energy γ-rays, a liquid flow dosimetry, a photo-fission detector, etc. In order to meet a strong request for various application, a heavy irradiation with 14 MeV neutrons was conducted at FNS. Total neutron yield was 1.2×10^{18} after the 160 hours operation.

5.1 Bulk Shielding Experiment on a Large SS316/Water Assembly

C. Konno, F. Maekawa, Y. Ikeda, Y. Oyama, Y. Uno, Y. Verzilov, M. Wada and H. Maekawa

The combination of type 316 stainless steel (SS316) and water is one of the most promising candidates for the shielding blanket and vacuum vessel of International Thermonuclear Experimental Reactor (ITER). Experimental data on the shielding performance of SS316/water are, however, very few limited for validation of current design calculation accuracy. A bulk shielding experiment on SS316/water[1),2)] has been performed at the Fusion Neutronics Source (FNS) facility according to the task agreement for the '94 ITER/EDA R&D T-16.

The experimental assembly consisted of the source reflector of 0.2 m-thick SS316 and the test region which had a layered structure of SS316 and water as shown in Fig. 5.1.1. The total volume ratio of water to SS316 was adjusted to be 1 : 4 in the region to 940 mm depth in the test region and the local volume ratio decreased with the depth. Water tanks or polyethylene blocks of about 150 mm in thickness surrounded[1)] the rear part of the test region as shown in Fig. 5.1.1, to reduce room-returned background neutrons. The experimental data for neutron spectra in energy regions of MeV, keV and eV, neutron activation reaction rates such as $^{93}Nb(n,2n)^{92m}Nb$ and $^{197}Au(n,\gamma)^{198}Au$, fission rates of ^{235}U and ^{238}U, gamma-ray spectra and gamma-ray heating rates of SS316 were taken at the positions from the front surface to the depth of 914 mm in the test region.

The calculation of the experiment[2)] was performed using the Sn code DOT3.5 (P_5 expansion, S_{16} quadrature) and the Monte Carlo code MCNP-4. The cross section libraries for DOT3.5 were FUSION-J3[3)], FUSION-40[3)] and JSSTDL[4)], which were produced from JENDL-3.1, while those for MCNP-4 were FSXLIB-J3[5)] and FSXLIB-J3R2[6)] from JENDL-3.1 and JENDL-3.2, respectively. Table 5.1.1 defines the abbreviations of the calculations corresponding to the codes and libraries adopted.

All calculations agree with the measured neutron flux above 10 MeV within ± 10 %. As for the neutron flux from 10 keV to 1 MeV, the discrepancy between the measurement and calculation is at most ± 20 % except for the cases with DOT-F125 and DOT-F42 which underestimate the measurement by more 10 %. Figures 5.1.2 and 5.1.3 show the ratios of the calculated to the measured data (C/E) of fission-rate of ^{235}U and gamma-ray heating rate of SS316, respectively. MCNP-J31, MCNP-J32, DOT-J125 and DOT-J42 agree with the measured fission rate of ^{235}U within 25 %, except for the data on the front surface, where DOT

calculations overestimate by 50 %. The overestimation in DOT calculations is due to larger cross section of ^{235}U(n,fission) reaction in the thermal group. DOT-F125 and DOT-F42 underestimated the measured fission rate of ^{235}U by 40 - 50 % at the depth of 914 mm. This is mainly caused by the cross sections without self-shielding treatment. The calculated gamma-ray heating rates of SS316 by JENDL-3.1 show the similar C/E trend each other; the C/Es are 1.3 - 1.5 to the depth of 450 mm, while they decrease with the depth at the rear region. The difference between JENDL-3.1 and -3.2 is remarkable in the gamma-ray heating rate of SS316, where the C/Es of MCNP-J32 become better by about 15 % than those of MCNP-J31.

References

1) Konno C., et al. : "Bulk Shielding Experiments on a Large SS316/Water Assembly bombarded by D-T Neutrons, Volume I : Experiment", JAERI-Research 95-017 (1995).
2) Maekawa F., et al. : "Bulk Shielding Experiments on a Large SS316/Water Assembly bombarded by D-T Neutrons, Volume II : Analysis", JAERI-Research 95-018 (1995).
3) Maki K., et al. : "Nuclear Group Constant Set FUSION-J3 for Fusion Reactor Nuclear Calculations based on JENDL-3", JAERI-M 91-72 (1991, in Japanese).
4) Hasegawa A. : "JSSTDL 295n-104γ; a Common Nuclear Group Cross-Section Library Based on JENDL-3 Nuclear Data File", Proceedings of the second Specialists' Meeting on Nuclear Data for Fusion Reactors, JAERI-M 91-062 (1991) pp. 15-25.
5) Kosako K., et al : "FSXLIB-J3 : MCNP Continuous Energy Cross Section Library Based on JENDL-3", JAERI-M 91-072 (1991) (in Japanese).
6) Kosako K., et al : "FSXLIB-J3R2 : A Continuous Energy Cross Section Library for MCNP Based on JENDL-3", JAERI-Data/Code 94-020 (1994).

Table 5.1.1 Summary of the calculation codes and nuclear data libraries.

Abbreviation	Code	Transport cross section library	Self-shielding
DOT-F125	DOT3.5	FUSION-J3(JENDL-3.1, n:125group, γ:40group)	uncorrected
DOT-F42	DOT3.5	FUSION-40(JENDL-3.1, n:42group, γ:21group)	uncorrected
DOT-J125	DOT3.5	JSSTDL(JENDL-3.1, n:125group, γ:40group)	corrected
DOT-J42	DOT3.5	JSSTDL(JENDL-3.1, n:42group, γ:21group)	corrected
MCNP-J31	MCNP-4	FSXLIB-J3(JENDL-3.1)	———
MCNP-J32	MCNP-4	FSXLIB-J3R2(JENDL-3.2)	———

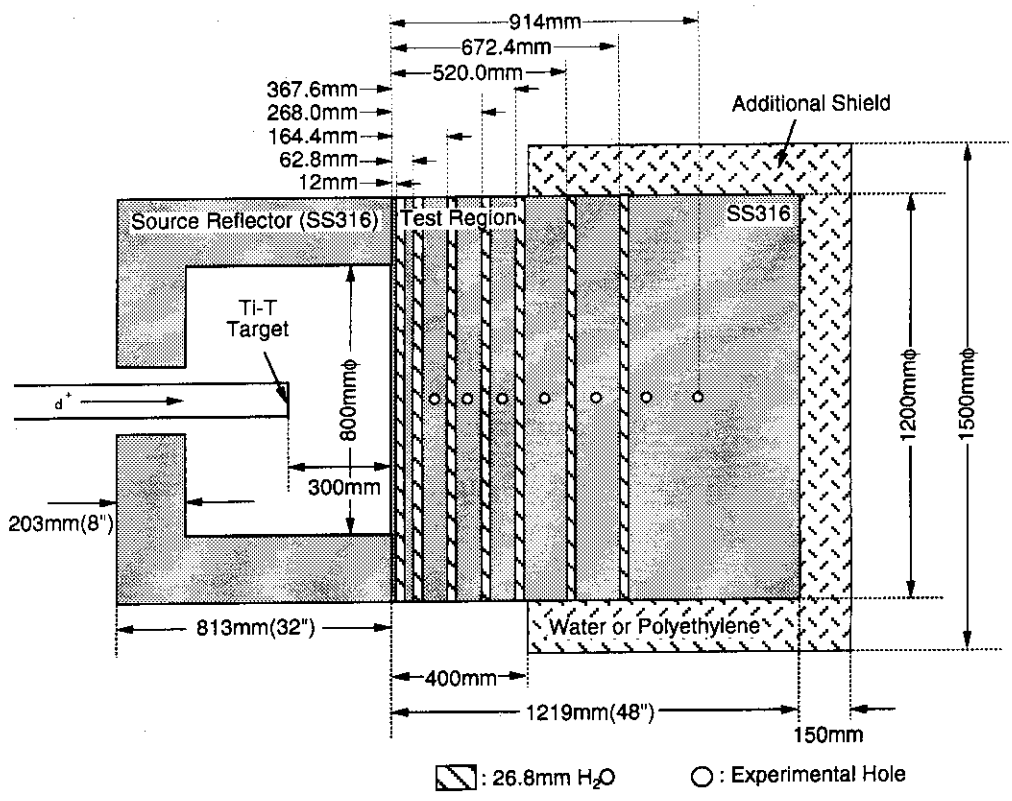

Fig. 5.1.1 Experimental Assembly.

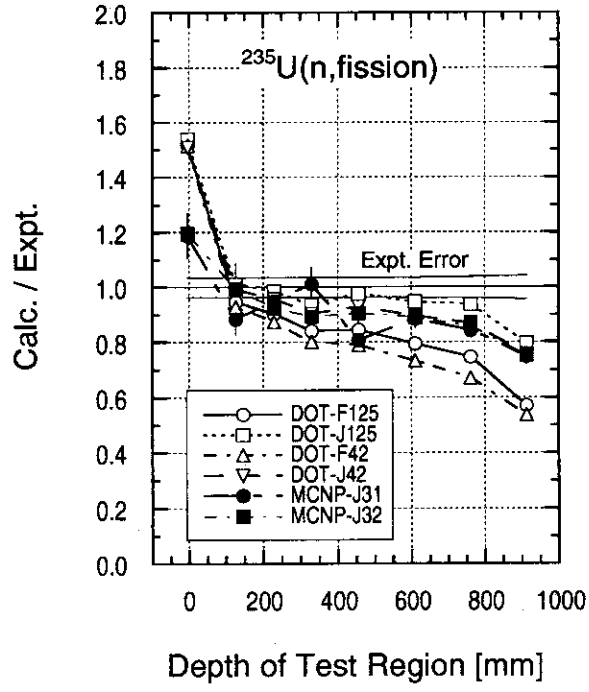

Fig. 5.1.2 Ratio of measured and calculated fission rate of ^{235}U.

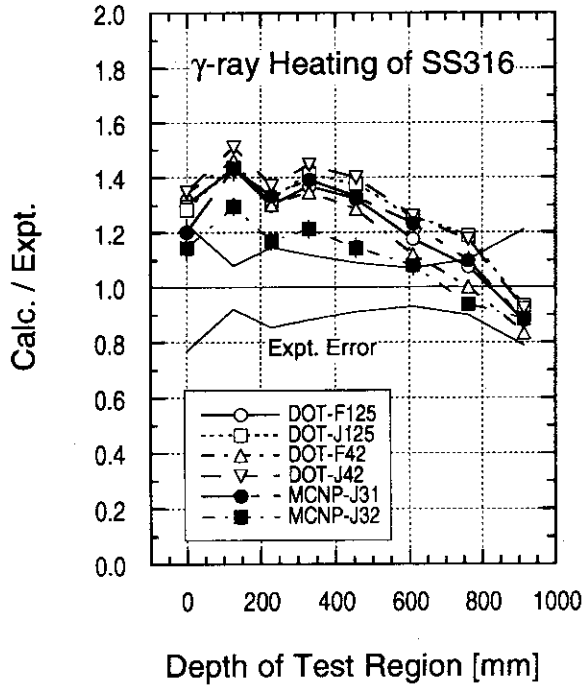

Fig. 5.1.3 Ratio of measured and calculated gamma-ray heating rate of SS316.

5.2 Reduction of Room-returned Background in SS316/water Bulk Shielding Experiment

C. Konno, F. Maekawa, Y. Ikeda, Y. Oyama, Y. Uno, M. Wada and H. Maekawa

It was found from the preliminary bulk shielding experiment[1] of type 316 stainless steel (SS316) and water that room-returned background neutrons significantly affected the experimental data associated with low energy neutrons below 1 MeV and gamma-rays in the test region deeper than 700 mm. In order to reduce room-returned neutrons as much as possible, the survey calculations[2] by DOT-DD[3] with DDXLIB-J3[3] were performed and necessary additional shield was determined. Figure 5.2.1 shows the calculation model. Two cases were examined : one was a thicker source reflector to reduce leakage neutrons from the source reflector, and the other was to put a polyethylene surrounding the rear part of the test region to reduce incoming background neutrons. The thicker (400 mm in thickness) source reflector reduced the background only by a half (signal to background ratio [S/N] $\approx$ 1), but the polyethylene shield of 100 mm in thickness for the rear part of the test region was found to be very effective (S/N $\geq$ 10). Thus the final experimental assembly was determined as shown in Fig. 5.1.1 of Sec. 5.1, where the thickness of the additional shield was adopted to be 150 mm considering a margin due to calculation uncertainty.

Figures 5.2.2 and 5.2.3 show the measured neutron flux from 10 keV to 1 MeV, fission rate of ^{235}U, reaction rate of ^{197}Au(n,γ)^{198}Au reaction and gamma-ray heating rate of SS316 in the SS316/water assembly with and without the additional shield. These figures indicate clearly that the additional shield reduces the background effectively.

For the benchmark experiment, it is needed to quantify the amount of background. The fission rate of ^{235}U was adopted for estimating room-returned background neutrons since the most of room-returned background neutrons were expected to be less than 1 MeV and the response of ^{235}U(n,fission) has large sensitivity to low energy neutrons. Tungsten blocks of 102 mm in thickness were attached on the surface of the test region to reduce the fast neutron flux reaching to the regions of interest directly from the source. The ratios of the measured fission rate with the tungsten blocks to those without the tungsten blocks were shown in Table 5.2.1. The ratios in the region between 400 mm and 800 mm are almost the same (the average is 0.266). This reason is that the attenuation coefficient for fission rate of ^{235}U is almost constant in the deep positions. Hence, if there are no background neutrons from outside, the ratio at the depth of 914 mm was also expected to be 0.266. The ratio of 0.321 means that the measured data at 914 mm include background neutrons. If the fission rate by

background neutrons is defined as x, the following equation can be satisfied.

$$\frac{1.030\times10^{-31}-x}{3.214\times10^{-31}-x}=0.266.$$

From this equation, the fission rate x by background neutrons is calculated as 2.385 x 10^{-32}. The fraction of the background is estimated to be 8 % at 914 mm, while the effect of background neutrons is considered to be negligibly small at the position of 756 mm. It should be noted that calculations tend to underestimation by about 10 % at the depth of 914 mm since the measured data which are sensitive to lower energy neutrons include background by about 10 %.

References

1) Konno C., et al. : "Bulk Shielding Experiments on a Large SS316/Water Assembly bombarded by D-T Neutrons, Volume I : Experiment", JAERI-Research 95-017 (1995).
2) Konno C., et al. : "Pre-analysis of SS316 and SS316/Water Bulk Shielding Experiments", JAERI-Tech 94-019 (1994).
3) Mori T., et al. : "One-, Two and Three Dimensional Transport Codes Using Multi-Group Double Differential Form Cross Sections", JAERI 1314 (1988).

Table 5.2.1 Measured fission rates of ^{235}U with and without tungsten blocks.

Distance from the front surface of the test region [mm]	^{235}U(n,fission) without tungsten [1/source]	^{235}U(n,fission) with tungsten [1/source]	Ratio of ^{235}U(n,fission) with to without tungsten blocks
127	2.40E-27	1.64E-27	0.682
229	9.92E-28	3.85E-28	0.388
330	3.63E-28	1.09E-28	0.299
457	4.39E-29	1.20E-29	0.273
610	8.84E-30	2.25E-30	0.255
762	1.55E-30	4.19E-31	0.271
914	3.21E-31	1.03E-31	0.321

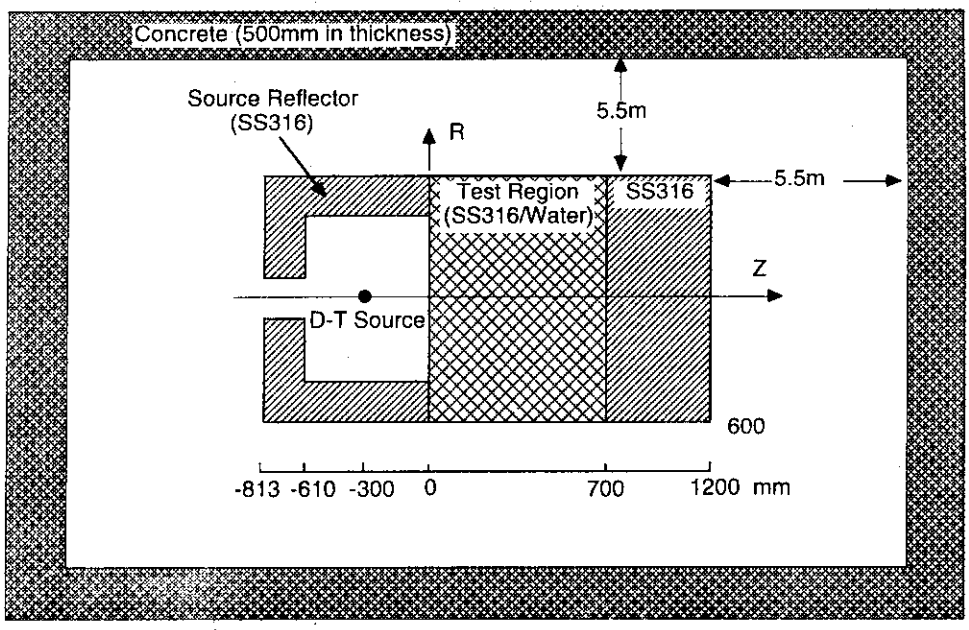

Fig. 5.2.1 Calculation model.

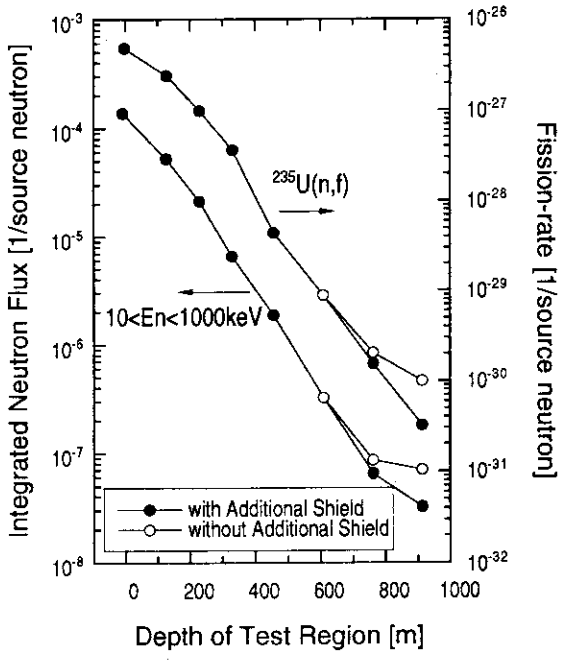

Fig. 5.2.2 Measured neutron flux from 10 keV to 1 MeV and fission rate of ^{235}U with and without the additional shield.

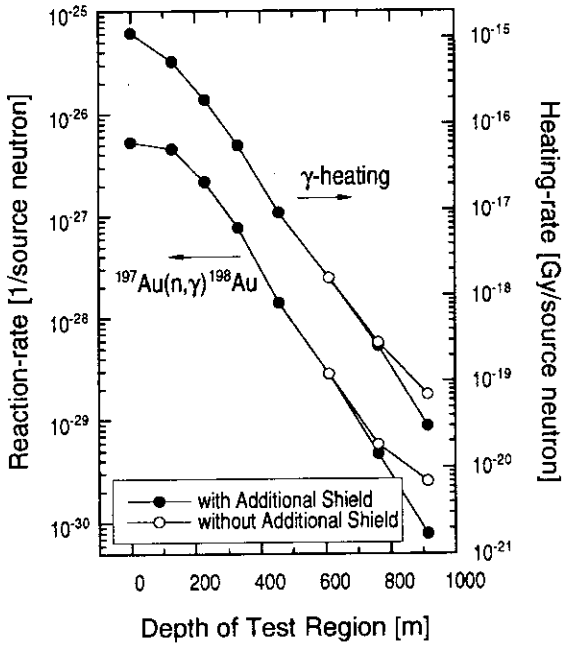

Fig. 5.2.3 Measured reaction rate of ^{197}Au(n,γ) and γ-heating rate of SS316 with and without the additional shield.

5.3 Estimation of Calculation Uncertainty on Shielding Parameters Based on SS316 and SS316/Water Bulk Shielding Experiments

C. Konno, F. Maekawa, Y. Ikeda, Y. Oyama, Y. Uno, M. Wada and H. Maekawa

The mission of the fusion reactor shielding experiments is to validate the shielding design calculations for the critical shielding parameters such as nuclear heating and damage in superconducting magnet (SCM). We estimated those parameters directly or indirectly by using the experimental data of the type 316 stainless steel (SS316) and SS316/water bulk shielding experiments[1), 2)] and identified the uncertainty in the calculations for these parameters in SS316 and SS316/water bulk shield designs.

Fast neutron flux (En ≥ 0.1 MeV), helium production of SS316, displacement per atom (DPA) of copper, and nuclear heating of copper (SCM part) and epoxyglass (electrical insulator) were selected as the critical shielding parameters, which are requested in ITER design. The parameters related to neutrons were estimated by multiplying the neutron spectra by the responses (reaction cross section data) based on JENDL-3.1. The measured spectra were used for neutrons above 10 MeV and from 10 keV to 1 MeV, while the calculated neutron spectra by MCNP-4 with JENDL-3.1 library (MCNP-J31) were adopted for the neutron spectra from 2 to 10 MeV and below 10 keV due to the insufficient experimental data. The errors of the estimated values were derived from the experimental errors and statistical errors of MCNP-J31.

Nuclear heating is produced by both neutrons and gamma-rays. Neutron heating rates were calculated by the neutron spectra and the neutron KERMA factor based on the JENDL-3.1. Gamma-ray heating rates were deduced by multiplying the measured gamma-ray heating rate of SS316 into the ratio of calculated gamma-ray heating rate of the specified material to that of SS316 by MCNP-J31.

Figures 5.3.1 and 5.3.2 show the contribution fraction of specified energy neutrons and total gamma-rays for each critical shielding parameter at the depth of 914 mm in the SS316 and SS316/water assemblies, respectively. These fractions were obtained from the neutron spectra calculated by MCNP-J31 and the responses based on JENDL-3.1. Neutron flux from 10 keV to 1 MeV and gamma-ray are dominant in the SS316 shield, while the fraction of neutron flux above 1 MeV increase in the SS316/water shield. The fraction of neutron heating rate of epoxyglass is much larger than that of copper since epoxyglass consists of light nuclei such as hydrogen, carbon and oxygen.

The estimated shielding parameters (ES) are plotted in Fig. 5.3.3 and 5.3.4. The errors of the estimated parameters were about 10 %. As for the calculations (C) by DOT3.5 and MCNP with JENDL-3.1 and -3.2 summarized in Table 5.1.1 of Sec. 5.1 on SS316 and

SS316/water bulk shield, we calculated the safety factor defined as the following equation;

Safety Factor = (ES + Error of ES) / (C - Error of C),

where, Error of C is zero in DOT calculations. The safety factors at the depth of 914 mm, the deepest position, are shown in Table 5.3.1 and 5.3.2 for SS316 and SS316/water shield, respectively. The safety factors for SS316/water are much smaller than those for SS316 and are comparable to the recommended safety factor of 1.5 in ITER/CDA[3]. Note that these safety factors are valid to only bulk shield. Overall safety factors for ITER shield will be larger than 1.5 due to the very complex structured shield of ITER. Further research is required to extrapolate the safety factors to ITER shield.

References

1) Konno C., et al. : "Bulk Shielding Experiments on Large SS316 Assemblies bombarded by D-T Neutrons, Volume I : Experiment", JAERI-Research 94-043 (1994).
2) Konno C., et al. : "Bulk Shielding Experiments on a Large SS316/Water Assembly bombarded by D-T Neutrons, Volume I : Experiment", JAERI-Research 95-017 (1995).
3) ITER Conceptual Design Report, ITER DS No. 18 (1991).

Table 5.3.1 Safety factor at the depth of 914 mm in the SS316 assembly.

	MCNP -J31	MCNP -J32	DOT -J125	DOT -J42	DOT -F125	DOT -F42
Neutron Flux [En>0.1MeV]	1.75	1.56	1.75	2.38	3.66	4.75
He production of SS316	1.60	1.49	1.54	1.62	3.15	3.39
Cu DPA	1.47	1.40	1.45	1.52	3.16	3.44
Nuclear heating of Cu	1.34	1.60	1.47	1.69	2.65	3.82
Nuclear heating of Epoxyglass	1.39	1.51	1.45	1.63	2.82	3.65

Table 5.3.2 Safety factor at the depth of 914 mm in the SS316/water assembly.

	MCNP -J31	MCNP -J32	DOT -J125	DOT -J42	DOT -F125	DOT -F42
Neutron Flux [En>0.1MeV]	1.42	1.44	1.40	1.73	1.66	2.10
He production of SS316	1.25	1.18	1.14	1.26	1.23	1.38
Cu DPA	1.34	1.33	1.27	1.38	1.49	1.66
Nuclear heating of Cu	1.43	1.42	1.29	1.31	1.37	1.45
Nuclear heating of Epoxyglass	1.33	1.32	1.25	1.37	1.42	1.59

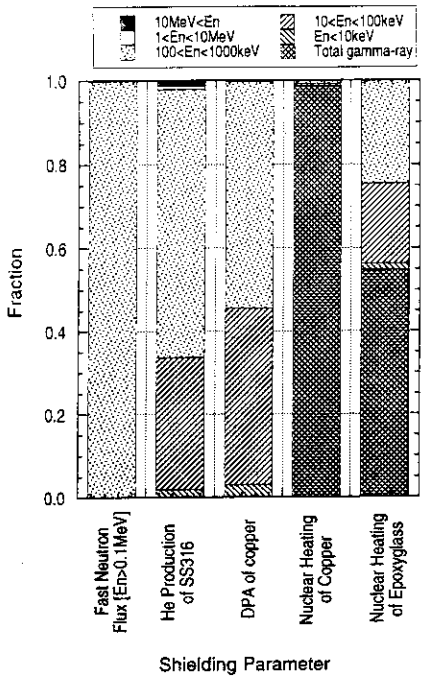

Fig. 5.3.1 Contribution fraction of specified energy neutrons and total gamma-rays for each shielding parameter at 914 mm in the SS316 assembly.

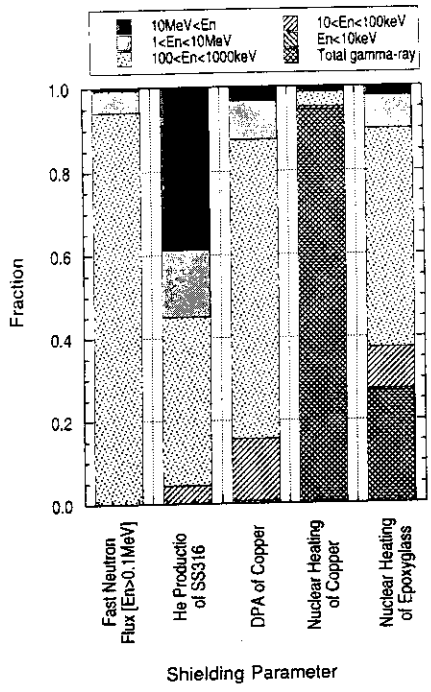

Fig. 5.3.2 Contribution fraction of specified energy neutrons and total gamma-rays for each shielding parameter at 914 mm in the SS316/water assembly.

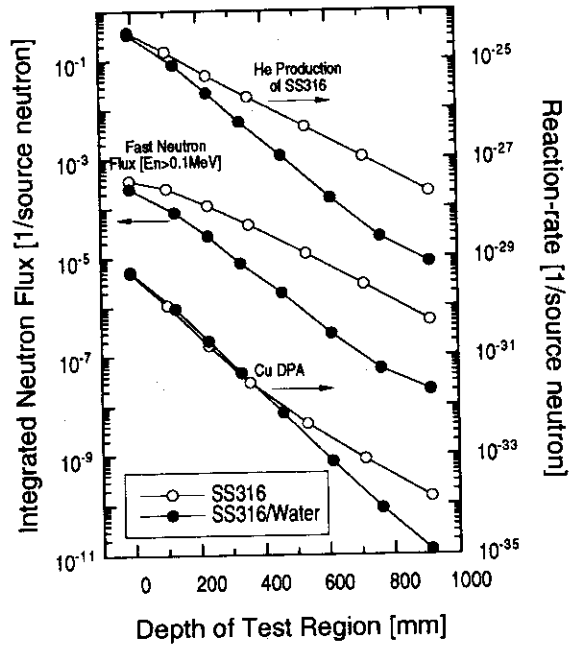

Fig. 5.3.3 Estimated neutron flux above 0.1 MeV, helium production of SS316 and copper DPA.

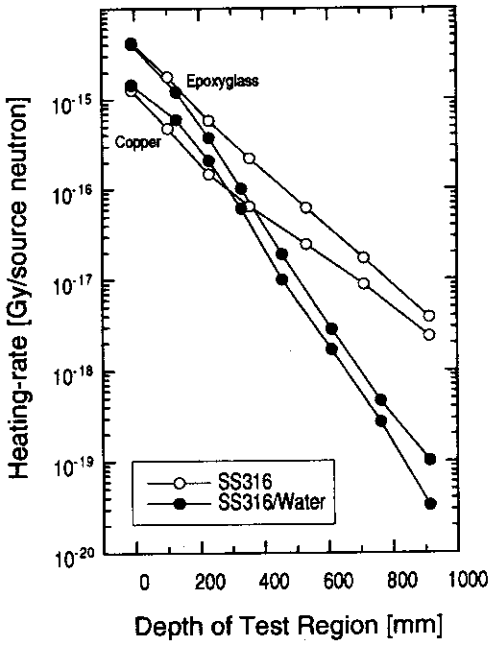

Fig. 5.3.4 Estimated nuclear heating rate of copper and epoxyglass.

5.4 Induced Radioactivity Measurements under Pulsed Mode Irradiation with 14 MeV Neutrons

Y. Ikeda, A. Kumar[1], Y. Uno, H. Maekawa, M. Z. Youssef[1]
and M. A. Abdou[1]

In the previous extensive experimental efforts carried out over last decade of collaborative program between USDOE and JAERI, the major focus had been on developing and demonstrating the techniques for measurement of neutron induced activity under a steady state condition. According to ITER/EDA R&D Task agreement of T-16, induced radioactivity experiments under pulsed operation was performed as against the steady state operation. The objectives of the experiments were to verify the algorithm for the induced radioactivity calculation undere a pulsed mode operation and to provide experimental data to validate overall calulation in a realistic operation scenario.

Foils of Nb, Fe, Al, V, Ni, and Mg were used, and we measured induced radioactivities in the following isotopic products: (i) ^{25}Na, and ^{24}Na of magnesium, (ii) ^{62m}Co, ^{62g}Co, ^{57}Ni, ^{58}Co, and ^{57}Co of nickel, (iii) ^{52}V, ^{51}Ti, and ^{48}Sc of vanadium, (iv)^{53m}Fe, and ^{56}Mn of iron, (v) ^{27}Mg, and ^{24}Na of aluminum, and (vi)^{90m}Y, and ^{92m}Nb of niobium. The half lives of these products varied from 1m (^{25}Na) to 271 d (^{57}Co). The unit pulse length was chosen to be 3 min in order to enhance the reduction effect on radioactivity levels comparing to those under the continuous irradiation. Three duty factors were applied: 10, 20 and 50% for the pulsed operation. The total number of pulses was either 3 or 10. Two kinds of power levels were used for various neutron pulse trains: (a) power level was held as constant as possible, (b)power level was significantly varied from pulse to pulse within a pulse train. The experimental data was processed to obtain ratio of inventories in pulsed to continuous operation scenarios for each of the observed radioactive isotope.

The comparison between calculation and experiment clearly demonstrates the capability of the technique developed. We have compared the radioactive inventories generated during pulsed operation to those under continuous operation. Both the calculations and the experiments indicate that the pulsed operation leads to large reduction in the radioactive inventories when both power and fluence are held constant. The reduction of activity level accentuates further with reduction in duty factor. Also, both our calculations and experiments confirm that the shapes of the pulses inside a pulse train also impact the relative amount of radioactivity generated in a pulsed mode of operation. We clearly observe a reduction in radioactive

1; School of Engineering and Applied Science, University of California at Los Angeles (UCLA), Los Angeles, CA 90024, USA

inventories for values of $t_{1/2}/p$ (half life/pulse duration) lying in the range of 1 to 10, as predicted by analytical formulae. In fact, random power pulse trains show even larger reduction in radioactive inventory: the ratio of inventories drops to ~0.14 for $t_{1/2}/p = 3.15$ (^{27}Mg) for a duty factor of 20 % and a pulse train of 10, whereas it would have hit a minimum of 0.3316 for $t_{1/2}/p = 3.5281$ for constant power level. We further find that, if the goal of pulsed operation is to reduce the radioactive inventory over a set time-period and a set total fluence, it is advised to operate, instead, with a continuous operation mode (or an operation mode with larger duty factor) over same length of time, but with appropriately reduced power level.

The present experimental results confirm the reduction predicted by the analytical algorithms under pulsed mode irradiation. It is, therefore, evident that the design safety margin should take into account the factors of reduction according to the parameters of pulse mode operation.

References

1) Attaya H., Gohar Y., and Smith D., "US-ITER Activation Analysis," Fusion Technology, 19, 1837-1842 (1991).

2) Bartels H.W., "Taking Credit for pulsed operation in ITER in the activation calculations", Interoffice memorandum, ITER JCT (March 24, 1994).

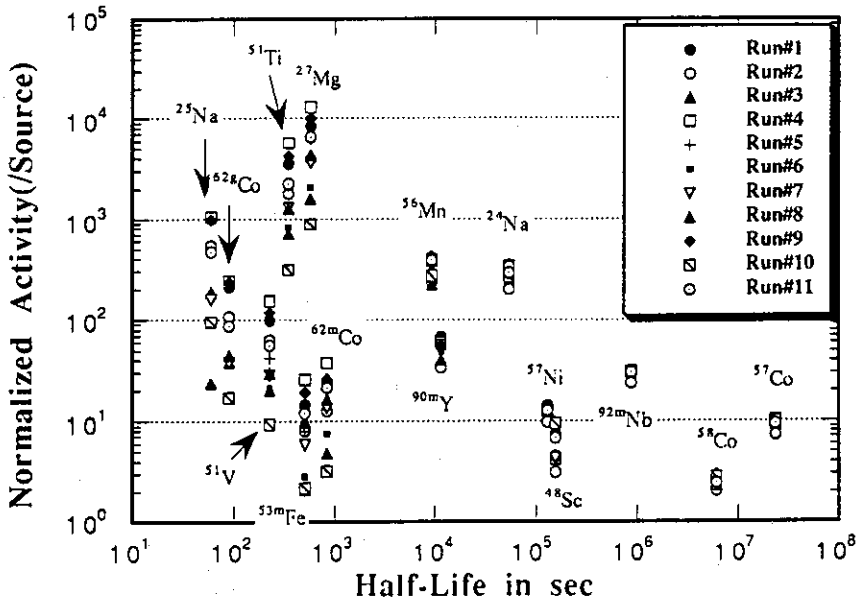

Fig. 5.6.1 Normalized radioactivities at the end of irradiation for all cases as a function of half-lives.

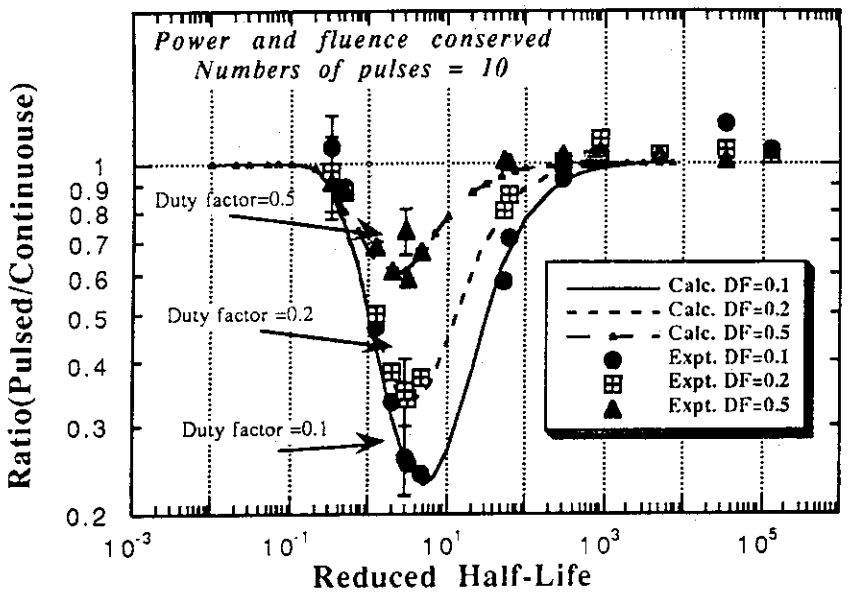

Fig. 5.6.2 Experimental and calculated ratios of inventories for pulsed to continuos operation for a pulse train comprising 10 pulses as a function of $t_{1/2}/p$ (half life/pulse duration).

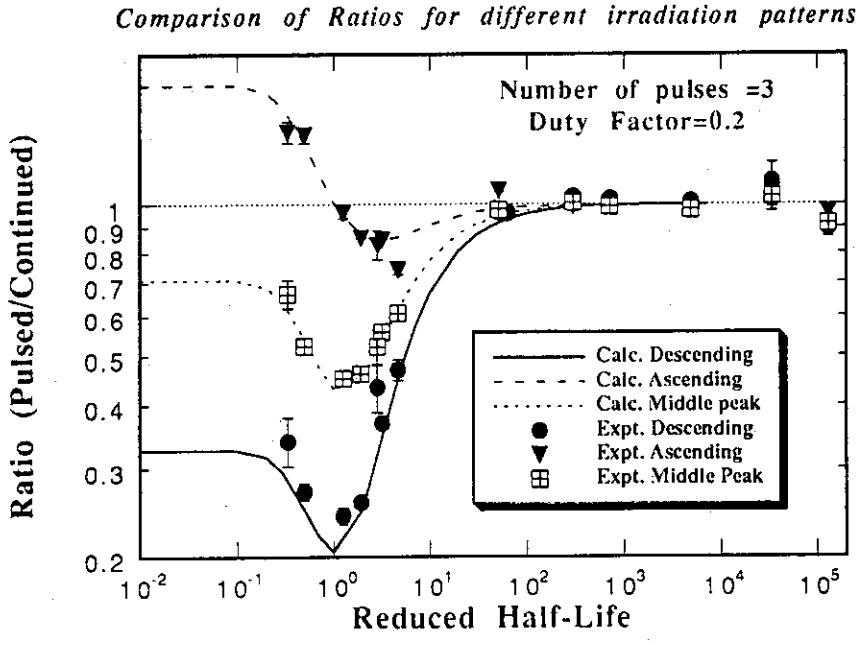

Fig. 5.6.3 Experimental and calculated ratios of inventories for pulsed to continuos operations for a pulse train comprising 3 pulses as a function of $t_{1/2}/p$ (half life/pulse duration).

5.5 Direct Nuclear Heating Measurements On First Wall/Pfc/Blanket Structural Components

Y. Ikeda, A. Kumar[1], F. Maekawa, Y. Uno, H. Maekawa, M. Z. Youssef[1] and M. A. Abdou[1]

The experiments on nuclear heating were carried out under the joint task with U.S.A. as assigned by ITER/EDA R&D sub-task of T16 in order to meet the strong need for validating the nuclear data relevant to nuclear heat deposition in fusion reactor structural components. The major technique applied was based on the microcalorimeter which has been developed previously in the last JAERI-USDOE collaboration[1,2]. The task covered additional experiments of γ-heating measurements with TLD (Thermo-Luminescent Dosimeter) and reaction rate distribution measurements with foils activation technique. The measurements were conducted on typical plasma facing and structural materials, i.e., stainless steel 316, beryllium, graphite, copper, zirconium, and tungsten. The cross sectional view of the assembly is shown in **Fig. 5.5.1**. The central zone of the assembly consisted of SS-316 blocks with a central channel hole of 50 mm in diameter. The calorimeter with thermal sensors, thermister (TM), was placed at very close position to the D-T neutron target, and irradiated with 3 to 5 minutes duration neutron pulses separated by 3 to 5 minute. The D-T neutrons were generated by bombarding a tritiated target with a 20 mA deuteron beam of 350 keV. The neutron irradiation history was recorded with a multi-channel scaling with 10 seconds duel time. The derivatives of relative temperature change are shown in **Figs. 5.5.2** for very first probe of stainless steel 316 in the reference assembly. There is a TM each at front and rear of this probe. It is observed that at the onset of each neutron pulse, the temperature reverses its course and starts to rise, and at the end of the neutron pulse, it reverts to its original course to decrease with the similar slope as prior to the arrival of the neutron pulse.

The calculations have been performed using 3-D transport code MCNP, and 2-D codes DOT3.5/GRTUNCL, and JENDL-3.1 data libraries. The foil activation rates were calculated using IRDF-90 version 2 dosimetry file. **Figure 5.5.3** shows the measured distribution of the volume averaged heating rates in the probes along the central channel along with values calculated by both DOT3.5 and MCNP. As observed, there are excellent agreements among the data in the distributions. The comparison for all other six materials was also made. We observed, however, large differences between the calculation and the experiment, particularly for probe materials of tungsten and zirconium.

In summary, the experimental approach with a microcalorimeter has demonstrated that this technique offers a promising way to provide experimental data. The experiment

---

1; School of Engineering and Applied Science, University of California at Los Angeles (UCLA), Los Angeles, CA 90024, USA

validating the adequacy of design calculations is possible with an accuracy of ± 10 % for the materials near the plasma chamber, first wall and blanket region for the neutron and gamma mixed radiation field. It was also shown that the importance of the γ-ray in the region far from the plasma could be covered by the TLD.

References

1) Kumar A., Ikeda Y. and Konno C., "Experimental Measurements and Analysis of Nuclear Heat Deposition Rates in Simulated D-T Neutron Environment: JAERI/USDOE Collaborative Program on Fusion Neutronics Experiments," Fusion Technol. 19 (1991) 1979 .

2) Ikeda Y., Kumar A., et al., "Measurement and Analysis for Nuclear Heat Depositions in Structural Materials Induced by D-T Neutrons," Fusion Technol. 21 (1992) 2190.

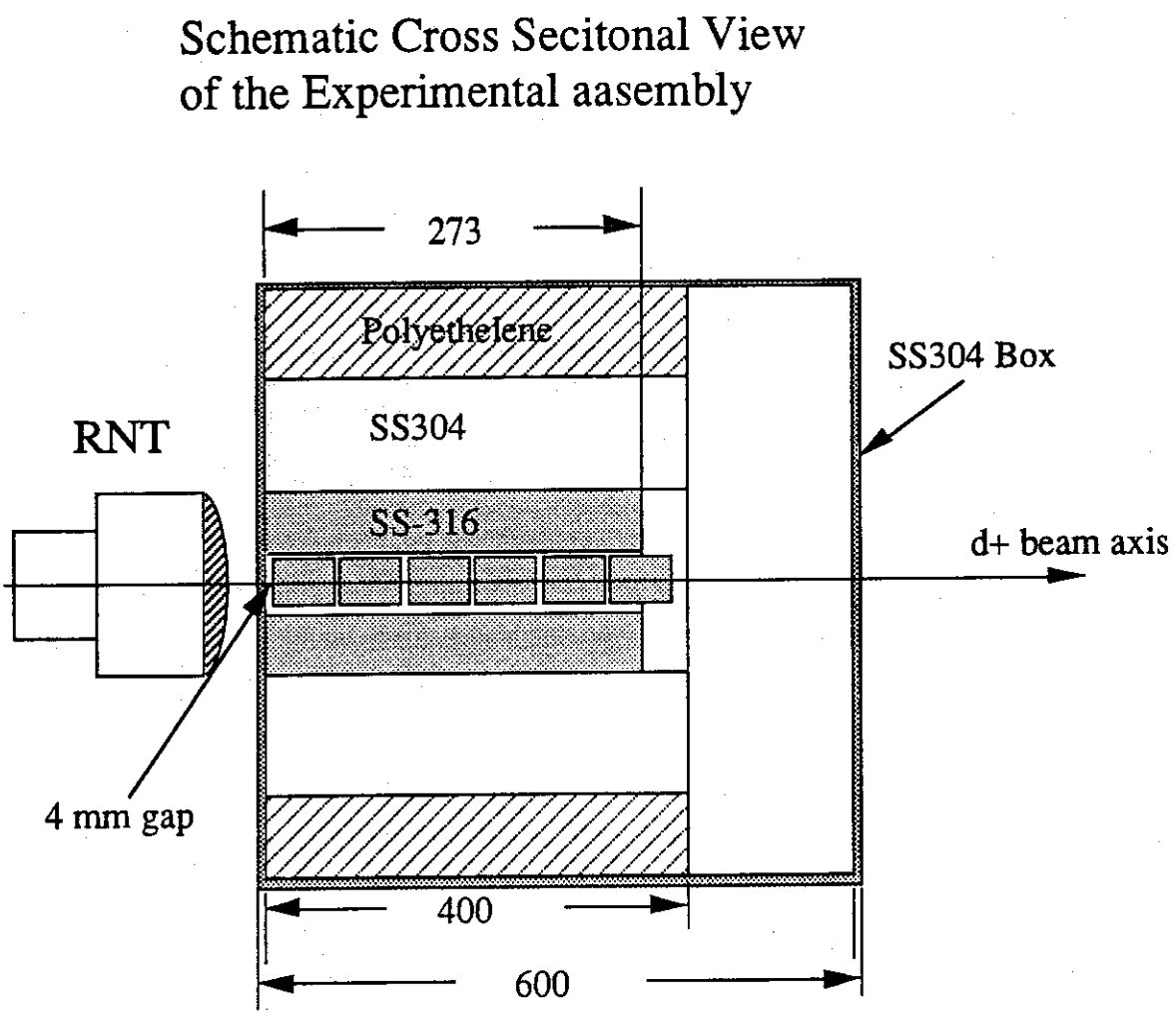

Fig. 5.5.1 Schematic cross sectional view of the experimental assembly

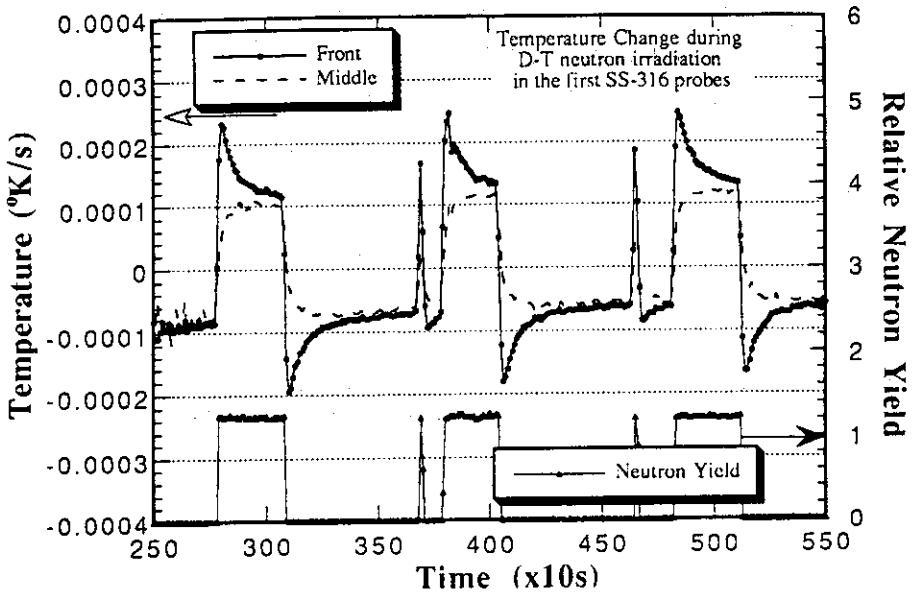

Fig. 5.5.2 Temporal derivative of temperature of a stainless steel 316 probe subjected to spaced D-T neutron pulses (Actually resistance change per cycle is shown. It is proportional to the temporal derivative of the temperature).

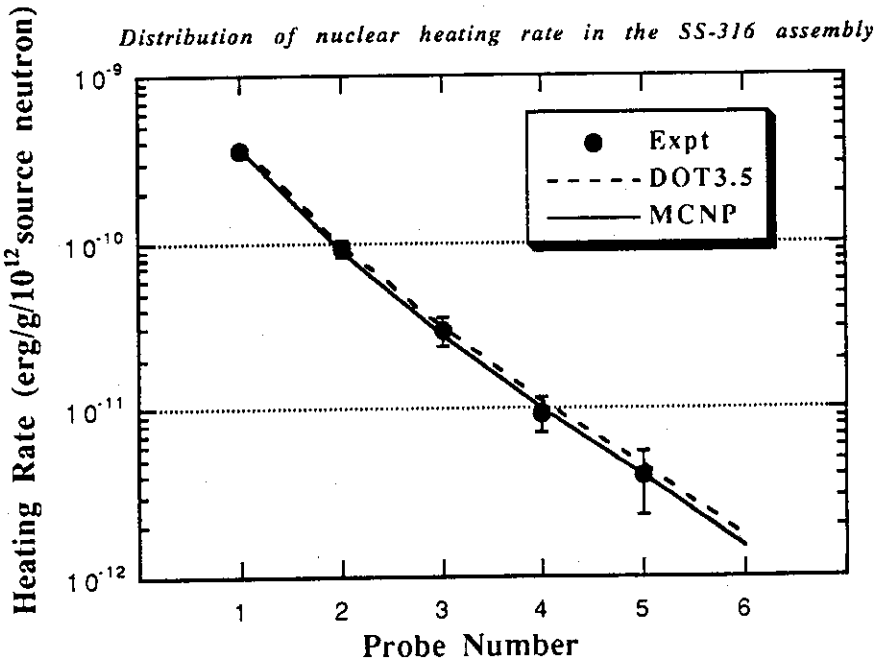

Fig. 5.5.3 Comparison of calculation and measurement for distribution of volume averaged nuclear heating rates over each probe of SS-316 inside the reference assembly. The calculations have been done using MCNP with FSXLIB-J3 and DOT3.5 with FUSION-J3.

5.6 Experiment on ^{16}N Production in Water with 14 MeV Neutron Irradiation and Associated 6 MeV Gamma-ray Characteristics

Y. Ikeda, D. L. Smith[1] and Y. Uno

Water is assumed as the coolant for ITER structural components, e.g., First Wall, Blanket, Shield, Vacuum Vessel, Diverter, etc. which are to be exposed to a high intense 14 MeV neutron flux from D-T plasma. The 14 MeV neutrons activate oxygen in water via the reaction of $^{16}O(n,p)^{16}N$ ($T_{1/2}$=7.13 sec). The flowing water carries radioactivities of ^{16}N through channels at the openings between TF coils. The decay of ^{16}N follows high energetic γ-rays of 6.1 and 7.1 MeV. A preliminary study showed that the activated water introduces additional sources for critical nuclear responses, e. g., the peak organic insulator dose and the peak nuclear heating in TF coil. This consideration addressed an urgent requirement for experimental validation of overall design related to the water activation issues. To realize the impact of ^{16}N in water produced by 14 MeV neutrons, a benchmark experiment was conducted. The experiment consisted of two parts. The first part was experiments on the ^{16}N radioactivity production with 14 MeV neutron irradiation as a function of water flow rate to characterize the radioactive source distributions all around inside the vacuum vessel. The second part was for the high energy photon attenuation benchmark experiments with SS304, Cu shield material configurations incorporating flowing water with ^{16}N. **Figure 5.6.1** shows the experimental setup for the γ-ray attenuation benchmark.

Dose rate at the TF coil in ITER was estimated based on the present experimental results. In order to extrapolate the data, several approximations were assumed as follows; (i) only the water channels at the first wall are taken into account, (ii) as each blanket has a total area of 26 cm^2 for the cooling channel (0.5 cm^2 x 52 channels), and (iii) the total number of modules is ten along the one sector, and the total cross section is 260 cm^2. If all water flow in the whole blanket is taken into account, the dose rate from the activated water should be multiplied by a factor of 4.7 by deriving from the summation of activities obtained from one-dimensional calculation. In addition, the following factors should be taken into accounts for the estimation; (iv) cross section for the $^{16}O(n,p)^{16}N$ reaction, (v) resident time of water flow in the blanket, and (vi) multiple coolant pipes nearby the TF coil. The additional factor to be multiplied becomes 2.73 (1.25 x 1.56 x 1.4). Finally, we have an estimation of dose rates at the surface of TF coil as 7.1 x 10^6 R/h at 8.5 cm and 1.7 x 10^6 R/h at 56 cm. The parameters for the estimations are summarized in **Table 5.6.1**.

Note that the criteria reported by the TAC-4 in the ITER project is as follows: Peak

---

1; Argonne Antional Laboratory, USA.

nuclear heating at TF coil = 5.89 x 10^{-2} mW/cm^3, peak organic insulator dose = 1.94 x 10^8 rads and average nuclear heating = 1.91 W/cm^3. From the preliminary experimental results, the dose of 1 x 10^6 R/h is possiblely obtained. The dose rate of 1 R/h is almost 1 rad for 1 MeV photon. Thus only 200 hr operation is allowed if the criteria is valid. If the ITER operation of 3 MWa/m^2 is scheduled, it is essential to reduce the dose by placing some shield materials.

We also have considered the attenuation characteristics of such high energy photons. From γ-ray spectra measured by the NaI(Tl), attenuation profiles were derived for different shield configurations for SS-304 and copper. **Fig. 5.6.2** depicts the attenuation profiles of the total γ-ray intensity, the γ-ray intensities integrated over energy regions (<3 MeV: low and >3 MeV: high), along with the dose rate obtained with GM counter. As expected, high energy γ-ray decrease rapidly as a function of the thickness. The attenuation profile is reasonably following the exponential curve with absorption coefficient of the 6 MeV photon. However, it was found that attenuation of the total γ-rays and GM dose was around 1/5 with 200 mm thick SS304. Less attenuation was shown for the low energy γ-rays. The results addressed very critical problem for a shielding design for protection of the high energy γ-ray dose due to ^{16}N against the TF coil heating and the organic insulator dose. All results indicate that without serious consideration of this activated water flow, ITER operation scenario should be drastically changed. As noted, there are lot of assumptions and unknown factors in the design to arrive at the final estimation. These assumptions have still considerably large uncertainties According to the present study, it is clear that we need to verify this design related critical issues by performing experiments with well defined and closely simulated conditions for the water flow and neutron environment.

Table 5.6.1 Estimation of dose rate at TF coil due to activated water flow

Item	ITER	FNS#1	Factor[1)]	FNS#2	Factor[1)]
Neutron wall load(W/m^2)	1 x 10^6	17.3	5.8 x 10^4	143	7.0 x 10^3
Channel section	260 cm^2	0.718 cm^2	3.62 x 10^2	0.13 cm^2	2.0 x 10^3
Resident Time (sec)	0.45	0.20	2.2	0.36	1.25
Length of outlet loop	7 m	25 m		32 m	
^{16}N Decay	0.8	0.3	2.7	0.12	6.7
Active length	1 m	0.085 m		1.25 m	
Dose rate (R/h)	5.5 x 10^5	4.4 x 10^{-3}	1.25 x 10^8		
Dose rate (R/h)	1.3 x 10^5			1.1 x 10^{-3}	1.17 x 10^8

1) values to be multiplied

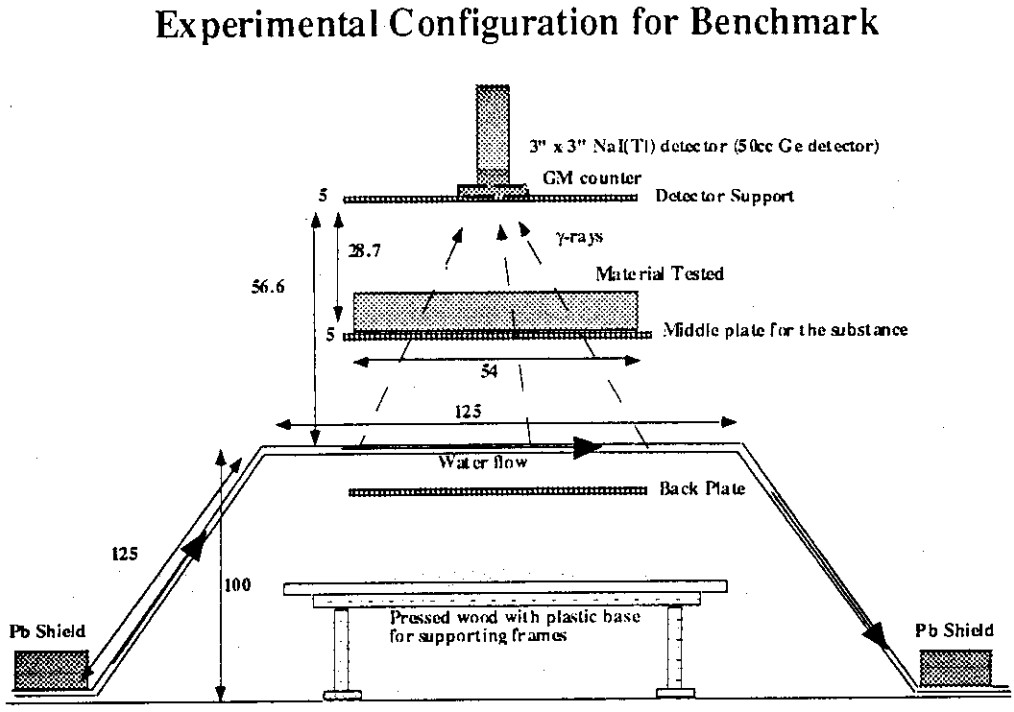

Fig. 5.6.1 ^{16}N photon attenuation benchmark configuration.

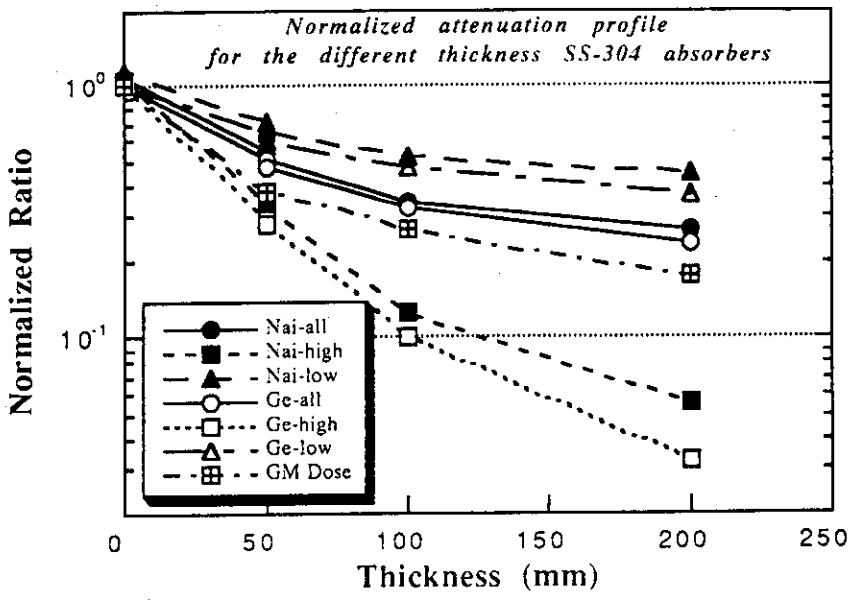

Fig. 5.6.2 Normalized attenuation profile of γ-ray flux and dose rate for SS304 shields.

5.7 Benchmark Experiment on a Tungsten Slab Assembly Bombarded by D-T Neutrons and Its Analysis

F. Maekawa, C. Konno, Y. Oyama, Y. Ikeda, M. Wada, Y. Uno and H. Maekawa

Tungsten is a inevitable material for fusion applications. It is used as a shielding material because of its high density and large absorption cross section for both neutrons and photons, and also as a high-temperature resistant material such as the diverter plates of fusion devices. In the nuclear designs of fusion devices, high accuracy of cross section data for tungsten is required. In order to provide benchmark data of tungsten, an integral experiment was carried out with D-T neutrons.

A slab assembly in cylindrical shape, 457 mm in diameter and 507 mm in thickness, made of tungsten alloy (W: 94.8 wt%, Ni: 3.1 wt%, Cu: 2.1 wt%), was placed at 200 mm from the D-T neutron source of the 80° beam line of Fusion Neutronics Source (FNS) facility. Measurements were carried out at 0, 76, 228 and 380 mm positions on the central axis of the assembly. The following energy-differential and energy-integral quantities for both neutrons and gamma-rays were obtained;

(i) neutron spectra above 1 MeV by a liquid organic scintillation detector, NE213,
(ii) neutron spectra between 3 keV and 1 MeV by proton recoil gas proportional counters,
(iii) reaction rate distributions for the $^{27}Al(n,\alpha)^{24}Na$, $^{93}Nb(n,2n)^{92m}Nb$, $^{115}In(n,n')^{115m}In$, $^{186}W(n,\gamma)^{187}W$ and $^{197}Au(n,\gamma)^{198}Au$ reactions by the foil activation method,
(iv) gamma-ray spectra by a deuterated liquid organic scintillation detector, BC-537, and
(v) gamma-ray heating rates by TLD with the atomic density extrapolation method.

The experimental data were compared with results of transport calculations with three evaluated nuclear data files, JENDL-3.2, -3.1 and FENDL/E-1.0 in order to verify accuracy of the files. The continuous energy Monte Carlo code MCNP-4A was employed with the cross section libraries FSXLIB-J3R2 [1], FSXLIB-J3 and FENDL/MC-1.0 [2], respectively. The two-dimensional SN code DOT-3.5 were also employed with the JSSTDL library of neutron 125 and gamma-ray 40 groups based on JENDL-3.1. The JENDL Dosimetry File was commonly used to derive reaction rates through out the analyses. The measured and calculated neutron spectra at 380 mm position are shown in Fig. 5.7.1. Calculated to experimental ratios (C/Es) for three reactions and the gamma-ray heating rate are presented in Fig. 5.7.2. Figure 5.7.3 shows the measured and calculated gamma-ray spectra at 228 mm position.

Transmission behavior of 14 MeV neutrons can be seen in C/Es of the $^{93}Nb(n,2n)^{92m}Nb$ reaction rate. The JENDL-3.2 agrees within 10 % with the experiment, while C/Es by JENDL-3.1 and FENDL tend to be larger as the thickness increases. The most probable reason of the tendency is due to difference of the (n,2n) cross section at 14 MeV; 2.15 b for JENDL-3.2, and 1.99 b for JENDL-3.1 and FENDL, and this experiment supports JENDL-3.2.

A broad peak of neutron spectrum below 10 MeV centered around 0.1 MeV is seen in Fig. 5.7.1. Most part of neutrons in the broad peak is formed by secondary neutrons from the (n,2n) reaction. The followings are found for the broad peak by considering Fig. 5.7.1 and Figs. 5.7.2 (b), (c).

(i) When JENDL-3.2 or -3.1 are used, the calculated spectra are softer than the measured one, however, total number of neutrons in the broad peak is almost appropriate since the C/Es of ^{197}Au(n,γ) reaction are close to 1.0.

(ii) The shape of spectrum by FENDL is the closest to the measured one among the three. But as recognized from the C/Es of ^{197}Au(n,γ) reaction, total number of neutrons in the broad peak by FENDL is much smaller than the measured one.

As for secondary gamma-rays, both gamma-ray spectra and heating rate by JENDL-3.1 are more than 5 times as large as the experiment at 228 and 380 mm positions. This fact was pointed out through the present benchmark analysis, and the secondary gamma-ray data of tungsten were reexamined in the evaluation of JENDL-3.2. As a result, much improved secondary gamma-ray data are stored in JENDL-3.2. Accuracy of the secondary gamma-ray data in FENDL is almost equal to those in JENDL-3.2.

References

1) Kosako K., et al., "FSXLIB-J3R2: A Continuous Energy Cross Section Library for MCNP Based on JENDL-3.2," JAERI-Data/Code 94-020 (1994).

2) MacFarlane R. E.: Private Communication, LANL (1994).

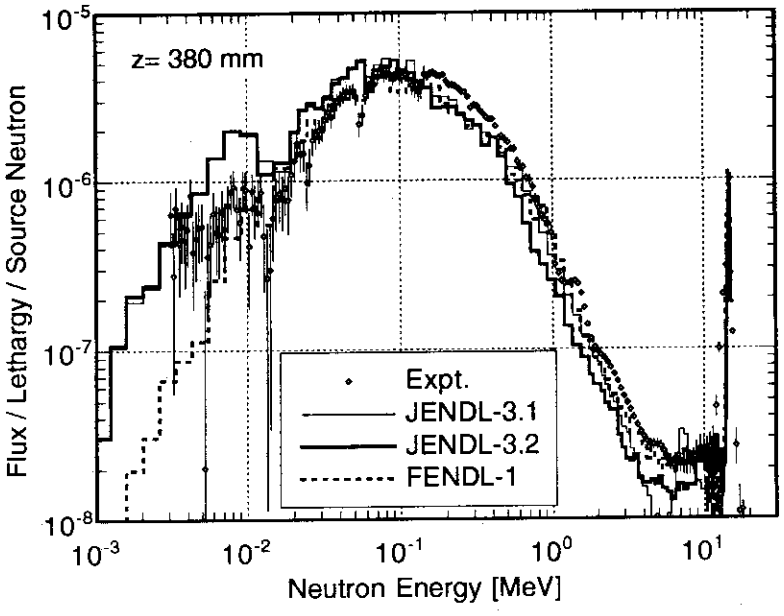

Fig. 5.7.1 Measured neutron spectrum at 380 mm depth in the tungsten assembly comparing with calculated ones with JENDL-3.2, -3.1 and FENDL/E-1.0.

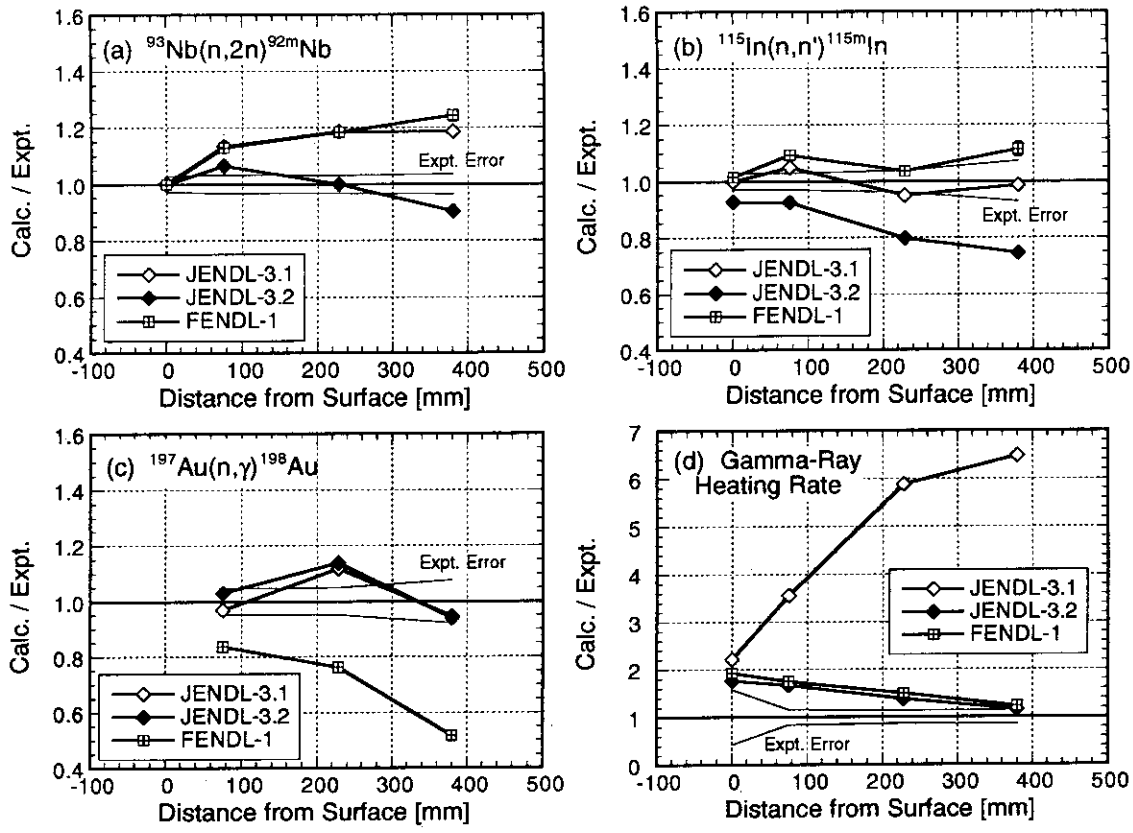

Fig. 5.7.2 Calculated to experimental values for (a) ^{93}Nb(n,2n)^{92m}Nb, (b) ^{115}In(n,n')^{115m}In, (c) ^{197}Au(n,γ)^{198}Au and (d) gamma-ray heating rate in the tungsten assembly.

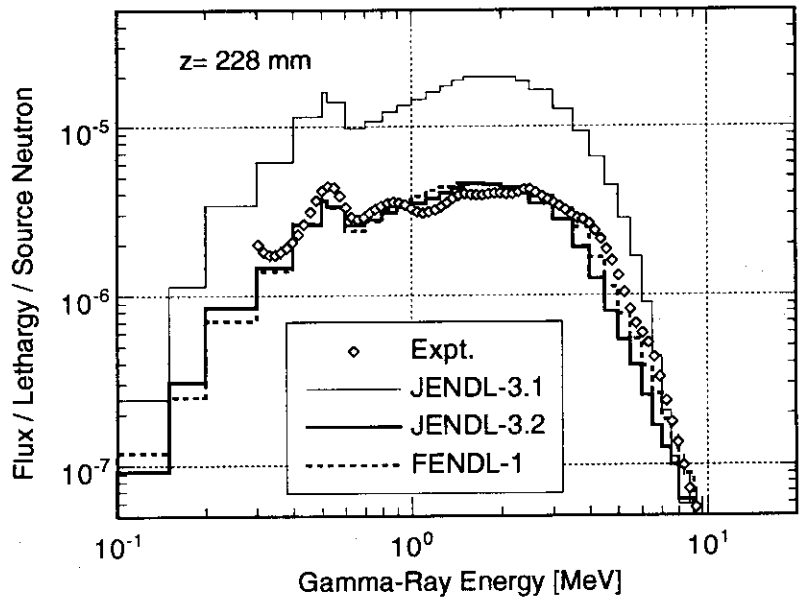

Fig. 5.7.3 Measured neutron spectrum at 380 mm depth in the tungsten assembly comparing with calculated ones with JENDL-3.2, -3.1 and FENDL/E-1.0.

5.8 Improved Measurement of Gamma-Ray Heating Rate by TLD

F. Maekawa and Y. Oyama

The technical procedure of gamma-ray heating rate measurement in a medium with plural kinds of thermoluminescent dosimeters (TLDs) was proposed by Tanaka, et al.[1] We have been applied[2] the method to many benchmark experiments for fusion neutronics with five types of TLDs; BeO, ^{7}LiF, Mg_2SiO_4 (MSO), Sr_2SiO_4 (SSO) and Ba_2SiO_4 (BSO). D-T neutrons were bombarded to an experimental assembly of simulated fusion blanket or shield, and gamma-ray heating rates were measured at several measuring positions in the assembly. The measured gamma-ray heating rates were compared with the results of benchmark calculations to estimate accuracy of secondary gamma-ray data in evaluated nuclear data libraries, such as JENDL-3. As a result, considerable discrepancies, more than twice in some cases, between the measured and calculated gamma-ray heating rates were sometimes found. The most probable reason of the discrepancies lied in inaccurate cross section data, but several experimental procedure to be improved were also found. The followings were examined in the experiment.

(i) TLDs have wide dynamic ranges typically more than 4 order of magnitude. But the dynamic range with good linearity is not so wide because of low signal to noise ratios in a low-dose region and appearance of supra-linearity in a high-dose region. Hence durations of the irradiations were adjusted to attain appropriate dose for the TLDs. The optimum dose was equivalent exposure dose between 5×10^{-5} - 5×10^{-3} [C/kg] of Co-60 in the air. Linearity of the TLDs except BeO in the dose range including a calibration error of the TLD reader was better than 5 %, and that of BeO was better than 10 %.

(ii) Since TLDs of MSO, SSO and BSO have sensitivity to daylight, TLDs were treated in dark places. Thin aluminum foil was used as a packing material to prevent the TLDs from being exposed by daylight.

(iii) The D-T neutron target also emits gamma-rays which are produced by interactions of the D-T neutrons with the structural material of the target. The gamma-ray spectrum was experimentally determined, and also calculated by a Monte Carlo transport calculation with the MCNP code precisely simulating the geometry of the target. Both spectra agree with each other, and it assures validity of the spectrum of the calculation. In a benchmark analysis of the experiment, calculations not only with source D-T neutrons but also with source target gamma-rays were executed. Gamma-ray heating rates associated with the target gamma-rays were estimated and they were subtracted from the measured gamma-ray heating rates.

As a result, the overall errors of the measured gamma-ray heating rates, previously given

around 20 - 30 %, have been reduced to typically about 10 - 15 %.

In order to demonstrate reliability of the improved measuring method, a measurement of gamma-ray heating rates in an iron shield assembly was carried out at the Fusion Neutronics Source (FNS) facility. Outline of the experiment was almost the same as described in Ref 2). A benchmark calculation of the experiment was performed with the Monte Carlo transport code MCNP-4A and cross section library based on ENDF/B-VI.1. The MCNP-4A is thought as one of the most accurate transport calculation code because of use of continuous energy cross section. Cross section data of iron in ENDF/B-VI.1 are also regarded as highly accurate due to the following reasons. (1) Iron is one of the most fundamental material and its cross section have been deeply investigated. (2) According to benchmark tests for neutron, calculated neutron spectra with ENDF/B-VI.1 agreed within about 10 - 20 % with the experimental data in any energy ranges between 14 MeV and 1 eV. (3) Explicit attention was paid to energy-balance of the secondary gamma-ray data, which largely influences the calculated gamma-ray heating rates, through its evaluation.

The measured and calculated gamma-ray heating rate inside the iron shield to 800 mm in depth are compared in Fig. 5.8.1. Errors of the measured data are 8 - 11 % except the 0 mm position where error is 26 %. The errors were reduced to nearly the half of those of the previous experiment [2]. It is clearly seen in the figure that the agreements between the measured and calculated gamma-ray heating rates are very excellent at all measuring positions even at the 800 mm position where the heating rate attenuates nearly 3 orders of magnitude from the beginning. Neutron and gamma-ray spectra change a lot depending on the penetration thickness; prominent 14 MeV neutrons and gamma-rays from threshold reactions near the front surface, and lower energy neutrons less than 1 MeV and gamma-rays from (n,γ) reactions in deeper part of the assembly. In spite of the change of neutron and gamma-ray environment, all the calculated heating rates are within the error ranges of about 10 % of the measured heating rates. This excellent agreement is the powerful evidence not only that the calculation including the cross section data of ENDF/B-VI.1 are valid but also that the improved measurement are highly reliable.

References

1) Tanaka S. and Sasamoto N.: J. Nucl. Sci. Eng., 22, 109-119 (1985).

2) Yamaguchi S., et al.: Fusion Eng. Des., 10, pp. 163-169 (1989).

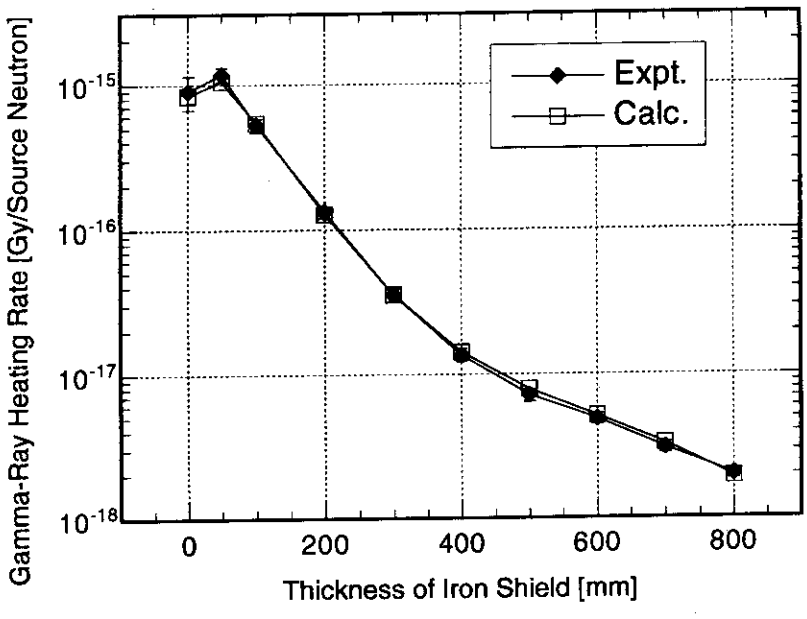

Fig. 5.8.1 The measured gamma-ray heating rate inside the iron shield up to 800 mm in depth in comparison with the calculated ones by MCNP-4A with ENDF/B-VI.1.

5.9 An Investigation into the Possibility of Performing Radiography with Gamma-Rays Emitted from Water that has been made Radioactive by Irradiation with 14-MeV D-T Fusion Neutrons.

D. L. Smith[1], Y. Ikeda and Y. Uno

Most conceptual designs for D-T fusion reactors incorporate water cooling. However, the water becomes temporarily radioactive from $^{16}O(n,p)^{16}N$ reactions induced by $^{3}H(d,n)^{4}He$ fusion neutrons. Reported studies of this phenomenon generally examined various related detrimental effects. The present investigation explores a potential beneficial application of this radioactivity to radiography. This is accomplished using 6.129 and 7.115 MeV photons generated by the decay of 7.13 second ^{16}N. The concept is demonstrated here by using D-T neutrons with a loop of water flow.

A simple radiography apparatus was constructed by circulating pure water between the D-T neutron target region and a remote location where photon transmission measurements were conducted using an arrangement of a collimated photon source and a detector. **Figure. 5.9.1** shows a schematic configuration of overall water loop with 14 MeV neutron source and transmission measurement. The initial γ-ray source was designed to provide a well collimated beam with rectangular shape of 25 x 100 mm^2 cross sectional area. As the photon detector, a 5" x 2" NaI(Tl) scintilator was employed. Lead shield with 25 mm gap, the geometrical level of which was aligned to the photon source collimator opening, restricted spatially the γ-ray which is transmitted through the object materials. The geometrical arrangement for the emission measurement is given in **Fig. 5.9.2**. Four objects with distinct features made of SS304, Cu and Pb, were examined in this work. As scanning the object with a 10 mm step perpendicularly to the photon beam, the photon flux in a energy region higher than 3 MeV was recorded for each step. A typical γ-ray spectrum from activated water measured with NaI(Tl) is shown in **Fig. 5.9.3**. In **Figs. 5.9.4 and 5.9.5**, the results for the cases of a SS304 block with a hole at the center and a Pb block sandwiched with two Cu plates are presented. The dashed lines in the figures correspond to values estimated by the photon attenuation for the full width of the materials.

These measurements demonstrated that features like hidden holes and discontinuities in atomic number could be identified easily by observing variations in photon transmission. Spatial resolutions consistent with the geometry of this apparatus were observed in all instances.

1; Argonne National Laboratory, USA.

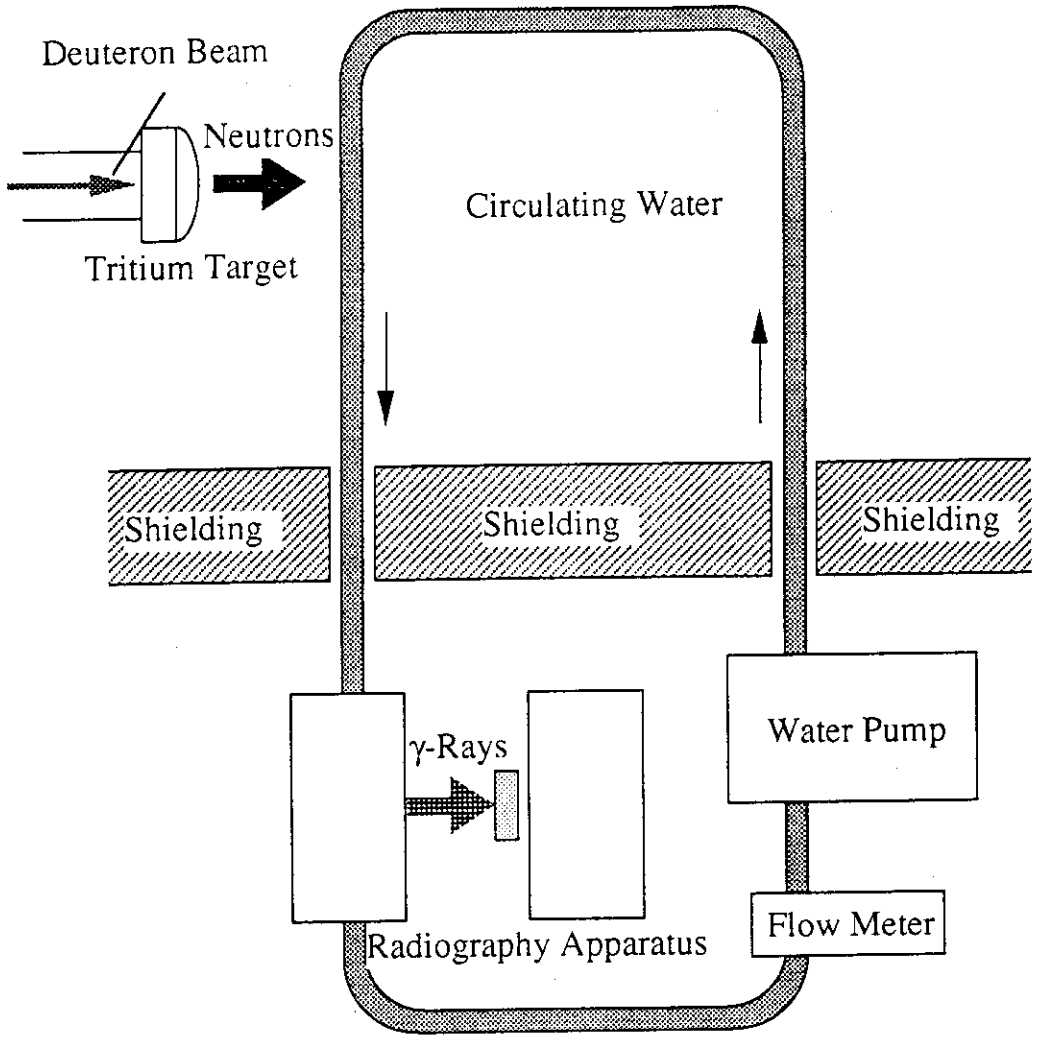

Fig. 5.9.1 Overall water loop layout

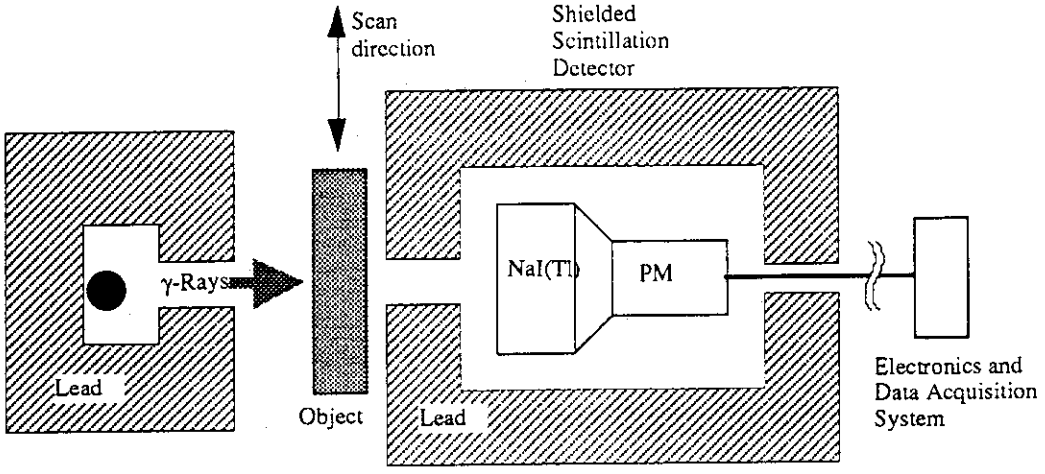

Fig.5.9.2 Transimission measurements configuration

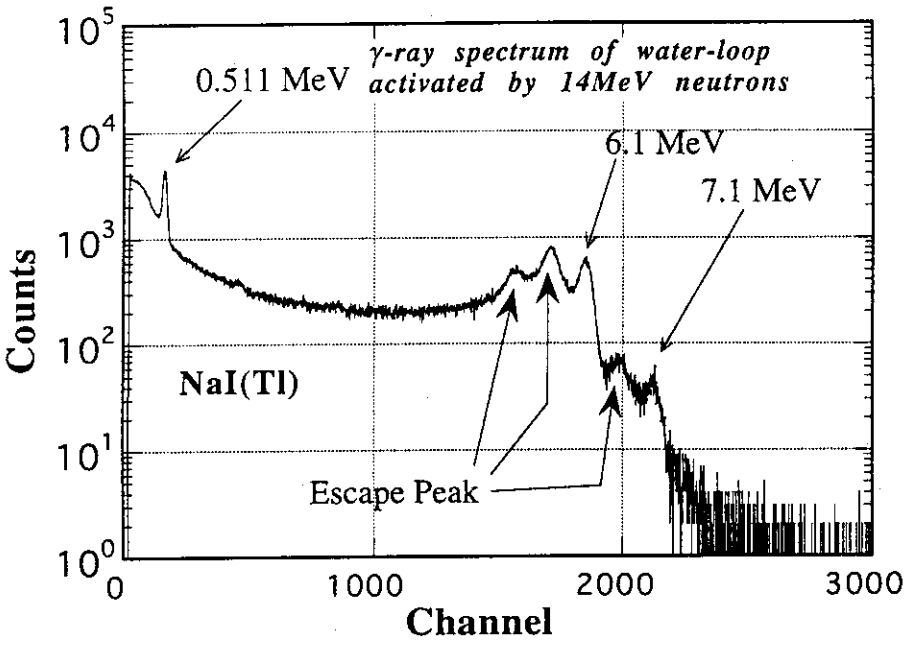

Fig. 5.9.3 Typical γ-ray spectrum measured with the NaI(Tl) detector

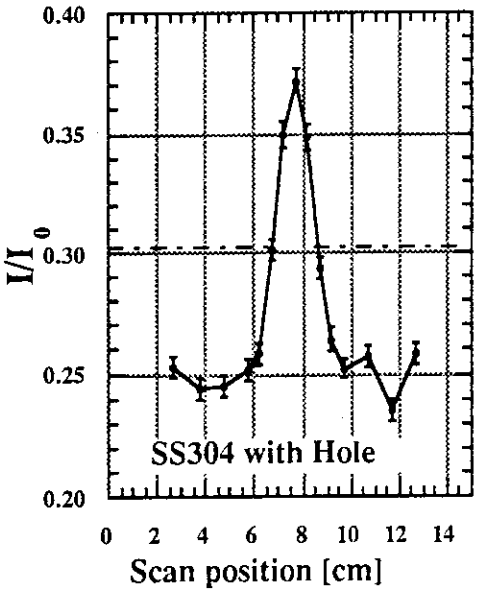

Fig. 5.9.4 Transmission profile of γ-ray flux SS304 with hole

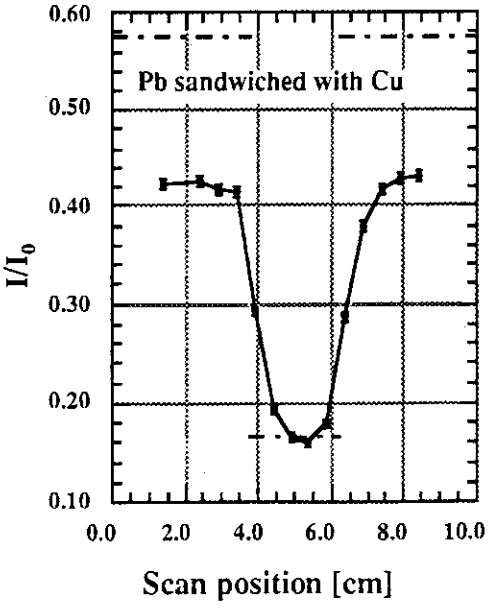

Fig. 5.9.5 Transmission profile of γ-ray flux for Pb sandwiched by Cu plates

5.10 A Novel Binary-acid Method for Solving Lithium Carbonate Pellet in Tritium Production Measurement with Liquid Scintillation Counting

Yu. M. Verzilov, F. Maekawa and Y. Oyama

A measurement of tritium activity in materials play an essential part in the fusion reactor blanket experiment[1] and a neutron flux monitor with $^{6}Li(n,\alpha)^{3}H$ reaction[2]. In such studies, lithium-containing pellets are usually irradiated by neutrons and the tritium produced in them is measured with a liquid scintillation counter. Due to basic principle of liquid scintillation counting for low energy β-emitter, it is necessary to bring tritium into contact with the scintillator molecules of the scintillation solution. However, lithium-containing materials to be irradiated are usually incompatible with the scintillation cocktail in solubility characteristics.

To overcome this problem various techniques were developed for different types of materials. In the present study, the wet-chemistry procedure for Li_2CO_3 is the subject of interest. This lithium compound was selected because of the high storage stability of the tritium in the irradiated pellet and non hygroscopic salt. The wet-chemistry procedure of the conventional technique, Dierckx method[3], consists of three main steps: 1) dissolution of pellet, 2) removal of lithium salts from the pellet solution by using hydrofluoric acid and centrifugion, 3) incorporation of the pellet solution into the liquid scintillator. Figure 5.10.1 illustrates the sample processing scheme and the main parameters of this technique. This technique has the following disadvantages. The figure of merit (FOM) is not so high. The FOM is given by the capability for measurement of low level activity of tritium, defined as the product of the pellet solubility and the counting efficiency of the solution-cocktail mixture. The remaining lithium acetate is liable to make the scintillation solution unstable and to reduce the tritium counting efficiency. To overcome these disadvantages and to simplify preparation procedure a new dissolving technique has been developed.

The present sample processing scheme for scintillation counting is shown in Fig. 5.10.2. It is very simple and does not require to remove lithium salt from the solution. A mixture of two different acids, HNO_3 (61%) and CH_3COOH (100%), strong and weak acids, respectively, has been proposed as a new binary acid solvent from a preliminary study and the following view point. In order to provide high solubility of lithium salt it is best to use an acid. Since strong acid, HNO_3, can dissolve a pellet of mass greater than CH_3COOH, this method makes it possible to prepare more concentrated solution of the pellet. However, this benefit is lost after the incorporation of the pellet solution into the liquid scintillator, because the small quantity of free nitric acid considerably quenches scintillations. Figure 5.10.3

shows the relation of counting efficiency to the sample content for different solvents. For reference, a quenching effect of water is also plotted in the same figure. From the figure it is seen that the strong acid leads to a rapid decrease in counting efficiency. Therefore, first the amount of the strong acid that is not enough to dissolve the whole pellet should be dropped, and the remained part of the pellet can be dissolved by the acetic acid.

The optimum acid volume ratio was determined by FOM and the sample compatibility in relation to the acid volume ratio and the pellet weight. Seven solvent compositions with the different acid-volume ratios were prepared. The first solvent contained only the nitric acid. Its volume was estimated by chemical equation. The others contained the mixture of two acids varying the mixing ratio. These solvents were prepared by gradually reducing the volume of nitric acid and by adding the acetic acid until the pellet was dissolved completely. A comparison between the two sets of the samples with different weights of 0.8 g and 1.2 g in terms of FOM was shown in Fig. 5.10.4. The optimum is obtained by the highest FOM value within the clear fluid region due to good compatibility.

A comparison of the capability for measurement of low-level tritium between the present and the conventional techniques was made by the FOM. The higher FOM denotes the capability for measurement of the lower level tritium activity. The main parameters of the conventional techniques were taken from the table in the reference[4]. They are summarized in Table 5.10.1 together with the calculated FOM.

In contrast to the conventional techniques, all preprocessings of the present one are performed in a standard scintillation vial, without removal lithium salts. Thus, the present technique is very simple and convenient, and at the same time it has higher FOM. From Table 5.10.1 one can see that the present technique can improve the FOM by a factor of ~ 2.

References

1) Maekawa H., Oyama Y. and Ikeda Y.: Proc. Int. Conf. on Nuclear Data for Science and Technology, May 9 -13, 1994, Gatlinburg, Tennessee, USA, p. 866 (1994).
2) Body Z., in: Handbook on Nuclear Activation Data, Technical Reports Series No.273 (IAEA, Vienna, 1987).
3) Dierckx R.: Nucl. Instr. and Meth., 107, 397 (1973).
4) Maekawa F., Maekawa H.: Report JAERI-M 93-017, Japan Atomic Energy Research Institute (1993).

Table 5.10.1. Comparison of measuring techniques for Li_2CO_3 pellets.

Organization & technique	Pellet weight (g)	Counting efficiency (%)	Figure of merit (g·%)
CEA/Cadarache Dierckx'	0.7	26.6	18.6
IGA/EPFL Dierckx'	0.7	20.6	14.4
ENEA Dierckx'	0.7	22.7	15.9
Osaka Univ. Dierckx'	0.5	18.6	9.3
Tokyo Univ. Dierckx'	0.6	29.8	17.9
JAERI Present tech.	**1.4**	**21.7**	**30.4**

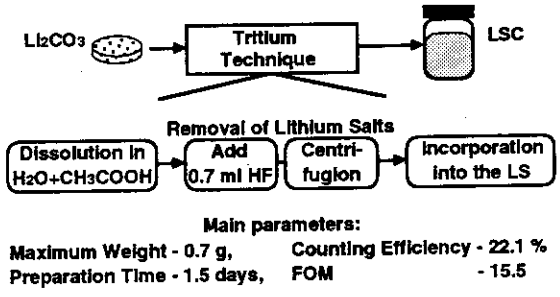

Fig. 5.10.1 Sample processing scheme of the Dierckx's technique.

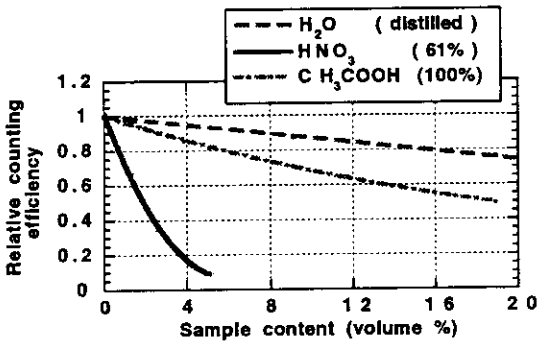

Fig. 5.10.3 Effect of the sample volume on counting efficiency for Clear-sol.

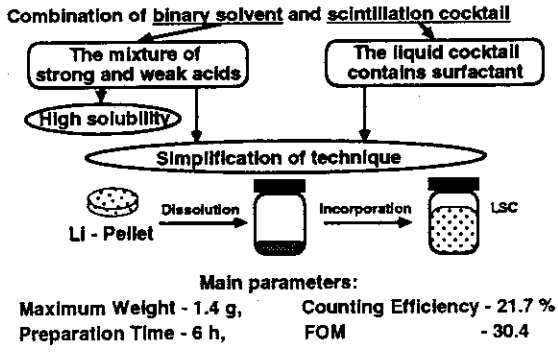

Fig. 5.10.2 Basic principle and the sample processing scheme of the new technique.

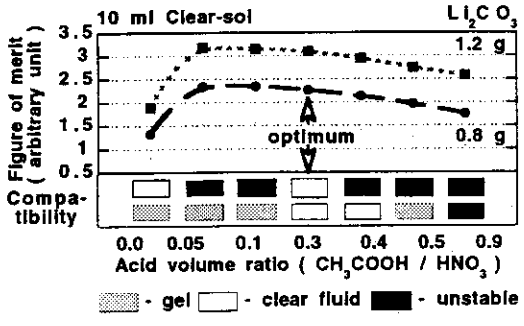

Fig. 5.10.4 Effect of the chemical composition and increasing pellet weight on figure of merit and sample compatibility.

5.11 Simple and Efficient Technique for Measurement of Low Level Neutron Flux

Yu. M. Verzilov, F. Maekawa and Y. Oyama

The dosimetry reactions $^{31}P(n,\gamma)^{32}P$, $^{32}S(n,p)^{32}P$ and $^{35}Cl(n,\alpha)^{32}P$ can be conveniently used to measure neutron fluxes even at large penetration depths because of large sensitivity of these detectors. They are characterized by the same reaction product, ^{32}P ($E_{\beta max}$ = 1.71 MeV), which is measured by using the liquid scintillation counting equipment. Since this nuclide exhibit β emission with energy above 263 keV of the threshold energy for the excitation of Cherenkov radiation in water, Cherenkov response may be used for the measurement of β activity.

Remarkable advantages of this technique are extreme simplicity of sample preparation and ability to count in aqueous systems without use of organic fluors. A comparison between the sample processing schemes for Cherenkov radiation counting and liquid scintillation counting is shown in Fig. 5.11.1. The main disadvantage is low detection efficiency as compared with liquid scintillation counting. The maximum theoretical detection efficiency in water for ^{32}P can be calculated by integrating the number of events above 263 keV and comparing this to the total emission. This value is about 86%, and the experimental detection efficiency is about two times less than the theoretical result when the ordinary liquid scintillation counting equipment[1] is used.

The main efforts were given to this study, to select the compounds for the dosimetry reactions and to improve detection efficiency for Cherenkov radiation counting. The selected compounds are listed in Table 5.11.1. They were proposed from the preliminary study due to the availability of compounds in high purity, ease of forming the compound into pellets and good water solubility. The improvement is based on some properties of Cherenkov radiation. Classical theory of this phenomenon indicates that at first a significant portion of the emission occurs in the ultraviolet spectral region and at second it has a highly directional light. If the ultraviolet photons can be converted to the visible region and if these photons give an isotropic spatial distribution, the counting efficiency should be distinctly improved.

The use of waveshifters in Cherenkov counting is the most important method for increasing total light output[2]. Among the tens of compounds to be used as waveshifting agents, Triton X-100 was selected because the aqueous Triton X-100 was not affected by solutions of interest. Optimum concentration of aqueous Triton X-100 (34%) increases ^{32}P counting efficiency by a factor about 1.3 as compared to water. In order to decrease the influence of the highly directional Cherenkov light on the counting efficiency, it is useful to use the vial with the frost walls. Cherenkov measurements ^{32}P activity were made using

three different vials: glass, polyethylene and Teflon. It has been found that the instrumental figure of merit for Teflon is almost twice as much as that of glass.

Consequently, the counting efficiency of ^{32}P in the Teflon vial filled with aqueous Triton X-100 (34%) was 66%, or 1.5 times as large as that in the glass vial filled with pure water. Although this is lower than the efficiency of liquid scintillation counting, the figure of merit, FOM, are much larger, because the volume of the aqueous sample for counting is much lager. Figure 5.11.2 shows comparison of FOM for measurement of ^{32}P in irradiated pellet of NH_4Cl after dissolution pellet in water. From the figure one can see that Cherenkov radiation counting can improve the FOM for LSC method by a factor of ~ 3.

References

1) Ross H.H. and Rasmussen G.T.: Liquid Scintillation Counting, Vol.1, ed. by Peng C., p.363, (Academic Press, New York, 1980).

2) Elrick R.H. and Parker R.P.: Int. J. Appl. Radiat. Isotopes 19, 263 (1968).

Table 5.11.1 Chemical compound and the maximum weight of activation detectors for Cherenkov radiation counting

Reaction	Threshold energy (MeV)	Compound	Max. weight for 100cc Teflon vial (g)
$^{31}P(n,\gamma)^{32}P$	—	$HN_4PH_2O_2$	51
$^{32}S(n,p)^{32}P$	2.3	$CH_3SO_2CH_3$	18
$^{35}Cl(n,\alpha)^{32}P$	3.7	NH_4Cl	25

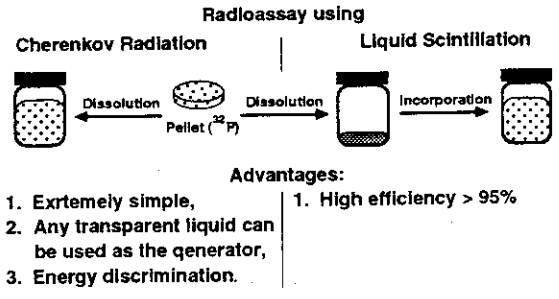

Fig. 5.11.1 Comparison of sample processing schemes for liquid scintillation counting and Cherenkov radiation counting.

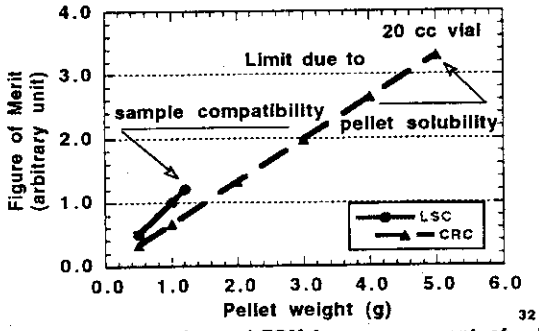

Fig. 5.11.2 Comparison of FOM for measurement of ^{32}P in NH_4Cl pellet by using Liquid Scintillation Counting (LSC) and Cherenkov Radiation Counting (CRC).

5.12 Neutron Irradaition Characteristics in International Fusion Materials Irradiation Facility

Y. Oyama, K. Noda, K. Kosako[1] and N. Yamano[1]

International Fusion Materials Irradiation Facility (IFMIF) is proposed under a collaboration of International Energy Agency (IEA). The facility generates fusion-like neutrons using d-Li reactions with 30-40 MeV and 250 mA deuterons. Two deuteron beams with an angle of 10 degree are injected to a flowing Li jet target with a square beam spot of 50 mm x 200 mm in typical size. Each beam current is 125 mA. Neutron field and damage parameter analyses were performed for an irradiation field generated by the above-mentioned deuteron beam to get basic information for making fusion materials test strategies using this facility.

First the analysis was made by the same analytical formulation as in Ref 1. The neutron field near the Li-jet target was calculated by considering neutron production reaction models and deuteron deceleration process in lithium layer. The difference from the previous analysis was in the two beam configuration. This configuration required completely three dimensional cordinates as shown in Fig. 5.12.1. The obtained neutron spectrum and angular distribution of emission yield are given in Fig. 5.12.2 and 5.12.3. The volumes with some typical neutron flux levels for fusion materials testing were estimated together with distributions of displacement damage and gas production rates for the uncollided neutrons.

The similar analysis was performed for the following four standard sample loading models in front of the target which were specified in IEA IFMIF-CDA preparatory activity: 1)Fe 50%, Void 50%, 2)Fe 50%, NaK30%, Void 20%, 3)SiC 50%, Void 50% and 4)SiC 50%, NaK 30%, Void 20%. The calculation was carried out by the Monte Carlo code GMVP with the HILO/86-J3 library that was modified from HILO/86 library by combining with JENDL-3.1. The energy and angular distributions of source neutrons were given by the analytical model mentioned above and used for the external volume source of the GMVP calculation. The calculated spectrum averaged in the loading sample is compared in Fig. 5.12.4 to the first wall spectrum of SSTR proposed by JAERI for the DEMO reactor. The flux distributions were caluculated inside the test regions filled with the standard loading samples as shown in Fig. 5.12.5. The flux-volume and dpa-volume relations were obtained for these standard loading samples. The dpa-He gas production ratio was also estimated inside the standard samples. In addition, the other parameters related to materials irradiation, such as nuclear heating, activation and nuclear transmutation, were evaluated.

---

[1] Sumitomo Atomic Energy Industries Ltd.

References

1) Oyama Y. , Yamaguchi S., Kosako K and Maekawa H.:" Calculation of Neutron Field Generated at Thick Li Target Bombarded with 10-40 MeV Deuterons for Energy Selected Neutron Irradiation Test Facility," JAERI-M 92-191 (1992)

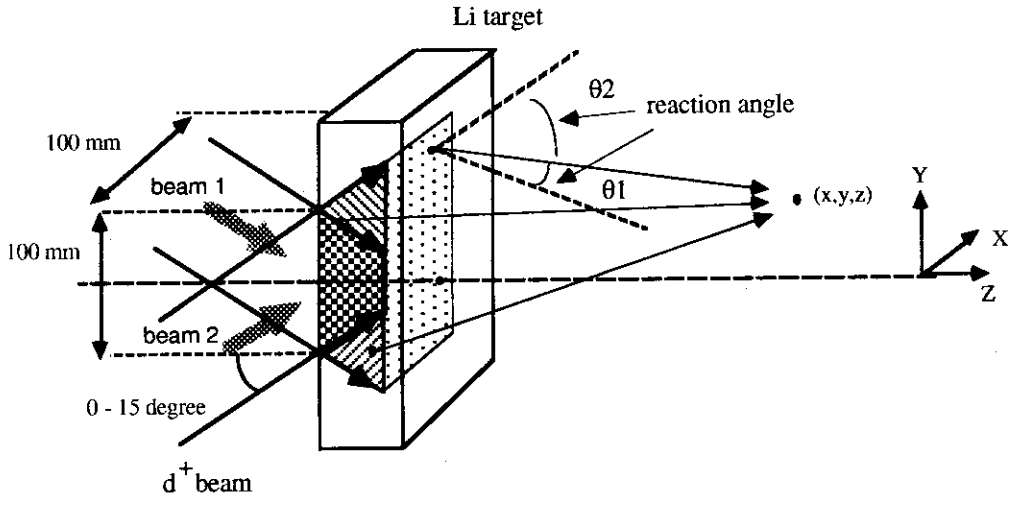

Fig. 5.12.1 Neutron Flux and Spectrum Calculation Model at Positions in Irradiation Field

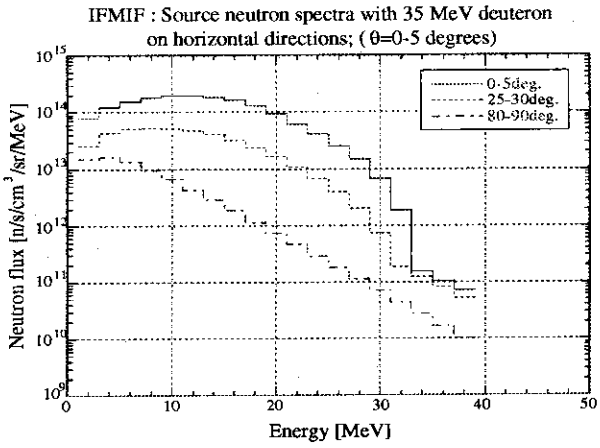

Fig.5.12.2 Neutron emission spectra for different angles

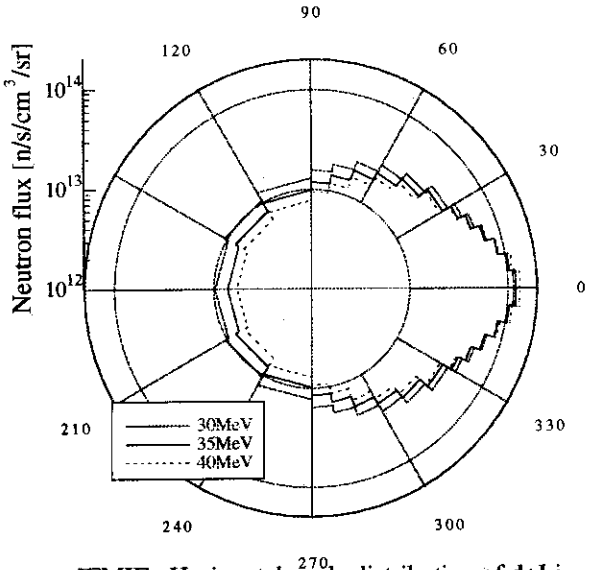

IFMIF : Horizontal angle distribution of d+Li neutron source

Fig. 5.12.3 Angular distribution of emitted neutrons on vertical plane

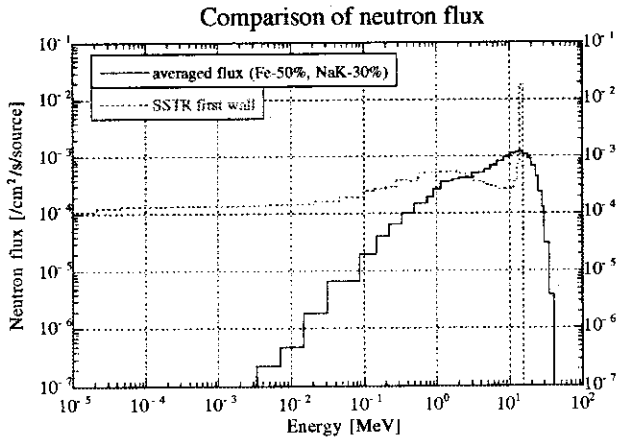

Fig. 5.12.4 Comparison of neutron spectra betwee SSTR and IFMIF

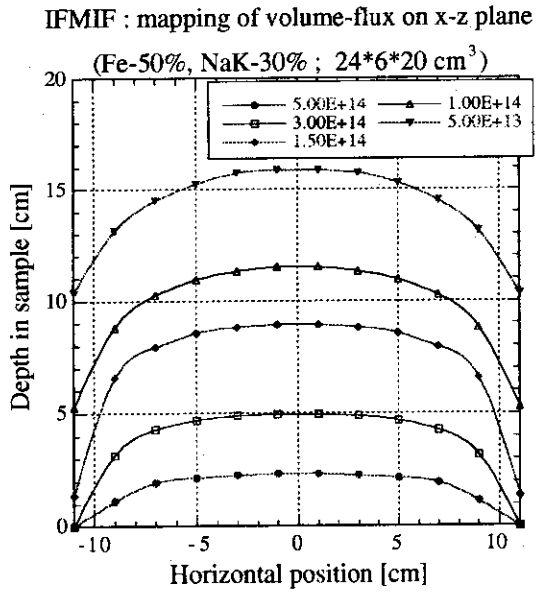

Fig. 5.12.5 Contour distribution of neutron flux in front of the target

6. Radiation Shielding

Studies on high energy radiation shielding have been made for the purpose of establishing a technological base of the wide utilization of intense proton accelerators. Four related works are reported in this category.

The neutron spectra and reaction rate distributions streaming through a labyrinth of the TIARA facility were measured to provide benchmark data and to estimate calculation accuracy of codes. Neutrons were generated by Cu(p,n) reactions in a thick copper target bombarded with 67 MeV protons. Neutrons and gamma rays were measured using activation detectors, fission chambers, solid state track detectors, TLDs, BC501 and bonner detectors and a rem-counter. Comparisons between the experiment and calculation using the Tesch's formula showed satisfactory agreement of factor three.

A point-kernel shielding code PKN-H, for the intermediate (0.01-400 MeV) energy source neutrons, was developed. Attenuation data of the code were prepared for water, concrete and iron by the one dimensional calculation using ANISN-JR with HIRO86R library. Finite medium effect can be corrected in the three dimensional combinatorial geometry calculation. Usefulness of the code was verified by comparing the attenuation results between the PKN-H and conventional Sn codes, such as, ANISN-JR and DOT4.2.

An energy response calculation code SSNRES has been developed for solid state nuclear track detectors applicable to the neutrons in the 100 keV to 20 MeV energy range. Simulation calculation results were compared with the experimental ones measured for various mono-energetic neutrons in the range, 100 keV to 15 MeV. Agreement was good in the whole energy range. Detection mechanisms are discussed by showing separately the contributions of various charged particles produced in the detector and radiator.

Effective dose per unit fluence for an anthropomorphic phantom was derived from equivalent doses of 13 kinds of tissues and organs. The doses were calculated assuming that they were irradiated with photons of eleven discrete energies from 1 MeV to 10 GeV. The effect of electron transport was analyzed by changing the exposure direction to the phantom. The dependence of dose equivalents on the geometry and depth was also analyzed for the same range of photon energy.

6.1 Measurements of Neutron Spectra and Reaction Rate Distributions Streaming Through Labyrinth

H. Nakashima and JAERI–Universities Collaboration Working Group for Accelerator Shielding Study

A lot of labyrinths are designed for entrance ways in high– and intermediate–energy accelerator facilities in order to reduce the intensity of radiations by multiple scattering. Radiation streaming through the labyrinths depends on the geometry of labyrinths and the characteristics of radiation generated in the facilities. Though it is important to estimate radiation streaming through labyrinths as well as radiation transmission through bulk shields, only a few experimental data for radiation streaming have been reported. Therefore, neutron spectra and reaction rate distributions streaming through a labyrinth was measured to provide benchmark data and to estimate the accuracy of calculational methods for radiation streaming.

Experiment has been carried out using the labyrinth of Light Ion Room 2 (LIR2) of TIARA as shown in Fig. 6.1.1. The target room has a dimension of 8.5 m x 7.5 m of cross section and 4.5 m in height. The attached labyrinth has cross sections of 1.5 m wide and 3.5 m high at the 1st and 2nd legs, and of 1.5 m wide and 3.0 m high at the 3rd leg. Neutrons was generated in the thick Cu–target in the LIR2 via Cu(p,n) reaction using 67–MeV protons. The incident proton beam intensity was monitored by a Faraday cup attached to the target, and the generated neutron intensity was also measured by ^{238}U and ^{232}Th fission chambers. Source neutron energy spectra and angular distributions were measured by eight kinds of activation detectors: ^{209}Bi for neutron up to 20 MeV, Al, Ti, Ni, Co, Nb, and In for neutrons in several MeV region and Au for thermal neutron. Measurements and the used detectors in the LIR2 and labyrinth are summarized in Table 6.1.1.

The neutron energy spectra measured by the BC501A and Bonner Ball detectors at three points along the lines in the labyrinth are shown in Fig. 6.1.2. The figure shows that the maximum energy of each spectrum decreases from about 35 MeV to 10 MeV and the ratio of thermal neutron to fast neutron increases with increasing the number of the legs and the distance from the entrance of the labyrinth, because of the multiple scattering of the high energy neutron in the labyrinth. Figure 6.1.3 shows the comparison of neutron dose equivalent rate in the labyrinth between measurement by the rem–counter and a design calculation of the labyrinth by Tesch's formula[1]. The design calculation was normalized by the ratio of the neutron yield generated by

67-MeV proton to that of 90-MeV proton, because the calculation was done so as to satisfy the specified design criteria assuming source neutron generated in a thick Cu target by 10μA-protons having the energy of 90 MeV[2]. The calculation is in agreement with the measurement within a factor of three. The result suggests that the calculation using the formula was adequate in the shield design of the labyrinth of TIARA.

Reference

1) Tesch K., et al., Particle Accel., 12, 169 (1982).

2) Watanabe H., et al., JAERI TIARA Annual Report Vol.2, 211 (1993).

Table 6.1.1 measurements and the used detectors in the LIR2 and labyrinth.

	in LIR2	in labyrinth
neutron spectra		BC501A [a] and Bonner Ball
fast neutron reaction rate	^{238}U and ^{232}Th fission chambers and SSNTD [b]	^{238}U and ^{232}Th fission chambers and SSNTD
thermal neutron flux	Au activation foil and TLDs	TLDs
gamma-ray exposure dose rate	TLDs	TLDs
neutron dose equivalent		rem-counter

a) BC501A liquid scintillation counter, b) solid state neutron track detector

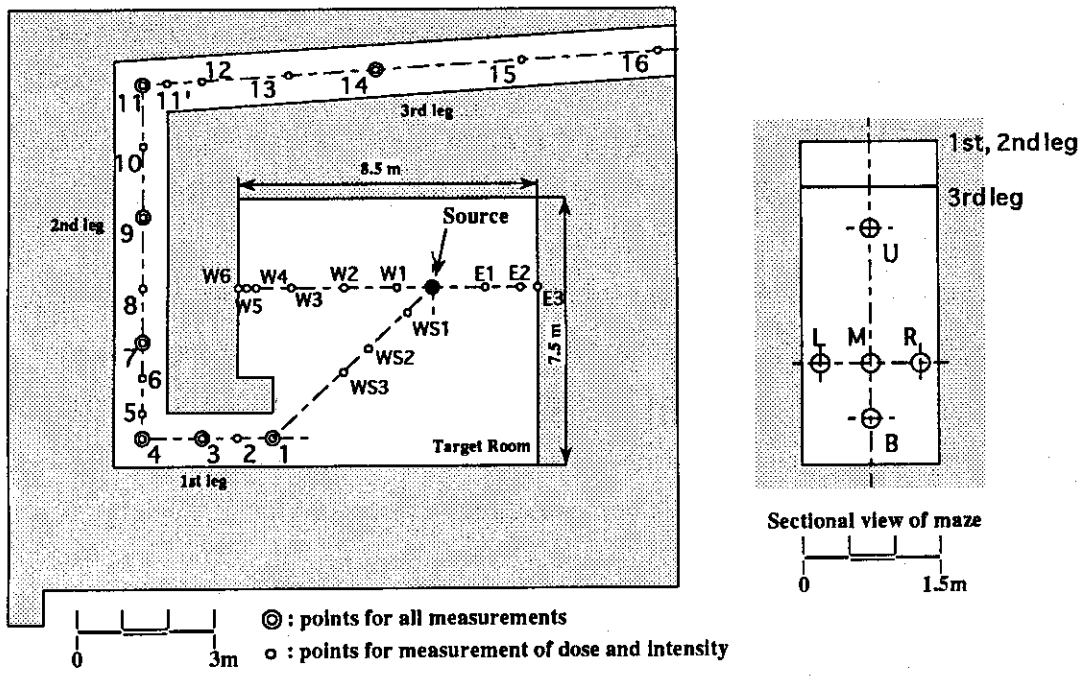

Fig. 6.1.1 A Plane view of LIR2 and measurement points for labyrinth streaming experiment.

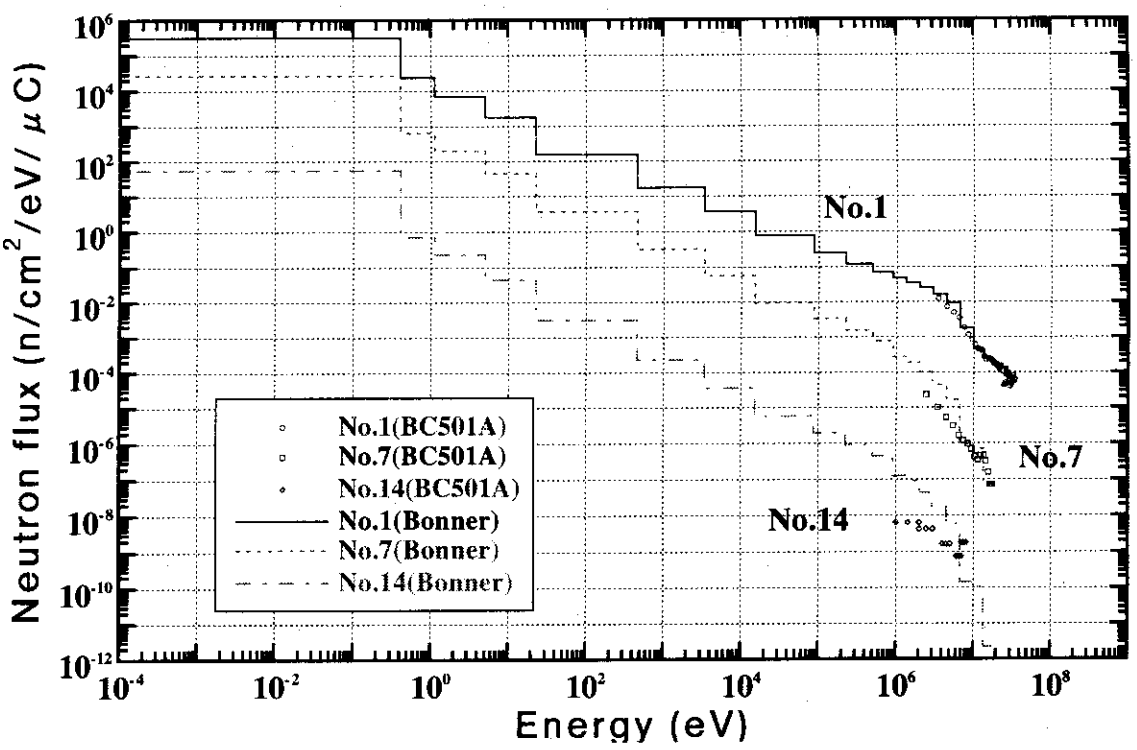

Fig. 6.1.2 Neutron energy spectra measured by a BC501A and Bonner Ball detectors in the labyrinth.

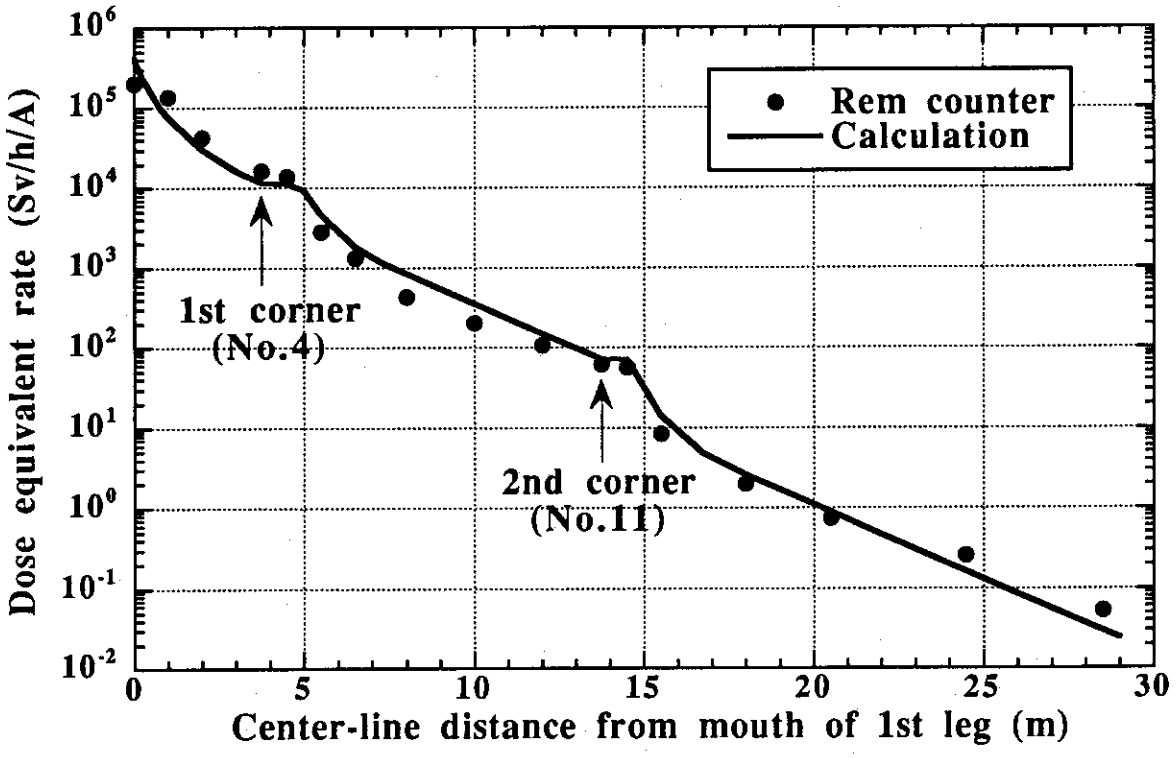

Fig. 6.1.3 Comparison of neutron dose equivalent rate between the measurement and calculation along the labyrinth.

6.2 Development of a Point Kernel Shielding Code (PKN-H) for Intermediate Energy Neutron Source Up to 400MeV

H. KOTEGAWA, Y. SAKAMOTO and S. TANAKA

Neutrons make the most substantial contribution to the total dose equivalent behind a concrete shield wall of proton accelerator facility. For the shielding calculations, Monte Carlo codes such as HETC and FLUKA has been proved to be especially useful for estimation of neutron production, but the use of these codes is too hard to carry out the thick shield calculations because of the limitation of computer resources. At high energy region above 1 GeV, Moyer model based on a point kernel method is very useful for proton incident problem, whereas such a useful method is not known for intermediate energy region under 1 GeV.

In the present study, a point kernel shielding code PKN-H[1] for the intermediate energy neutron source was developed. As for the attenuation data, the neutron and secondary gamma-ray dose equivalent rates were calculated in infinitely thick shields of water, ordinary concrete and iron of spherical geometry for 55 isotropic monoenergetic neutron sources from 0.01 to 400 MeV with the one dimensional discrete ordinates transport code, ANISN-JR, using macroscopic cross section library HILO86R[2] which was a revised version of HILO86 library. The conversion factors from fluence to dose equivalent were supplyed from ICRP Publication-51. These attenuation factors were parametrized by fitting to a 4th-order polynomial exponential formula in the neutron build-up region and to two kinds of simple exponential attenuating formula in the equiliblium spectrum region. Moreover, the correction factors for the finite medium effect were also calculated and installed in the PKN-H code.

The characteristics of PKN-H code are described as follows.

1)Neutron and secondary gamma-ray dose equivalents in water, ordinary concrete and iron shields for 55 monoenergetic neutron volume sources from 0.01 to 400 MeV are capable of calculation quickly and easily in 3-dimensional combinatorial geometry(CG).

2)The multi-layer calculation is carryed out using equivalent shielding distance.

3)The finite medium effect correction is taken into account at air region behind shields.

4) PKN-H is advantageous to dose equivalent calculations in deep penetration with useful attenuation lengths which are fitting parameters in equiliblium spectrum region for monoenergetic neutron source.

Fig.6.2.1 shows neutron and secondary gamma-ray dose equivalents calculated by PKN-H and ANISN-JR for 250 MeV source neutrons. A point source is placed at the center of a concrete tunnel. Neutrons penetrate the 1 m inner radius and 9m thick concrete wall shield. The PKN-H and ANISN-JR calculations were made in spherical geometry. For both neutron and secondary gamma-ray dose equivalents, the results of the PKN-H agree well with those of ANISN-JR from inner surface of concrete to 10 m in radius. The PKN-H with no consideration of the finite medium effect denoted by PKN-H/inf shows a little overestimation outside the concrete. If the correction for the finite medium effect is made, a better agreement is obtained as shown by the PKN-H/fini.

Consequently, PKN-H needs short cpu time, and its handling is quite tractable in comparison with the transport calculation codes, and its usefulness has been verifyed by comparing with the sophisticated transport codes; ANISN-JR, DOT4.2 and MCNP-4A for typical shielding problems. In multilayered shields, however, for example in iron-concrete double layer, which is a typical situation in a proton accelerator facility, neutron and secondary gamma-ray spectrum changes drastically on the boundary region of two shields. Such a drastic change is not taken into account in PKN-H at present.

References

1) Kotegawa,H., et al.:"PKN-H:A Point Kernel Shielding Calculation Code For Neutron Source Up to 400 MeV",JAERI-Data/Code 95-004(1995).

2) Kotegawa,H., et al.:"Neutron-Photon Multigroup Cross Sections for Neutron Energies Up to 400MeV:HILO86R -Revision of HILO86 Library-",JAERI-M 93-020(1993).

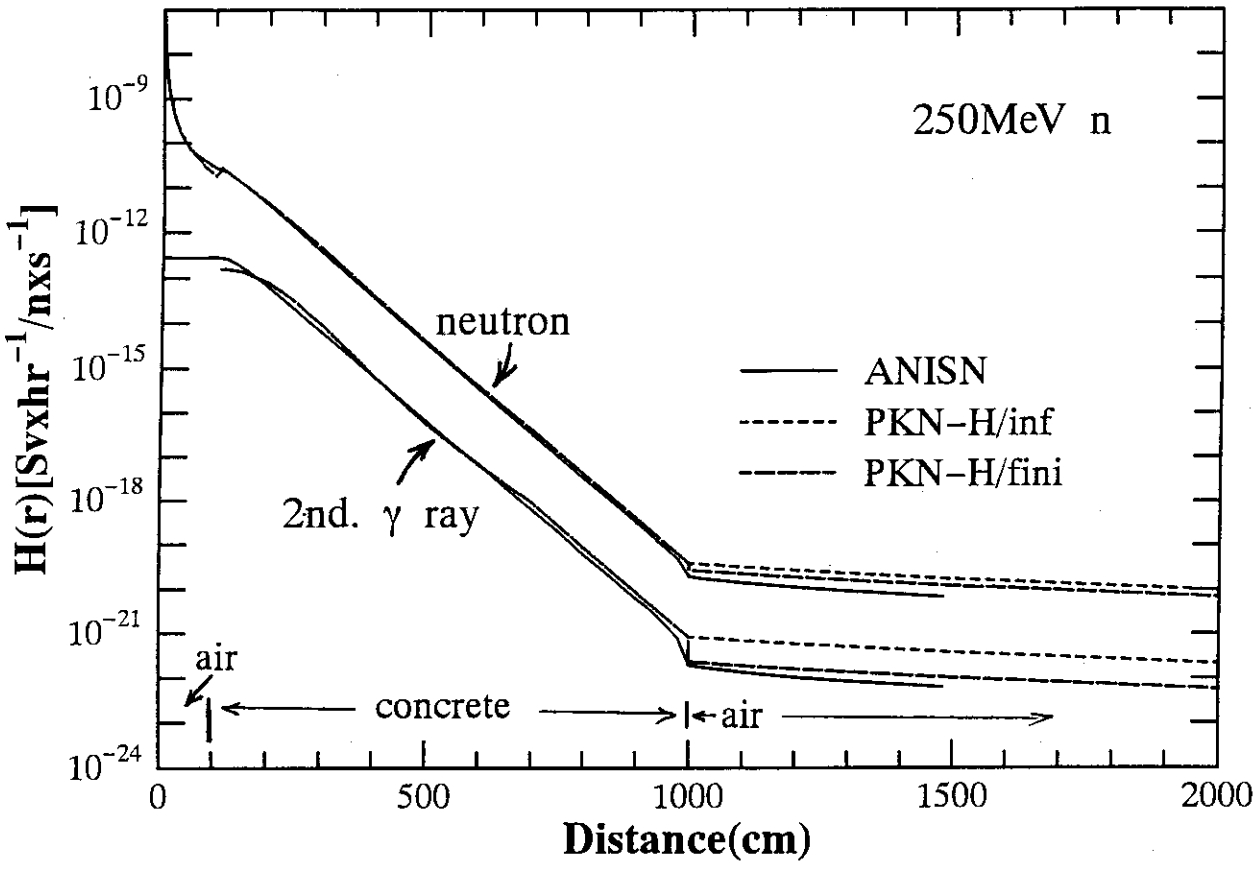

Fig.6.2.1 Calculational results of PKN-H of neutron and secondary gamma-ray dose equivalent for 250 MeV neutron penetrating through 9 m thick concrete in comparison with that of ANISN-JR

PKN-H/inf means PKN-H calculation without finite medium effect, and PKN-H/fini means that with finite medium effect.

6.3 Monte Carlo Calculation of Energy Response of SSNTDs to Neutrons up to 20 MeV

Y. Nakane, H. Nakashima and S. Tanaka

Solid state nuclear track detector (SSNTD) has been used in many fields of application because of its long-term stability, small size, low cost and insensitivity to gamma-rays. Energy response of the SSNTD depends on the kind of detector, the thickness and composition of a radiator and the conditions of etching. Therefore, an energy response calculation code system SSNRES has been developed for SSNTDs to neutrons in the energy range from 100 keV to 20 MeV. Charged particle production and transportation in the radiator and the detector were calculated with SCINFUL code[1] in SSNRES. Almost all reactions with a carbon were taken into account by using the reaction cross sections taken from ENDF/B-V, while the cross section of the $^{12}C(n,n')3\alpha$ reaction was derived from the evaluated cross section by Antolkovic[2]. The SCINFUL was modified so as to consider the reactions of O(n,n), O(n,n') and O(n,α) by introducing cross sections based on ENDF/B-VI. For calculation of transportation, ranges of 10 kinds of charged particles in the radiator and the detector were calculated with SPAR[3] and RSTAN[4] codes.

In the calculation, the shape of SSNTD was considered as a cylinder with a radius of 4 mm and the length of 2.4 mm. The polyethylene radiator of 1.4 mm thick was attached in front of the detector of 1.0 mm thick. Composition of the detector were the same as that of CR-39 (Allyl diglycol carbonate). Neutrons were vertically and uniformly injected on the surface of the radiator. The energy cutoff of charged particles was chosen to 30 keV, and the LET cutoff in the etch-removed layer was chosen to 5 keV/μm. The number of histories of calculation was so determined that the fractional standard deviation of calculation was less than 3%. The relation between the critical angle and LET of charged particle was based on Stafford's results[5], being adjusted so as to reproduce our measurements. Results of SSNTD response calculation are shown in Fig. 6.3.1 with experiments.

The responses of two type of detectors (TS-16N and MR-3) were measured[6] for the energy range from 100 keV to 15 MeV by using monoenergetic neutrons at the Fast Neutron Laboratory (FNL) of Tohoku University, and the response of MR-3 type detector was also measured using a ^{252}Cf source at a radiation standard facility in JAERI. Irradiated SSNTDs

were etched chemically for 15.5 hours in a circulating bath of 5 N NaOH solution at a temperature of 70℃. The thickness of the etch-removed layer was approximately 10 μm. All etch pits including linelike pits visible through the optical microscope of 400 times magnification were counted.

It is found that the calculated total response is in good agreement with experimental one in Fig. 6.3.1. The neutron response increases gradually with increasing neutron energy up to 8 MeV, while it decreases rapidly above 10 MeV because the LET of a recoil-proton in the etch-removed layer decreases. The response at 20 MeV is about one fifth of that at 8 MeV. Fine structure of neutron response observed in the energy range from 300 keV to 8 MeV is influenced by the resonance of elastic cross sections of carbon and oxygen.

In Table 6.3.1, the percentage of counted charged particles in the calculation is listed for five points of neutron energy and for 10 kinds of particles produced in the radiator and the detector. Recoil-proton of H(n,n) reaction and proton produced by the reaction with carbon are counted separately. In the table, all particles except recoil-proton are produced by the reacton with carbon and oxygen. The charged particles produced in the radiator are dominant in response at neutron energies of 3 and 10 MeV. Particles produced in the detector are dominant in response at neutron energy below 0.5 MeV because particles produced by the low energy neutrons have so short range that the particles produced in the radiator cannot reach the detector. The fractions of particles produced in the radiator and the detector are comparable at 20 MeV. More than 90% of etch pits are caused by recoil-protons in the neutron energy from 3 MeV to 10 MeV. On the other hand, the percentage of charged particles produced by the reactions with carbon and oxygen increases drastically from about 10% at 10 MeV to about 87% at 20 MeV.

References

1) Dickens J. K. : ORNL-6463 (1988).
2) Antolkovic B., et al. : Nucl. Phys., A394, 87 (1986).
3) Armstrong T.W. and Chandler K.C. : ORNL-4869 (1973).
4) Bichsel H. : private communication (1992).
5) Stafford P. M., et al. : Nucl. Tracks Radiat. Meas. 14, 373 (1988).
6) Yasubuchi S. : Private communication (1994).

Table 6.3.1 The percentage of counted charged particles produced in the radiator and the detector

Neutron Energy	0.2 MeV		0.5 MeV		3 MeV		10 MeV		20 MeV	
	Rad	Det	Rad	Det	Rad	Det	Rad	Det	Rad	Det
p(recoil)	11.2	68.4	25.0	47.8	87.4	3.0	89.5	0.1	12.5	0.1
p(carbon)									14.8	0.4
d										
α							0.8	2.2	22.4	12.1
^{9}Be							0.1	0.7	0.6	0.4
^{11}B										1.2
^{12}B										0.4
^{12}C	0.4	13.9	0.5	18.3	0.6	5.8	0.2	3.6	2.7	17.5
^{13}C								0.6		0.9
^{16}O		6.1		8.4		3.2		2.2		14.0
total(%)	11.6	88.4	25.5	74.5	88.0	12.0	90.6	9.4	53.0	47.0

The fractions of proton produced by the reaction of the carbon are negligibly small.
Rad: the fraction produced in the radiator
Det: the fraction produced in the detector

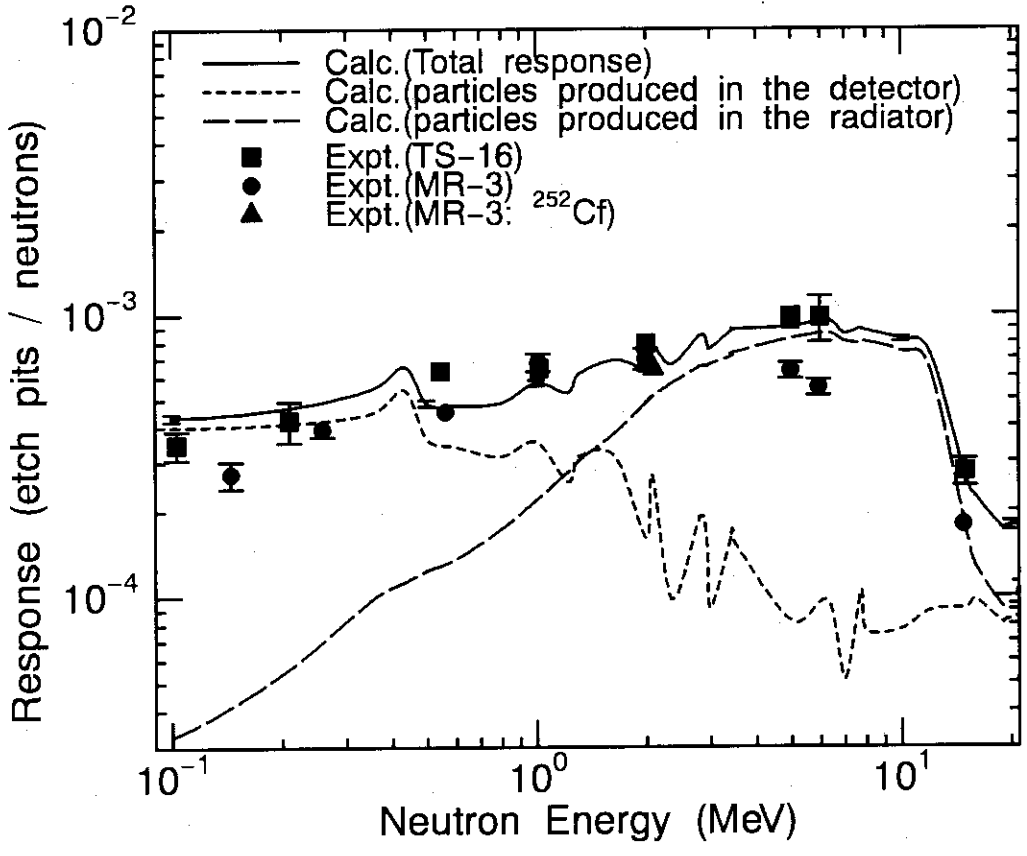

Fig. 6.3.1 Calculated and measured responses of SSNTDs to neutrons

6.4 Evaluation of Fluence to Dose Equivalent Conversion Factors for High Energy Radiations (III)

– Effective Dose for Photons Higher than 10 MeV –

Y. Sakamoto, S. Tanaka, O. Sato *, N. Yoshizawa *, S. Furihata *, S. Iwai **
and T. Uehara **

Along with the increase of high current and high energy accelerator facilities, the evaluation of effective dose for high energy photons and neutrons has come up to an important problem from the view point of radiation protection.

Equivalent doses in tissue and organs at 11 photon energies from 1 MeV to 10 GeV have been calculated with the EGS4 code [1] for AP (anterior–posterior: uniform parallel beam from the front side of the body to the rear side) and PA (posterior–anterior: uniform parallel beam from the rear side to the front side) geometries. The anthropomorphic phantom placed in a vacuum environment, which was represented using MARS [2] geometry package, was irradiated by aligned and expanded photons. For each energy, about 5 million histories were tracked to attain the stochastic error of the effective dose within a few percent. The effective dose per unit photon fluence was derived from the equivalent doses with the tissue weighting factors specified for 13 kinds of tissue or organs in ICRP60.

The calculating cutoff energy for photons was fixed to 0.1 MeV below that photons gave all energy to media. As for electrons and positrons, the cutoff energy was set to 0.5 MeV corresponding to the Continuous Slowing Down Approximation (CSDA) range of 0.18 cm in water, which would give no significant effect to the absorbed dose calculation in tissue and organs. In this approximation, electrons or positrons are assumed to lose energy continuously along their tracks, with a mean energy loss per unit pathlength given by the stopping power. Additional calculations with a cutoff energy higher than incident photon energy also were tried to examine the effect of a neglect of secondary electron transport using kerma approximation adopted in ICRP51.

Figure 6.4.1 shows the effective doses obtained for AP and PA conditions with and

* Mitsubishi Research Institute, Inc.
** Mitsubishi Heavy Industries, Ltd.

without electron transport. The difference between the effective doses calculated with and without secondary electron transport in AP and PA geometries grows large with increasing the incident photon energy from 10 MeV [3]. The effective doses for 10 GeV photons calculated without electron transport become 2 decades larger than those calculated with electron transport. The values with electron transport in PA geometry are larger than those in AP geometry at the energy above 10 MeV. The energy deposition due to energetic electrons or positrons with large penetration depth produced from high energy photons contributes to the equivalent doses in tissue and organs strongly. Therefore, the equivalent doses in PA geometry are large for a testis and a breast located at the front side, while there has been observed only a little difference of the equivalent doses for an ovary and the remainder located in the middle of the body.

Figure 6.4.2 shows the comparison of (a) the dose equivalent at 1-cm depth on the principal axis of ICRU sphere with 30-cm diameter, (b) the maximum dose equivalent on the principal axis of ICRU sphere, (c) the dose equivalents at 1-cm, 10-cm and 20-cm depth in a slab with 30-cm thickness, (d) the maximum dose equivalent in a slab and (e) the effective doses calculated with the anthropomorphic phantom in PA or AP geometry in the photon energy range from 1 MeV to 10 GeV [3]. The good agreement was observed between the energy dependence of dose equivalents at 1-cm depth in a ICRU sphere and a slab. The dose equivalent at 10-cm depth in a slab agree with the effective dose calculated in PA geometry at the energy above 10 MeV. The dose equivalent at deeper position than 1-cm depth of a slab phantom can be used as the operational quantity for the effective dose of high energy photons.

References

1) Nelson W.R., Hirayama H. and Roger W.O.: "The EGS-4 Code System", SLAC-265 (1985).
2) West J.T. and Emmett M.B.: "MARS: A Multiple Array System Using Combinatorial Geometry", NUREG/CR-0200, Vol.3, sect.M9(1980).
3) Sato O.: "The Calculation of Effective Dose for Photons Higher than 10 MeV", p.76-84, Proceedings of the Workshop on Dosimetry for External Radiations, January 19-20, 1995, JAERI, Tokai, JAERI-Conf 95-007 (1995), (in Japanese).

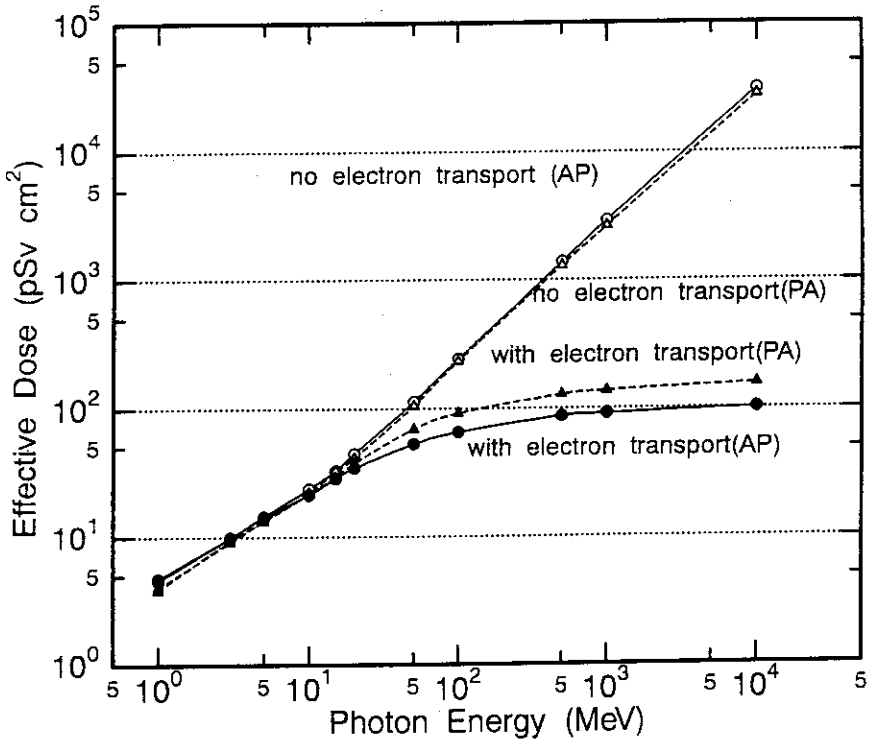

Figure 6.4.1 Effective doses calculated with and without secondary electron transport for PA and AP conditions vs. incident photon energy

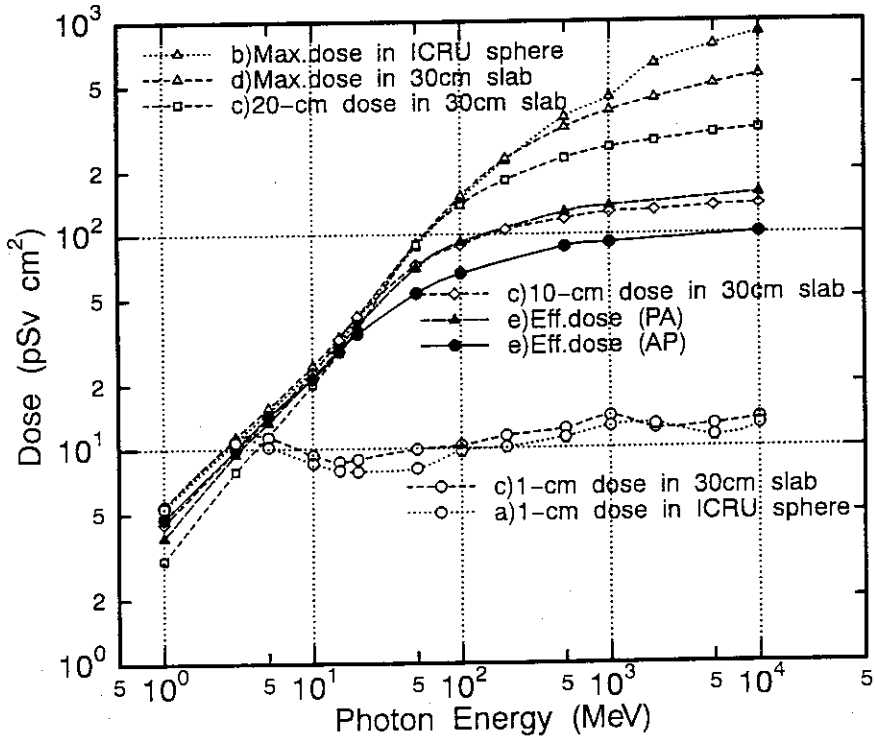

Figure 6.4.2 Effective doses (PA and AP conditions) and dose equivalents in 30 cm-slab or ICRU sphere vs. incident photon energy

7. Reactor and Nuclear Instrumentation

In R&D works of reactor and reactor-relevant instrumentation, efforts were made to test performance characteristics of fuel failure detection (FFD) system, to investigate the feasibility of a position sensitive neutron detector and to explore the method to assess nondestructively the material degradation in aged RPVs (reactor pressure vessels). The FFD system was developed for HTTR (high-temperature engineering test reactor) that is just under construction in the Oarai-site of JAERI. The FFD system adopts a wire precipitator to catch noble-gaseous fission products. The improvement of FFD performance has been tried out by utilization of a nuclide-separation type wire precipitator that was newly invented. The feasibility study of position sensitive neutron detector has been carried out, aiming at development of an advanced reactor-power-distribution monitoring system. The detector is of a fission counter and employs a delay-line structure of electrodes to detect positions where fission occurs. In the present stage of study, theoretical and analytical approaches are conducted. The proposed method for nondestructive measurement of material degradation in aged RPVs is based on measurement of magnetic coercivity of RPV steel and named "Magnetic Interrogation Method (MIM)". The MIM relies on that the radiation hardening of RPV steel is followed by the increase of its coercivity. In the implementation of MIM, nondestructive measurement of nonmagnetic overlay-clad thickness of RPV is very essential. Main topics in nuclear instrumentation are R&D works of nondestructive measurement to assess α -radioactivity in TRU wastes. The works have been carried out to develop methods to inspect the wastes returned from overseas. Now, the works are shifted to treat with domestic wastes and new studies are started to develop a high sensitive system to measure very low level TRU wastes by combination of passive and active neutron assays and gamma-ray CTs.

As concerns fundamental researches in the field of instrumentation and measurement, light emission characteristics of various scintillators have been experimentally investigated to explore the feasibility of a new two-dimensional radiation detector in which semiconductor light sensors are applied together with scintillators. Also, some efforts are made to contribute to fusion researches. One of topics is development of neutron emission profile monitor.

All the above are performed in Sensing Technology Laboratory.

7.1 Development of a Directional Neutron Detector for Neutron Emission Profile Monitor

J. Kaneko, K. Ara, Y. Ikeda and H. Maekawa

Neutron emission profile monitors are used on fusion plasma diagnostics[1] and nuclear fuel safety research[2]. These diagnostic systems need huge multiple channel neutron collimators and neutron detectors. In plasma diagnostics, only a few multiple channel neutron collimators can be adopted to a nuclear fusion device because of their huge size and heavy weight. This results in lack of lines of sight and view points, and then it corrupts spatial resolution and accuracy of neutron emission density on reconstructed profiles.

The authors have been developing a directional neutron detector for reducing the size of multiple channel neutron collimator. Figure 7.1.1 shows schematically the principle of directional neutron detection. This detector is a kind of recoil proton telescope and consists of three parts; a radiator, a recoil proton collimator and a charged particle detector. The recoil proton collimator limits the scattering angles that allow recoil protons to enter the charged particle detector. The detector can have directional sensitivity by using the recoil proton collimator and energy discrimination.

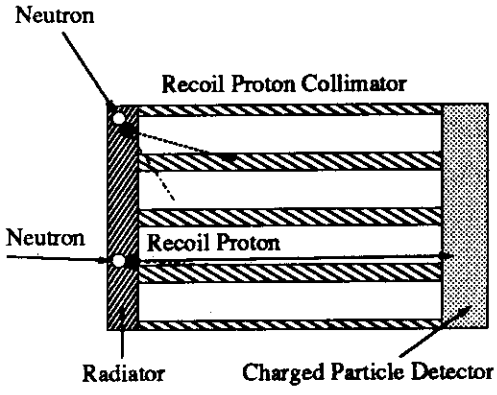

Fig. 7.1.1 Principal of directional neutron detection

Table 7.1.1 Detector components

Radiator;	Polyethylene	30 mm × 30 mm × 1 mm
Recoil Proton Collimator;		
#1	Aluminum,	25 mm × 25 mm × 2 mm, ϕ 1.4 mm × 188 holes
#2	Aluminum,	30 mm × 30 mm × 2 mm, ϕ 0.8 mm × 492 holes
#3	Lead,	25 mm × 25 mm × 2 mm, ϕ 1.4 mm × 188 holes
Scintillator; CsI(Tl),		25 mm × 25 mm × 2 mm

The response function of the developed directional neutron detector was measured for 14 MeV neutrons at the facility of Fusion Neutron Source (FNS). In this measurement a CsI(Tl) scintillator and a photo multiplier were used as a charged particle detector. A CsI(Tl)

scintillator was chosen for rise time pulse shape discrimination. Components of the detector are listed in Table 7.1.1.

Figure 7.1.2 shows a measured response function, where one can see three regions of alpha, proton and background gamma. The proton region is induced by recoil protons and (n, p) reactions in the scintillator that decrease the signal-to-noise ratio. Figure 7.1.3 indicates proton energy spectra for several neutron incident angles. These spectra were measured with rise time discrimination. There is a marked decrease of counts in the high energy region with the increase of neutron incident angles. Directional sensitivity is shown in figure 7.1.4, and relative efficiency becomes half at 25 degrees.

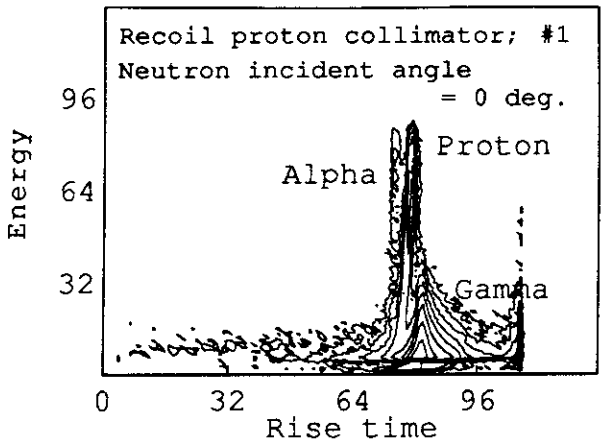

Fig. 7.1.2 A response function for 14 MeV neutrons

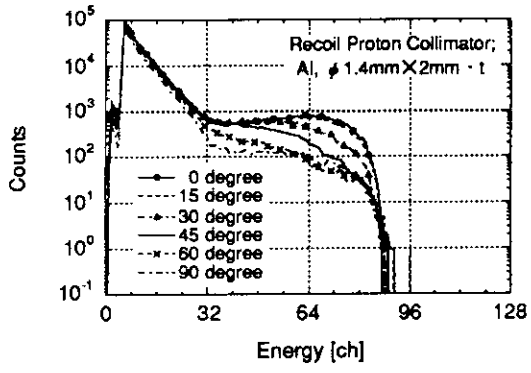

Fig. 7.1.3 Proton energy spectra for several neutron incident angles

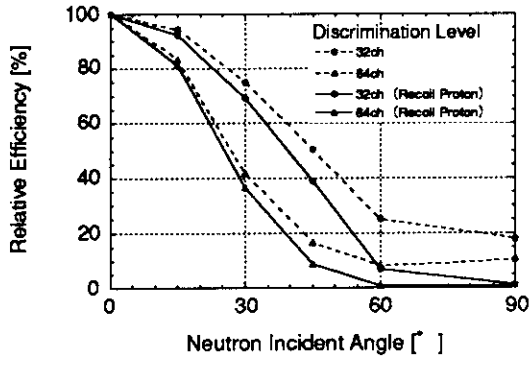

Fig. 7.1.4 Directional sensitivity

Applying suitable scintillator geometry, this detector can get directionality for 14 MeV neutrons only by energy discrimination. A scintillator that has fast decay time and low cross section about (n, p) and (n, α) reactions is important for this detector.

References

1) Adams J. M., et al. : Nucl. Instrum. Meth., A329, 277, (1993)

2) Baumung K., et al. : Nuclear Technology, 71, 353, (1985)

7.2 Investigation of Nondestructive Method for Measuring the Overlay-clad Thickness of Reactor Pressure Vessel

K. Sakasai and K. Ara

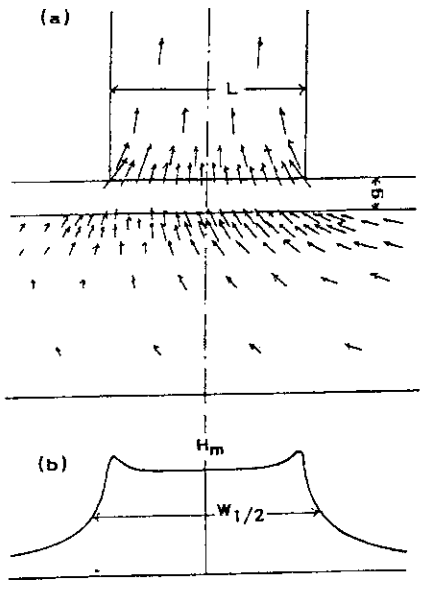

Fig.7.2.1 Magnetic field distribution in the vicinity of the pole of a magnetic yoke. (a) flow of the magnetic flux and (b) magnetic field distribution perpendicular to the surface of the RPV wall.

The authors have proposed a new method, MIM (Magnetic Interrogation Method), for nondestructive measurement of radiation damage of reactor pressure vessel (RPV)[1)-2)]. The method relies on good correlation[3)] between the levels of radiation-induced hardening and magnetic coercivity change in RPV. On the other hand, the nonmagnetic or very weak (negligible) magnetic overlay-clad ranges in its thickness from about 5 mm to 10 mm in RPV, and it differs from part to part of RPV. Since a part of RPV is magnetized from its inner-wall side through the overlay-clad by a magnetic yoke and the coercivity distribution in RPV is estimated by MIM, it is necessary to know the thickness of the clad before implementation of the MIM.

When the RPV is magnetized from the state of zero magnetization to about saturation with the MIM, flows of magnetic flux in the vicinity of the pole of the yoke become as shown Fig. 7.2.1(a) and one can obtain a magnetic field distribution being perpendicular to the surface of the overlay-clad as shown Fig. 7.2.1(b). Then the normalized center value H_m/NI and half-width $W_{1/2}$ in the field distribution pattern can be determined, where NI is "ampere-turns" applied to the magnetic yoke. Supposing these values are directly related to the overlay-clad thickness g, one may know the value of g from H_m/NI and $W_{1/2}$.

The above idea was examined through magnetostatic analyses with a commercially available software. Figure 7.2.2 illustrates the system

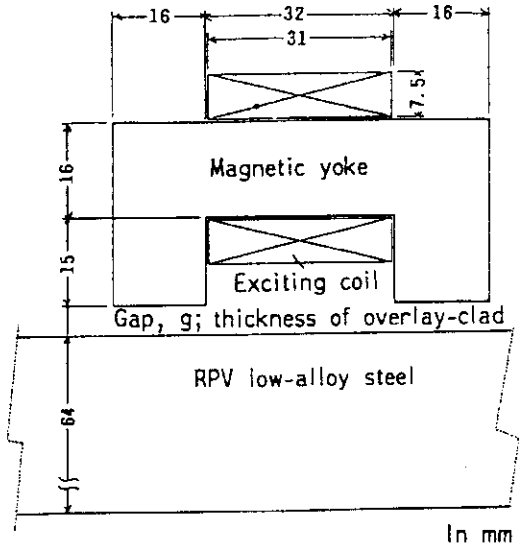

Fig.7.2.2 Two-dimensional system geometry for magnetostatic analyses.

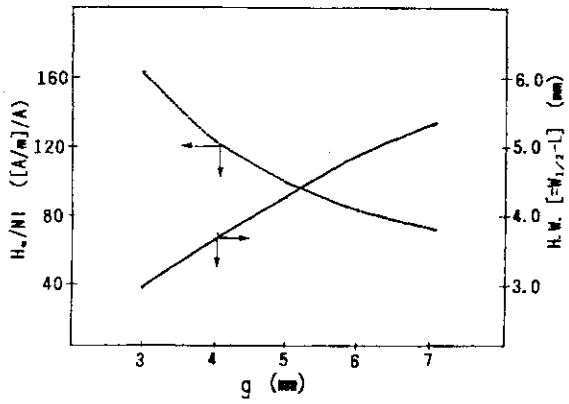

Fig.7.2.3 Results of magnetostatic analyses; H_m/NI and H. W. (=$W_{1/2}$-L) as a function of g, where L is the width of the yoke pole.

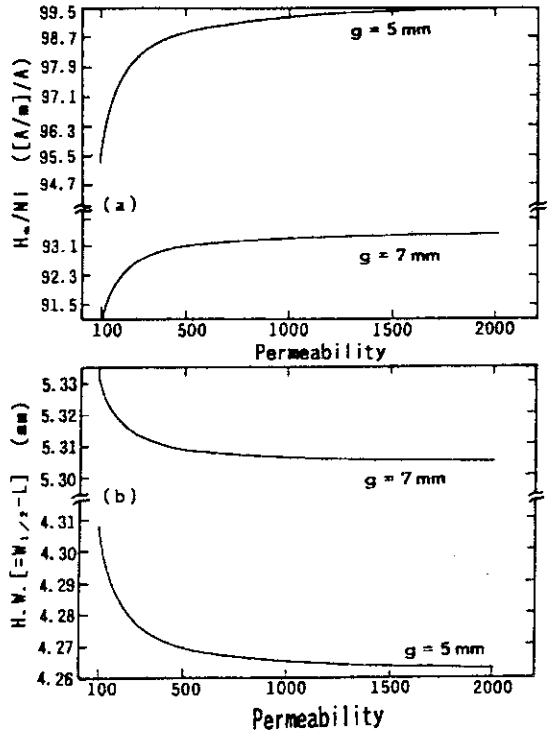

Fig.7.2.4 Results of magnetostatic analyses; (a) H_m/NI and (b) H. W. (=$W_{1/2}$-L) as a function of RPV steel permeability.

geometry for the analyses. Here the gap g represents the thickness of the overlay-clad. The magnetic field distributions were evaluated on the plane being 0.25 mm distant from the edge of the pole of the yoke.

Assuming the permeability of the yoke and RPV steel as 10^3, the relations between H_m/NI (or $W_{1/2}$) and g were calculated. The results are shown in Fig. 7.2.3. In the figure, instead of $W_{1/2}$, H.W. (=$W_{1/2}$-L) is indicated on the right ordinate, where L is the width of the pole of the yoke. Then, the changes of H_m/NI and $W_{1/2}$-L with variations of permeability of RPV steel were calculated for the cases of g = 5 mm and g = 7 mm, with the yoke permeability of 10^5. The results are shown in Fig. 7.2.4. One sees that H_m/NI and $W_{1/2}$-L depend only on g when the permeability of RPV steel is large enough. A simple calculation showed that the value of g can be determined within the ambiguity of 0.025 mm by magnetizing the RPV steel to a level where its permeability becomes larger than 500.

References

1) Ara K. et al., 1993 Fall Meet. of the Atom. Energy Soc. Jap., paper D-11(1993)

2) Ara K. et al., JAERI-Review 94-009, 184(1993)

3) Popp K. et al, Kernenergie, 29, 22(1986)

7.3 Development of Nuclide-Separation Type Wire Precipitator for Noble-gas Fission Products

M.Kishimoto, M.Katagiri, H.Ito, H.Yoshida, M.Fukushima, H.Ohkawa and T.Saruta

In high temperature gas-cooled reactors (HTGRs), the noble-gas fission products (FPs) are released into the primary coolant system from normal nuclear fuels. Therefore, for detecting fuel failure of HTGRs, a detector having high sensitivity and fast response is needed to quantify concentrations of noble-gas FPs released from nuclear fuels and to determine the precise fuel failure fraction. The wire precipitator is a very sensitive detector suitable for measuring radioactive noble-gas FPs released from nuclear fuels. The authors have been developing a fuel failure detection system using the nuclide-separation wire precipitator [1]. We applied it to the measurement of noble-gas FPs released from a coated particle fuel sample irradiated in the Japan Material Testing Reactor (JMTR) and examined the response characteristics of the precipitator to three noble-gas FPs, i.e., ^{88}Kr, ^{89}Kr and ^{138}Xe. Figures.7.3.1 and 7.3.2 show the schematic diagram of the nuclide-separation precipitator and the fuel failure detection experimental equipments using FGS gas-swept capsule of JMTR respectively. The main body of precipitator is of the Mark XI precipitator made by the Plessey Company Limited in the UK. We altered the volume of precipitation chamber from 1000cm^3 to 120 cm^3 and adopted the 6 mm thick CaF(Eu) scintillator to measure the beta particle up to 5 MeV emitted from the daughter nuclei of noble-gas FPs precipitated on the wire.

(1) Dependency of radioactivity concentration on soak time

We change the time which noble-gas FPs is precipitated on the wire (soak time) and measured the dependency of radioactivity concentration on sork time. Figure 7.3.3 shows the radioactivity concentration calculated from the response functions of precipitator into account [1].

(2) Dependency of radioactivity concentration on flow-rate of sampling-gas

When the flow-rate of sampling-gas changes, the precipitation rate of noble-gas FPs changes by the dilution effect of page-gas. We measured the dependency of radioactivity concentration on flow-rate of sampling-gas. In Figure7.3.4, we show the measured results. The radioactivity concentrations of ^{88}Kr and ^{138}Xe are about independent on the flow-rate of sampling-ga;. But that of ^{89}Kr increases with the flow-rate.

(3) Dependency of counting rates on precipitation voltage

We measured the dependency of precipitation rate of noble-gas FPs on the precipitation voltage. Figures7.3.5 and 7.3.6 show the measured results for the flow-rates of sampling-gas of 25cm^3/min and 100cm^3/min respectively.

References

1) M.Katagiri. et al. : Nucl. Inst. and Meth. A327(1993)463-468

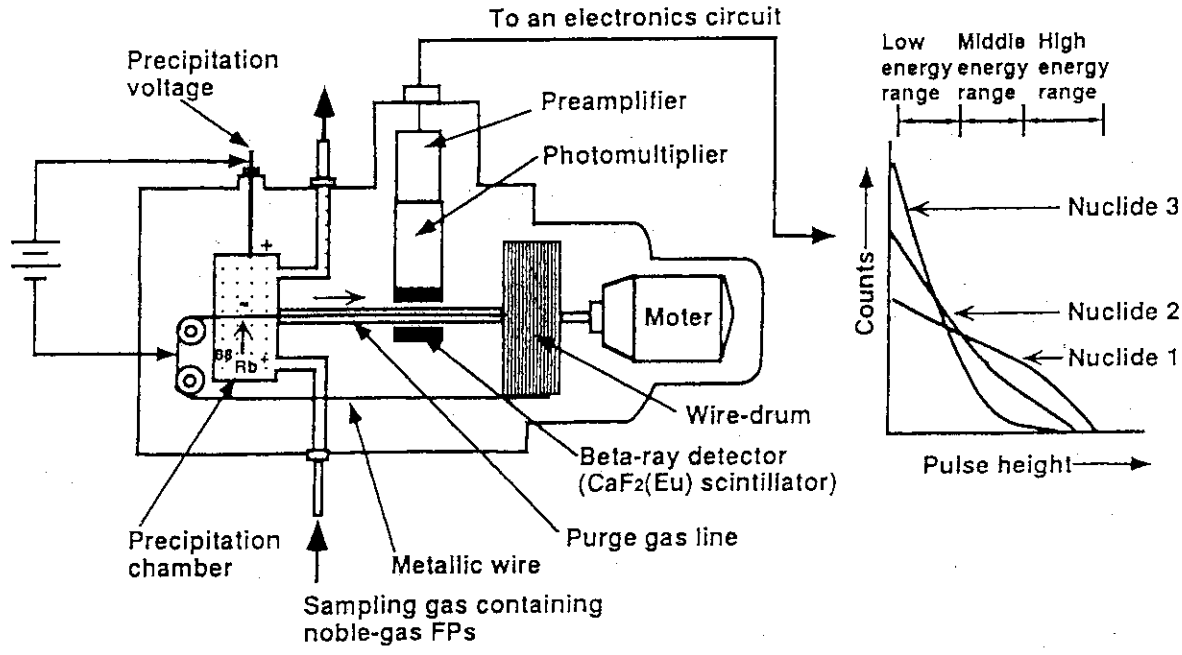

Fig.7.3.1 Schematic diagram of nuclide-seperation wire precipitator

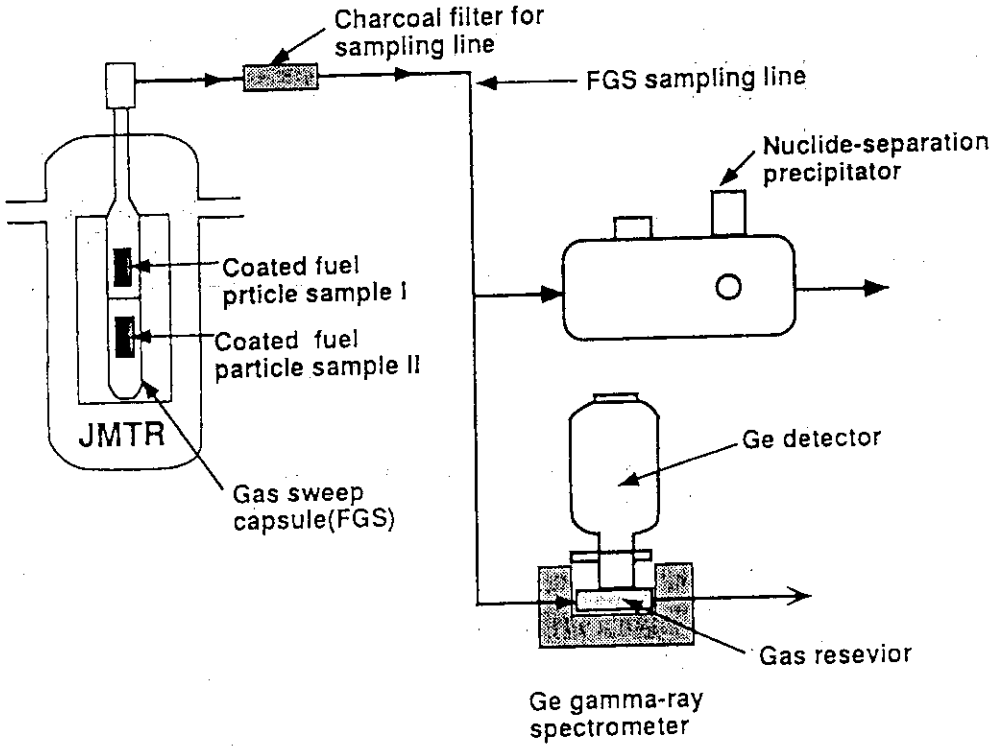

Fig.7.3.2 FFD experimental equipments using FGS gas-sweep capsle in JMTR

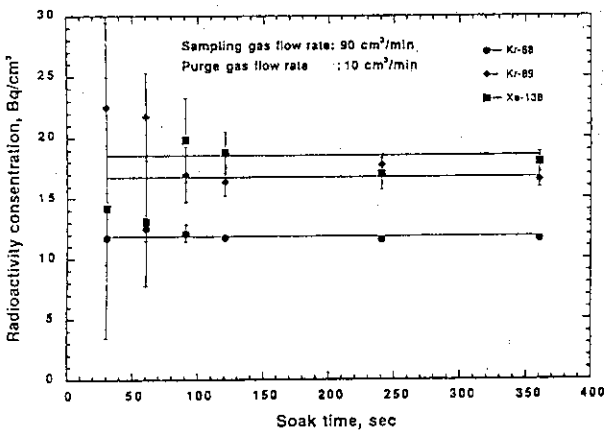

Fig.7.3.3 Dependency of radioactivity concentration on soak time

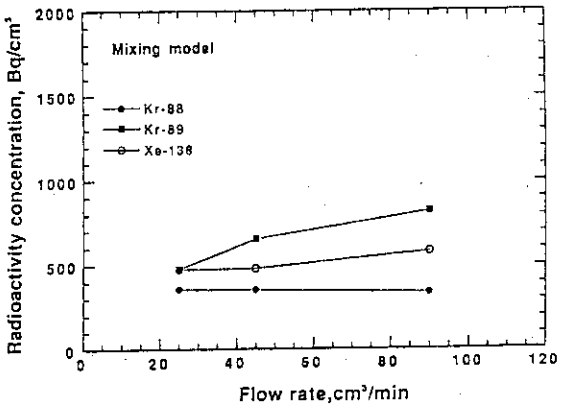

Fig.7.3.4 Dependency of radioactivity concentration on flow-rate of sampling-gas

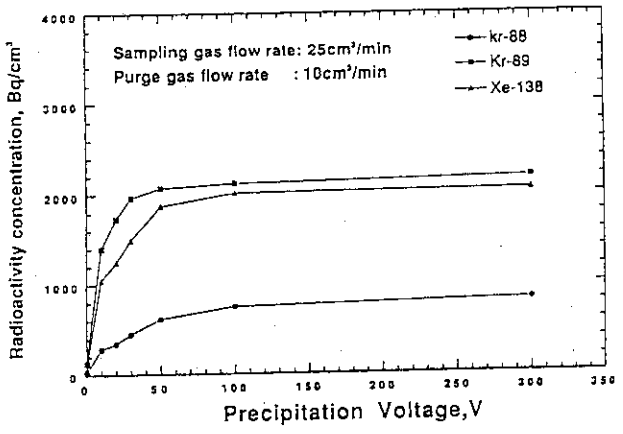

Fig.7.3.5 Dependency of counting rates on precipitation voltage under sampling-gas flow-rate of 25cm³/min

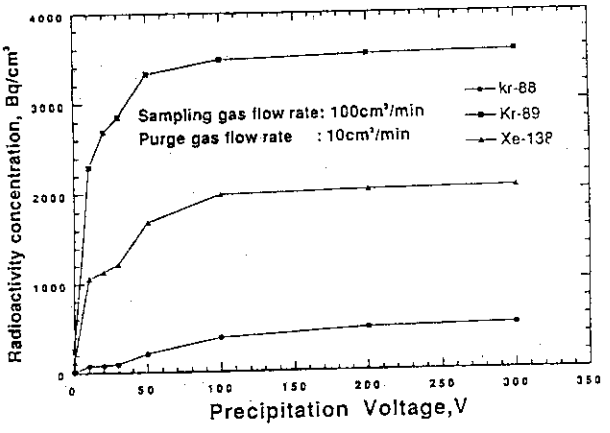

Fig.7.3.6 Dependency of counting rates on precipitation voltage under sampling-gas flow-rate of 100cm³/min

7.4 Measurement of Scintillation Pulse Shapes

H. Yagi, H. Itoh and M. Yamada

The experimental investigations have been performed for the scintillation response that include the relation between the emission spectra and the decay time. As the first stage, the emission spectra of the typical inorganic scintillators had been measured.[1] As the following stage, the emission pulse shapes have been measured. These results support the development of X-ray image sensor that is integrated scintillator on the semiconductor photo detector for the synchrotron radiation. It is necessary to know the relation between the emission spectra and the decay time, for the development of the advanced phoswich detector that is applied to measure the α emit nuclide.

Voltage pulse shapes appear on an accumulating capacitance charged by the output current of the photo multiplier, and these are observed by the sampling oscilloscope. The voltage pulses are integral forms of the scintillation emission pulses on the integrating circuit. The voltage pulse signals are observed through the emitter-follower circuit that has smaller distortion than the one by the band width limitation on the voltage amplifier circuit. When the computer takes the data from the oscilloscope, three steps of signal processing are performed to obtain better pulse shapes. At the first step, pulse height discriminating process make a stable trigger level. Following step, pulse shape discrimination reject piled up pulses. At the finals, the taking voltage pulse data are accumulated by the averaging process and are corrected by the circuit time constant. The scintillation emission pulse shapes are obtained by the arithmetic differentiation of the corrected voltage pulse data.

The approximation of multi-components linear functions for the logarithmic emission pulse shapes are performed to estimate the decay time constant of the scintillation emission. These results show that the NaI(Tl) has two components of decay time and the ZnS(Ag) has four or more components. The output wave form of the shaping amplifier is simulated by the giving four components to the ZnS(Ag) for convenience sake. Typical emission pulse shapes and the estimation of these decay times for the NaI(Tl) and the ZnS(Ag) scintillators were shown in Figure 7.4.1. A change of pulse shapes by the light spectrum shift using the optical filters for the ZnS(Ag) is shown in Figure 7.4.2. The results support the effects of the optical filters for the phoswitch detector that is combined two scintillators with the different decay times.[2]

References

1) Itoh H., Asano Y., Yamada M. and Yagi H.: Proc. Fall Meet. of AESJ, p.356, 1993.
2) Usuda S. and Tayama T.: Proc. Annual Meet. of AESJ, p.594, 1994.

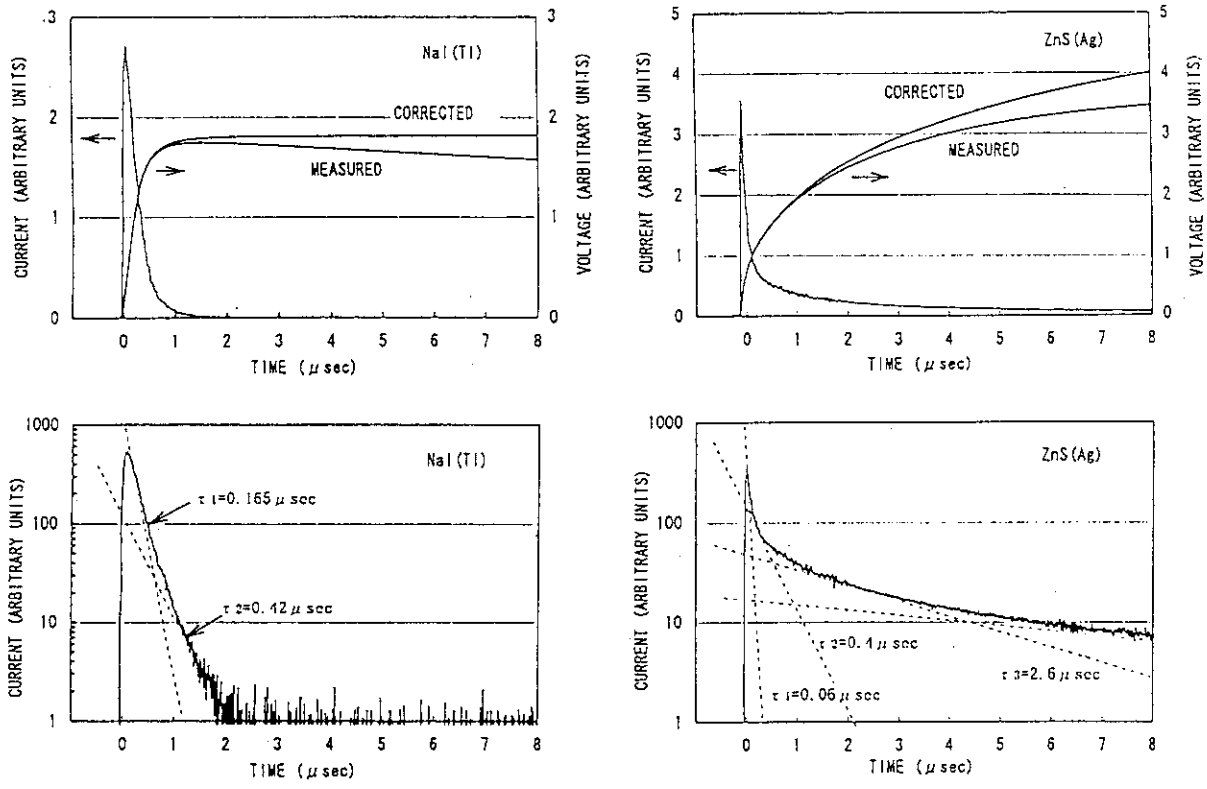

Figure 7.4.1 The scintillation emission pulse shapes of the NaI(Tl) and the ZnS(Ag)

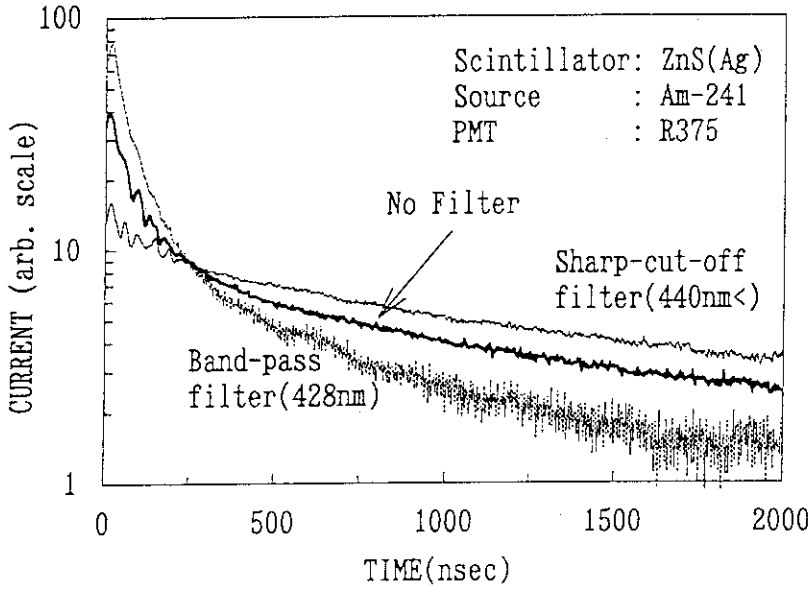

Figure 7.4.2 A change of pulse shapes by the light spectrum shift using the optical filters for the ZnS(Ag)

7.5 General-purpose Electric-cooled Germanium Gamma-ray Detector Using Two Stirling Refrigerators

M. Katagiri, Y. Kobayashi, Y. Taguchi* and T. Uchida*

A germanium gamma-ray detector is indispensable to gamma-ray spectroscopy. Since the germanium detector is normally operated in a cryostat cooled by liquid nitrogen, it takes much time for keeping liquid nitrogen in the cryostat. Therefore, a maintenance-free germanium detector system has been required from various fields. We developed a small electric-cooled germanium gamma-ray detector using a Stirling refrigerator for cooling a detector element [1]. However, a large germanium detector element having the relative detection efficiency more than 10% cannot be used because the cooling faculty of the Stirling refrigerator is low. Therefore, we have developed a general-purpose electric-cooled germanium detector having the relative detection efficiency more than 10%.

Schematic construction of the developed electric-cooled germanium detector is illustrated in Fig. 7.5.1. Two Stirling refrigerators are used to cool down a germanium detector element to liquid nitrogen temperature (77K) instead of a dewar containing liquid nitrogen. A Model SRS-2110 made by Sumitomo Heavy Industry Co. was used as the Stirling refrigerator The cooling faculty of this refrigerator is 1.5 W at 80K when it works in the operation condition of AC 15V and 4.0A. The refrigerator consists of a compressor, a connection pipe, a cooling system with a displacer and an AC power supply. Two cold heads of the cooling system cooled by the displacer are connected by an inverse-T shape fitting.

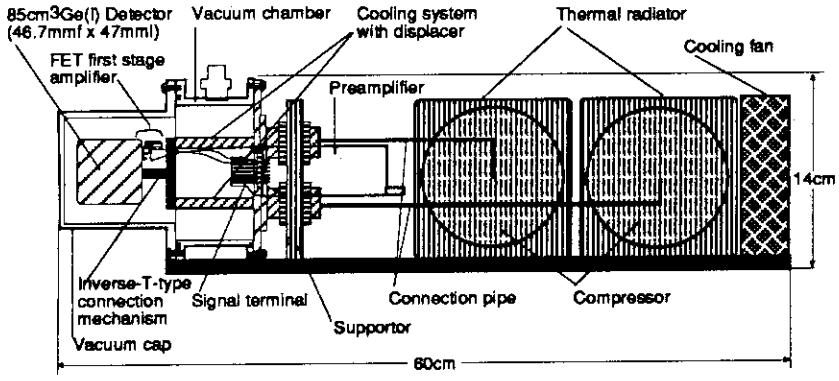

Fig. 7.5.1 Schematic construction of a developed general-purpose electric-cooled germanium detector using two Stirling refregirators

A $85cm^3$ (46.7mmϕx 47mml) closed-end high purity germanium detector is attached at the center of the fitting. This detector has a relative detection efficiency of 14%. Moreover, the first stage circuit of a preamplifier(ORTEC-120) is installed near the germanium detector to reduce the microphonic noise which is produced by the vibration of the Stirling refrigerators. A size of the detector is 60cml x 15cmh x 15cmw.

---

* Sumitomo Heavy Industry Corporation, Tokyo

The measurement of cooling characteristics was carried out by operating two Stirling refrigerators with AC 15V of the rated voltage. The result is shown in Fig. 7.5.2. The lowest cooling temperature is 77K. The operation time of 6 hours is necessary to cool down the temperature.

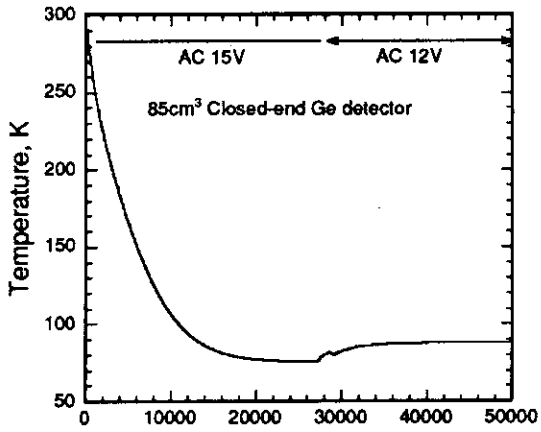

Fig. 7.5.2 Cooling characteristics of general-purpose electric-cooled germanium detector

After cooling down, AC voltage was reduce to 12V and the temperature was kept at 89K. The performance of the detector was measured by a ^{60}Co gamma-ray source. The dependency of FWHM energy resolution on shaping time of a spectroscopy amplifier(CANBERRA-2021) was measured. The shaping time is changed from 0.5μsec to 4 μsec. The results are shown in Fig. 7.5.3. The best FWHM energy resolution is obtained when the shaping time is 2μsec. The energy resolution for 1.33MeV gamma-rays is 2.06keV and that for the pulser is 1.34keV. On the other hand, the energy resolution for 1.33MeV gamma-rays is 2.08keV and that for the pulser is 1.20keV if the AC power supply of the refrigerators is stopped for a short time. From these results, it is revealed that the developed germanium detector has the FWHM energy resolution as same as that of a conventional germanium detector using liquid nitrogen.

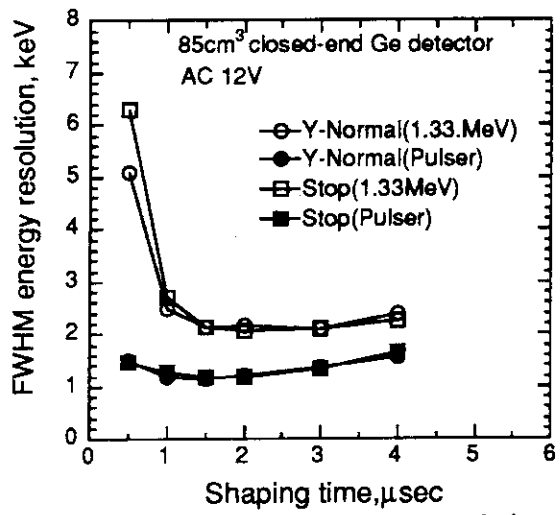

Fig. 7.5.3 Dependency of energy resolution on shaping time of a spectroscopy amplifier

Therefore, we investigates the reasons of good energy resolution. The variation of weight(size) of the germanium detector element can be considered as one of the reasons. The dependency of FWHM energy resolution on shaping time of a spectroscopy amplifier was measured by using a $14cm^3$ germanium detector instead of the $85cm^3$ germanium detector. The results of comparison with $14cm^3$ and $85cm^3$ germanium detector are shown in Fig. 7.5.4. Both dependencies of the energy resolution are almost same. The energy resolution for 1.33MeV gamma-rays is 2.17keV and that for the pulser is 1.44keV. On the other hand, the energy resolution for 1.33MeV gamma-rays is 2.58 keV and that for the pulser is 1.88keV in case that this $14cm^3$ germanium detector was attached at one Stirling refrigerator. It is revealed that the weight of the germanium detector element is not related to the improvement of the energy resolution.

Next, the difference of phase of operational AC voltages between two Stirling refrigerators can be considered as one of the reasons. Measurements of the energy resolution carried out in condition of the same phase and the inverse phase between two Stirling refrigerators. However, both results are same. It is revealed that the phase difference of operational AC voltages is not related to the improvement of energy resolution.

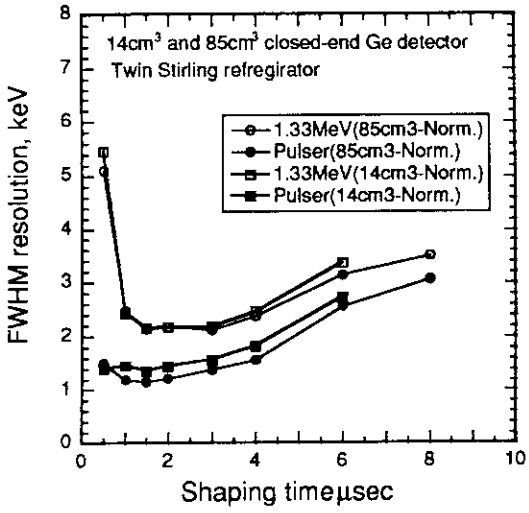

Fig. 7.5.4 Comparison of dependency of energy resolution on shaping time for $14cm^3$ and

From above experimental results, it is estimated that the reason is the use of two Stirling refrigerators, itself. Therefore, the analysis of the mechanical vibrations produced by the Stirling refrigerators was carried out to inquire the improvement reason of the FWHM energy resolution. Signals of mechanical vibrations were measured by using an accelerator sensor. The sensor was attached at three positions, e.g., front, side and top of a germanium detector element and the frequency spectra of output signals were analyzed by a spectrum analyzer. The difference of the frequency spectra between a one-refrigerators-type germanium detector and a two-refrigerators-type germanium detector was obtained. The $14cm^3$ germanium detector was used for these experiments. Typical comparison results at the top position are shown in Fig. 7.5.5. Two spectra are distributed in the range from 1kHz to 15kHz. The spectrum for the two-refrigerators-type germanium detector is lower of 10dB than that for the one-refrigerators-type germanium detector. Moreover, comparison results for other two position were almost same.

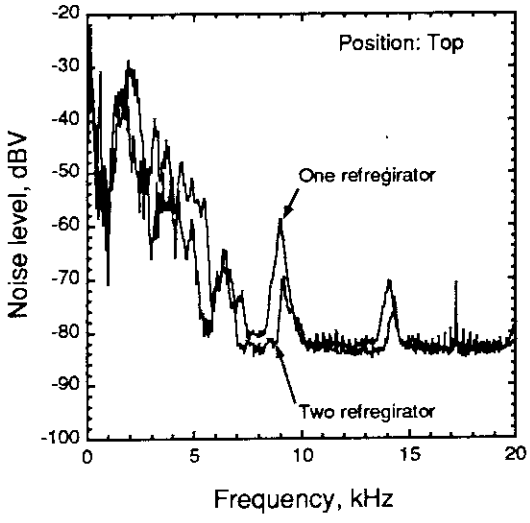

Fig. 7.5.5 Typical frequency spectra of mechanical vibration measured by a spectrum analyzer

Therefore, it is confirmed that the use of two refrigerators contributes to the improvement of energy resolution for the two-refrigerators-type germanium detector.

Reference

1) Katagiri M. and Ito H.: KEK Proceeding 94-7, Radiation Detector and Their Uses, 1174(1994).

7.6 Calculation Method for Pulse Height Distributions of Fission Counters

H. Yamagishi

A calculation method for pulse height distributions (PHDs) of fission counters (FCs) was studied to design a high sensitive fission counter. Figure 7.6.1 shows a schematic diagram to explain the fundamental operation configuration of the FC. As a neutron sensitive material, uranium oxide (U_3O_8) is made coating with a thin thickness on the surface of inner-electrode (Anode) and outer-electrode (Cathode). Generally, electrode gap is of a few millimeters (mm). As ionized gas, mixture gas of ($Ar+N_2$) is filled with a pressure of several atmospheres (atm) in the counter vessel. In this study, electric charges at the FC output, generated by detecting neutrons, were calculated to investigate the PHDs.

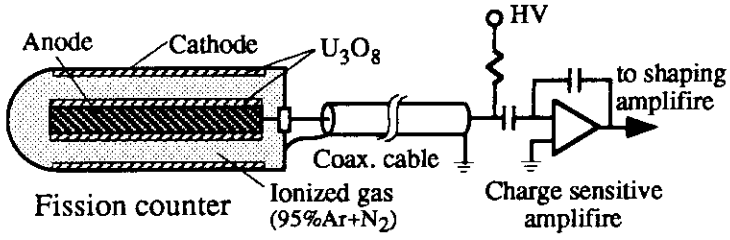

Fig. 7.6.1 Fundamental operation configuration of fission counter

Figure 7.6.2 shows the schematic diagram of calculation model for the case that fissions occur in the inner-electrode. Two fission fragments (FFs) produced in U_3O_8 of the electrodes fly to opposite direction, respectively: the probability of FF flight is uniform in all directions. Either fragment goes into the electrode gap and ionizes the gas. The FC provides a signal pulse of a small electric charge by one fission. The stopping power (dE/dx) of materials to heavy ion such as FFs is given by Eq. (7.6.1) which is an experimental equation proposed by Bridwell and Moak[1), 2)].

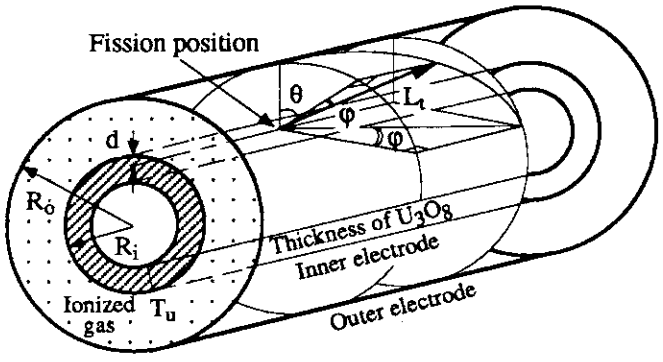

Fig. 7.6.2 Schematic diagram for calculation of pulse height distributions of fission counter (In case that the fission position is in the inner-electrode)

$$\left(\frac{dE}{dx}\right)\left[MeV/\left(kg/m^2\right)\right]=\frac{2064.5}{A_2}\sqrt{\frac{TA_1Z_2}{Z_1}} \quad \text{---------- (7.6.1)}$$

where T is an energy (MeV) of a heavy ion; A_1 and Z_1, mass and atomic number of the heavy ion; A_2 and Z_2, mass and atomic number of a material (Uranium, Oxygen, Argon or Nitrogen).

The stopping power $(dE/dx)_{mix}$ of a chemical compound and mixture is given by Eq. (7.6.2).

$$\left(\frac{dE}{dx}\right)_{mix}\left[MeV/\left(kg/m^2\right)\right]=\sum_i \omega_i\left(\frac{dE}{dx}\right)_i \quad \text{---------- (7.6.2)}$$

where ω_i, weight percentage of i element; $(dE/dx)_i$, stopping power for i element.

As shown in Fig. 7.6.2, if the fission occurs in U_3O_8 of the inner-electrode, the length (L_t) of the track where the FF flies is given by Eq. (7.6.3).

$$L_t[m]=\frac{-2(R_i-d)\cos\theta+\sqrt{\left\{2(R_i-d)\cos\theta\right\}^2+4\left\{R_o{}^2-(R_i-d)^2\right\}}}{2\cos\varphi} \quad \text{------- (7.6.3)}$$

where R_i and R_o, radiuses of the inner-electrode and outer-electrode, respectively; d, the depth from the surface of inner-electrode where fission occurs; φ and θ, angles of the flight direction in the electrode gap.

In case of the FCs, flight distance (ℓ_f kg/m^2) of the FFs in the FC is given by $\ell_f \approx \rho L_t$ because most of the FFs fly through the thin U_3O_8 coating, then in gas and finally reach the opposite electrode. The ρ is density of the ionized gas. The energy loss (E_{GS}) of FF in ionized gas is a function of ℓ, φ and θ; and is given by Eq. (7.6.4). The electric charge (P_h) produced in the FC is calculated by Eq. (7.6.5).

$$E_{GS}(\ell,\varphi,\theta)=\int_0^{\ell_{GS}}\left(\frac{dE}{dx}\right)_{GS}dx_{GS} \quad \text{---------- (7.6.4)}$$

$$P_h(\ell,\varphi,\theta)=\frac{1}{w_{GS}}\int_0^{\ell_{GS}}\left(\frac{dE}{dx}\right)_{GS}dx_{GS} \quad \text{---------- (7.6.5)}$$

where ℓ_{GS}, the flight distance of FF in ionized gas with angles of φ and θ; $(dE/dx)_{GS}$, the stopping power of mixture ionized gas; w_{GS}, w-value. The energy loss of FF in the thin U_3O_8 coating can be deduced by the same way as those in the case of ionized gas.

In case that a fission occurs in the side of outer-electrode, equations for the calculation of electric charge can be deduced by the same way as those in the case of inner-electrode. A PHD is constituted with pulses which are generated by the FFs produced in the inner-electrode and in the outer-electrode.

The PHDs were calculated with following conditions: R_i=11mm, R_o=12mm, electrode gap=1mm, thickness of U_3O_8 =1mg/cm^2, ionized gas=95%Ar+N_2, gas pressure=5 atm or 2 atm, w-value of mixture gas=26.4 MeV. Specifications of the FFs are as follows: light FF (energy T_L=97 MeV, A_{L1}=95, Z_{L1}=38), heavy FF (T_H=65 MeV, A_{H1}=139, Z_{H1}=54).

Experimental measurements of PHDs were performed by using a FC having specifications as above mentioned. The FC has a gas valve for refilling ionized gas.

Figure 7.6.3 shows the calculated result as compared with the experimental result. The calculated result shown is due to signal pulses of the FC on detection of neutrons; it does not

contain pulses due to alpha-rays. In the experimental result, the PHD in a lower pulse height region with high pulse-count-rates is due to alpha-rays. The pulse height of the most frequent pulses in the experimental result is of 0.81×10^{-13} coulombs (C) and that of the calculated result is of 0.87×10^{-13} C. A broken line in Fig. 7.6.3 shows the calculated PHD modified with a factor of 0.93. The PHD of broken line agrees well with the experimental results. Figure 7.6.4 shows PHDs for the condition of gas pressure of 2 atm. The pulse heights of experimental and calculated results were 0.38×10^{-13} and 0.39×10^{-13} C, respectively. The PHD shown by a broken line is of a factor of 0.97 as compared with the calculated result. The calculated result shown by a solid line agrees well with the experimental results. From above considerations, it is proved that the error of pulse height calculation by the implemented method is less than 7%.

After this study, we made a computing code for design of fission counters: this will be useful for development of high sensitive fission counters and position sensitive fission counters.

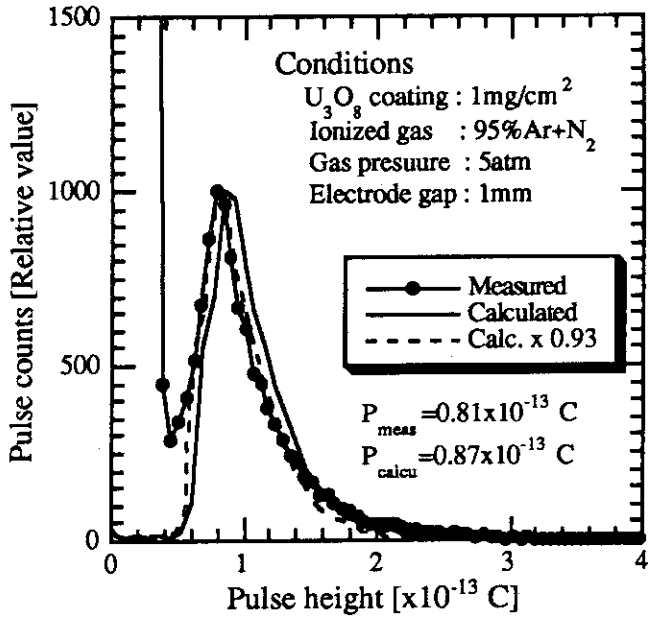

Fig. 7.6.3 Calculation results and measured result of pulse height distributions for fission counter (Gas pressure : 5atm)

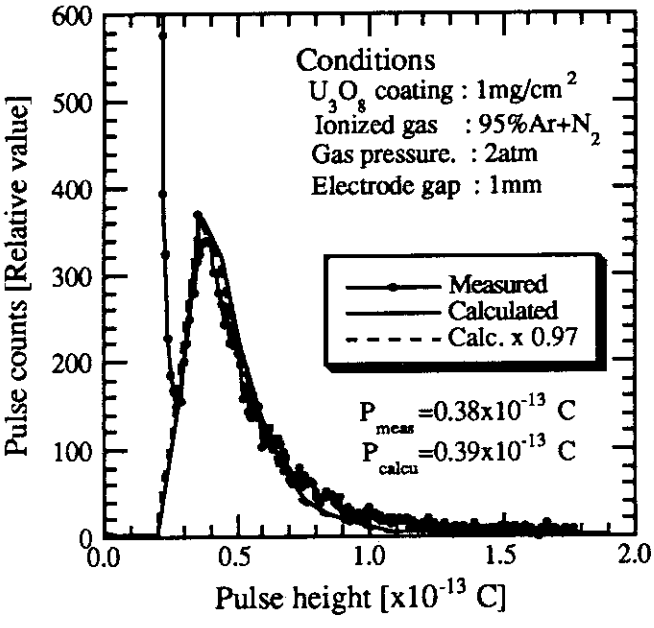

Fig. 7.6.4 Calculation results and measured result of pulse height distributions for fission counter (Gas pressure : 2atm)

References

1) Bridwell, L., and Bucy, S., *Nucl. Sci. Eng.* 37:224 (1969)

2) Bridwell, L., and Moak, C. D., *Phys. Rev.* 156:242 (1967)

7.7 Ten Year Study on the Development of Nondestructive Measuring Techniques for Returning Wastes from Overseas

H. Gotoh[*1], M. Haruyama and M. Takase[*2]

JAERI started a research program named "Development of Verification Instruments for Returning Wastes from Overseas Reprocessing" at the beginning of the year 1985 under a contract between JAERI and the Science and Technology Agency(STA) of the government, basing on the special national account of developing electric resources. Ten Japanese electric power companies had made contracts with French and English fuel reprocessing establishments on the reprocessing of Japanese spent fuels. And wastes accompanying the recovered plutonium were also scheduled to be returned to the native country.

The research program selected two kinds of techniques to be studied; the active neutron method using a pulsed d-t neutron source(the differential dieaway technique, DDT) and the passive neutron method. The program was planned as a six year project in the beginning, because the first shipping of wastes was expected to start soon after the end of the program. When the course of original project finished, an additional course was planned especially focusing on the study of verifying heterogeneous wastes produced by containing metal recalled parts from reprocessing facilities; such as piping and pumps. The additional course extended to the end of October 1994 in making a full project of ten years and ten months length.

In the first stage of the project with a length of five years and three months, we designed and constructed measuring systems for the two methods, made many kinds of simulated packages of returning wastes, performed measuring experiments and finally obtained detection sensitivities of TRU materials contained in waste packages. The main results were reported elsewhere in these series of annual reports.

In the second stage of the project with a length of residual five years and seven months, we concentrated our efforts on the solving of heterogeneity problems of waste packages and on the establishment of the technical basis for future domestic commercial reprocessing of the spent fuels.

Several topics to be memorized will be described hereafter. One of the topics is the tolerance of neutron detectors to high gamma-ray dose rate anticipated from wastes originated in the reprocessing. We adopted a fast electronic circuits with a time constant of 50 ns for the processing of pulses from neutron detectors. It permitted us to use ^{3}He proportional counters

---

[*1] Present address: Higashiishikawa 1181-25, Hitachinaka-shi, Ibaraki-ken

[*2] On leave from Chiyoda Maintenance Co. Ltd., Oarai-machi, Higashiibaraki-gun, Ibaraki-ken

in an environment of 1,000 rad/h of gamma-ray intensity, about 100 times larger than that permitted to ordinary electronics for proportional counters. At the other hand it sacrificed the neutron detection efficiency as high as 47%.

The fast electronics also permitted us to record counts even in the slowing down time region without an appreciable counting loss in the active neutron method, then the record gave us an expectation of distinguishing types of waste matrices by the difference of slowing down times. The difference was very small because we used an enough volume of moderator for neutron economy. The difference will become large and stable if we use a proper volume of moderator.

Monte Carlo-type programs were important in conducting studies in both active and passive neutron methods. MORSE and then MCNP were used in early stages of the program. Although they worked well in the study, we changed the program to MVP which had been developing in the same department because of its speed and its expected flexibility. All the three programs mentioned above are satisfactory in calculating the detection sensitivity in passive neutron method. The measurable quantities in active neutron method are complicated because the detecting process contains two stages of nuclear reactions, and any of the programs are not adequate in calculating the measurable quantities in the present states.

We adopted a special electronic system in the passive neutron method. All the time intervals between neutron detection pulses are recorded. The histogram data taken by the system have a large redundancy compared with data obtained by ordinary shift-register-type analyzers. We succeeded in formulating an analytical expression for the distribution function of the time intervals.

Many works in passive neutron method reported previously have interests in the determination of spontaneous fission rate and do not mind the (α,n) neutron emission rate. The reason is that the former is determined only by nuclear properties and the solution is stable, whereas the latter is related to both nuclear properties and the chemical state of TRU materials and the solution is often unstable. The authors believe that the (α,n) neutron emission rate should be evaluated more because it contains an additional information on TRU materials in spite of its complicated relationship to the α-activity.

In conclusion, if we want to guarantee the strength of the α-activity of a waste package with nondestructive means, the informations, what kinds of TRU elements are contained, what is their isotopic compositions, and in what pattern they are distributed in the package, are important whether in passive neutron method or in active neutron method.

Naoaki Wakayama[*3] was engaged in this work on the fiscal years 1984 through 1989.

[*3] Present address: Nippon Advanced Technology Co. Ltd., Tokai-mura, Naka-gun, Ibaraki-ken

He was at the time the head of the Reactor Instrumentation Laboratory, the host laboratory of the program. He designed all the electronic system and leaded the program. The instruments newly built in NUCEF are heavily indebted to his administrative leadership.

Makoto Suzuki[*4] spent four years in constructing the measuring systems and in the early stage of experiments. The authors are also greatly indebted to him on the formulation of the time interval distribution in stochastic process theory. Yoshitaka Takeuchi[*5] conducted the experiments of the first course. Yoichi Yoshimura[*6] majored the gamma-ray tolerance experiment of neutron detectors. Koji Sekine[*7] performed MORSE calculations in the first course. Toshihide Kawamura[*8] conducted the experiments in the second stage.

The authors thank to Masayuki Nakagawa and Takamasa Mori, who also belong to authors' department, for their permission to authors' access to MVP before publication and for their help in computation. The authors are much obliged to the staff of the Department of Reactor Engineering in their administrative efforts.

In the course of the program Samzil Las[*9] came to Japan under a cooperative program between STA and Indonesia. Recently Peija Tang[*10] came to Japan from China under a program of the same kind. They were not directly engaged in the work but helped us in making softwares for the calculation of (α,n) neutron emission rate. The discussions with them encouraged us and we expect that their experiences and the informations acquired in discussing with us will be helpful in the planning of their nondestructive measuring systems relating to fuel handling and fuel cycling.

The authors express their thanks, last but not least, to Katsuyuki Ara who has since April of 1990 been the principal researcher of the contract between JAERI and STA and the head of Reactor Instrumentation Laboratory (now Sensing Technology Laboratory) to which the authors have belonged.

[*4] Present address: Sasanodai 73, Asahi-ku, Yokohama-shi, Kanagawa-ken

[*5] Present address: Naganuma-cho 762-8, Hachioji-shi, Tokyo-to

[*6] Present address: Mitsubishi Atomic Fuel Mfg. Co. Ltd., Tokai-mura, Naka-gun, Ibaraki-ken

[*7] Present address: Nippon Sogo Kenkyusho Co. Ltd., Shibuya-ku, Tokyo-to

[*8] Present address: Miyama Co. Ltd., Asahi-mura, Higashiibaraki-gun, Ibaraki-ken

[*9] Present address: Radioactive Waste Management and Technology Center, Tangerang, Indonesia

[*10] Present address: China Institute of Atomic Energy, Beijing, China

8. Reactor Control, Diagnosis and Robotics

The H^{∞}, optimal reactivity filter using H^{∞} estimation theory has been proposed to estimate the time-varying net reactivity of a nuclear reactor. The methodology has been tested by computer simulation and has been compared with other techniques, such as Kalman filtering techniques.

A real-time nuclear power plant monitoring using hybrid intelligence system that consists of artificial neural network and real-time expert system has been developed as a prototype diagnosis system for Borssele Nuclear Power Plant (NPP). In the system the artificial neural network, having three layered autoassociative structure, is used for modelling of the plant with limited number of signals. The expert system is provided for improving man-machine interface and synthesizing anomaly diagnosis of NPP.

The benchmark analysis of acoustic noise signals for detection of sodium/water reaction due to sodium leak was continued. This year, the benchmark test has been focused on not only estimations of the start time and duration but also the location estimation of sodium/water boiling. The autoregressive (AR) modeling techniques are applied instead of the Twice Squaring method in the present benchmark test.

A new control concept, called Image Based Visual Servo (IBVS), is investigated for robot arm control. This method utilizes image feature value directly so that this is suited for real time feedback control. The objective is to control the end effector position of the arm specified on image. The IBVS controller performance is evaluated experimentally.

The Control and A.I. Laboratory is in charge of this chapter.

8.1 Frequency Characteristics of H_∞ Optimal Reactivity Filter

K. Suzuki, J. Shimazaki and K. Watanabe

It is necessary to estimate the time-varying net reactivity of a nuclear reactor on-line and in real-time for optimal reactor control and reactivity anomaly detection. The reactivity has traditionally been determined from measurements of the neutron density using an inverse kinetics equation. Various analog and digital methods of estimating the reactivity have been developed on this basis. However, the neutron density signal fluctuates because of the noises that are induced by signal detection system. The reactivity estimates obtained by such methods may themselves fluctuate significantly because the inverse kinetics equation involves differentiation of the neutron density signal with respect to time. One possible alternative to this problem, one not using the time derivative, is to apply modern optimal estimation techniques based on the state variable concept. Digital Kalman filtering technique was successfully applied to the problem of determining the coefficients of a specified time function according to which the reactivity was assumed to change.[1)]

Note that design criteria of the Kalman filter, which reconstructs the full state vector from measurements of the system output, is to minimize the variance of the reconstruction error. Difficulty is often encountered in the design of Kalman filters because the design specification for the estimates is given beforehand in the frequency domain. For this reason the design method is not always suitable for handling such a specification. Using H_∞ estimation theory, therefore, we have developed a design method that explicitly takes into account the filter design specification and provides a sufficiently stable filter.[2),3)]

The aim of this article is to state the frequency characteristics of the H∞ optimal reactivity filter designed by the method. We observed the ratio of peak-to-peak amplitude between that of the estimate and that of the true net reactivity when we added the sinusoidal reactivity input disturbance with a certain magnitude and frequency.[4)] The ratio was defined by $M:=\frac{\hat{\rho}}{\rho}$ where the symbols $\hat{\rho}$ and ρ denote the peak-to-peak amplitude of the estimate and that of the input reactivity, respectively. Let us use the symbol M_H for the H_∞

optimal filter (with the minimum value 7.375 for the adjusting parameter γ) and the symbol M_K for the Kalman filter. Figure 8.1.1 shows the dependence of M_H and M_K on the frequency of the sinusoidal reactivity input with a magnitude of 10 cents. It reveals a slow decline of M_H and rapid one of M_K with increasing the frequency of the input. The behavior of M_H is attributed to the selection of the frequency weighting which has the magnitude of −20 dB in the frequency range from zero to the cutoff frequency of 0.15 Hz.

In addition, our interest was also directed to a phase lag between the estimate and the input reactivity. The phase lag was defined by $\Phi:=2\pi f\tau$ where τ refers a time lag between them. Here, the Φ_H and Φ_K denote the phase lags of the H_∞ optimal filter and the Kalman filter, respectively. The dependence of Φ_H and Φ_K on the frequency of the sinusoidal reactivity input is shown in Fig. 8.1.2. It is apparent that the change of the Φ_H is small up to the frequency of 1.0 Hz, while that of the Φ_K is large. This may also be attributed to the frequency weighting mentioned previously. These observations indicate that the H_∞ filter generates more quickly and accurately than the Kalman filter.

References

1) Venerus J. C. and Bullock T. E. : Nucl. Sci. Eng., **40**, 199(1970).

2) Suzuki K., Shimazaki J. and Shinohara Y. : JAERI-M 93-040(1993).

3) Suzuki K., Shimazaki J. and Shinohara Y. : J. Atom. Ener. Soci. Japan, **36**, 79(1994).

4) Suzuki K., Shimazaki J. and Watanabe K. : Nucl. Sci. Eng., **119**, 128(1995).

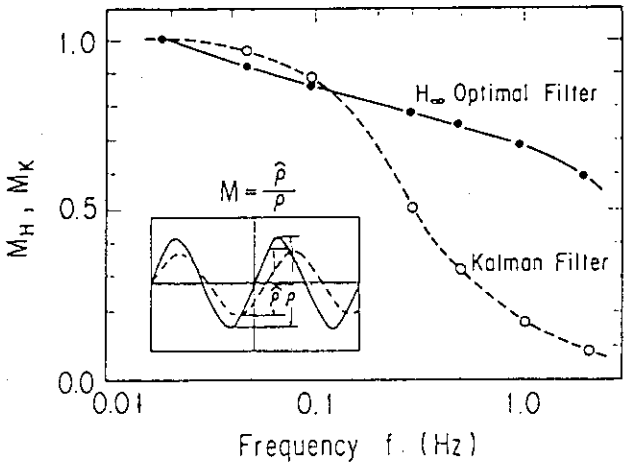

Fig. 8.1.1 Dependence of M_H and M_K on the exogenous reactivity frequency

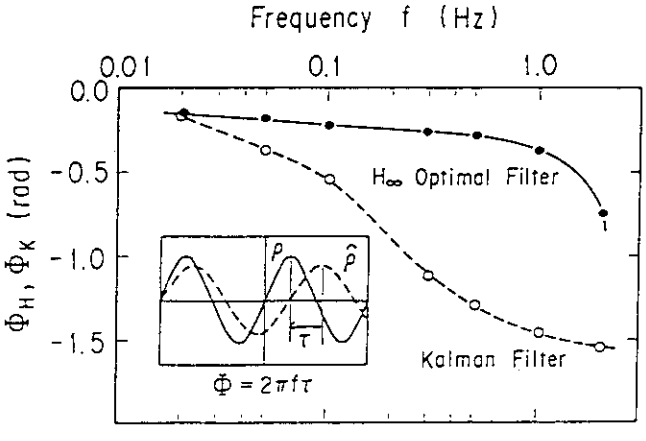

Fig. 8.1.2 Dependence of Φ_H and Φ_K on the exogenous reactivity frequency

8.2 Hybrid Intelligence System for Real-time Nuclear Power Plant Monitoring

K. Nabeshima, K. Suzuki and E. Türkcan*

The real-time nuclear power plant monitoring systems with artificial neural network (ANN) were developed for Borssele nuclear power plant (NPP).[1)-3)] However, they might be much improved to obtain sufficient performance over all possible reactor conditions including new operation mode that the ANN has never learned. The goal of plant monitoring is to infer the present status of the plant under operation from observation signals. For the construction of plant wide monitoring, therefore, it is of benefit to complement the shortage of the ANN by using an expert system.[4),5)] One of major advantages of the expert system is to have a capability to gather a lot of expert knowledge and make it utilizable in complex decision environments. Any known correlation between plant status patterns and operation mode can be written into the expert system as an a priori set of rules. In the present hybrid monitoring system consisting of ANN and expert system, the expert system is used as a decision agent which works based on the information from both ANN and human operator. The information of other sensory signals is also fed to the expert system, together with the outputs which ANN generates from the real-time plant signals. Fig. 8.2.1 shows the hybrid intelligent system architecture for plant wide monitoring of a nuclear power plant.

One of the main tasks of expert system is to make advisory display for operators from the view point of man-machine interface. In this system, the schematic plant figure is displayed with the values of measured and estimated by ANN. When the expert system detects anomaly, the color indicating the signal value changes from green to red. This is quite advantageous to the operator to identify which signal is exceeded the fault severity level. When an operator click the signal value on the display, the time series plotting figure appears as shown in Fig. 8.2.2.

The testing data, consists of 3700 patterns, are used for illustrating hybrid intelligent monitoring system performance. The results obtained from two process signals are given in Fig.8.2.3. Potentially invalid sensor signals are included in the testing data. Several pulsive noises can be seen frequently in the signal of feed-water pressure in steam generator-1 (SG1) after 690 minutes. At most of the off-normal points the deviation of only feed-water pressure signals in SG1 exceed its fault severity level, so that this anomaly is caused not by the system but might be a trouble of the electrical circuit of data acquisition system. The expert system displays the sensor error of feed-water flow of SG1 on the screen, as shown in Fig. 8.2.2, when the deviation of feed-water pressure in SG1 exceeds the fault severity level at 739

---

* Netherlands Energy Research Foundation ECN, The Netherlands

minutes.

In this study, the neural network is mainly used for modelling of the plant with limited number of signals, and the expert system is used for synthetic anomaly diagnosis of NPP. It is shown that complex and dynamic system like nuclear power plant can be modelled by ANN and the hybrid system is effective to enhance the reliability and operability of nuclear power plant. It is expected that the hybrid system discussed here is useful as an intelligent surveillance system to support the plant operator in nuclear power plant.

References

1) K. Nabeshima, E. Türkcan and Ö. Ciftcioglu: ECN-RX--93-066, The Netherlands,1993.
2) K. Nabeshima, E. Türkcan and Ö. Ciftcioglu: AIR'94, May 30-June 1, 1994, Tokai.
3) K. Nabeshima, et al.: ICONE-3, April 23-27, 1995, Kyoto.
4) K. Nabeshima, K. Suzuki and E. Türkcan: 9th Power Plant Dynamics, Control & Testing Symposium, May 24-26, 1995, Knoxville.
5) K. Nabeshima, K. Suzuki and E. Türkcan: SMORN-7, June 19-23, 1995, Avignon.

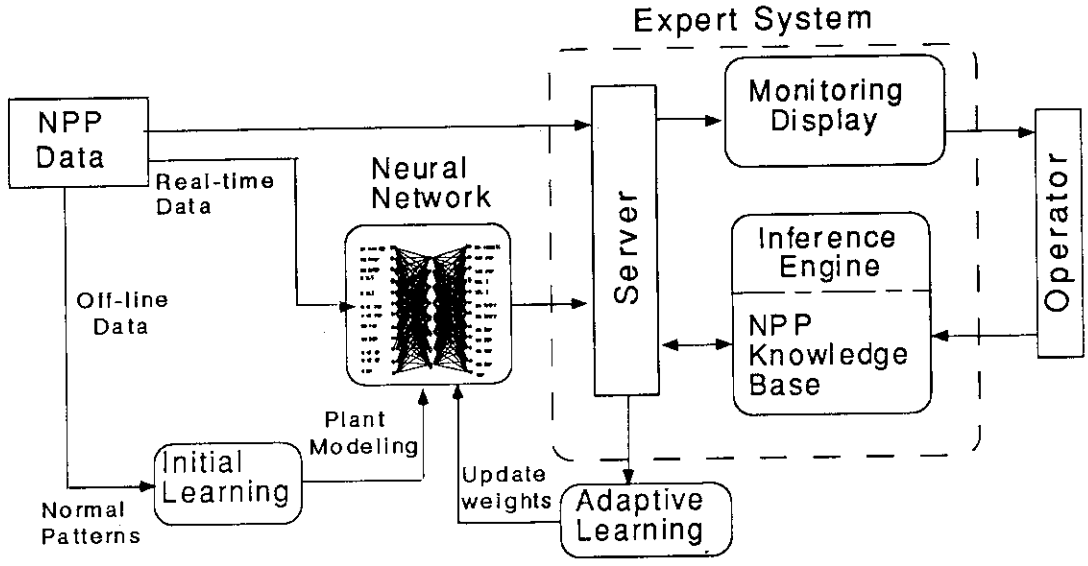

Fig. 8.2.1 Diagram of hybrid AI system

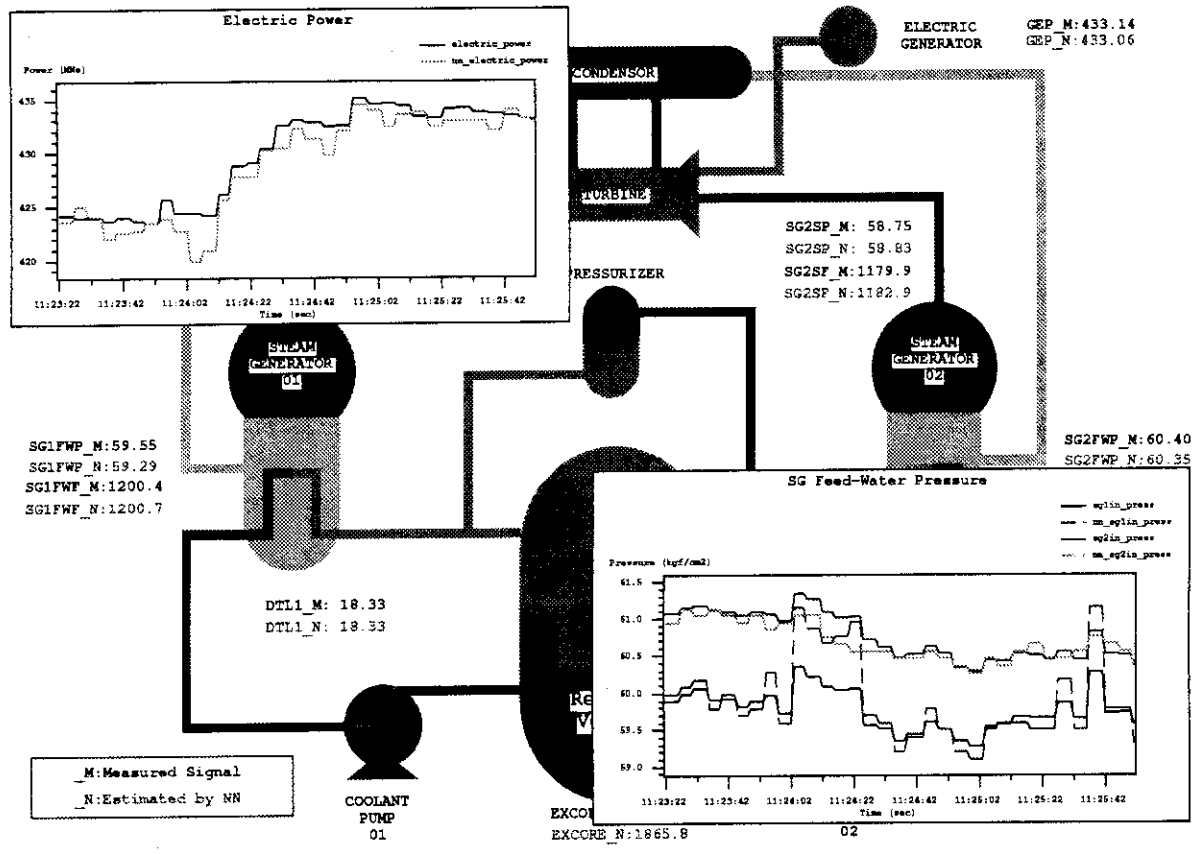

Fig. 8.2.2 Monitoring display by hybrid AI system

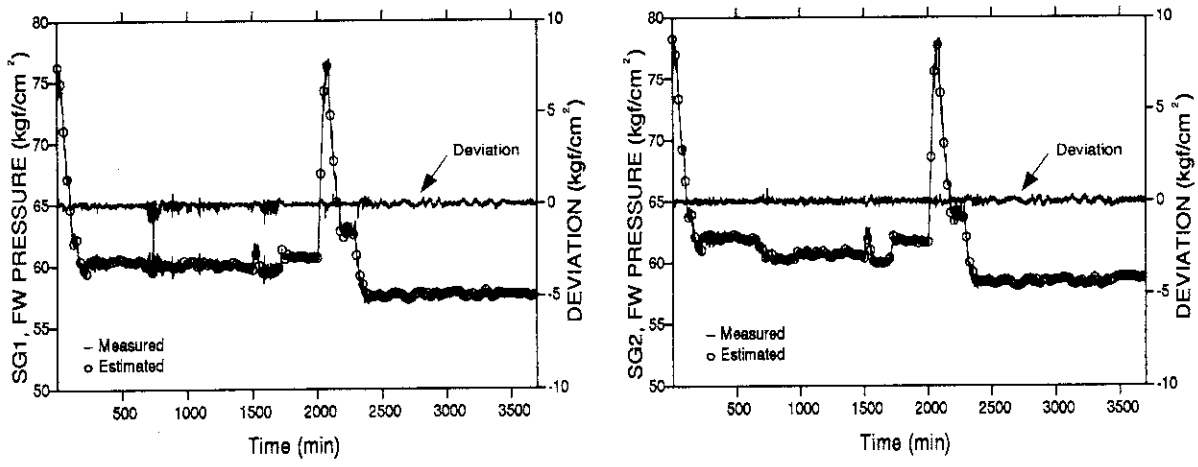

Fig. 8.2.3 Measured signals and estimated values by hybrid AI system

8.3 1994 Benchmark Test on Acoustic Detection of Sodium/Water Reaction

K. Hayashi, K. Watanabe, N. Ishikawa and Z. Zheng*

In the IAEA extended coordinated research program of on acoustic signal processing for the detection of sodium boiling or sodium/water reaction in LMFBR, the working group has been performed benchmark tests on the detection methods since 1989. The main objective of the benchmark tests concerns how to detect an onset of sodium/water reaction from acoustic signals with high sensitivity and accuracy. The performances and detection margins of various detection methods have been evaluated through cross comparisons among the test results. The 1994 benchmark test has been focused on not only estimations of the start time and duration but also the location estimation of sodium/water reaction in Steam Generator Unit. The test data were synthesized by CEA France using the leak signals for a mean leak rate of 3.8 g/s measured by a British team at the ASB loop and the background signals measured by UKAEA at Prototype Fast Reactor Superheater 2. The major differences between this benchmark and the former ones are that (1) 4 channels instead of single channel were proposed enabling multi-channel analysis and (2) digital data were supplied instead of analog data. The tasks of the benchmark test were as follows;

1) Determine the leak start times and duration for the 5 mixed signal sets;
2) Assess the advantage of multichannel analysis over monochannel processing for acoustic leak detection;
3) Evaluate, if possible the location of the leak;
4) Assess the reliability and false trip rate of their techniques.

Although the Twice-Squaring method[1] we developed was successfully applied to such estimation problem in the previous benchmark test, it has a difficulty in the analog filtering to separate both leak and background signal components locating at very near frequencies. Therefore, we applied the autoregressive (AR) modeling techniques[2] in the present benchmark test. In practice, the background signal whitening filter built by univariate AR model was newly applied to enhance the leak noises and to suppress the background noises in the sensor signals. This is a linear simple digital filter suppressing only background noises in sensor signal.

Fig. 8.3.1(a) shows an example of the resultant signal of the background signal whitening filter. Fig. 8.3.1(b) shows typical wave forms of both background and leak pulses containing in the resultant signal and Fig. 8.3.1(c) shows their PSDs. It is found that background and leak pulses have clear features to classify their states, respectively.

---

* Visit researcher, Nuclear Power Institute of China.

That is, the features of the filtered background pulses are narrow peaks in the frequency range from 15 kHz to 20 kHz and wide peaks in the range at least covered from 20 kHz to 40 kHz. On the other hand, the feature of the filtered leak pulse is the low frequency component at about 2.5 kHz and the middle frequency components distributed from 27 kHz to 38 kHz.

We analyzed all test signals using this filter. The results of the analysis for the five sets of test data are given in Table 8.3.1.

Table 8.3.1. The start time and duration of the leak

set Name	Start Time(s)	Duration Time(s)
set0	1.873s	5.469s
set1	1.218s	4.032s
set2	2.015s	5.390s
set3	1.608s	5.502s
set4	2.0s	5.0s

It is concluded that the signal processing using the UAR background signal whitening filter can detect reliably the leak signals with signal-to-noise ratio down to about -20 dB. Even if the sensor signal contains the non-boiling or non-leak large pulse components with a frequency range similar to the leak noise, they can be classified by spectral information.

In the estimation problem of the leak location, the differences of the start-up times among the leak pulse waves were not found. Therefore, we tried an estimation method using the time constants of the acoustic signal propagating paths based on the multivariate AR modeling techniques.

The time constants of acoustic propagating paths on the surface and in the inside of the ASB loop vessel were evaluated by the MAR modeling method using the leak small pulse data. However, the analysis results were not consistent physically and this method is still under development.

References

1) Hayashi K., et al. : "Autoregressive Techniques for Acoustic Detection of In-Sodium Water Leaks - The Results of 1994 Benchmark Test on Detection of Sodium/Water Reaction-," Presented for Research Coordination Meeting on Acoustic Signal Processing for the Detection of Sodium Boiling or Sodium/Water Reaction in LMFBR, Kslpakkam, India, 1-3 November 1994.

2) K. Hayashi et al.: A Method of Nonstationary Noise Analysis Using Instantaneous AR Spectrum and Its Application to Borssele Reactor Noise Analysis, Progress in Nuclear Energy, 1988, Vol.21, pp.707-716.

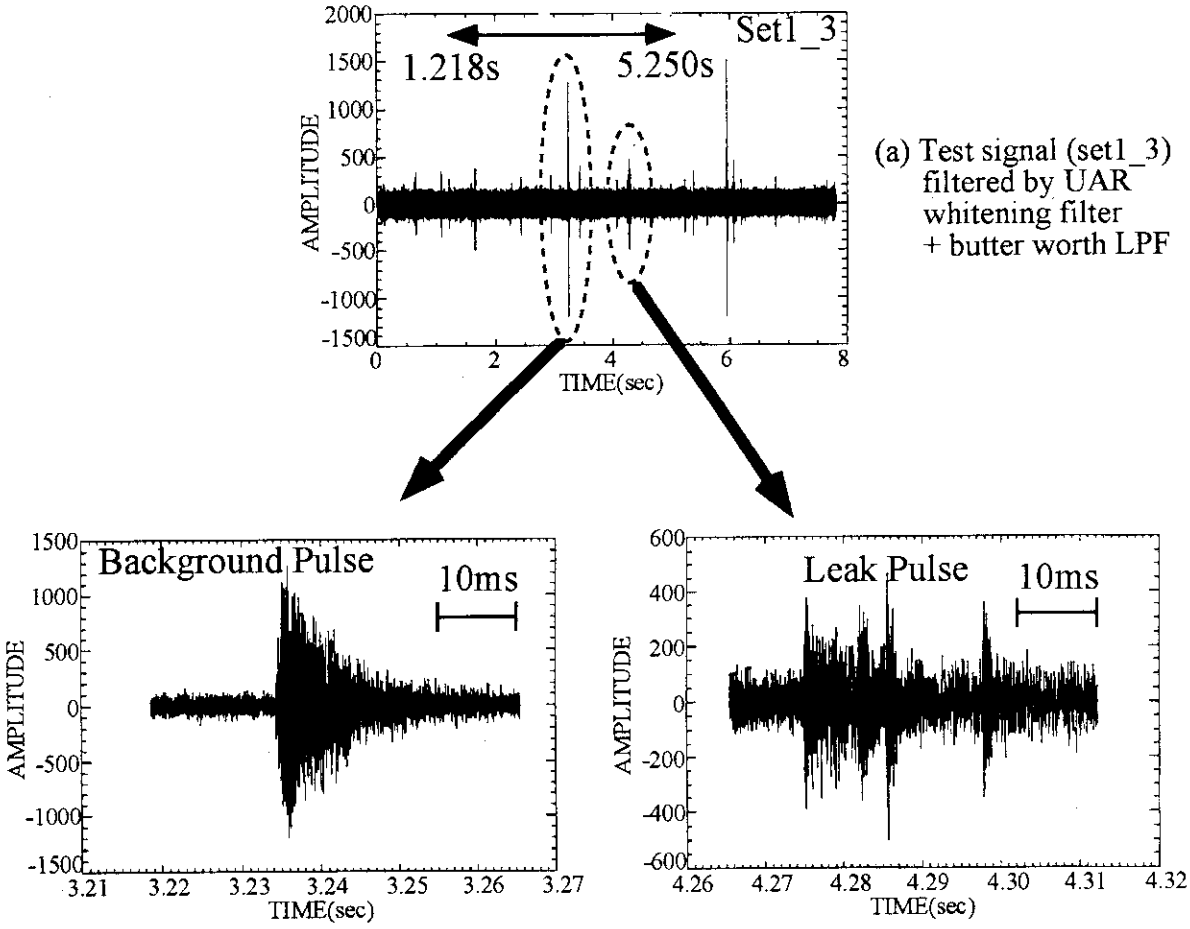

(a) Test signal (set1_3) filtered by UAR whitening filter + butter worth LPF

(b) Wave forms of typical large pulses in filtered test signal

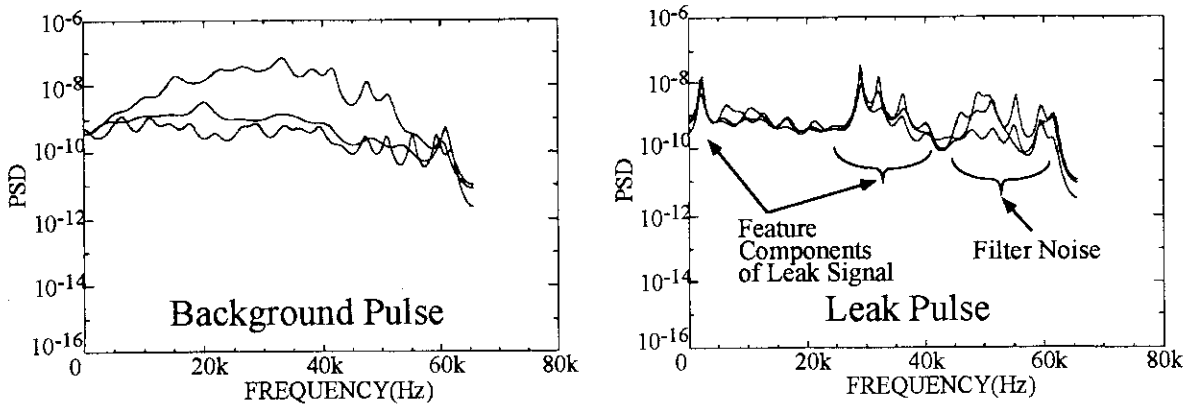

(c) PSDs of typical large pulses in filtered test signal

Fig.8.3.1 Typical wave forms and spectral patterns of background pulse and leak pulse in filtered test signal (set1_3)

8.4 Experimental Evaluation of Image Based Visual Servo Controller for Robot Arm

N. Ishikawa, K. Suzuki, Y. Fujii and H. Usui

We investigate new control concept, called Image Based Visual Servo(IBVS)[1], from the experimental point of view to check the feasibility for robot arm control. Main difference between the conventional control and present one lies in the quantity used as control reference. The conventional method utilizes 3-dimensional position information as control reference, while the present method utilizes image feature value directly. Direct use of the image feature value for control saves much computational time so that this control concept is suited for real time feedback control. In this report, we present the result of experiment for evaluating the IBVS controller performance.

The objective is to control the end effector position of the arm specified on image. End effector position is measured by TV camera which faces to the robot arm. The block diagram of this control system is depicted in Fig. 8.4.1. In this experiment, we utilize only one rotational joint and adopt digital PI controller. Digital PI controller can be obtained by discretizing original analog controller. Analog PI controller is given in the form of

$$u(k) = k_p(e(t) + k_i \int e(t)dt) \tag{1}$$

where k_p is proportional gain and k_i is integral gain. u(t) is control signal and e(t) is error signal measured on the image, that is, $e = X_{PX}^{ref} - X_{PX}$, where X_{PX} is the end effector position on image and X_{PX}^{ref} is its reference value. Discretization of Eq.(1) at the sampling time T_S yields

$$u(k) = k_p(e(k) + k_i T_s \sum_{i=0}^{k} e(i)) \quad . \tag{2}$$

Eq.(2) is written in the form of recurrence formula as

$$u(k) \leftarrow u(k) + k_1 e(k) + k_2 e(k-1) \tag{3}$$

where

$$k_1 = k_p(1 + k_i T_s), \quad k_2 = -k_p .$$

Eq. (3) is implemented on personal computer as a control law.

In order to consider the controller performance, what should be done first is to measure the time delay of vision system. Figure 8.4.2 shows the experimental result. In this figure, dotted line indicates the angle position measured by encoder, while solid line

indicates one that obtained from vision. From this result, we find that the delay time is about 40[msec].

Figure 8.4.3 shows the control result of visual servo control by means of digital PI controller with K_p = 0.0045, K_i = 0.85 and T_s = 30[msec]. The control reference on the image is given to be 40[pixels]. Controller gain is found by trial and error. Setting of K_p = 0.0055 causes unstable oscillation. This indicates that this control system is very sensitive to the controller gain because of the computational delay. Some predictive method is desired to eliminate the effect of time delay.

Reference

1) L. E. Weiss, et al.: "Dynamic sensor based control of robots with visual feedback", IEEE Trans. Robot and Automation, Vol. 3, No 5, pp404 - 417 (1987)

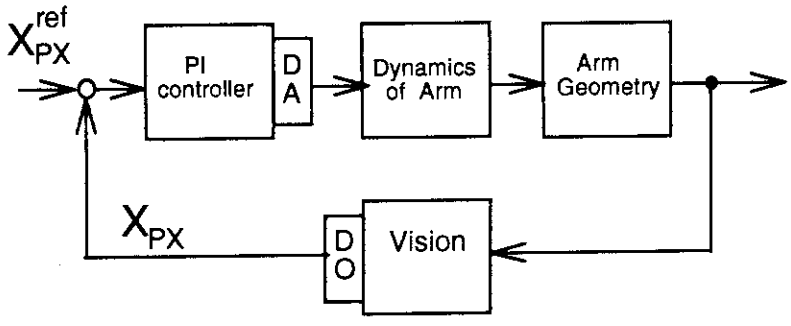

Fig. 8.4.1 Block diagram of IBVS control by digital PI controller

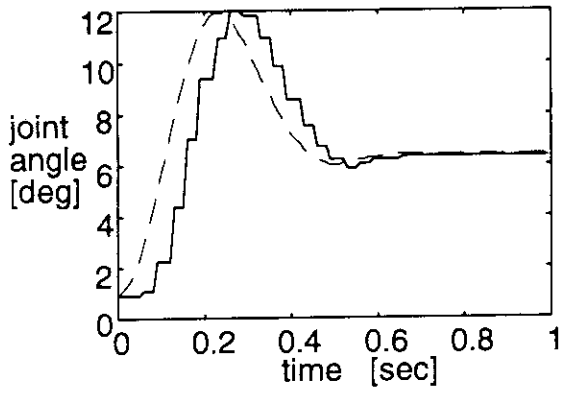

Fig. 8.4.2 Experimental result of delay system measure of vision

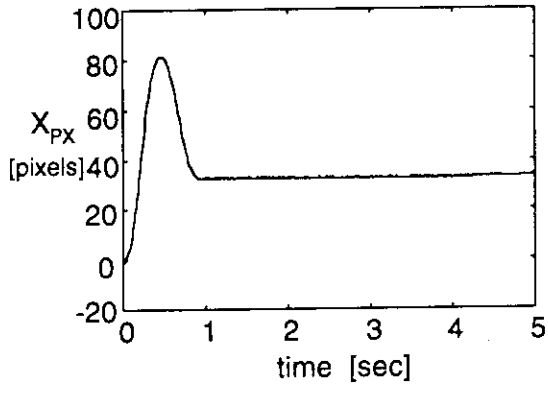

Fig. 8.4.3 Response of IBVS control

9. Heat Transfer and Fluid Flow

There are three major subjects of research associated with heat transfer and fluid flow. The first subject is the development and verification of the best-estimate codes for thermal-hydraulic analyses of light water reactors (LWRs). The REFLA/TRAC code is a best-estimate code with two-fluid model being developed at JAERI to provide advanced predictions of thermal hydraulic behaviors during postulated accidents in LWRs. The code uses the TRAC-PF1 code developed by the US Nuclear Regulatory Commission (USNRC) as the framework and adopts physical models developed at JAERI. The code has been assessed and verified for various transients and accidents in pressurized water reactors (PWRs) by FY 1993. In the FY 1994, the assessments of the code were performed to check the applicability to analyses of thermal-hydraulic transients in passive safety reactors. The models for the pressure drop evaluation have been modified to predict the natural circulation behavior more accurately. The model for the void fraction evaluation in a large vertical pipe or secondary side of the steam generator was also assessed for the analyses of passive safety reactors. The COBRA-TF code, which is a three-field subchannel code being developed originally by the USNRC, has also been assessed as the detailed analysis code for prediction of critical heat flux in core.

The second subject is on the fundamental studies such as the mechanism of critical heat flux (CHF) in the fuel assembly and two-phase flow structure in the vertical and horizontal flow channels. For developing a mechanistic model of countercurrent flow limitation in vertical channels, flow visualization experiments were carried out by means of the neutron radiography in the JRR-3M research reactor in JAERI.

The last subject is the transient thermal-hydraulic demonstration test program which is the second phase of the large scale reflood test program, aiming at the verification of the core integrity during the design basis events (DBEs) of LWRs. The demonstration test facility was initiated to be constructed in 1993. The test is scheduled to start in 1996 and end in 2000. Several calculations for major selected DBEs of PWRs were performed with the J-TRAC code to get information on initial and boundary conditions of tests.

9. Heat Transfer and Fluid Flow

There are three major subjects of research associated with heat transfer and fluid flow. The first subject is the development and verification of the best-estimate codes for thermal-hydraulic analyses of light water reactors (LWRs). The REFLA/TRAC code is a best-estimate code with two-fluid model being developed at JAERI to provide advanced predictions of thermal hydraulic behaviors during postulated accidents in LWRs. The code uses the TRAC-PF1 code developed by the US Nuclear Regulatory Commission (USNRC) as the framework and adopts physical models developed at JAERI. The code has been assessed and verified for various transients and accidents in pressurized water reactors (PWRs) by FY 1993. In the FY 1994, the assessments of the code were performed to check the applicability to analyses of thermal-hydraulic transients in passive safety reactors. The models for the pressure drop evaluation have been modified to predict the natural circulation behavior more accurately. The model for the void fraction evaluation in a large vertical pipe or secondary side of the steam generator was also assessed for the analyses of passive safety reactors. The COBRA-TF code, which is a three-field subchannel code being developed originally by the USNRC, has also been assessed as the detailed analysis code for prediction of critical heat flux in core.

The second subject is on the fundamental studies such as the mechanism of critical heat flux (CHF) in the fuel assembly and two-phase flow structure in the vertical and horizontal flow channels. For developing a mechanistic model of countercurrent flow limitation in vertical channels, flow visualization experiments were carried out by means of the neutron radiography in the JRR-3M research reactor in JAERI.

The last subject is the transient thermal-hydraulic demonstration test program which is the second phase of the large scale reflood test program, aiming at the verification of the core integrity during the design basis events (DBEs) of LWRs. The demonstration test facility was initiated to be constructed in 1993. The test is scheduled to start in 1996 and end in 2000. Several calculations for major selected DBEs of PWRs were performed with the J-TRAC code to get information on initial and boundary conditions of tests.

9.1 Large Scale Reflood Test Program II

T. Iguchi, M. Okazaki, T. Okubo, A. Ohnuki, K. Nakajima, H. Watanabe
Y. Watanabe, T. Sato, Y. Sudo, H. Akimoto

It was planned to perform "Transient thermal-hydraulic demonstration test program" as a part of "Large scale reflood test program II" sponsored by Science and Technology Agency of Japan. Transient thermal-hydraulic test program started in April, 1993 and is scheduled to complete in March, 2000.

The purpose of the test program is to demonstrate the core integrity during unexpected transients and accidents, i.e. design basis events (DBEs), of light water reactors (LWRs). To demonstrate the integrity, a test facility which can simulate the transient in-core thermal-hydraulic behavior during DBEs is constructed and simulation tests are to be performed with the test facility. The focused LWRs are pressurized water reactors (PWRs), boiling water reactors (BWRs), and their improved ones.

Schedule of the test program is shown in Fig.9.1.1. The construction of the test facility will be completed in 1995. The simulation tests will start in 1996.

In 1994, following activities (1) - (3) were performed.

(1) Design and construction of the test facility

The test facility was designed to have capability enough to simulate the transient in-core thermal-hydraulic behavior during DBEs. The designed test facility is shown in Fig.9.1.2. The test facility can supply coolant controlled at specified pressure, temperature and mass flow rate into a test section which simulates the core of reactors.

The major dimensions of the test facility are as follows: 1) Maximum pressure: 19.5MPa, 2) Maximum wall temperature: 647K, 3) Fluid: Demineralized water and steam, 4) Maximum flow rate into core: 11kg/s (5060kg/m^{2}s), 5) Core power: 6MW, 6) Cooling capacity: 5MW.

Test section consists of a 5x5 bundle test section and a heated tube test section. The bundle test section simulates a PWR core or a BWR core. Heated rods simulating nuclear fuels are electrical indirect heated rods. Clad temperature is measured with thermo-couples burried in the cladding.

Figure 9.1.3 shows the flow chart of the test. It is planned to perform transient tests for confirmation of the core integrity during DBEs and to perform separate tests for supplement of phenomenological understanding and quantitative evaluation. Convective heat transfer of film boiling and transition boiling under high pressure is studied with the separate tests. The void fraction in the core and the large-scale pipe under high pressure is also studied with the tests.

(2) Evaluation of code predictability

In order to perform simulation tests, it is necessary to know the core boundary conditions (Pressure, core power, flow rate and coolant temperature). It is planned to obtain the core boundary conditions through prediction with reliable analysis codes, i.e. J-TRAC, TRAC-BF1 codes. Hence, calculation with the codes was performed for major selected DBEs (Primary pump seizure accident, loss of flow accident, unexpected pressure reduction and SG pipe rupture accident of PWRs) and predictability of the code was investigated. It was found that the predicted result with the code agreed fairly well to that with a safety evaluation code.

(3) Supplemental tests

In order to evaluate the predictability of J-TRAC code on basic two-phase flow characteristics, a two-phase flow experiment was performed. The detail is described in the following section.

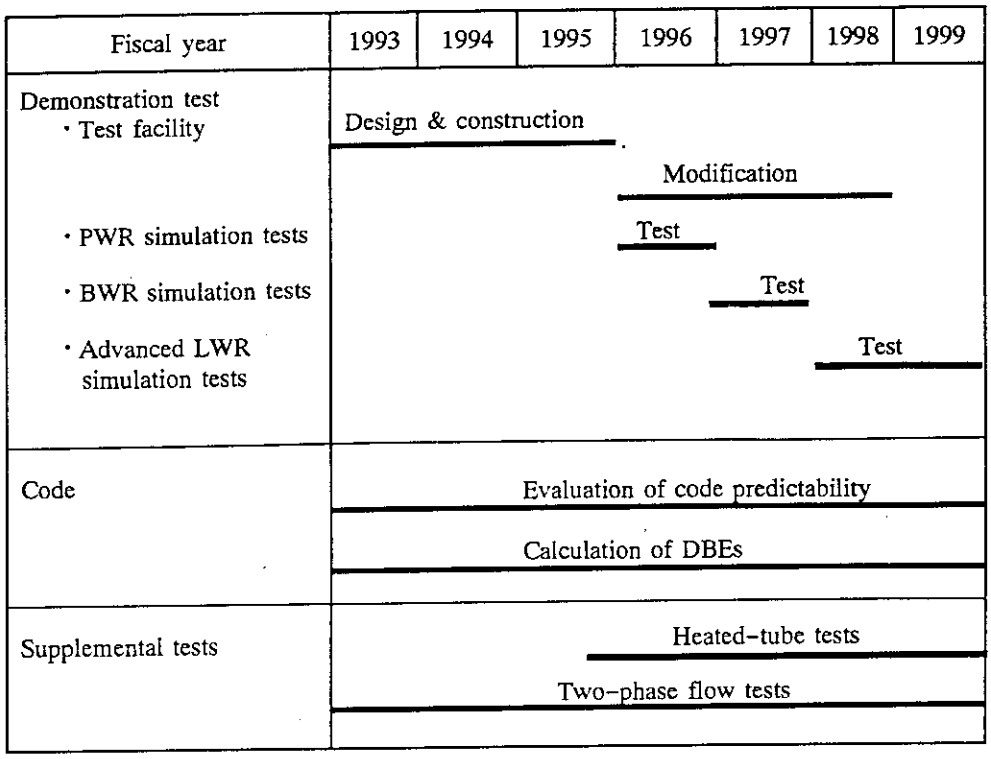

Fig. 9.1.1 Schedule of "Transient thermal-hydraulic demonstration test program"

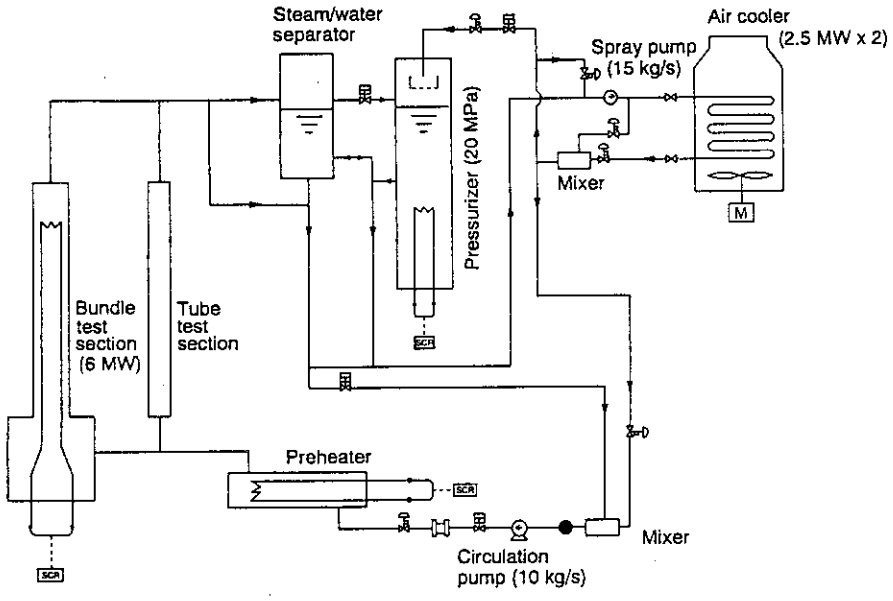

Fig.9.1.2 Transient thermal hydraulic demonstration test facility

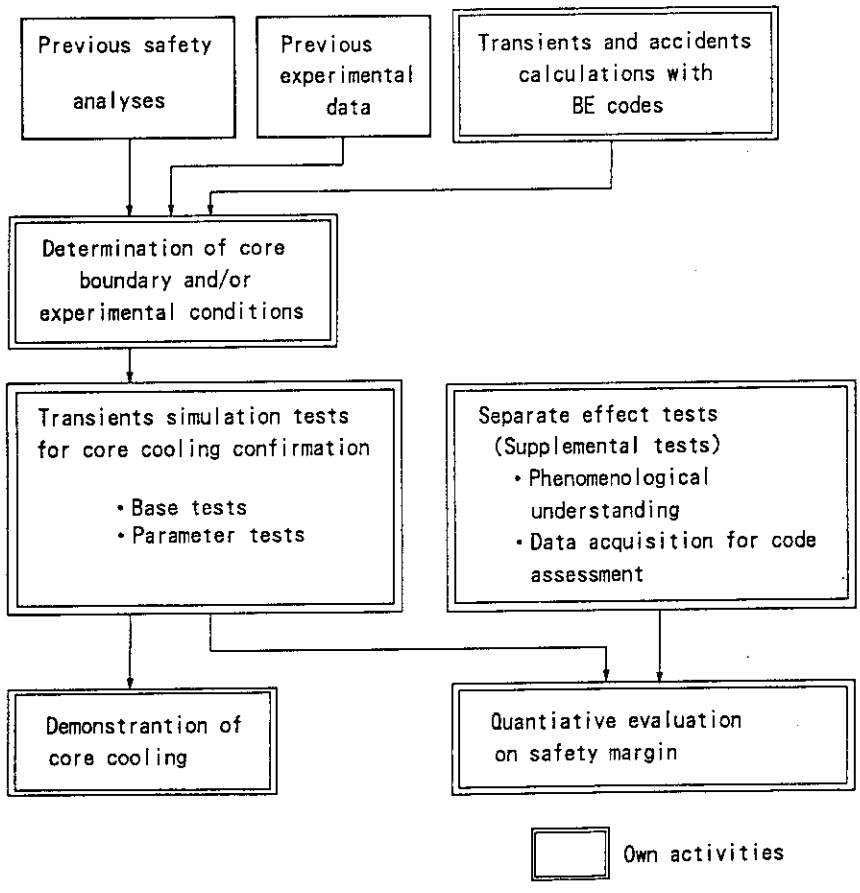

Fig. 9. 1. 3 Flow chart of the program

9.2 Analyses of Transient Phenomena Induced by Some Unexpected Events and Accidents

M. Okazaki, T. Iguchi, A. Ohnuki and H. Akimoto

In the transient thermal-hydraulic demonstration program[1], we are planning to simulate the phenomena in the core induced by abnormal events and accidents of commercial light water reactors. In order to achieve the test effectively for simulating the phenomena, we performed the analyses of transient phenomena in the primary system of 1100MWe PWR power plant to understand the causal sequence and the main factors which play an important role in the transient phenomena. The analyses were performed using J-TRAC code which was developed in JAERI based on the TRAC-PF1 code[2].

(1) The case of reduction of mass flow rate.

The pump seizure accident in PWR was dealt for this case. In the analysis, gap conductance between pellets and cladding was changed to very high value of 10,000 $BTU/ft^2h^\circ F$ after occurrence of accident, for the purpose of achieving the conservative evaluation concering the core cooling. Sudden change of gap conductance caused the rapid release of the stored heat in the pellets to the claddings and the film boiling flow took place in the core because of rapid temperature rise of claddings. The reactor tripped by the reduced flow in the loop where pump seizure occurred at 2 seconds after the initiation of accident. After the reactor tripped, core power decreased rapidly and so did the cladding temperature (Fig.9.2.1). In the calculation with the ordinary gap conductance film boiling did not take place. In this case the coolant temperature in the core increased more than the case of film boiling, which makes the higher pressure due to the volume expansion in the core.

In the case of loss of electric power for driving pumps, the pressure reached up to 16.2MPa (Fig.9.2.2) because the mass flow rate in the core decreased more and the temperature increased more than the case of pump seizure accident.

(2) The case of unexpected pressure reduction.

This case assumes that the pressurizer relief valve is sticked at the open position,

which reduces the pressure in the primary system due to steam discharge.

The calculated results by J-TRAC code using the license application condition agreed well with these of the license application (Fig.9.2.3). The calculated results of the license application showed that the reactor tripped at 40 seconds after the initiation of accident to prevent the DNB in the core. However the calculation by J-TRAC code showed that the temperature in the core was kept at subcooled condition (Fig.9.2.4).

(3) Flow stagnation in the core in split break LOCAs.

In early period of split break LOCA at the cold leg near the pressure vessel, the core inlet flow is reversed in particular range of break area, although the core outlet flow is kept normal. In such a case, flow stagnation occurs in the middle of core and rapid increase of void fraction may happen in the core. If the flow stagnation in the core occurs before reactor trip by pressure decrease, claddings temperature may increase intensively. In order to investigate such situations, we made the parametric calculations for the break area of 20, 40, 60 and 80 % of cold leg flow area. Flow stagnation in the core did not occur in the cases below 40% break. In 80% break reactor trip occurred before flow stagnation takes place. Flow stagnation and reactor trip occurred approximately at the same time in 60% break. From the result of 60% break, we could find that the flow stagnation in the core took place when the void fraction becomes large in the upper plenum due to the coolant discharge. If the single phase flow of steam appeared in the upper plenum, discharge flow decreased remarkably and the fluids flow from the intact loop cold leg to downcomer which were discharging through broken loop cold leg so far, partly start to flow into the core (Fig.9.2.5). Consequently the core was cooled rapidly by the filling water. Reactor power shows oscillatory change due to void fraction change (Fig.9.2.6).

References

1) Iguchi T., et al. : Reactor Engineering Department Annual Report, "9.1 Large Scale Reflood Test Program" JAERI-Review 1994.

2) Liles D.R., et al. : TRAC-PF1/MOD1 Correlations and Models, NUREG/CR-5069 LA-11208-MS (1988).

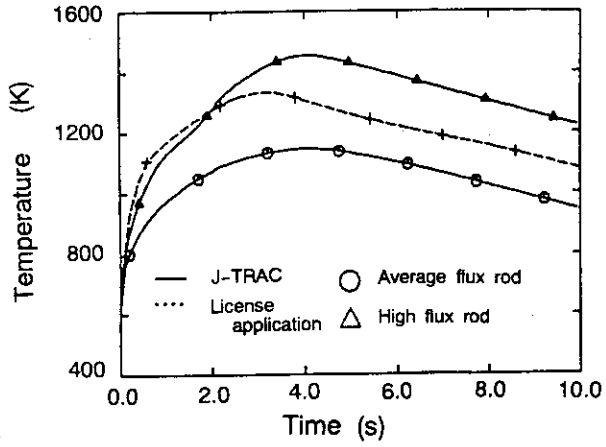

Fig.9.2.1 Maximum clad temperature (Reduction of mass flow)

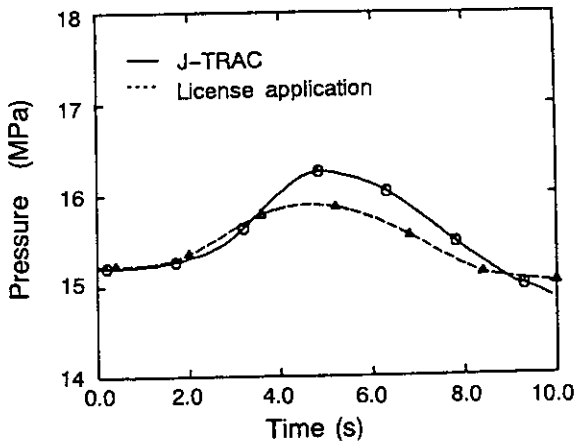

Fig.9.2.2 Pressure in the Pressurizer (Reduction of mass flow)

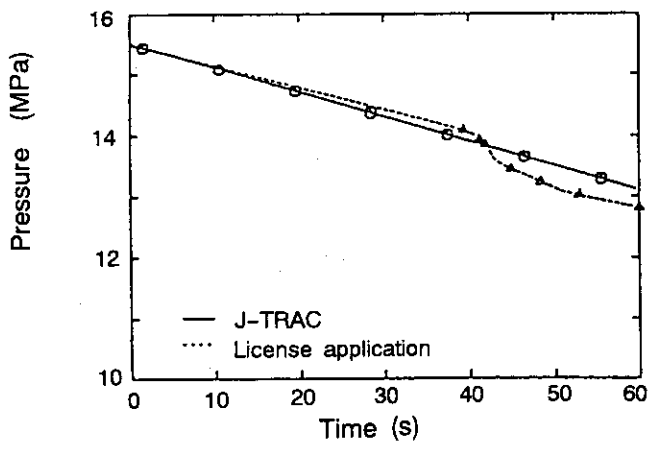

Fig.9.2.3 Pressure in the Pressurizer (Unexpected pressure reduction)

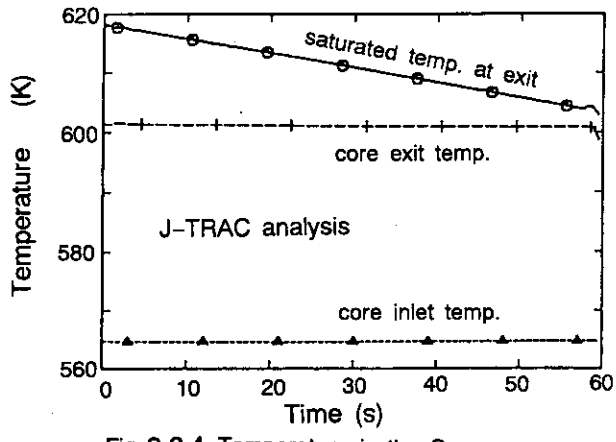

Fig.9.2.4 Temperature in the Core (Unexpected pressure reduction)

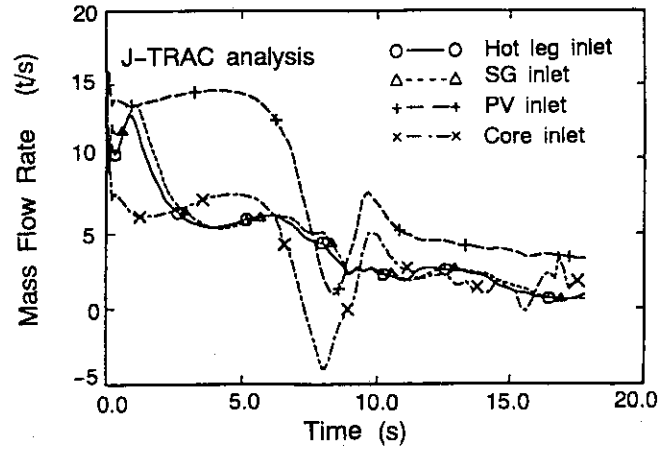

Fig.9.2.5 Mass Flow Rate in the Intact Loop (60% Split Break)

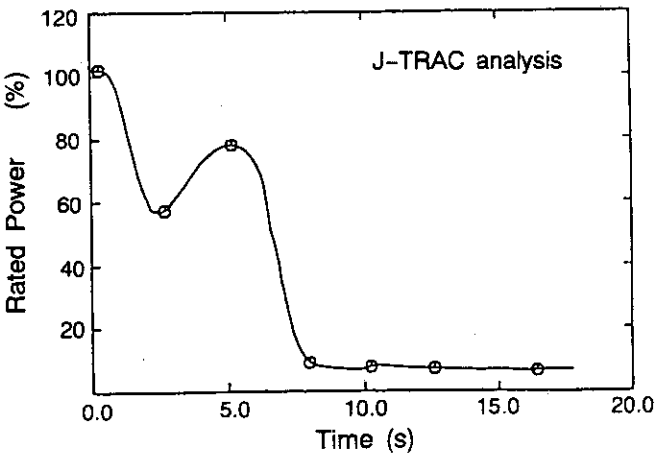

Fig.9.2.6 Reactor Power (60% Split Break)

9.3 Analysis of steam generator tube rupture accident in a 4-loop PWR with J-TRAC code

H. Akimoto, M. Okazaki, T. Iguchi, A. Ohnuki and Y. Sudo

An analysis of steam generator(SG) tube rupture accident in a 4-loop PWR is performed with J-TRAC code to give information on core boundary conditions for tests using the transient thermal-thermal hydraulic test facility, which aims at demonstrating the core integrity during design basis events of light water reactors.

A double-ended break of single U-tube was assumed. The calculational conditions were specified as close as possible to those of licensing calculation[1]. The calculated results with the J-TRAC code were compared with those of licensing codes to check the applicability of the J-TRAC code to the SG tube rupture accident. The timing of the reactor trip was input to 290 s using the value of the reference licensing calculation.

The input data of the J-TRAC code was developed based on that for the large break loss-of-coolant accident[2] by changing initial and boundary conditions for the SG tube rupture accident. Figure 9.3.1 shows input schematics at steam generator with a tube break. In Case 1 input, the break tube is modeled by a secondary pipe of a TEE component model, while it is modeled by a separate pipe in Case 2 input. Although the actual configuration is expected to be similar to that of Case 2 input model, Case 1 input was used because it was supposed that the licensing calculation was performed with the input model similar to Case 1 input model.

Figures 9.3.2 and 9.3.3 show mass flow through SG tube break and pressure at pressurizer, respectively. The case 2 shows lower mass flow and higher pressure than the Case 1. In the Case 2 calculation, high pressure drop was calculated along the single tube part connecting between SG plenum and break location and resulted in the lower mass flow rate at the break compared to the Case 1. It was found that the modeling of the ruptured tube has a remarkable effect on the pressure transient during the SG tube rupture accident.

Figure 9.3.4 shows calculated flow conditions at core with the J-TRAC code. Although the modeling method of the ruptured tube has a significant effect on the core pressure transient, it has a weak effect on inlet velocity, inlet fluid temperature and core power. Because the J-TRAC code can give information on core flow conditions, which

is not described in the final safety analysis report, it is considered that the J-TRAC code is an useful tool to specify the initial and boundary conditions for the transient thermal-hydraulic demonstration test facility.

References

1) Kyuushu electric power company : FSAR of Genkai 3&4 nuclear power plant, October 1982.

2) Akimoto,H., Ohnuki,A. and Murao,Y. : Development of REFLA/TRAC code for accident analyses of light water reactors - analysis of large break LOCA in a 4-loop PWR-, JAERI-Review 94-009 pp228-230, 1994.

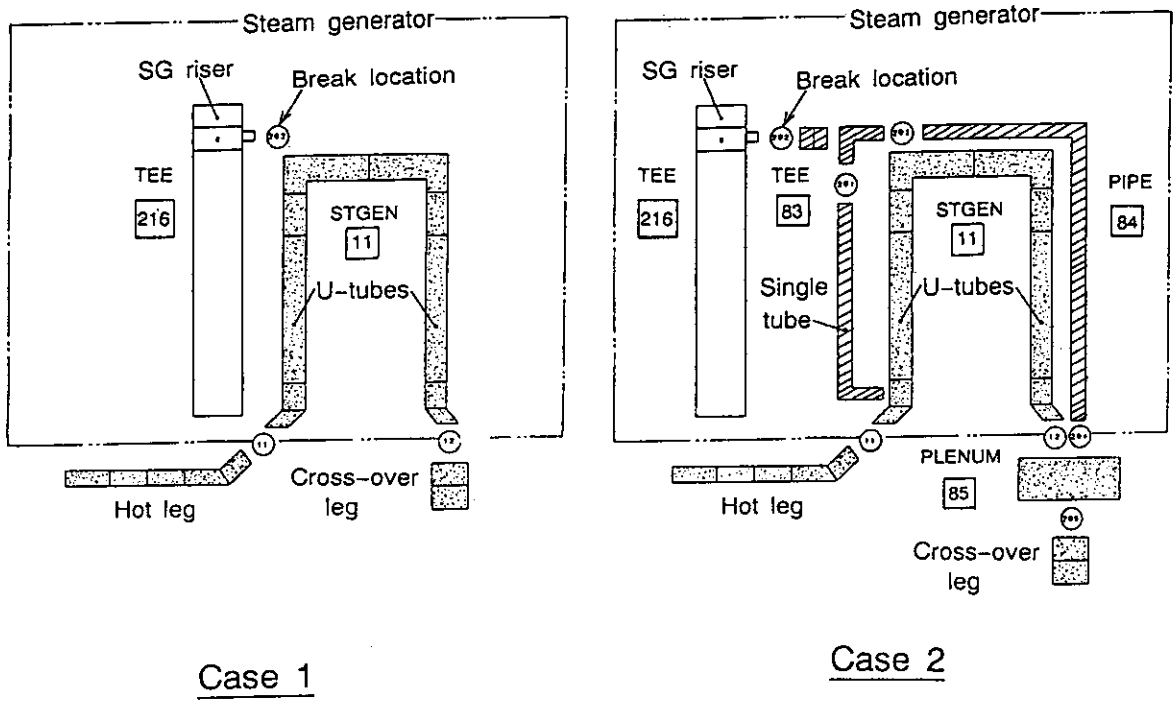

Fig. 9.3.1 Input schematic at steam generator

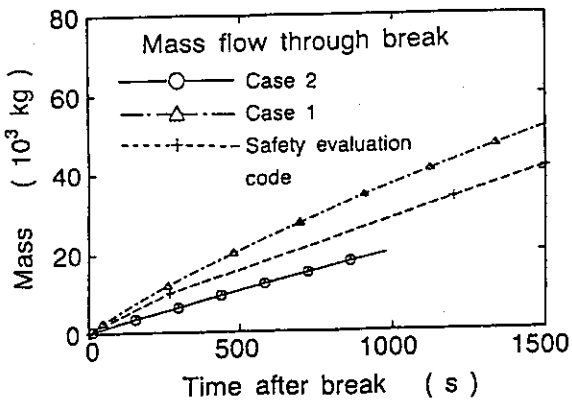

Fig. 9.3.2 Mass flow through break

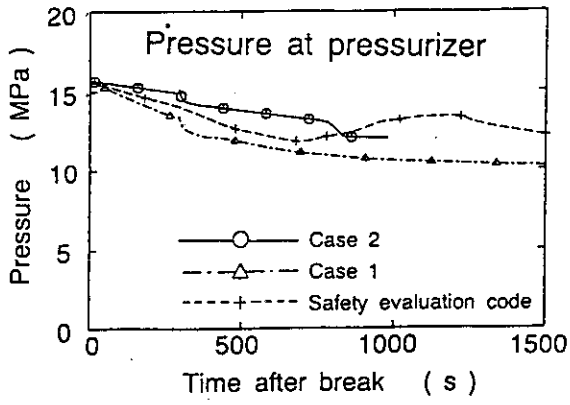

Fig. 9.3.3 Pressure at pressurizer

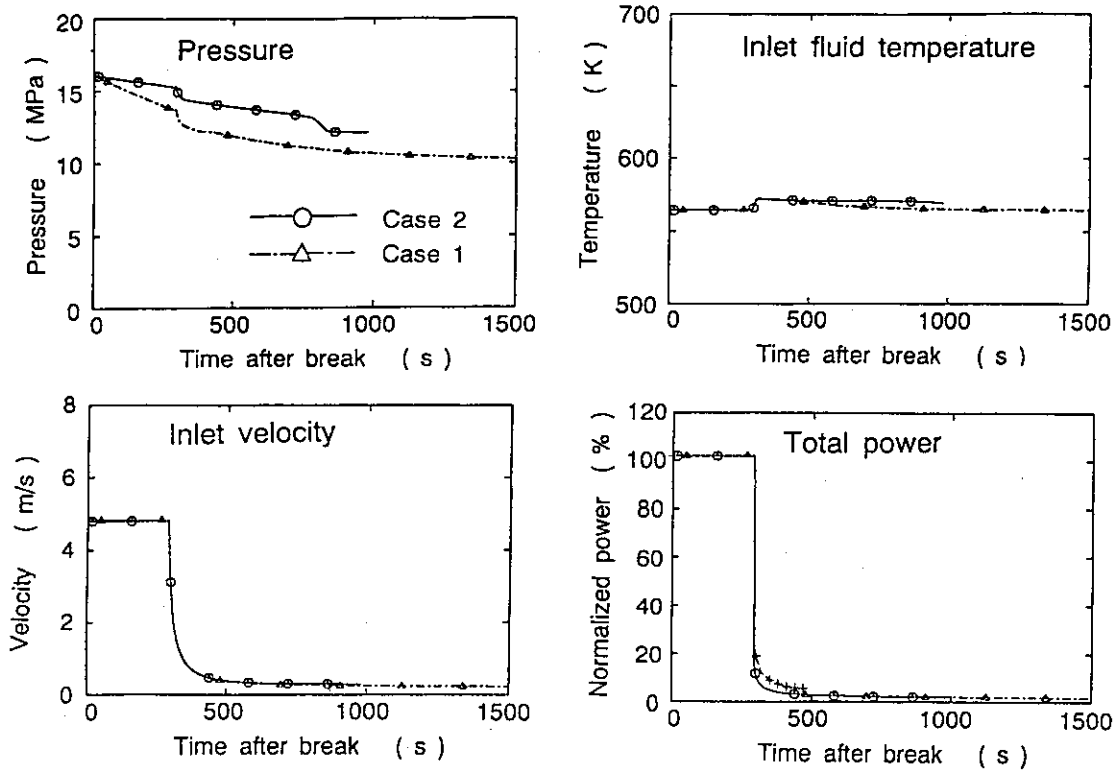

Fig. 9.3.4 Flow conditions at core

9.4 Flow Pattern and Its Transition in Gas-Liquid Two-Phase Flow along a Large Vertical Pipe

A. Ohnuki, H. Akimoto and Y. Sudo

The flow pattern and its transition were investigated experimentally in air-water two-phase flow along a large vertical pipe (hydraulic diameter: 0.48 m, length of flow path: 2 m). This study was performed to establish a data-base and to examine the flow structure in the large vertical pipe. Figure 9.4.1 shows the outline of experimental rig used in this study. The experimental rig is composed of a test section, an upper plenum located above the test section, a lower plenum located under the test section and the air and water sources. The test section is made of transparent acrylic resin to observe the flow pattern. The experimental conditions for air and water flow rates were as follows: superficial air velocity J_g: 0.02 - 0.87 m/s (at atmospheric pressure) and superficial water velocity J_l: 0.01 - 0.2 m/s. The pressure was atmospheric pressure at the top of upper plenum and the fluid temperature was around 35 C.

In order to examine the flow pattern and its transition along the large vertical pipe including a developing flow region, the followings were measured: (1) Flow pattern, (2) Differential pressure and sectional void fraction fluctuation and (3) Phase and local liquid velocity distributions in the radial direction near the top of test section. From the measurements, the following findings were obtained:

(1) No slug bubbles are recognized even under the condition where the slug flow is realized in a small-scale pipe.

(2) The bubbly flow pattern is changed from the uniform to the churn bubbly flow via the agitated bubbly flow with increasing J_g but the uniform bubbly flow is not attained under a low J_l due to the downward liquid flow near the wall.

(3) In the churn bubbly flow, the standard deviation, σ , of the void fraction fluctuation is larger than that in the uniform or the agitated bubbly flow.

Based on these findings, we classified the flow pattern by using the flow observation results and the magnitude of σ of the void fraction fluctuation. Figure 9.4.2 shows the flow pattern map proposed in this study. The boundary between the uniform and the agitated bubbly flow was determined by the flow observation results. The boundary corresponds to the downward liquid velocity near the wall of about -0.1 m/s. The boundary between the agitated and the churn bubbly flow was obtained by a threshold value of σ . The value of 0.04 was adopted

because the increasing rate of σ with J_g was low in the region less than the value. It is interesting that the boundary between the agitated and the churn bubbly flow corresponds to the criterion of bubbly to slug flow transition by Mishima-Ishii[1].

References

1) Mishima K. and Ishii M.: Flow Regime Transition Criteria for Upward Two-Phase Flow in Vertical Tubes, Int. J. Heat and Mass Transfer, Vol. 27 No. 5, pp. 723-737, (1984).

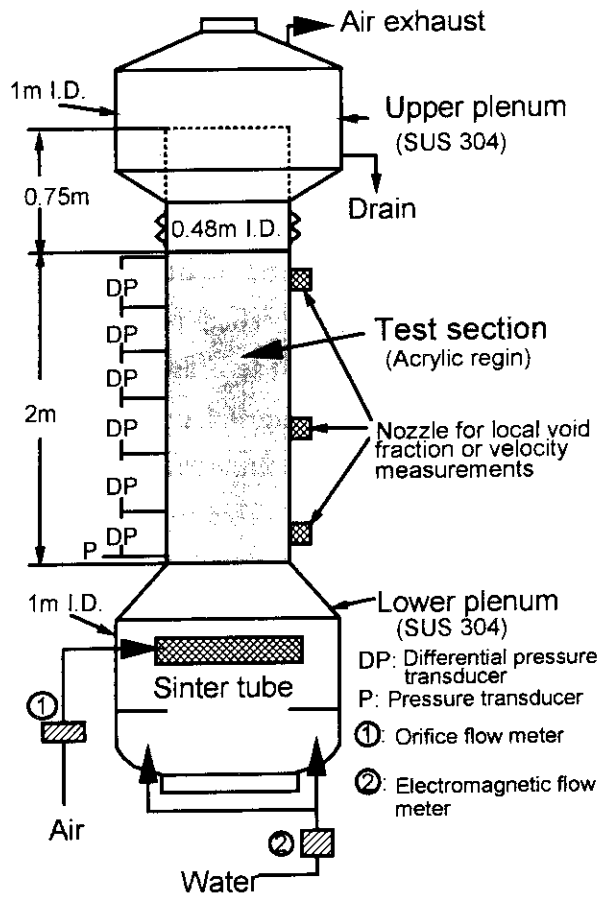

Fig. 9.4.1 Schematic of experimental rig

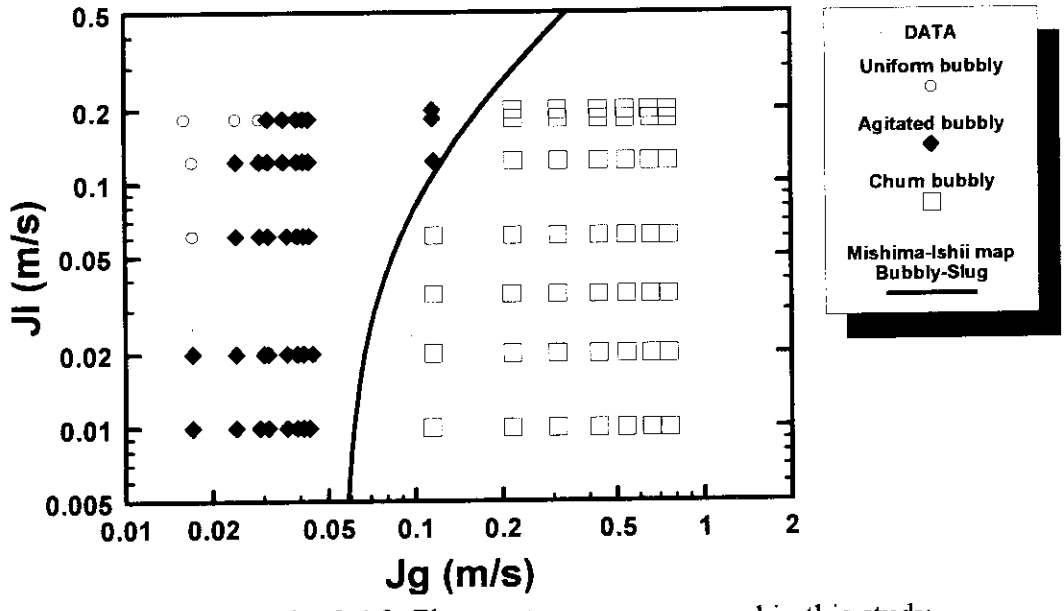

Fig. 9.4.2 Flow pattern map proposed in this study

9.5 Prediction of Average Void Fraction in a Large Vertical Pipe by Two-Fluid Model

A. Ohnuki and H. Akimoto

The void fraction in a vertical flow path with large hydraulic diameter is one of important quantities to determine the characteristic of natural circulation in a passive safety reactor. We are recently investigating the flow structure in a large vertical pipe (Inner diameter: 0.48 m) and the results for the flow pattern is described in Sec. 9.4. In this study, the applicability of interfacial friction models in two-fluid model code was assessed for the prediction of sectional average void fraction measured in the large vertical pipe.

The data were derived from differential pressure measurements by neglecting frictional and accelerated pressure losses. The assessed models were those in REFLA/TRAC[1] and TRAC-BF1[2] codes.

Figure 9.5.1 compares the data with various models under superficial water velocity $J_l = 0.18$ m/s. In the experiment, an uniform bubbly flow was observed in the flow rate condition indicated by A and an agitated bubbly flow was observed in those by B and C. The original model in REFLA/TRAC code underestimates the void fraction in the region of void fraction higher than about 0.25. A large slug bubble occupied the flow path is assumed in the original model in that region but no such slug bubbles were observed in the experiment. The maximum size of slug bubbles in the model was restricted to a certain value based on Kataoka's study[3] and the modified model (Modified REFLA/TRAC) gives better prediction in the region of void fraction up to about 0.4. The model in TRAC-BF1 code uses Wilson correlation for this subject and underestimates the void fraction. This tendency was also observed for steam-water data by Currier et al.[4]. The predictive accuracy is improved by removing the Wilson correlation and using the drift-flux type model in the TRAC-BF1 code.

Figure 9.5.2 compares the steam-water data by Currier et al. with the original model in REFLA/TRAC code and the modified model for the maximum size of slug bubbles. The original model underestimates the void fraction. The modified model gives higher void fraction than that by the original model and better prediction especially under a higher pressure.

The assessment results in this study indicate that the maximum size of slug bubbles in the model of REFLA/TRAC code should be modified to improve the predictive accuracy.

References

1) Akimoto H., et al.: Assessments of REFLA/TRAC Code for Various Postulated Accidents in PWR, Fifth Int. Topical Meeting on Reactor Thermal Hydraulics (NURETH-5), Vol. VI, pp. 1797-1803, (1992).

2) Borkowski J.A., et al.: TRAC-BF1/MOD1 Models and Correlations, NUREG/CR-4391 EGG-2680 R4, (1992).

3) Kataoka I. and Ishii M.: Drift Flux Model for Large Diameter Pipe and New Correlation for Pool Void Fraction, Int. J. Heat Mass Transfer, Vol. 30 No. 9, pp. 1927-1939, (1987).

4) Currier F., et al.: Joint US/EURATOM R&D Program Quarterly Progress Report, ACNP-63021, (1963)

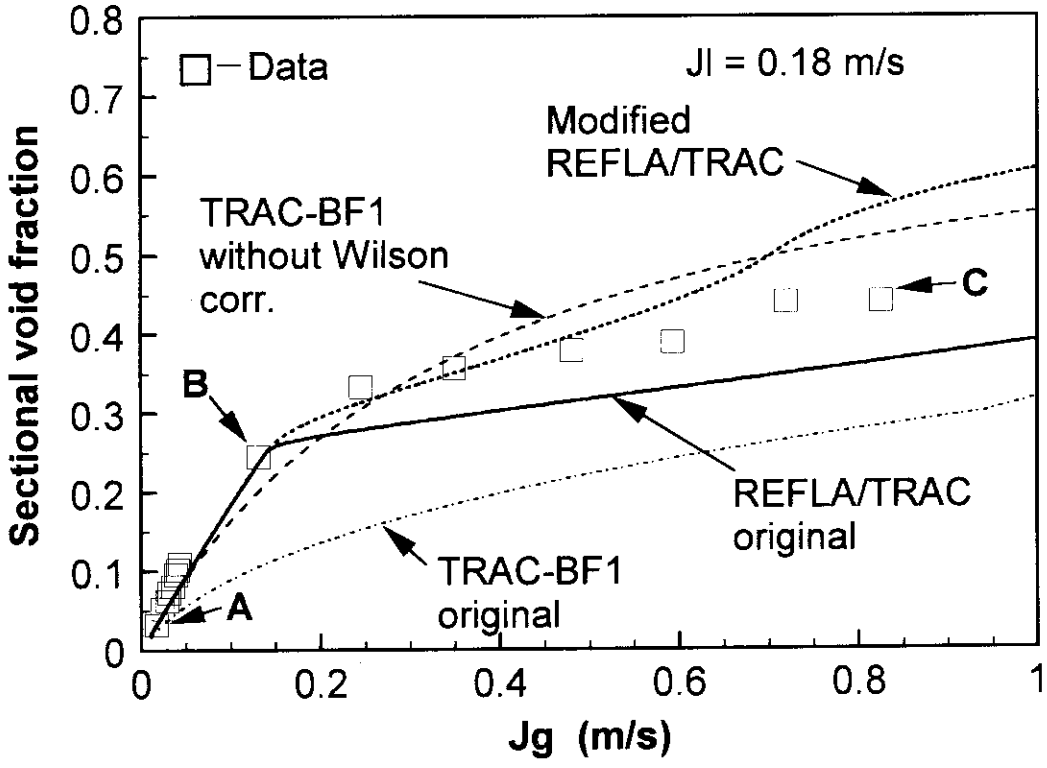

Fig. 9.5.1 Prediction of sectional average void fraction by two-fluid model

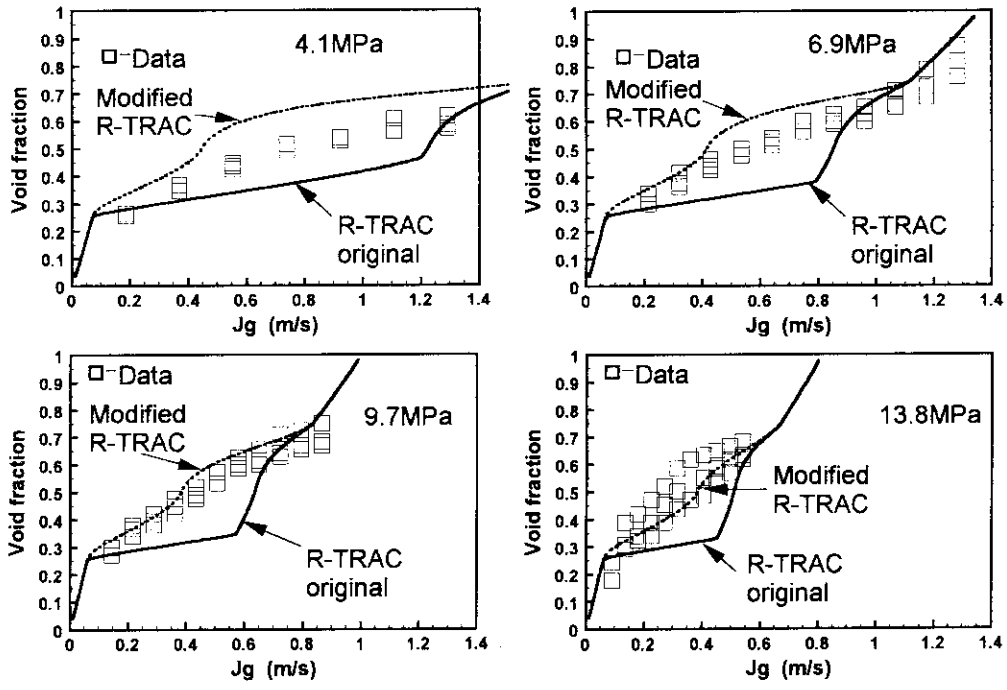

Fig. 9.5.2 Applicability to steam-water data by Currier et al.

9.6 CHF experiment in a rectangular flow channel heated from one side

H. Akimoto, M. Kaminaga and Y. Sudo

A high heat flux of 10 to 100 MW/m^2 is required to be cooled in various areas; a new rotating target for DT neutron source at FNS (Fusion Neutronics Source)[1], an advanced research reactor with high neutron flux, the diverter of fusion reactors, etc. The required heat flux is more than ten times of the conventional heat flux. A forced convection with highly subcooled water at a high velocity is one of promising cooling methods for the heat removal under such high heat flux conditions. An experiment was performed to measure the critical heat flux (CHF) for the system cooled by highly subcooled water at a high velocity.

Figure 9.6.1 shows the schematic of the test section used in the present experiment. The water flows through a rectangular flow channel of 3 mm in height, 12 mm in width, and 50 mm in length. The exit of the channel is opened to the atmosphere. The one side of the flow channel is heated by the copper film of 9 μm thick on the printed wiring board electrically. Each experiment was performed at a constant inlet water temperature, T_j, and a constant inlet water velocity, V_j, increasing supplied power to the copper film step by step. The heat flux on the copper film was calculated from the measured voltages at every 12 mm section and measured electric current. The temperature of the copper film was calculated from the change of the electric resistance. The critical heat flux was determined by the burnout of the copper film. The flow behavior in the channel was observed through transparent polycarbonate resin.

Figure 9.6.2 shows an example of measured boiling curves in the present study. The particular test, shown in Fig. 9.6.2, was performed at inlet water temperature of 30 $^\circ$C, inlet water velocity of 10 m/s, and outlet pressure of 0.1 MPa. The burnout of the copper film occurred at exit of the test section. The data in Fig. 9.6.2 were calculated using the measured voltage at the 12 mm section in the 1 mm upstream of the test channel exit. In the test in Fig. 9.6.2, no bubble was observed when the heat flux was low. This observation indicates that the copper film is cooled by the forced convection of the single-phase water. A tiny bubble was observed when the wall temperature was more than about 120 $^\circ$C. It can be considered that so-called subcooled boiling was initiated at about 120 $^\circ$C. Once the subcooled boiling is initiated, the slope of the boiling

curve is increased because the heat transfer due to boiling is added to the heat transfer due to the forced convection. Figure 9.6.2 shows that the contribution of the forced convection is very important in the system cooled by a highly subcooled water at a high velocity.

Figure 9.6.3 shows measured heat transfer coefficient due to the forced convection. The Reynolds number, Re, and the Nusselt number, Nu, were defined by

$$Re = \frac{V_l D_h}{\nu_l}, \qquad Nu = \frac{h_l D_e}{k_l},$$

where V_l indicates liquid velocity, D_h hydraulic equivalent diameter of test channel, ν_l kinematic viscosity of water, h_l measured heat transfer coefficient due to forced convection, D_e thermal equivalent diameter of test channel, and k_l heat conductivity of water, respectively. Measured heat transfer coefficients are about 1.8 times those by Dittus-Boelter[2] or Petukhov-Gnielinski[3] correlations. It is supposed that the high heat transfer due to the forced convection is caused by the high turbulence in the vicinity of the water inlet.

Figure 9.6.4 shows measured critical heat flux, q_{CHF}. The measured q_{CHF} is about 1.5 times that calculated by Katto's[4] or Celata's[5] models. It is supposed that the high q_{CHF} in the present study is caused by the high turbulence in the vicinity of the water inlet. It is necessary to study more on the effect of the configuration of the water inlet and the length of the heated section in order to clarify the effect of the turbulence at the water inlet on q_{CHF}.

References

1) Tanaka,S., et al.: JAERI-M 86-105, (1986), (in Japanese).

2) Dittus,F.W. and Boelter, L.M.K : Univ. Calif., Pubs. Eng. 2, p.443, (1930).

3) Gnielinski,V.: Int. Chem. Eng.,Vol.16 (2) p.359, (1970).

4) Katto,Y.: Int. J. Heat Mass Transfer, Vol.33 p.1921, (1990).

5) Celata,G.P,et al. : Int. J. Heat Mass Transfer, Vol. 37 (2),p.237, (1994).

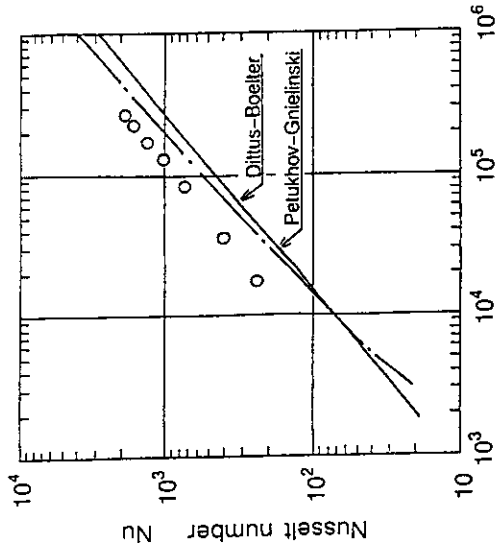

Fig. 9.6.3 Heat transfer coefficient due to forced convection

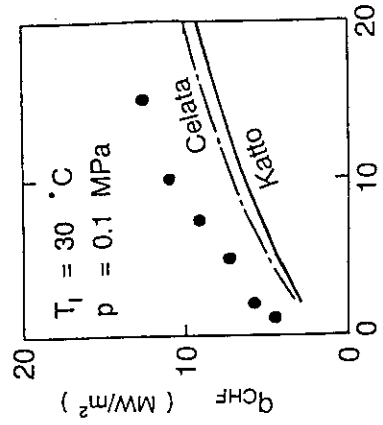

Fig. 9.6.4 Critical heat flux

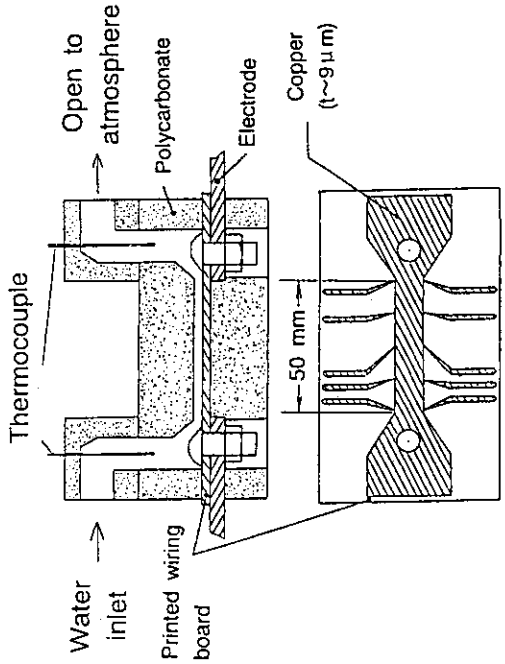

Fig. 9.6.1 Test section

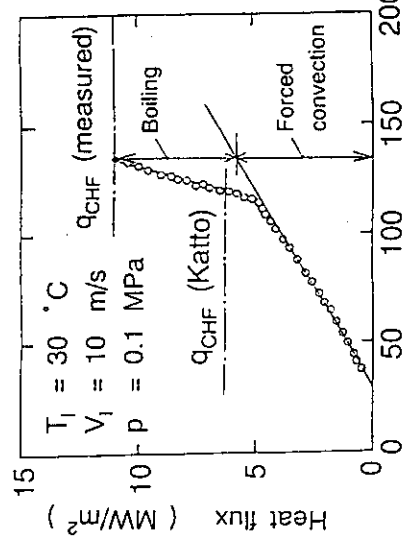

Fig. 9.6.2 Boiling curve

10. Transmutation System

The research activities on transmutation system includes the conceptual design studies on proton accelerator-based transmutation systems and the relevant basic researches such as the code system development and the spallation experiment.

The preliminary conceptual design study was made on proton accelerator-driven liquid TRU alloy target/blanket system for transmutation of minor actinides (MAs) and long-lived fission products (LLFPs). Neutronics and thermal-hydraulic calculations were made on the liquid alloy system. The system was modified to increase the number of coolant channels in the blanket region about three times as many as that of the original design and to contain not only Pu and Np but also Am and Cm in the liquid alloy. It was shown that this system with an effective neutron multiplication factor of 0.91 can transmute about 200 kg TRU per year and generate a thermal power of 1350 MW in operation with a proton beam of 1.5 GeV and 33 mA. Burnup calculations were made for three type of proton accelerator-based transmutation system; the solid system with tungsten target and TRU alloy blanket, the chloride molten-salt system, and the TRU alloy system. The evolution of actinide composition with burnup time was calculated up to 1800 days for each system at average neutron fluxes of 2, 5,10 x 10^{15} n/cm^2/s respectively.

In the code system development, the experimental data of fission cross section from 20 MeV to 10 GeV were surveyed for the proton-induced reactions of an actinide ^{238}U and a subactinide ^{209}Bi and were compared with predictions computed by the cascade codes. The calculated cross section for the neutron-induced fission reaction of ^{235}U was compared with the Rapapart's measured data which had been evaluated in JENDL 3.2 in the lower energy range below 20 MeV. One parameter in the high energy fission model proposed by Nakahara was adjusted to fit with the measured data for a 300 MeV proton-induced reaction. As the result the modified fission product mass distribution showed better agreement with measure ones in a wide energy range than the original one. The total cross sections for nucleon-nucleus reaction stored in the cascade code NMTC/JAERI were modified based on the Pealestein's systematic data. This modification has considerably improved the agreement between calculation and measurement for the transmission in the iron shielding experiment with 67 MeV protons and the threshold reaction in the spallation experiment with 500 MeV protons.

In the spallation experiment, the spectra of neutrons emitted from the thick lead target irradiated by protons with energies of 500 MeV and 1.5 GeV were measured in six directions by using the time of flight (TOF) method in the KEK facility, Tsukuba. The neutron spectrum above

14 MeV was determined by the TOF analysis, whereas the unfolding method was applied to the energy region below 14 MeV to correct the time fluctuation due to scattering. The spectrum calculated with the cascade code NMTC/JAERI and the neutron transport code MCNP 4.2 was in good agreement with the measured one below 15 MeV and underestimated by a factor of two in the range from 20 MeV to 70 MeV. The spectra of neutrons emitted from thin targets such as C and Au pellets irradiated by 67 MeV protons were measured in seven directions in the TIARA facility at the Takasaki Research Establishment. The spectra calculated with the above codes overestimated the measured data by a factor of two to three in the forward direction in the whole energy range and underestimated them in the backward direction for energies above 20 MeV. Adoption of the preequilibrium reaction model in the cascade code has comparatively improved the agreement between calculation and measurement up to 40 MeV.

In this chapter the Transmutation System Laboratory is in charge of paragraphs 10.1 -10.3 and the Radiation Shielding Laboratory in charge of paragraphs 10.4 -10.6.

10.1 Neutronics Analysis of the Accelerator-based Liquid TRU-alloy Target and Molten-salt Blanket Transmutation System

T. Sasa, K. Katafuchi*, T. Nishida and T. Takizuka

Neutronics design study of the accelerator-based liquid TRU-alloy target and molten-salt blanket transmutation system[1] was performed.

The subcritical core in this system is composed of a liquid TRU-alloy target, a molten-salt plenum, a graphite moderator with cooling channels, a proton beam path with a beam window and a graphite reflector. Compositions of the liquid TRU-alloy and molten-salt are TRU-Co-Ce and LiF-BeF_2 respectively. Liquid TRU-alloy is based on the fuel studied in the LAMPRE[2] program at Los Alamos National Laboratory. In this system, liquid TRU-alloy acts both as target and fuel. The subcritical core is about 2 m in diameter and 2 m in height. Spallation neutrons and heat are mainly generated in the target region located at the center of the blanket. Liquid TRU-alloy is forced to circulate by the molten-salt's flow and the heat is removed by the molten-salt through the blanket channel. Reaction products in the liquid TRU-alloy are also transferred to the molten-salt in the blanket region. Molten salt is led to external heat exchangers and an on-line spallation/fission product removal facility to remove the heat and reaction products in the molten-salt and finally returned to the core.

Several points were revised to satisfy the JAERI's accelerator-based transmutation guideline. The major modifications were

1. Addition of Am and Cm in the liquid TRU-alloy target,
2. Rise up the thermal output due to the increase of the transmutation amount of TRUs.

A spallation calculation code system NMTC/JAERI[3] and a Monte Carlo transport code system MCNP-4A[4] were used for the calculation. FSXLIB-J3[5], the JENDL-3.1-based cross section library, was used for the MCNP calculation. NMTC/JAERI calculates the high energy nucleon reaction and particle transportation in the energy range from 15 MeV to 3.5 GeV. Below the energy range of 15 MeV, calculation was connected to the MCNP-4A code system. Criticality calculation was also performed with the MCNP-4A code system and FSXLIB-J3 library.

The calculation results for the original and the revised models of the system are tabulated in Table 10.1.1. Figure 10.1.1 shows the neutron spectra per incident proton in the target, blanket and molten-salt regions for the revised model. From the result, the spectrum in target region was almost same as one in the original model. Spectra in the blanket region and

---

* Tokai University

the molten-salt region became slightly softer than the original model and the average neutron energy was also become lower. In order to transmute TRU mainly by fission reaction, blanket material might be substituted with other materials.

References

1) Sasa T. et. al. : JAERI-Review 94-009 (1994)
2) Hannum W. H. and Kirkbride L. D. : LA-3384-MS (1966)
3) Nakahara H. and Tsutsui T. : JAERI-M 82-198 (1982)
4) Briesmeister J. F. ed. : LA-12625-M (1993)
5) Kosako K. et. al. : JAERI-M 91-187 (1991)

Table 10.1.1 Calculated results for the original and the revised models

Calculation model			Original	Revised
• Spallation neutron yield per proton		(n/p)	45.5	44.9
• Effective neutron multiplication factor			0.895	0.908
• Fission reaction rare		(reacions/p)		
Neptunium			71.4	56.2
Americium			-	30.8
Curium			-	8.16
Plutonium			74.2	98.0
• Capture reaction rate		(reactions/p)		
Neptunium			200.2	182.1
Americium			-	131.1
Curium			-	7.75
Plutonium			37.9	43.5
• Average neutron energy				
Target region		(MeV)	1.721	1.220
Blanket region		(MeV)	0.705	0.595
• TRU inventory and transmutation rate				
Neptunium	Inventory	(kg)	644.1	784.1
	Transmutation rate	(%/year)	11.0	15.8
Americium	Inventory	(kg)	-	540.4
	Transmutation rate	(%/year)	-	12.8
Curium	Inventory	(kg)	-	79.6
	Transmutation rate	(%/year)	-	23.2
Plutonium	Inventory	(kg)	249.9	491.8
	Transmutation rate	(%/year)	29.8	44.1
• Thermal output		(MWt)	455	1350
• Proton beam energy		(GeV)	1.5	1.5
• Proton beam current		(mA)	15.6	34.5

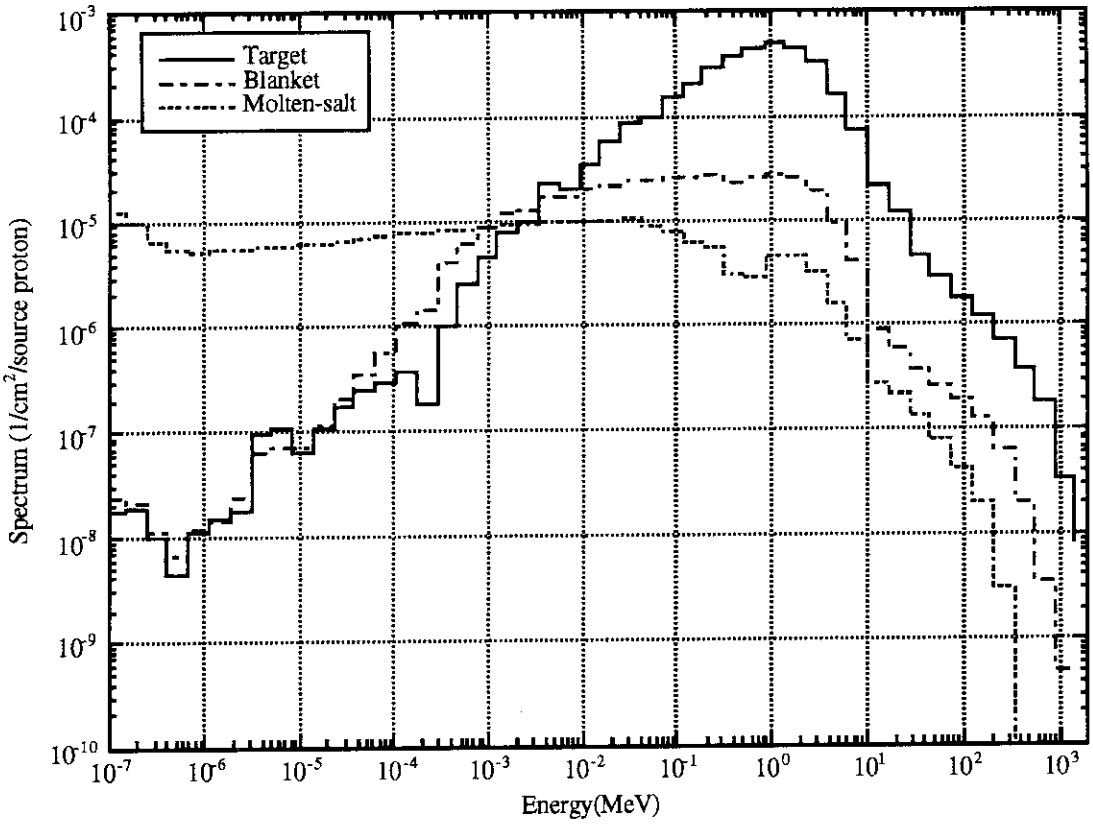

Fig.10.1.1 Calculated neutron spectrum in target, blanket and molten-salt region

10.2 Burnup Calculations for Accelerator Driven Transmutation Systems

T. Nishida, T. Sasa, H. Takada, T. Takizuka, Y. Okuda*

The effective and safer management on long-lived radioactive nuclides in the spent nuclear fuel is one of most important issues for the future application of atomic energy in the 21 Century. The three types of accelerator-based transmutation system for minor actinides (MA: Np, Am, Cm) and long-lived fission products(LLFP) are conceptually being studied at JAERI to develop the promising technology alternative to the undergraund repository one. In the present report the burnup calculations for these systems have been done to examine the transmutation capability and tne nuclear safety of these systems through one cycle time.

The code system SPACE, which was being developed for design study on an accelerator-based system, has been extended to calculate burnup characteristics for the accelerator-based MA transmutation systems. The new version of the burnup code COMRAD[1] based on the Beteman method was prepared to speed up the computation. Figure 10.2.1 illustrates the flow chart producing the one group cross section libraries of actinides for the burnup calculation. JSSTDL is the standard cross section library with the 295 group structure and was prepared for many nuclides including higher actinides corresponding to JENDL3.2[2] at JAERI. The program MACROJ produced both effective microscopic and macroscopic cross sections for the nuclides used in transmutation systems with JSSTDL. The one dimensional transport code ANISN computes the 295 group neurton spectrum for simplified models of transmutation system, using the macro cross sections. The one group cross sections were degenerated by averaging the microscopic cross sections with the neutron spectrum.

The burnup calculations by COMRAD were carried out for three csaes of (a) tungsten target/MA alloy fuelled[3)-5)], (b) MA molten salt[6)-8)] and (c) MA eutectic alloy target/graphite blanket[9),10)] transmutation systems, where the decay data library JDDL was used. The calculation conditions and the initial atom number densities of main actinides for each system are summarized in Table 10.2.1. Figures 10.2.2 - 10.2.4 represent the composition of minor actinides dependent on the burnup time under the contant neutron flux 5×10^{15} n/cm^2/s upto 1800 days in the active region of (a), (b) and (c) systems respectively. Figure 10.2.5 shows the dependence of neutron effective multiplication factors for three transmutation systems on burnup time until 1800 days. The effective neutron multiplication factors were recalculated by the code TWOTRAN-II [11] for each system with renewed compositions of actindes on some burnup steps. It has been recognized that all systems always keep the subcritical state with sufficient margin although k_{eff} swings to the positive side at the initial burnup stage.

* Sumitomo Atomic Power Industries, INC.

References

1) Naito Y., Hara S., Ihara H., Katakura J. : JAERI-M 86-121 (1986).
2) Koyama K., Minami K., Taji Y., Miyasaka S. : JEARI-M 7155, (1977).
3) Takizuka, T. et al. ; Proc. 5th Int. Conf. Emerg. Nucl. Systems, Karlsruhe (1989).
4) Mizumoto, M., et al.: 16th Int. Linear Accelerator Conf. LINAC-92, Ottawa (1992).
5) Takizuka, T. et al. : Proc. 2nd Inform. Exch. Meeting, Argone, 397 (1993).
6) Nishida T. et al. : Proc. ICENES'93, Makuhari, 419 (1993).
7) Katsuta, H., et al. : Proc. OECD/NEA Inter. Inform. Exchan. Meeting, 242 (1993).
8) Kato, Y. et al. : Proc. OECD/NEA Specialist Meeting of Accelerator-based Transmutation, 92-02 ISSN 1019-6447, Swiss, 133 (1992).
9) Katsuta, H. et al. : Proc. ICENES'93, Makuhari, 424 (1993).
10) Sasa T., Takizuka T., Nishida T., Katsuta H. and Takahashi H. : Proc. Inter. Symp. Global Enviro. Nucl. Energy System, Susono (1994).
11) Lathrop K. D., Brinkley F. W. : LA-4848-MS (1973).

Table 10.2.1 Calculation conditions

Average neutron flux : 2, 5, 10 x 10^{15} n/cm^2/s		
Burn up step (day) : 50, 100, 200, 300, 400, 500, 600, 700, 800, 900, 1000, 1100, 1200, 1300, 1400, 1500, 1600, 1700, 1800		
Initial actinide number density in active zone (x 10^{24}n/cm^3)		
System (a)	Np237	3.1573E-3
	Pu238	2.5483E-5
	Pu239	7.9443E-4
	Am241	1.2915E-3
	Am243	5.8206E-4
	Cm 243	1.4554E-6
	Cm244	2.4686E-4
	Cm245	1.3473E-5
System (b)	Np237	2.287E-3
	Pu238	1.403E-5
	Pu239	4.423E-4
	Am241	1.075E-3
	Am243	4.884E-4
	Cm 243	1.221E-6
	Cm244	2.080E-4
	Cm245	1.140E-5
System (c)	Np237	5.2629E-3
	Pu238	3.2064E-5
	Pu239	9.9960E-4

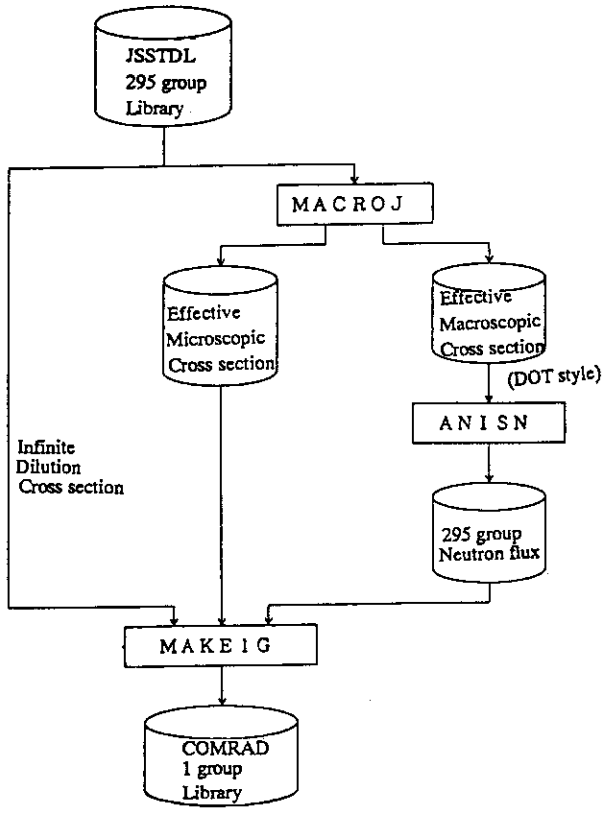

Fig.10.2.1
Flow cahrt for producing the one group cross section library

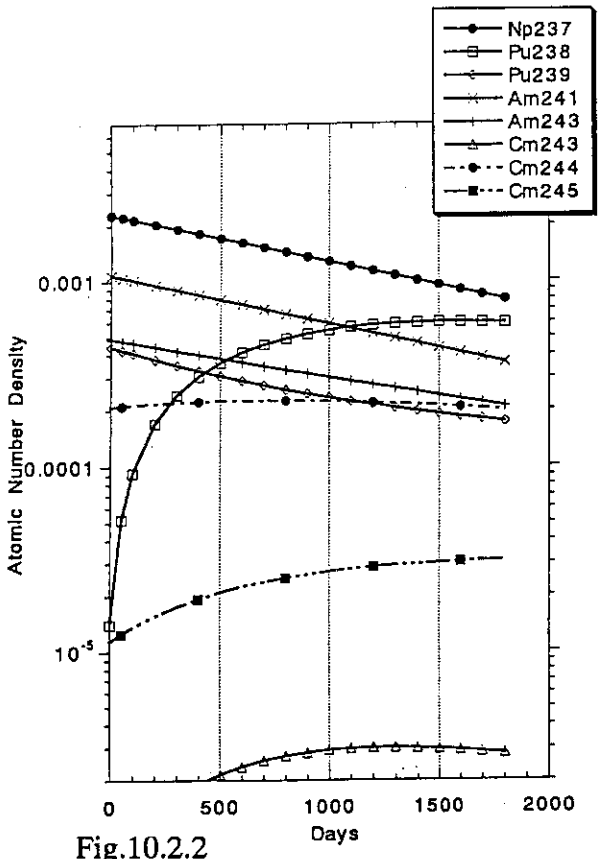

Fig.10.2.2
Time evolution of atom number density of actinide in the tungsten target/metal fuel system

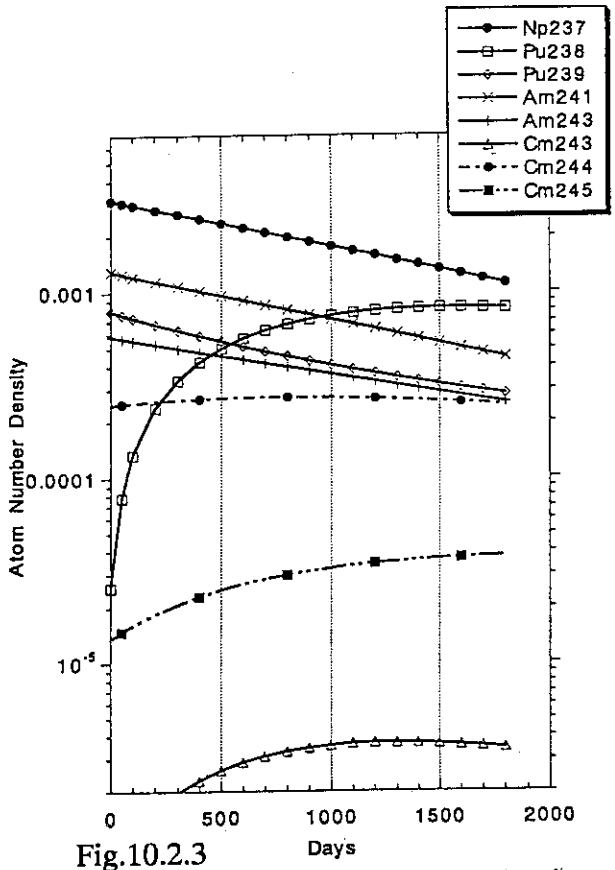

Fig.10.2.3
Time evolution of atom number density of actinide in the molten salt fuel system

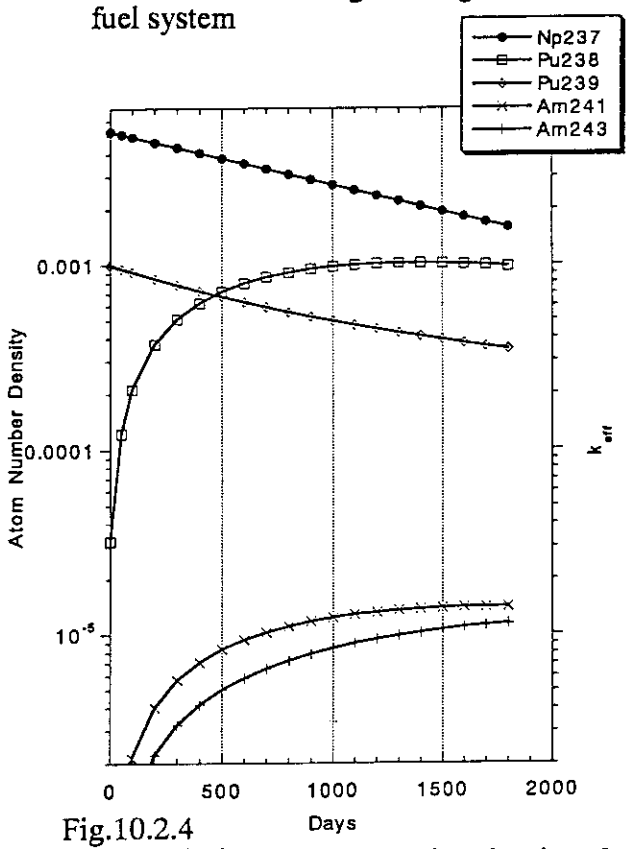

Fig.10.2.4
Time evolution of atom number density of actinide in the eutectic alloy target system

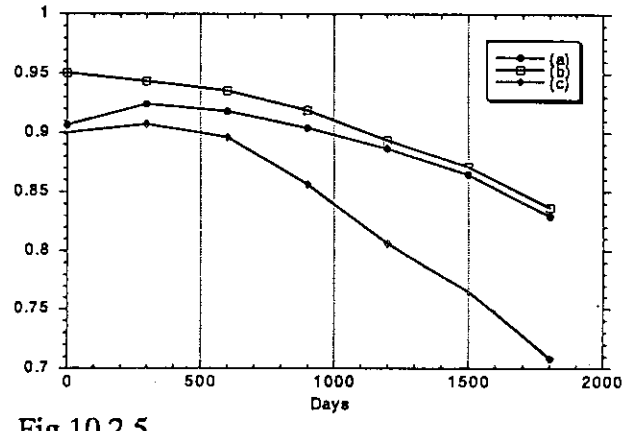

Fig.10.2.5
Dependence of neutron effective multiplication factors on burnup time for (a) solid metal fuelled, (b) molten salt fuelled and (c) eutectic alloy target systems

10.3 Benchmark Evaluations of High Energy Fission Model for the Cascade Code

T. Nishida, N . Yoshizawa*, H. Takada, T. Fukahori, Y. Nakahara,

Evaluations of fission cross section and reaction product for actinides in the high energy range above 20 MeV are important to estimate exactly the amount of radioactive wastes transmuted in the high energy particle-driven system. These give the considerable influence on the number of spallation neutrons which drive the transmutetion system as source neutrons. Benchmark calculations were made to evaluate the accuracy of the high energy fission (HEF) models implemented by Nakahara[1] and Atchison[2] into the high energy cascade codes NUCLEUS[3] and HETC/KFA2[4] respectively.

Experimental data of fission cross sections for ^{238}U(p, fission)[5-9] in the high energy from 10 MeV to 10 GeV were surveyed and compared wtith predictions by both model as seen in Fig 10.3.1. Although experimental data are relatively distributed among authors, both code's predictions agreed within 50 % to them. High energy fission reaction of subactinides should be also taken into accounts because their fission cross sections increase with the particle energy increasing. Figure 10.3.2 shows comparison of experimental data of fission cross sections for ^{209}Bi(p, fission) [5, 6, 7, 9] with predicted cross sections. The large discrepancy near the threshold energy for the reaction is observed between calculated and experimental data and there is a room to improve the disagreement. For neutron-induced fission cross section of ^{235}U, the adjustment between predictions by both codes and data in the cross section library was examined as seen in Fig. 10.3.3. These fission cross sections are considerably smaller than one evaluated in JENDL 3.2[10] at 20 MeV. It is considered that the discrepancy is due to the constant geometrical cross section used in both HEF models and the modification of the total cross section, taking into acounts its energy dependence, is needed. These predictions also were compared with experimental data[11] from 20 MeV to 1 GeV and overestimated experimental ones by 50 % above 50 MeV. Here the corss sections calculated in HETC/KFA2 are larger by about 30 % than those in NUCLEUS.

These codes calculated the residual mass distribution after ^{238}U(p, fission) reaction with proton energy of 300 MeV[8] as seen in Fig. 10.3.4. The residual nuclei in the mass number range from 100 to 140 are produced mainly from the high energy fission reaction. NUCLEUS has given the broader mass distribution than HETC/KFA2. This comes from the fact that the adjustment on the width of Gaussian curve representing the fission product mass distribution is not sufficient in Nakahara model.[12] The width, which is determined dependent severely on the excitation energy of fissioning nucleus, was surveyed to fit to the measured

* Mitsubishi Research Institute Inc

data in this case as appeared in Fig.10.3.5. The width has been selected to have the maximum width at the excitation energy of 15 MeV, where the mass distribution is denoted by thick line against measured data denoted with closed circles. The thin curve with open circles represents the original distribution without modification. In Fig. 10.3.6 we compared the mass distributions calculated by the modified Nakahara model with experimental data[13] for the case of ^{238}U(p, fission) reaction with proton energy of 2.9 GeV and both distributions showed the good agreement.

References.

1) Nakahara Y. and Tsutsui T. : JAERI-M 82-198 (1982)
2) Atchison F. : Jul-Conf-34, (1980).
3) Nishida T., Nakahara Y. and Tsutsui T. : JAERI-M 86-116, (1986)
4) Cloth P., et al. : KFA-IRE-E AN/12/88, (1986).
5) Khan H. A., et al. : Phys. Rev. **C29**, 2199 (1984).
6) Byshenkov V. S., et al. : Sov. J. Nucl. Phys. **17**, 496 (1973).
7) Kon'shin V. A., et al. : Sov. J. Nucl. Phys., **2**, .489 (1966).
8) Stevenson P. C., et al. : Phys. Rev., **111**, 886 (1958).
9) Steiner H. M., et al. : Phys. Rev., **101**, 807 (1956).
10) Shibata K., et al. : JAERI 1319 (1990).
11) Rapaport J., et al. : LA-11078-MS (1987).
12) Nishida T., et al. : PSI Proc. 92-02, ISSN 1019-6447, 535 (1992).
13) Friedlander G. : IAEA, Vienna (1965).

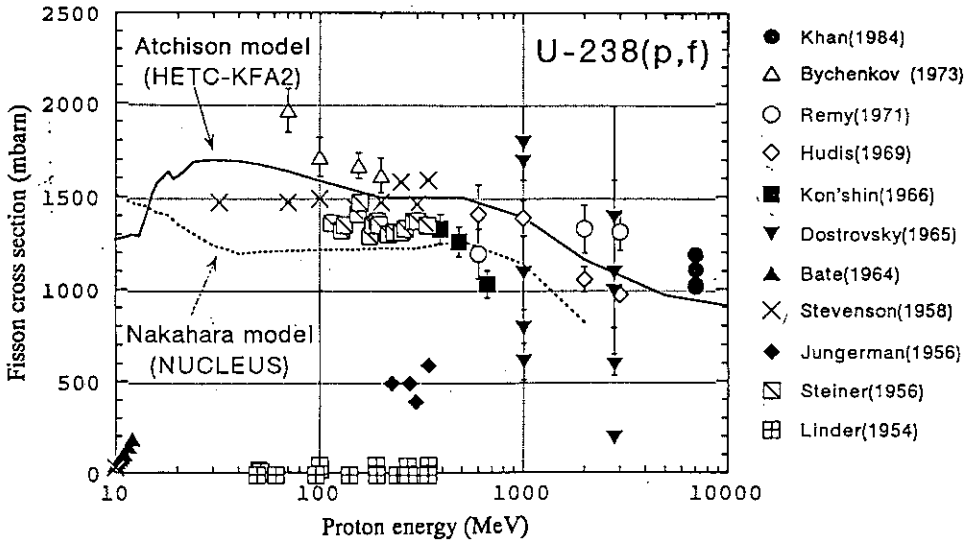

Fig. 10.3.1 High energy fission cross sections calculatedby both HEF models and experimental data for ^{238}U(p, fission) reaction

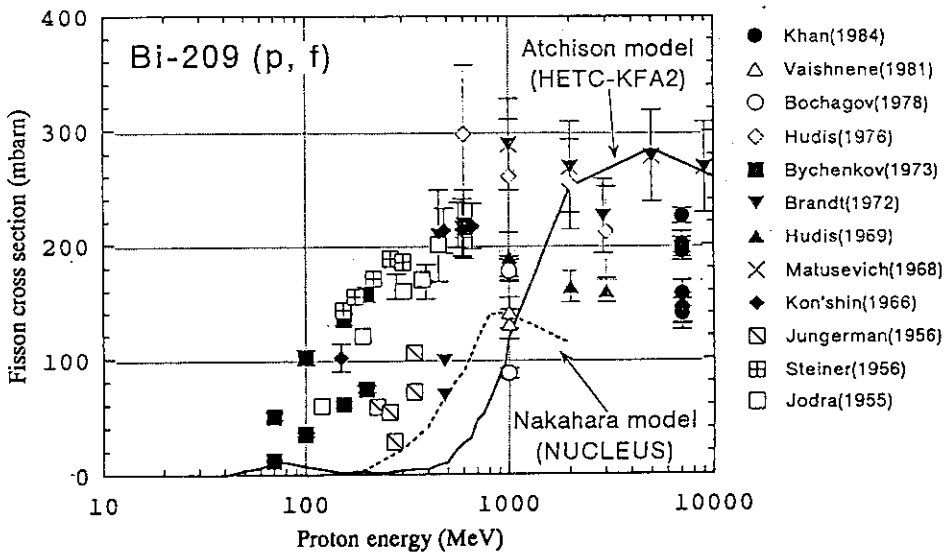

Fig. 10.3.2 High energy fission cross sections calculated by both HEF models and experimental data for ^{209}Bi(p, fission) reaction

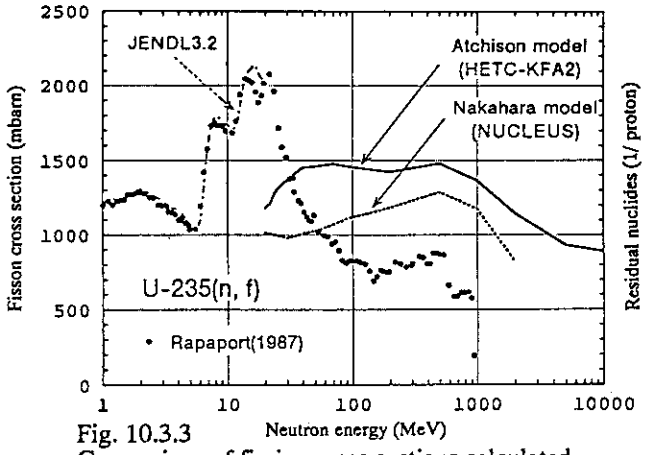

Fig. 10.3.3 Comparison of fission cross sections calculated by both HEF models with JENDL3.2 data below 20 MeV and experimental data above 50 MeV for ^{235}U(n,fission) reaction

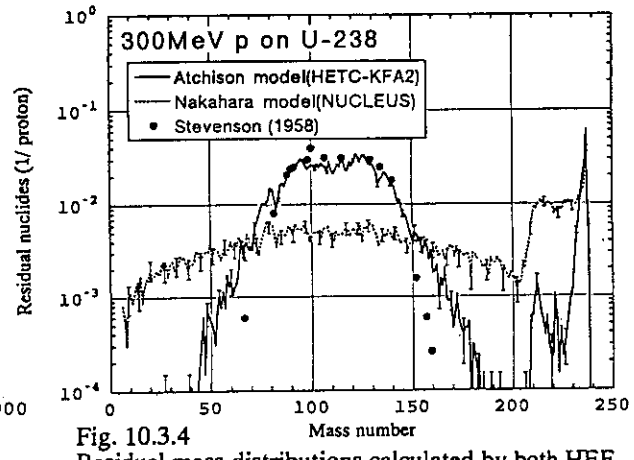

Fig. 10.3.4 Residual mass distributions calculated by both HEF models and experimental data for ^{238}U(p, fission) reaction with proton energy of 300 MeV

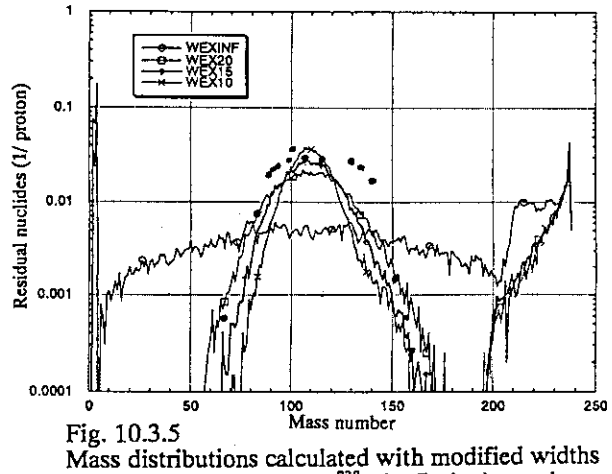

Fig. 10.3.5 Mass distributions calculated with modified widths for experimental data for ^{238}U(p, fission) reaction with proton energy of 300 MeV

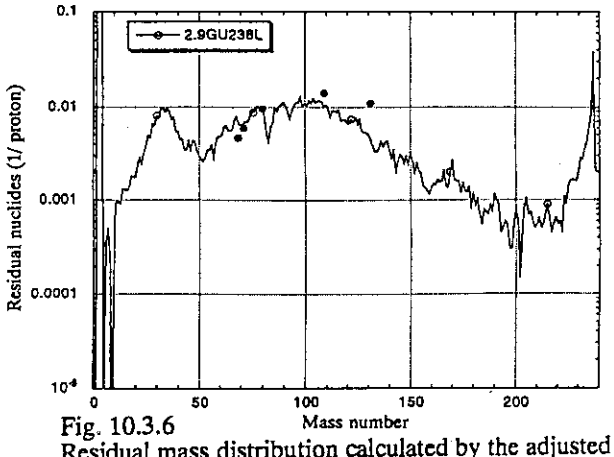

Fig. 10.3.6 Residual mass distribution calculated by the adjusted Nakahara model and experimental data for ^{238}U (p,fission) reaction with proton energy of 2900 MeV

10.4 Correction of The Treatment of Nucleon-Nucleus Reaction Cross Sections in Nucleon Meson Transport Code NMTC/JAERI

H. Takada and H. Nakashima

In the design study of accelerator-based transmutation systems, Nucleon Meson Transport Codes such as NMTC/JAERI[1] and HETC-KFA2[2] have been widely employed in the neutronics calculation in the energy region above 20 MeV where there are few available nuclear data files for the calculation yet. It was found through an analysis of a neutron transmission experiment[3] that the calculation of HETC-KFA2 with the nucleon-nucleus elastic collision improved its accuracy quite well. On the basis of this result, the treatment of the nucleon-nucleus collision cross section and the transport calculation procedure in NMTC/JAERI, in which the nucleon-nucleus collision has not been considered yet, was modified using a little different data and method from those adopted in HETC-KFA2.

At first, the systematics proposed by Pearlstein[4] was included in NMTC/JAERI to obtain the elastic and the non-elastic collision cross sections of nuclear reactions. In Fig.10.4.1, the total, the elastic and the non-elastic cross sections for Fe obtained by the systematics are compared with those used in HETC-KFA2. In both codes, the type of the collision is determined according to the fraction of the elastic and the non-elastic cross sections by a random sampling. As for NMTC/JAERI, the geometric cross section has been used as the total cross section irrelevant to the incident energy. The value is 1.37 barn for Fe. It is easily deduced,therefore, that original code estimates the mean free path of a travelling neutron too long in the energy region below 100 MeV.

At second, the treatment of a pseudo event in a nuclear reaction was changed in the computation procedure. Here, the pseudo event corresponds to the phenomenon that an incident particle passes through a target nucleus without making a single collision. So far, the sampling to find a next collision point was repeated in the computation procedure of NMTC/JAERI and HETC/KFA2 when the pseudo event occurred. This event is regarded as an elastic collision. In this modification, the pseudo event was prohibited and the trial for the nuclear reaction calculation was repeated until a real event occurred because the nuclear reaction calculation was selected as the non-elastic collision by the sampling.

In order to investigate the influence of the modified cross sections and the computation procedure, the analysis for the neutron transmission experiment with the quasi-monoenergetic

neutrons produced by Li(p,n) reaction induced by 67-MeV protons was carried out by modifying HETC-KFA2 in the same manner as for NMTC/JAERI. In Fig.10.4.2, the calculated result is compared with the previous one of HETC-KFA2 in which the elastic collision was taken into account. It is observed that the calculated result with the modified version estimates the neutron spectra by 20 to 30 % lower than the previous result so that better agreement is obtained with the experimental result.

Another analysis was also carried out using modified NMTC/JAERI for the integral spallation experiment with a lead assembly which size is 60 cm in diameter and 100 cm in length. In the experiment, 500 MeV protons were injected in the target with the diameter of 16 cm and the length of 30 cm which was placed at 20 cm behind the top surface. In Fig.10.4.3, the calculated neutron spectra at the depth between 30 and 32.5 cm in the radial positions of 10 and 20 cm are shown for the case that a tungsten alloy was installed as the target. With inclusion of the systematics of Pearlstein, the neutron spectra in the energy region between 20 and 70 MeV is estimated rather lower than the results obtained with the default version.

In Fig.10.4.4, comparison is made between the experimental and the calculated results for the axial distributions of the yield of $^{nat}Ni(n,x)^{56}Co$ in the tungsten target installed lead assembly for 500 MeV proton incidence. The threshold energy of the reaction is about 20 MeV. The production cross section for $^{nat}Ni(n,x)^{56}Co$ was calculated with the code NUCLEUS which corresponds to the nuclear reaction calculation part of NMTC/JAERI. The calculated reaction rates with modified NMTC/JAERI significantly improve the results of the original version which employs the geometric cross sections. The results with modified NMTC/JAERI agree with the experimental results reasonably well because the transport of the neutrons with the energies between 20 and 50 MeV is estimated correctly.

It is concluded from this work that the transport calculation with NMTC/JAERI for neutrons with the energies below 70 MeV has been greatly improved by considering the nucleon-nucleus collision cross sections correctly with the systematics of Pearlstein.

References

1) Nakahara, Y. and Tsutsui, T.: *JAERI-M* 82-198 (1982), (in Japanese).

2) Cloth, P., et al.: *Jül*-2203 (1988).

3) Nakashima, H., et al.: *JAERI-Review* 94-009, 160 (1994).

4) Pearlstein, S.: *Astrophys. J.*, **346**, 1049 (1989).

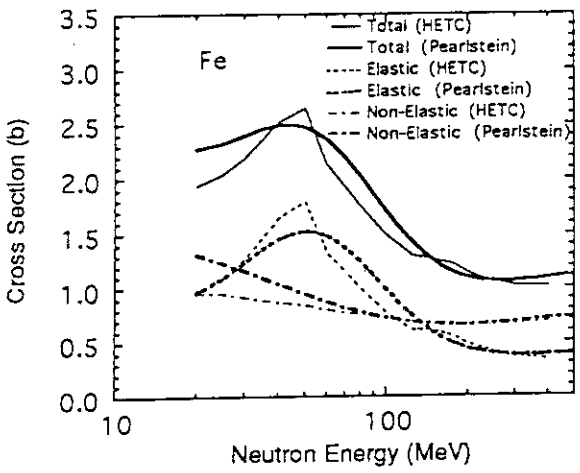

Fig.10.4.1 Total, elastic and non-elastic cross sections of Fe for neutron incidence.

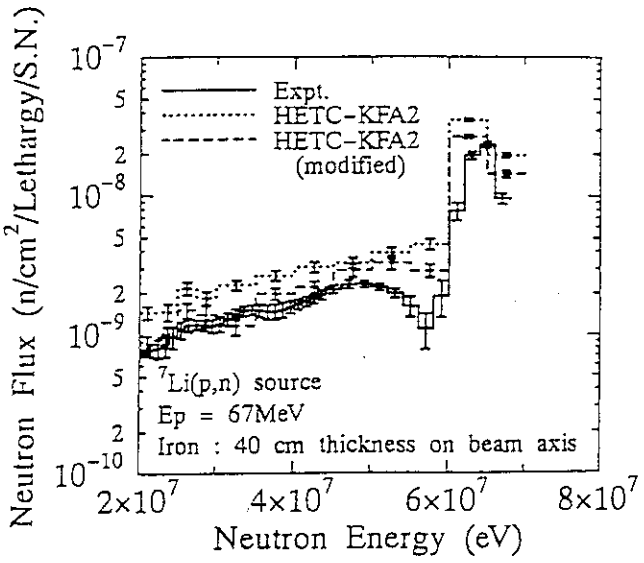

Fig.10.4.2 Energy spectra of neutrons transmitted through 40 cm iron shield for incidence of quasi-monoenergetic source neutrons produced by Li(p,n) reaction with protons of 67 MeV.

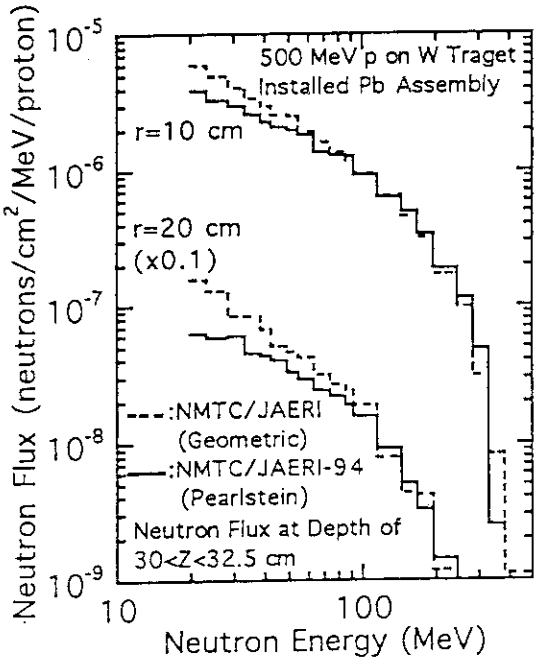

Fig.10.4.3 Calculated neutron energy spectra at the depth between 30 and 32.5 cm in the radial distances of 10 and 20 cm for 500 MeV proton incidence on tungsten installed lead assembly having the size of 60 cm in diameter and 100 cm in length.

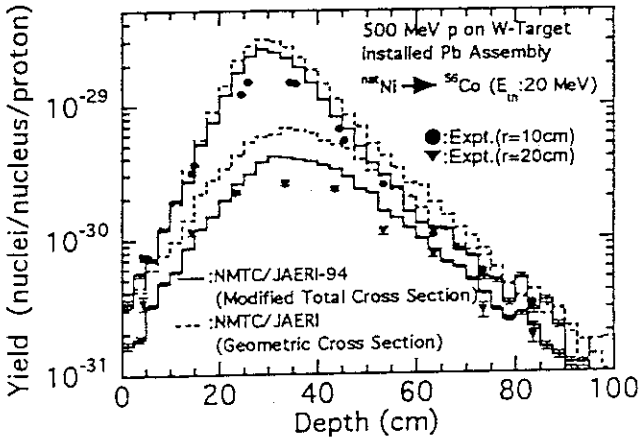

Fig.10.4.4 Experimental and calculated yields of ^{56}Co in ^{nat}Ni samples inserted into tungsten installed lead assembly for 500 MeV proton bombardment. The solid lines indicate the calculated results of NMTC/JAERI with cross sections evaluated by Pearlstein. The dashed lines stand for the results with the geometric cross section.

10.5 Measurements of Neutron Spectra from a Thick Lead Target Bombarded with 0.5 and 1.5 GeV Protons

S. Meigo, H. Takada, S. Chiba, K. Ishibashi*, T. Nakamoto*, N. Matsufuji*,
K. Maehata*, N. Shigyo*, Y. Wakuta*, Y. Watanabe** and M. Numajiri†

In order to validate and improve the nucleon-meson transport codes such as NMTC/JAERI[1] which have been used for neutronics calculations of accelerator driven actinide transmutation systems, we have measured proton induced neutron-production double-differential cross-section (DDX)[2]. In the present study, the neutron spectra from a thick lead target bombarded with 0.5 and 1.5 GeV protons were measured at 6 emission angles between 15° and 150° to investigate the transport of spallation neutrons in a medium. The experiment was performed at the π2 beam line of National Laboratory for High Energy Physics (KEK). The same detectors and electronic circuits as for DDX measurements were employed in the experiment. The spectrum calculation was also carried out by using NMTC/JAERI and the result was compared with the measured one.

In the experiment, a rectangular lead target having a size of 15 cm in length, 15 cm in width and 20 cm in thickness was used. The target was thick enough to stop 0.5 GeV proton completely, while it caused a loss of 0.24 GeV on average for 1.5 GeV protons. The NE-213 scintillators (5" ϕ x 5") with veto counters were used as the neutron detectors. The neutron energy spectra were derived by using the time-of-flight (TOF) and pulse height unfolding methods.

In the TOF method, the detector bias was set at half height of ^{137}Cs Compton edge (0.493 MeVee), which corresponds to the neutron energy of 1.8 MeV. The detection efficiency for the bias was calculated with SCINFUL[3] which included modified deuteron light output[4] and the angular distribution of H(n,n) reaction cross-section[5]. For the neutron above 80 MeV, the efficiency was calculated with the code Cecil[6]. The calculated curve by Cecil was connected to the one obtained by SCINFUL at 80 MeV.

From the calculation result of NMTC/JAERI, it was found that a neutron mostly scattered by the target nuclei more than once. The scattered neutron has some delay in the flight time compared with the one of which neutron comes out the target without scattering. Consequently, the energy spectrum obtained by TOF method is softer than the real one. In

---

* Department of Nuclear Engineering, Kyushu University
** Department of Energy Conversion, Kyushu University
† National Laboratory for High Energy Physics (KEK)

order to estimate this effect quantitatively, we also obtained the neutron energy spectra using the unfolding method. The unfolding was carried out with the code FORIST[7] by the use of the response matrix calculated with SCINFUL from the pulse height distribution of the neutron below 14 MeV. This energy was chosen because saturations were observed in the pulse height signal for neutrons with energies above 14 MeV.

The neutron spectrum obtained by the unfolding method is compared in Fig. 10.5.1 with the one obtained by the TOF method. In the region below 3 MeV, the spectrum obtained by the TOF method is estimated 50 % lower than that obtained by the unfolding. The cause of the difference can be explained by the ambiguity of the efficiency around the bias energy of 1.8 MeV, which is used in the TOF method. In the energy region between 3 and 14 MeV, on the other hand, the spectrum obtained by the unfolding method agree with the result of TOF quite well. These results show that the neutron spectra obtained by the unfolding method are more reliable than the ones obtained by the TOF method below 3 MeV and that the neutron scattering effect was negligibly small above 3 MeV. In consequence, the measured energy spectrum was finally determined by connecting the results of the TOF method with those of the unfolding method at 3 MeV.

In the calculation, the nuclear reaction and particle transport above 20 MeV were simulated with NMTC/JAERI in which nucleon-nucleus elastic cross-sections were modified as mentioned in 10.4. In the nuclear reaction calculation part, the level density parameter derived by Baba[8] was used. For the neutron transport calculation below 20 MeV, MCNP-4A[9] was employed with neutron cross-section library processed from the evaluated nuclear data file JENDL 3.2.

The calculated results are compared with the measured ones in Figs. 10.5.2 and 10.5.3. The calculated spectra are in reasonable agreement with the measured ones at every emission angle, for both incident proton energies although they underestimate the measured data by about 50 % in the energy region of several tens MeV.

References

1) Nakahara Y. and Tsutsui T. : JAERI-M 82-198 (1982).
2) Ishibashi K., et al. : JAERI-M 93-046 p.82 (1993).
3) Dickens J.K. : ORNL-6462 (1988).
4) Meigo S., et al. : JAERI-Review 94-009 p.268 (1994).
5) Arndt R.A., et al. : Phys. Rev., D35, 128 (1987).
6) Cecil R.A., et al. : Nucl. Instrum. Meth., 161 439 (1979).
7) Jonson R.H. and Wehring B.W. : ORNL/RSIC-40 p.33 (1976).

8) Baba H. : Nucl. Phys. A, 159, 625 (1970).
9) Briesmeister J.F., et al. : RSIC/CCC-200 (1991).

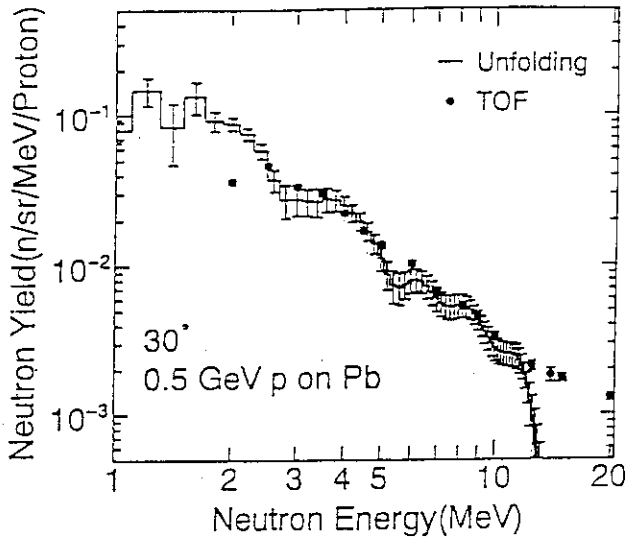

Fig. 10.5.1 Comparison of neutron spectra obtained by TOF and unfolding methods

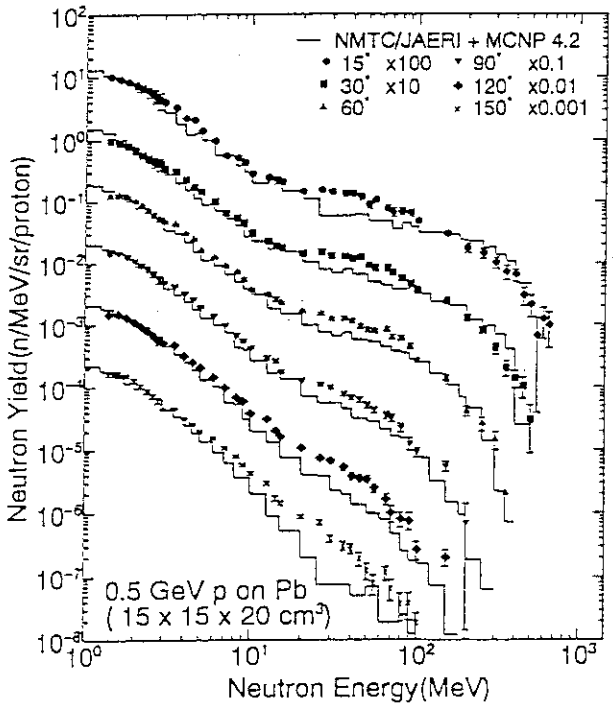

Fig. 10.5.2 Measured and calculated neutron spectra for 0.5 GeV proton

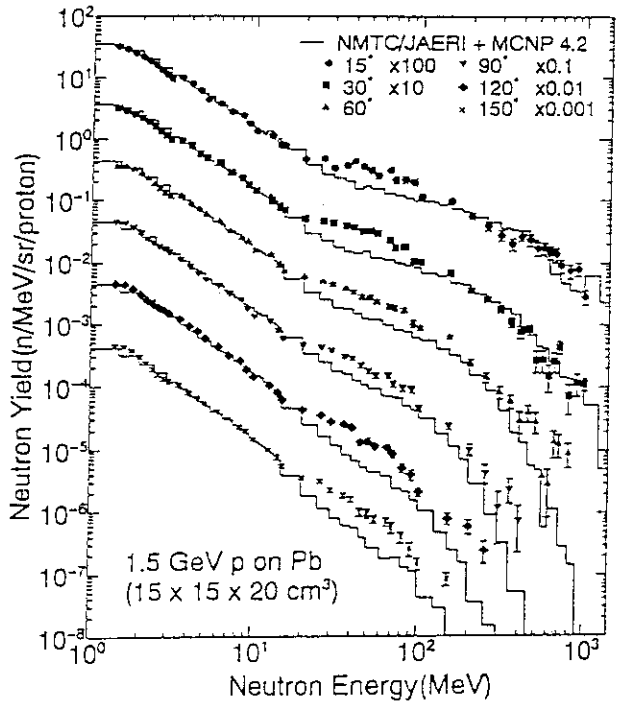

Fig. 10.5.3 Measured and calculated neutron spectra for 1.5 GeV proton

10.6 Measurements of Neutron Spectra from Stopping-Length Targets of C and Au Bombarded with 67-MeV Protons

H. Takada, S. Meigo, H. Nakashima, T. Sasa, S. Tanaka, K. Shin* and S. Ono*

It is important to validate and improve the nucleon meson transport code such as NMTC/JAERI[1] for detailed neutronics design study of an accelerator based transmutation system. In the present study, neutron energy spectra produced in stopping-length targets of C and Au were measured for 67 MeV protons at the HB-1 line of the TIARA at Takasaki establishment of JAERI in order to investigate the accuracy of NMTC/JAERI in the energy region of 20 to 67 MeV.

The experimental arrangement is shown in Fig. 10.6.1. As for the targets, 33-mm-thickness C and 6-mm-thickness Au were employed. Here, the diameter was 30 mm for both targets. Neutrons were measured by the time of flight method with a BC501A scintillator of 12.7 cm in diameter and 12.7 cm in length at emission angles of 0°, 15°, 30°, 45°, 60°, 90° and 120°, respectively. The flight path was 5.0 m for the measurements between 0° and 45°, and 2.5 m for those between 60° and 120°. The n-γ discrimination was made by the zero cross method with a pulse shape discriminator. The contribution of background neutrons caused by the room-scattering was estimated at every angles using a rectangular iron block with the size of 20 x 20 x 40 cm^3. In the experiment, the pulsed protons of 3-ns-width and 320-ns-interval were employed. The number of injected protons was counted with a current integrator connected to the target which was surrounded by a -500V suppressor mesh to repel secondary electrons.

In the calculation, NMTC/JAERI code was employed for nuclear reaction and particle transport calculations above 20 MeV, in which the modified nucleon-nucleus cross sections mentioned in 10.4 was included. The transport of the neutrons with the energies below 20 MeV was calculated by the code MCNP-4A[2]. Moreover, the calculation including the preequilibrium model proposed by Ishibashi et al.[3] were also performed because it has been pointed out[4] that the preequilibrium process should be taken into account in order to improve the accuracy of the code in the energy region below 160 MeV. For convenience, we call

---

* Division of Nuclear Engineering, Kyoto University

hereafter the calculation with the default version as "2-step calculation" and the one including the preequilibrium process as "3-step calculation".

In Figs. 10.6.2 and 10.6.3, the calculated results are compared with the experimental ones for C and Au, respectively. It is observed in both figures that the 2-step calculation significantly overestimates the experimental neutron spectra in the energy region above 20 MeV, which comes from the intranuclear cascade process, by factor of 3 to 10 at the forward angles from 0° to 30°. For the backward neutron emission beyond 90°, the results of 2-step calculation fall off steeply, and so estimate the experimental results too small. On the other hand, the 3-step calculation predicts backward neutron emission in the energy region above 20 MeV fairly well. The increase of the yield of the neutrons with the energies above 20 MeV leads to diminish the excitation energy of a residual nucleus so that the yield of the evaporation neutron decreases. The 3-step calculation agrees well with the experiment in the evaporation part which corresponds to the energy region below 10 MeV. For the energy region above 20 MeV, however, the calculation still overestimates the experiment.

In conclusion, the inclusion of the preequilibrium process improves the accuracy of NMTC/JAERI for the backward neutron emission and the evaporation part in the forward angles. It is necessary to modify the intranuclear cascade model to improve the overestimation by NMTC/JAERI for neutron spectra at the forward angles of 0° to 30°.

In this study, the experiment was carried out as a part of project collaboration research between JAERI and universities.

References

1) Nakahara, Y. and Tsutsui, T.: *JAERI-M* 82-198 (1982), (in Japanese).

2) Briesmeister, J.F., (Ed.): *LA*-12625 (1993).

3) OECD, "*Intermediate Energy Nuclear Data: Models and Codes*", OECD Publications, Paris, (1994).

4) Ishibashi, K., et al.: *Proc. of Int. Conf. on Nucl. Data for Sci. and Technol.*, Gatlinburg, Tennessee, May 9-13, 1994, p571 (1994).

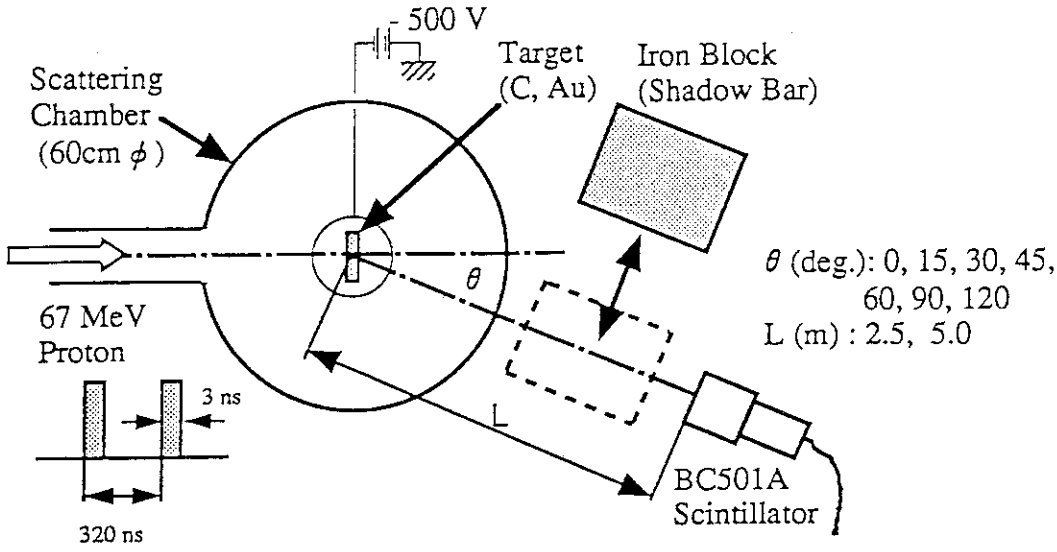

Fig. 10.6.1 Illustration of the experimental arrangement

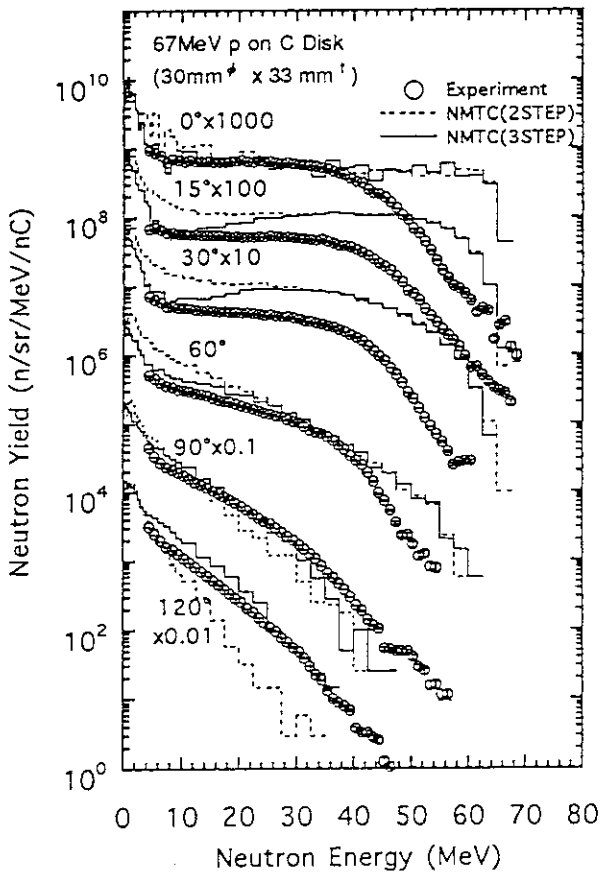

Fig.10.6.2 Neutron energy spectra for 67 MeV proton incidence on stopping-length C target. The dashed and the solid lines stand for the results of 2-step and 3-step calculation with NMTC/JAERI, respectively.

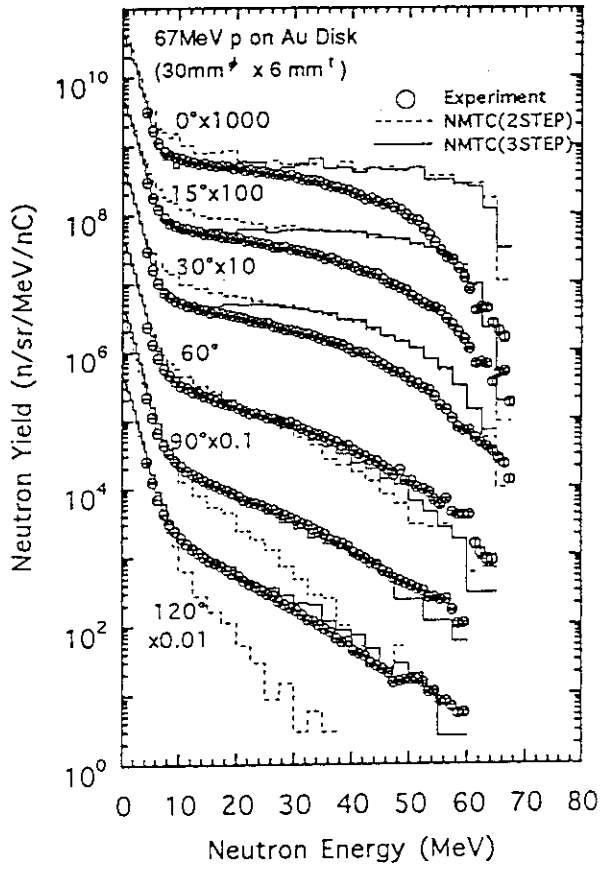

Fig.10.6.3 Neutron spectra for 67 MeV proton incidence on stopping-length Au target. The of lines are the same as for Fig.10.6.2.

11. Accelerator Development

A high intensity proton accelerator with an energy of 1.5GeV and a current of 10mA has been proposed for many basic research and nuclear engineering applications. As a part of the R&D works for the accelerator development, the 2MeV Radio Frequency Quadrupole (RFQ) and high power rf source were installed at the linac building and the beam test in JAERI has started in November, 1994. The maximum RFQ output current was 70mA and estimated transmission rate through the RFQ was about 70%. The duty factor was presently limited to less than 2% for these experiments due to the damage of the rf contact, To solve this problem, modification of the thickness for the rf contact (silver plated beryllium copper alloy) is investigated. The rf heating and the cooling capability for the drift tube linac (DTL) hot test model was examined by feeding the designed rf power of 130kW. The power dissipation experimentally obtained in the each DTL component was well predicted by the design calculation. While the multi-cusp proton ion (H+) source has been stably operated for the RFQ beam test with a beam current of about 120mA, the negative ion (H-) source was designed and partly fabricated. A mock-up experiment for the beam stopper has been made to investigate fabrication method and its thermal performance. The temperature rise and spatial distribution on the test piece were measured with the thermo-viewer and resulted in good agreement with the one-dimensional calculation.

A beam test of the superconducting rf linac FEL was performed to get an electron beam of ten and several amperes of peak current at the exist of the main accelerator at around 15MeV. Measured energy resolution of a pre-accelerated beam is about 3% in FWHM, and that of a fully-accelerated beam about 0.8% or less. Stable and large far-infrared (FIR) signals were observed around 25m by utilizing the Ge(Cu) detector equipped with the Stanford-type fast current amplifier.

At the superconducting booster for the tandem accelerator, acceleration ion beam tests were carried out with the eleven heavy ion beam species ranging from $^{35}Cl^{10+}$ to $^{197}Au^{25+}$ during the-period from April to November in 1994. The beam energy was measured by a solid state detector with Rutherford scattering for Au foil for resonator phase setting and by the beam analyzing magnet for the final output energy. The largest energy gain factor of 3.8 was obtained for $^{127}I^{27+}$. Installation of an experimental apparatus, recoil mass separator, started after the end of the beam test in December, 1994.

The chapters of 11.1-11.5, 11.6 and 11.7 were separately prepared in charge of Accelerator Engineering Laboratory, Free Electron Laser Laboratory and Accelerators Division, respectively.

11.1 A Progress in the High Intensity Proton Linear Accelerator Development

M. Mizumoto, S. Tanaka, Y. Suzuki, K. Hasegawa, H. Oguri, N. Ito, J. Kusano,
Y. Okumura, H. Murata*, Y. Touchi*, H. Ino**, H. Kitamura*** and M. Kawai****

High Intensity Proton Accelerator has been studied for many applications from basic researches to nuclear engineering. Proposed research areas based on the 1GeV-class proton accelerator are shown in Fig. 11.1. including OMEGA•Nuclear Energy Technology, Neutron Irradiation, Neutron Physics (Nuclear Data Measurement), Cold•Thermal Neutron Application (Intense Neutron Source), Meson•Muon Physics, Spallation Radio Isotope (RI) Beam Application and Medium Energy Experiment. The proton accelerator proposal was originated for various engineering tests for accelerator-based nuclear waste transmutation as a part of the OMEGA Project (Options Making Extra Gains of Actinides and Fission Products)[1]. Though the energy-related research work such as OMEGA is still an important part of the accelerator proposal, the emphases have been extended toward to the more basic side of the researches as indicated in the figure. Accordingly the whole project name was temporarily called the Proton Engineering Center and, then now is changed (still tentative) to the Neutron Science Research Center. The study groups for proposed six user facilities were set up voluntarily for each research area in addition to the accelerator development group. The accelerator development group includes accelerator-related experts for radiation shielding, radiation safety and beam diagnostics technologies. The first workshop (Proton Engineering Center Workshop) was held at the Tokai Research Establishment in February 7-8, 1995 with more than 200 participants from various research fields including accelerator experts and nuclear physics and material science user groups from inside-JAERI, universities, governmental institutes and also industries.

For such accelerator-related various applications, the proposed high intensity proton linear accelerator (ETA: Engineering Test Accelerator) is the linear accelerator with an energy of 1.5GeV and an average current of 10mA. The main characteristics of this accelerator is to accelerate the very high intensity beam current. In the conceptual and detailed design of the system, much attention has be paid in order to maintain the beam spill

* Sumitomo Heavy Industries Ltd.
** Mitsubishi Heavy Industries Ltd.
*** Mitsubishi Electric Corporation
**** Toshiba Corporation

as small as possible. As the research and development (R&D) work for the accelerator components, the low energy portion of the accelerator structures have been studied since 1991 because the beam quality is mainly determined at the low energy part. For the high intensity accelerator, it is of particular importance to maintain the good beam quality (low emittance; small beam size and divergence) to avoid the damage and activation of the accelerator structures.

Electromagnetic properties and heat removal problems are also important issues for the structural and mechanical design, because accelerator is required for high peak power and high duty (repetition rate x pulse width) operation. The full mock-up test structure of RFQ and hot test model of DTL, which are both operated by the full RF power, have been fabricated. The electromagnetic characteristics were measured with the electromagnetic field distribution and electric discharge property, and the thermal characteristics were also measured with temperature distribution, outgas condition and attainable vacuum range. The beam acceleration test with high brightness ion source, RFQ and one unit of RF source was made successfully with the beam current of 70mA (peak) and 5% duty.[2,3,4,5].

The conceptual and optimization studies for the high energy accelerator ETA have been carried out in collaboration with the Los Alamos National Laboratory. The accelerator cavities and RF system for high β structures dominate the accelerator size and construction cost for the ETA..

The design works for the front-end part of the ETA (10MeV, 10mA) has been continued for the next development step. The front-end part will be used for the purpose of the full mock-up test in the low energy portion of the ETA. Other accelerator systems and components in addition to the present R&D items are being studied: control system, beam diagnostics, beam stopper, radiation shielding, utility requirement and accelerator building.

References

1) Kaneko Y.:"The Intense Proton Accelerator Program", The 2nd International Symposium on Advanced Nuclear Energy Research – Evolution by Accelerator, Jan. 24–26, 1990, Mito p.25–33

2) Hasegawa K., et al.: "First Beam Test of the JAERI 2MeV RFQ for the BTA", Proc. of the 1994 International Linac Conference, Aug. 21–26, 1994, Tsukuba, Japan, p.113–115

3) Oguri H., "A High Brightness Hydrogen Ion Source for the BTA at JAERI", ibid., p381–383

4) Ito N. et al., "Fabrication and Tests of the DTL Hot Model in the R&D Works for the Basic Technology Accelerator (BTA) in JAERI, ibid., p119–121

5) Touchi Y. et al. "A RF System for the BTA", 4th European Particle Accelerator Conference, June 27–July 1, 1994, London, p1900–1902

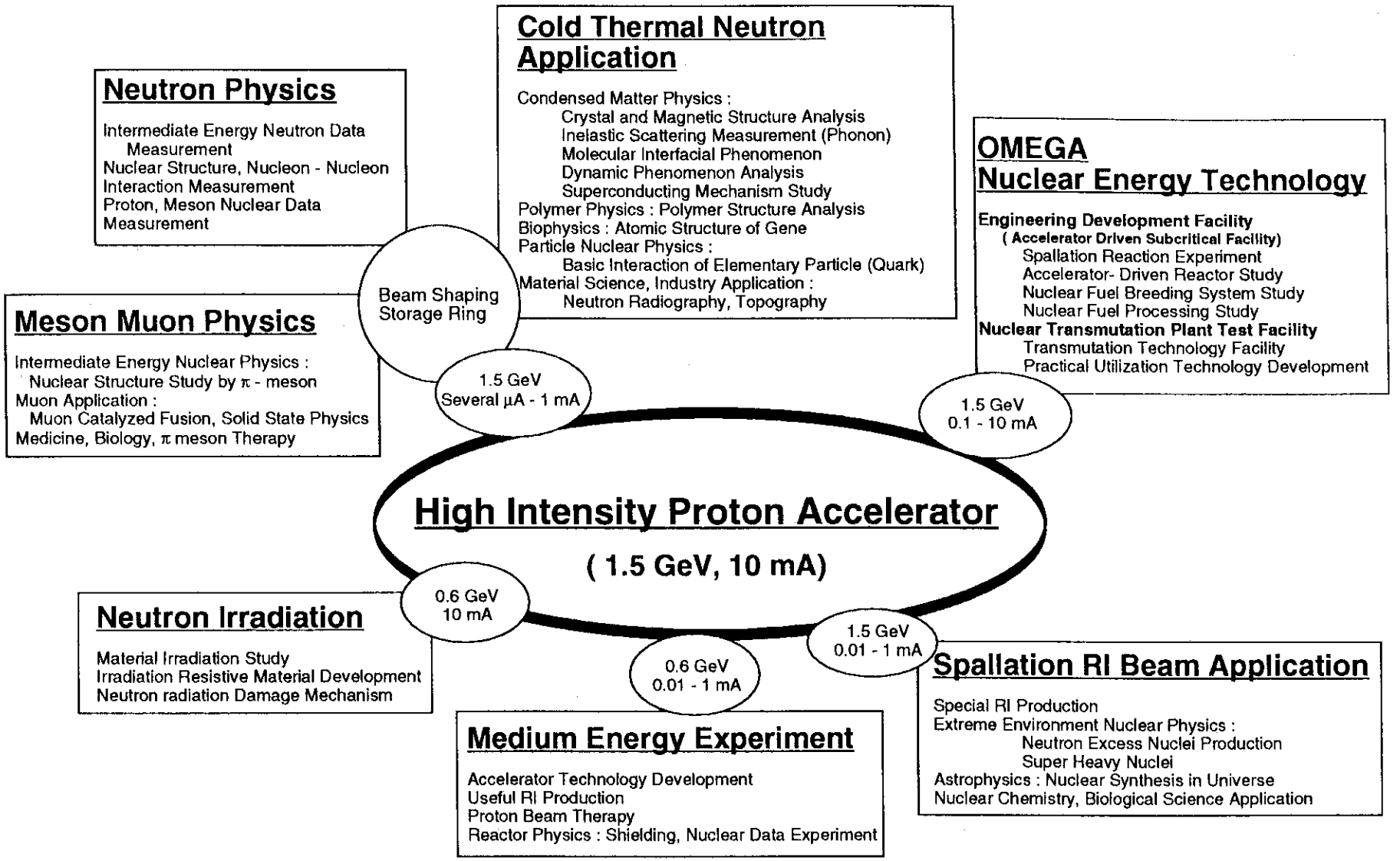

Fig.11.1 Applications of High Intensity Proton Accelerator

11.2 Beam Test of the JAERI 2 MeV Radio Frequency Quadrupole

K. Hasegawa, N. Ito, H. Oguri, J. Kusano, Y. Touchi*, H. Ino** and M. Mizumoto

The JAERI 2 MeV Radio Frequency Quadrupole (RFQ) is one of the main injector components for the Basic Technology Accelerator (BTA). The RFQ is designed to accelerate protons up to 2 MeV with a peak current of 100 mA and a duty factor of 10 %. To study the characteristics of the RFQ, the beam test has been carried out.

The first beam test was conducted for two weeks at the factory of Sumitomo Heavy Industries, Ltd. in February, 1994[1]. To study further properties in JAERI, the accelerator room at the linac building, where the 120 MeV electron linac had been operated for more than 20 years and it was shut down in December, 1993, was reformed for the RFQ beam test. A new cooling water system was equipped for the high power and high duty factor operation. The RFQ, the high power rf source and the control system were shipped from the factory to JAERI in March and April, 1994, and reinstalled. Relative electric field distribution was measured using the perturbation method to confirm the low power tuning results at the factory. After the conditioning with the high power rf and obtaining the permission to the radiation protection rule, the beam test in JAERI has been started since November, 1994.

The layout of the RFQ beam test is illustrated in Fig. 11.2.1. The high power rf source is located in the accelerator room and is connected to the RFQ with a WX-203D coaxial line. The proton beam from the ion source (IS) was focused by the two solenoids (Sol-1, 2) to match to the RFQ acceptance. The input and the output beam currents of the RFQ were measured by the Faraday cups of FC-2 and FC-3, respectively, and the RFQ transmission rate was deduced. The energy of the proton beam from the RFQ was measured by the compact magnetic energy analyzer (MEA) installed in the medium energy beam transport (MEBT) and was confirmed to be 2 MeV.

The maximum RFQ output current of 70 mA was obtained at the ion source extraction current of 155 mA. The ordinary RFQ operation current, however, was 50 – 60 mA at the ion source current of 125 – 135 mA to prevent an overheat to the ion source electrodes. The estimated transmission rate through the RFQ was around 70 %, although the precise measurement is difficult because the net proton fraction in the input beam is not clear due to the mass separation effects of the solenoids. There are several reasons to be considered for lower

---

* Sumitomo Heavy Industries, LTD. ** Mitsubishi Heavy Industries, LTD.

transmission than that of the designed value of 95 %. There could be an alignment error between the ion source, the solenoids, the RFQ and so on. There could be a mismatching between the RFQ acceptance and the ion source emittance. Transmission through the RFQ itself could be lower than the designed one for some reasons. To reveal the reason for the lower transmission rate, re-alignment of the components, proton fraction and emittance measurements of the injected beam are being prepared.

The maximum duty factor of 5 % was achieved at the first beam test[1], but in this beam test, it was limited less than 2 % due to the partial burn out of the rf contact. The silver plated spiral type rf contact, which is made of beryllium copper alloy, was used between the tank and the vane. To improve the heat transfer properties from the contact to the vane and the tank, a thicker silver plated type spiral contact and/or a C-type copper tube contact will be examined.

To achieve the designed beam current, the transmission rate and the duty factor, further beam test and R&D will be continued in 1995.

References

1) Hasegawa K., et al.: "First Beam Test of the JAERI 2 MeV RFQ for the BTA", 1994 Linear Accelerator Conference, Tsukuba, Japan, pp.113-115 (1994)

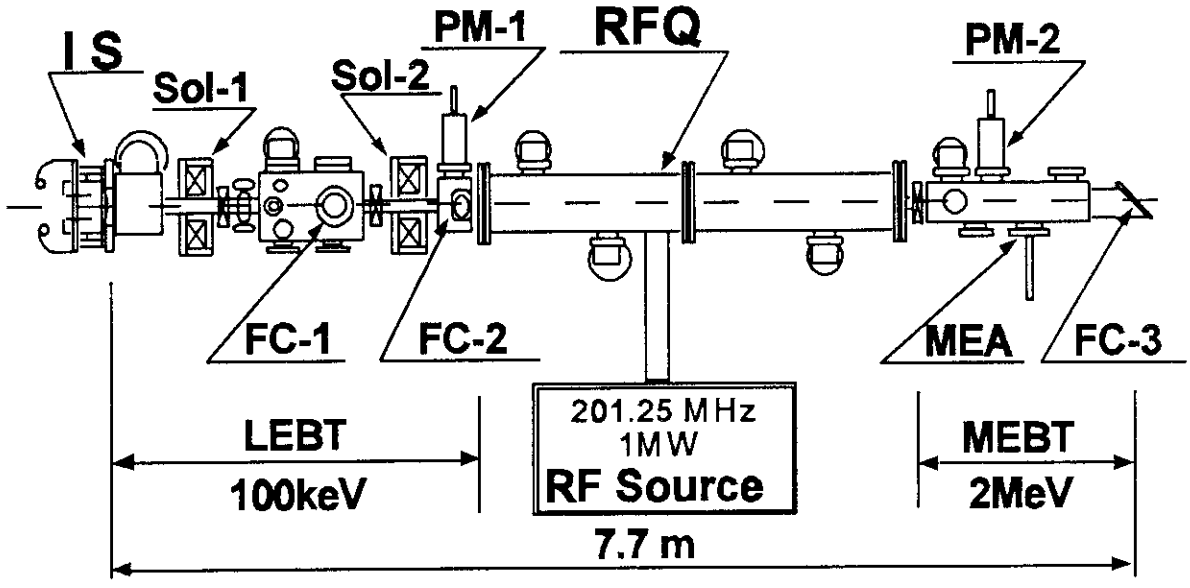

Fig. 11.2.1 Layout of the RFQ beam test

11.3 High Power Test of the Drift Tube Linac Hot Test Model for the BTA

N. Ito, H. Ino*, K. Hasegawa and J. Kusano

The hot test model of a drift tube linac (DTL) was fabricated in the R&D works for the BTA-DTL[1]. The main purposes of the hot test model are (1)development of the quadrupole magnets, (2)examination of the RF characteristics and (3)examination of the cooling capability. The hollow conductor type quadrupole magnets have been developed successfully and the RF characteristics have been examined in the cold tests[2]. As the final test of the hot test model, the high power test has been carried out to examine the RF heating and the cooling capability.

Figure 11.3.1 illustrates the experimental arrangement of the high power test. Quadrupole magnets were installed in the #0 and #1 drift tubes of the hot test model. RF power was fed by an RF amplifier through the coaxial tube. The RF signals from the directional coupler and the pickup loop were monitored to estimate input RF power. The bremsstrahlung X-ray spectra were measured by a HP-Ge detector to estimate the gap voltage. The flow rate and the temperature rise of the cooling water through each path were measured to obtain the value of power dissipation. After the conditioning for about a week, the input RF power up to 154kW was achieved with the duty factor of 12%, which exceeded prescribed power of 130kW to achieve an average field strength of 2MV/m. After that, however, the RF contact between the tank and the end plate was damaged by the RF discharge because of the insufficient contact and it became hard to operate at the duty factor of 12%. Therefore, the measurements were made at the duty factor up to 4%.

Figure 11.3.2 shows the bremsstrahlung X-ray spectra at the input RF power of 128, 139 and 142kW. In these measurements, a collimator and a shield were set up carefully to detect X-rays only from the first gap region. In this figure, both energy and yield of X-rays increase with the input RF power. Maximum energies in the X-ray spectra represent the gap voltage, since electrons are accelerated by the RF field. The gap voltages were estimated at the several conditions of input power and are in good agreement with the calculated values by the SUPERFISH code.

The RF heating and the cooling capability were examined by feeding the prescribed RF power of 130kW. Figure 11.3.3 shows the power dissipation obtained experimentally in the each element of the hot test model compared with the calculated value by the SUPERFISH code. Circles in Fig. 11.3.3 represent the experimental results when only RF power was fed, which are

---

* Mitsubishi Heavy Industries, LTD.

in good agreement with the calculated values. Triangles in Fig. 11.3.3 represent the experimental results when both RF power and excitation current of the quadrupole magnets were fed. The differences between the circles and the triangles indicate the influence of the quadrupole magnet heating. The increases of the power dissipation of the drift tube #0 and #1 were about 50 and 100 W, respectively, which were only a few percent of the quadrupole magnet heating. Most of the heating of the quadrupole magnet, ~7kW, was confirmed to be removed with the quadrupole magnet cooling water. The experimental results satisfy our cooling design.

In this high power test, we could not carry out the experiment under the higher duty operation because of the damage of the RF contact. After the high power test, the damaged RF contact was repaired and modified to make a better contact. In FY-1995, the high power test will be done at the duty factor up to 20% which is required for the BTA-DTL to accelerate proton at the duty factor of 10%.

References

1) Yokobori H., et al.: Reactor Eng. Dep. Annual Report, 215, JAERI-M 92-125 (1992).

2) Ito N., et al.: Proc. of the 1994 International Linac Conference, August 21-26, 1994, Tsukuba, Japan, Takata K. Editor, p113-115.

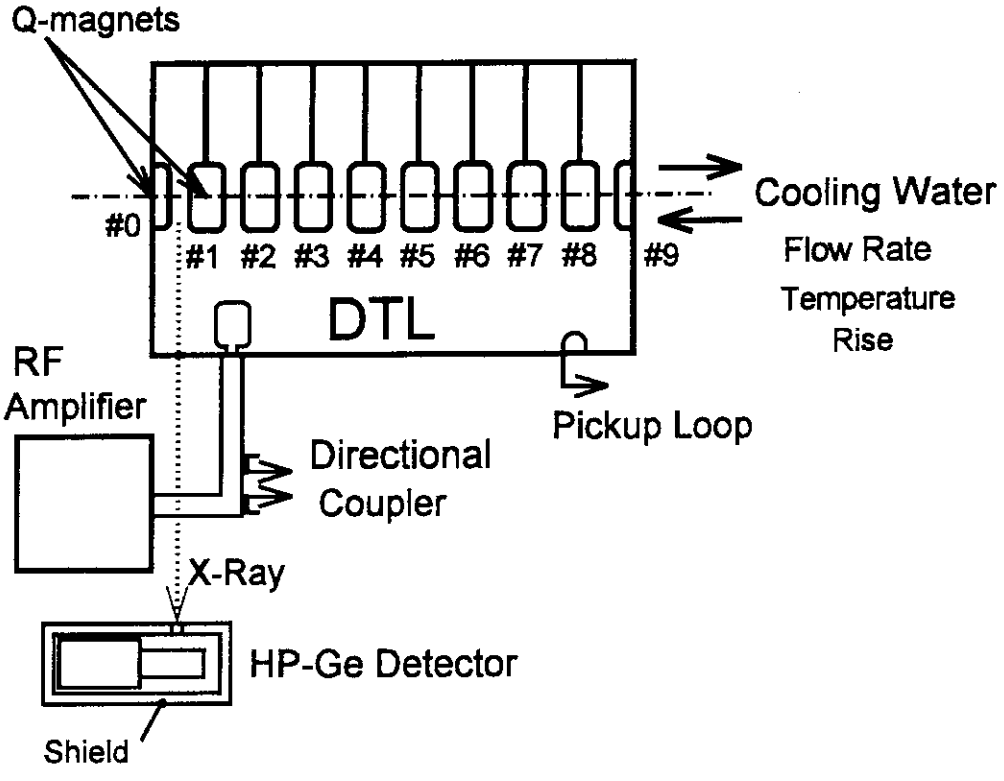

Fig. 11.3.1 Experimental arrangement of the high power test with the DTL hot test model.

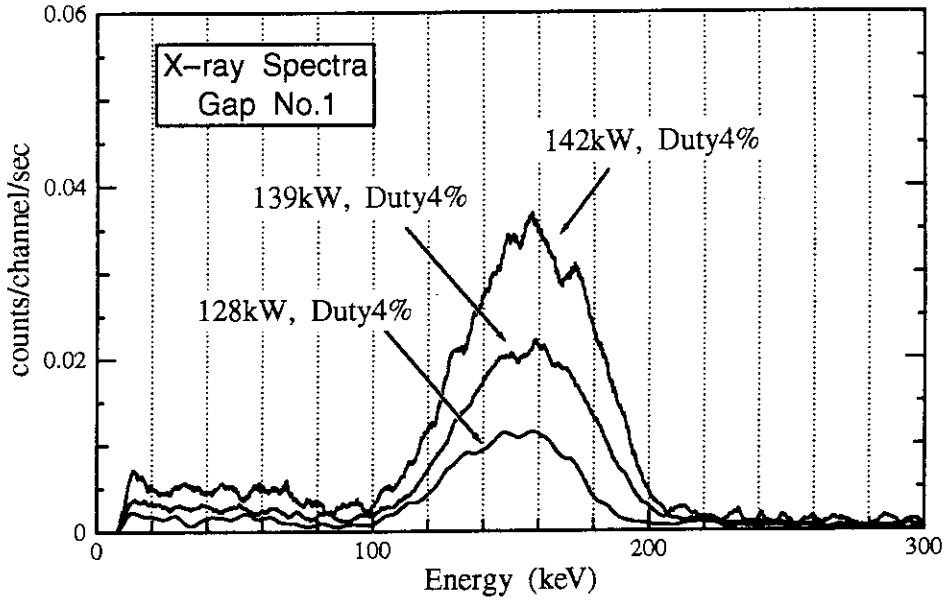

Fig. 11.3.2 Bremsstrahlung X-ray spectra measured with a HP-Ge detector.

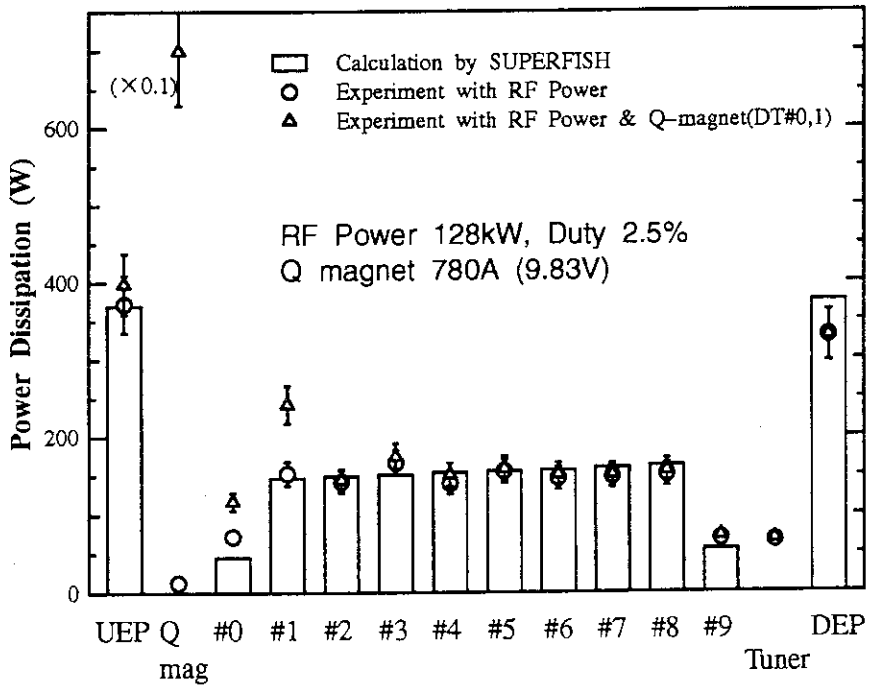

Fig. 11.3.3 Power dissipation of the elements of the DTL hot test model

#0～#9 : drift tube and stem

UEP : upstream end plate

DEP : downstream end plate

11.4 Performance of the High Brightness Ion Source for the BTA (II)

H. Oguri, J. Kusano, Y. Okumura, M. Mizumoto, K. Hasegawa, N. Ito, M. Kawai*, H. Kitamura** , Y. Touchi, H. Ino*** and T. Ono

Construction of a 1.5 GeV/10 mA (100 mA peak current with 10 % duty factor) proton linear accelerator ETA has been proposed for engineering tests of the nuclear waste transmutation and studies of the basic nuclear sciences.

A high brightness multicusp type proton ion source has been developed at JAERI since 1991[1]. In February 1994, the first RFQ beam acceleration test was performed at the test shop of Sumitomo Heavy Industries, Ltd.[2], and the ion source was successfully operated as the RFQ beam injector[3]. Since November 1994, the second RFQ beam test has been carried out at JAERI Tokai[4]. The performance of the ion source during the second beam test is described here.

To increase the extraction beam current from the ion source, the gap length of the extraction electrode was reduced from 18 mm to 14.4 mm in length. Figure 11.4.1 shows the new perveance characteristic of the ion source together with the previous data[3]. Optimum beam current increased from 95 mA to 136 mA at an acceleration voltage of 100 kV. The reduction of the gap length did not affect the stable beam extraction. During the beam test, a Faraday cup was used to monitor the beam current injected into the RFQ. The accurate measurement of the beam current using the Faraday cup was difficult because of a large amount of the secondary electrons emitting from the surface. To create a sufficient potential barrier to repel the secondary electrons, the geometry of the Faraday cup has to be optimized.

The impurities content in the ion beam was measured by the Doppler-shifted spectroscopy method[1]. A typical spectrum is shown in Fig.11.4.2. The peak at the wavelength of 656.3 nm is the Balmer-alpha light emitted from beam plasma particles. The four peaks at longer wavelength are the Doppler-shifted Balmer-alpha light emitted from beam particles. These peaks correspond to the H_1^+, H_2^+, H_3^+ and impurities such as OH^+, H_2O^+ and H_3O^+ from the right side of the spectrum, respectively. The peak height of the impurities became smaller by operating the ion source for long period. Figure 11.4.3 shows that the impurities content decreased with the operation time and reached a few percent after 500 minute operation.

---

* Toshiba Corporation

** Mitsubishi Electric Corporation

*** Mitsubishi Heavy Industries, Ltd.

Negative ion beam is required to inject into the storage ring at the high energy portion of the ETA. For the next stage of the ion source development, a negative hydrogen ion source of the volume production type has been designed. Negative ions are generated in a magnetically filtered multicusp plasma generator. The negative ion production is enhanced by seeding a small amount of cesium in the plasma generator. To obtain a high brightness negative ion beam, negative ions are extracted from multiple apertures and each beamlet is steered by electrostatic lens to merge into a single beamlet.

References

1) Oguri H., et al.: "A High Brightness Hydrogen Ion Source for the BTA at JAERI" , Proceedings of the 1994 International Linac Conference, Tsukuba, Japan (1994) 381
2) Hasegawa K., et al.: "First Beam Test of the JAERI 2MeV RFQ for the BTA", ibid., 113
3) Oguri H., et al.: Reactor Eng. Dep. Annual Report, JAERI-Review 94-009 (1994) 281
4) Hasegawa K., et al.: Reactor Eng. Dep. Annual Report, (April 1, 1994 - March 31, 1995) (1995)

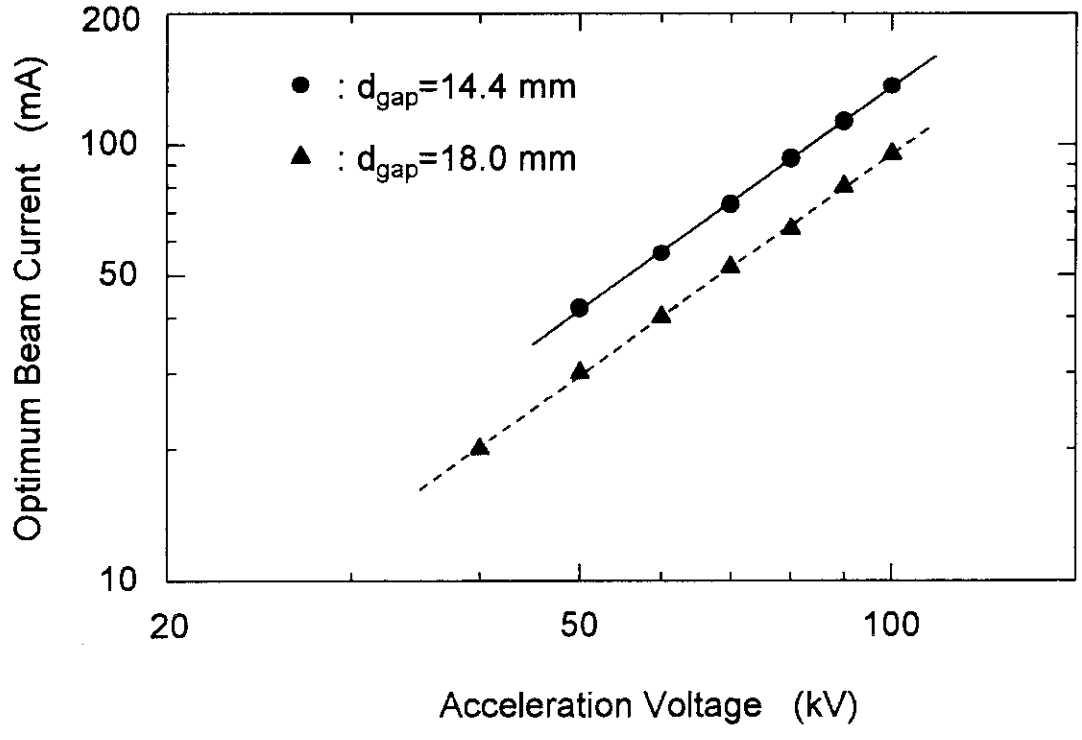

Fig.11.4.1 Perveance characteristic of the proton ion source.

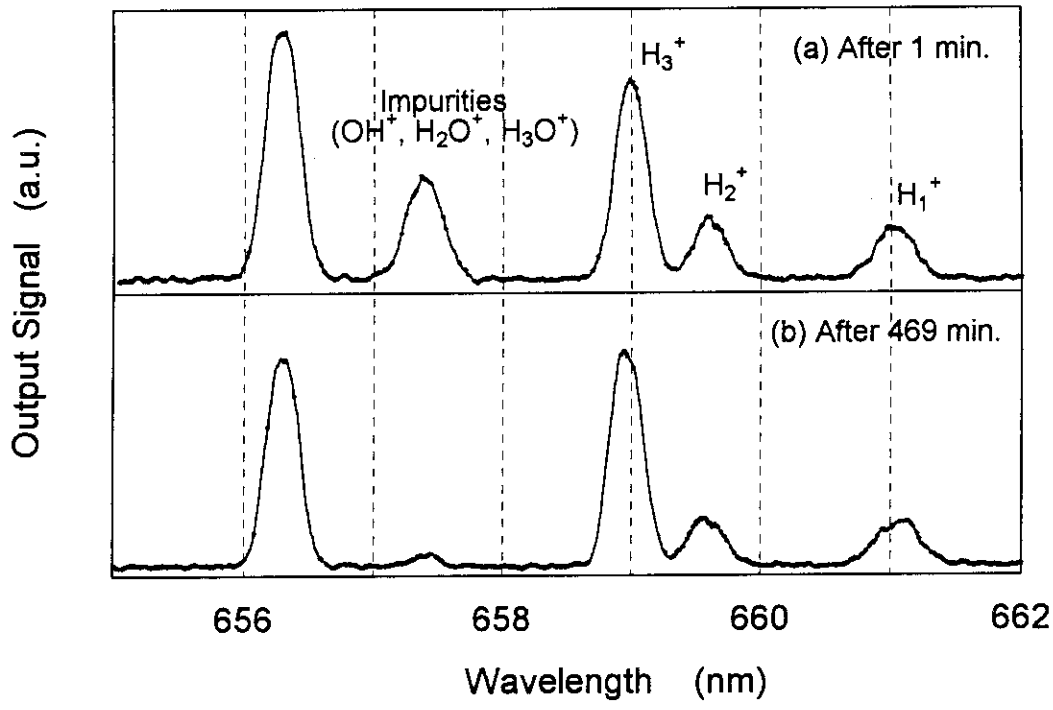

Fig. 11.4.2 Spectra of Balmer-alpha light after (a) 1 minute and (b) 469 minute operation.

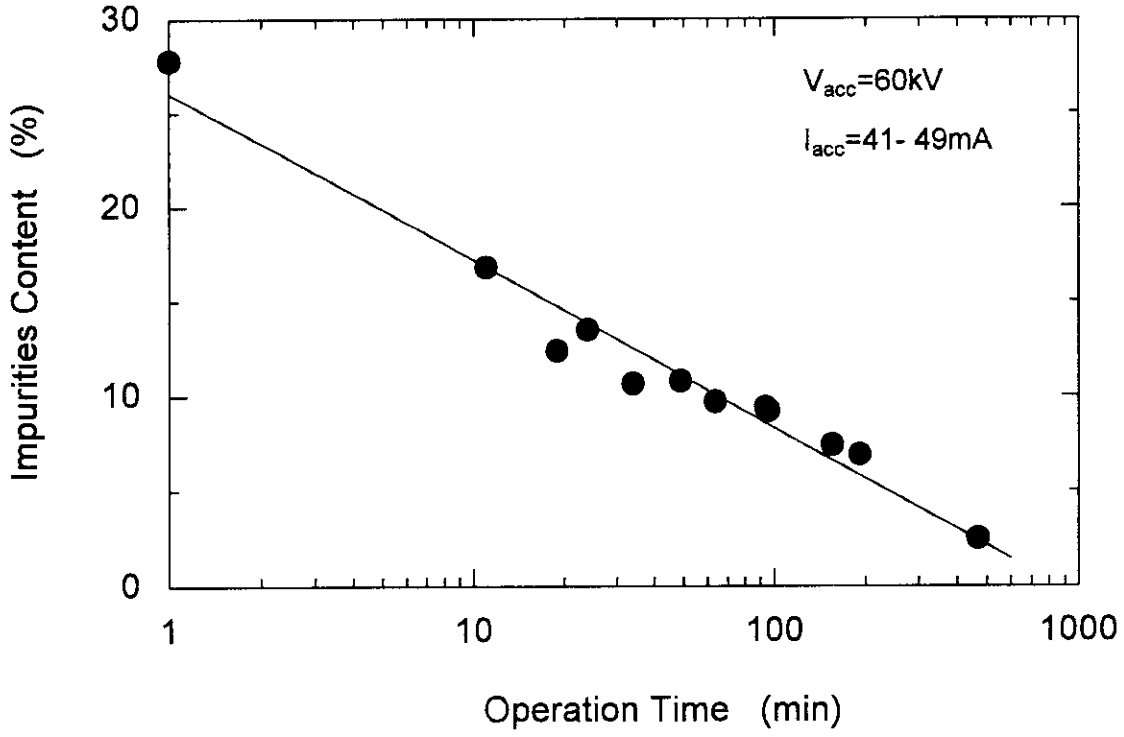

Fig.11.4.3 Reduction rate of the impurities content in the hydrogen beam.

11.5 Preliminary Mock-up Experiments for BTA Beam Stopper Using 2 MeV Proton Beam from RFQ

M. Kawai*, J. Kusano, K. Hasegawa, H. Oguri, N. Ito, Y. Touchi**,
H. Ino***, H. Kitamura****, K. Sato*, M. Mizumoto

The design study of the 10 MeV proton linear accelerator BTA (Basic Technology Accelerator) pulse-operated with a peak current of 100 mA, 100 Hz repetition rate and 1 ms duration is being made[1] together with the R&D study [2, 3] on accelerator components. For its high energy beam transport system, the conceptual design of a beam stopper with multilayered configuration using new material such as CC (carbon-fiber composite) material and functionally gradient material was made[4] to absorb 100 kW heat in average due to proton beam and to reduce parasitic neutron generation. In the present work, the mock-up experiments has been preliminarily made by using 2 MeV proton beam from RFQ[2] in order to investigate beam-stopper fabrication method and its thermal performance.

The mock-up sample is made of 12 pieces of 1.0 cm thick tile of CC and W-Cu alloy layers with 2 x 2 cm^2 area which are arrayed on a copper plate of 4 cm width, 12 cm length and 0.75 cm thickness supported by 1.0 cm thick stainless steel slab. In copper slab, flat water-channel of 0.25 cm x 3.0 cm is made for cooling. Figure 11.5.1 shows the experimental set up. The sample was located at 1.1 m downstream from the RFQ with a beam incident angle of 45 degree inclined. Temperature distribution on the sample was measured with a thermo-image camera and 5 thermocouples pasted on the side of the sample. The proton beam from the RFQ was bombarded with an intensity of 52 mA changing duty factor from 0.25% to 1.25%. This current gives about 40 MW/m^2 thermal loading to the sample in maximum. Cooling water was fed with a flow rate of 3, 4.5 or 6 l/min.

Figure 11.5.2 shows the beam stopper surface temperature at beam bombarding which was measured with the thermo-image camera for various beam-pulse widths, frequencies and water flow rates. The temperature is elevated by about 100 °C within 500 ns and it becomes higher in case of 1 ms pulse. The temperature elevation rate seems to be nearly independent of water flow rate. Off the beam-pulse, it suddenly falls to a quasi-steady state level which is determined by the total input beam power and flow rate, and slowly decreased.

The temperature change on the sample measured with the thermo-image camera forms distributions nearly expressed with Gaussian distribution: at beam bombarding, it is very similar to the beam profile measured with a wire-type beam profile monitor. The temperatures measured with the thermo-image camera during off the beam-pulse generally agree with those by the thermo-couples. One-dimensional calculation using analytic formulas

* Toshiba Corporation
** Sumitomo Heavy Industries, Ltd.
*** Mitsubishi Heavy Industries, Ltd.
**** Mitsubishi Electric Co. Ltd.

of random flow and heat transfer gives a fairy good result which consistent with the measurements, except for the cases of flow rate of 3 l/min.

Higher peek temperature was observed at just beam bombarding. It may become more severe in case of high duty beam operation. The detailed analysis considering time-dependent heat transfer will be made to establish the method of beam stopper design.

References

1) Mizumoto M., et al.: "High Intensity Proton Linear Accelerator for Nuclear Waste Transmutation," Proc. 7th Int. Conf. on Emerging Nuclear Energy System, 20-24 September 1993, Makuhari, p.453 (1993).

2) Hasegawa K., et al.: "First Beam Test of the JAERI 2 MeV RFQ for BTA," Proc. of 1994 International. Linac Conf., August 21-26, 1994, Tsukuba, p. 113 (1994).

3) Oguri, H., et al.: "A High Brightness Hydrogen Ion Source for the BTA at JAERI," ibid., p. 381 (1994).

4) M. Kawai, et al., "Design of 100 kW Proton Beam Stopper for BTA at JAERI," Proc. of the 19th Linear Accelerator Meeting in Japan, JAERI-Conf 94-003, p. 301 (1994).

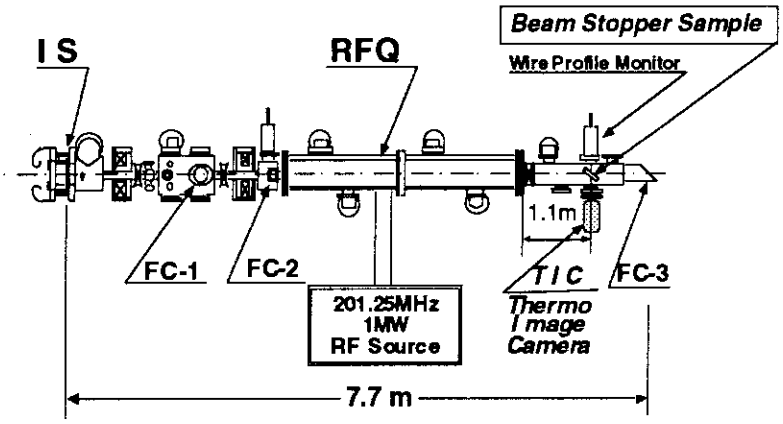

Fig. 11.5.1 Setup of Mock-up Experiments of Beam Stopper

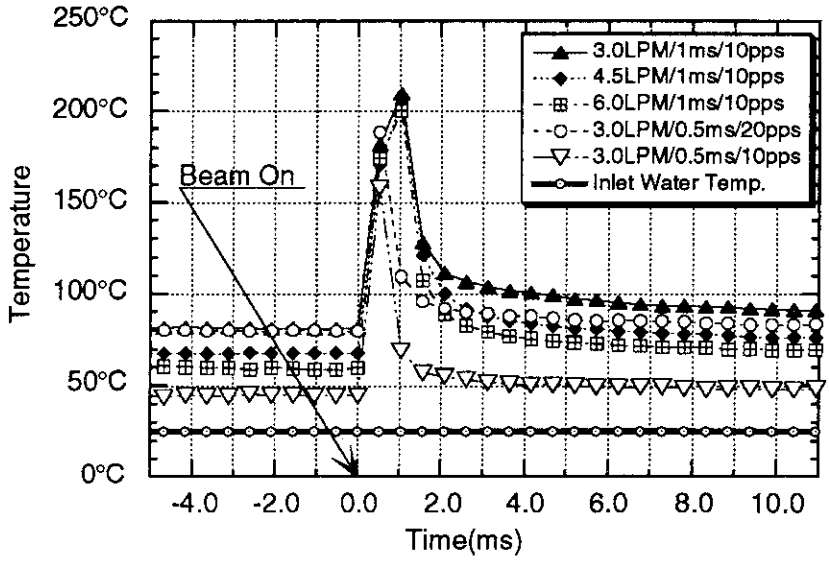

Fig. 11.5.2 Beam Stopper Surface Temperature at Beam Bombarding

11.6 Status of the JAERI Free Electron Laser Facility

E.J.Minehara, M.Sugimoto, M.Sawamura, R.Nagai and N.Kikuzawa

Introduction

As well known, a laser system consists of three major parts, i.e., a laser driver like a flash lamp, a gain medium like a glass or a crystal, and an optical resonator of paired mirrors. Since the invention of the laser in 1950's or 1960's, efficiency and average power level of the conventional lasers have been seriously limited to very low by their huge heat losses in the laser drivers and gain media, and damages in the mirrors. Because a free electron laser(FEL) has a high energy electron beam in alternating magnetic field as the gain media, we could neglect the heat losses in the FEL gain media. Unfortunately, as long as conventional normal conducting accelerators were used to produce the high energy electron beam as the FEL driver, we still have the large heat losses in the accelerator cavity wall of the FEL driver. Therefore, in order to make a highly-efficient, and high average power FEL, we resultantly have to minimize the heat losses in the driver to very low level in comparison with total rf power consumption. This is our motivation why we try to apply the superconducting rf linac accelerator to the JAERI FEL driver.

A developmental program[1,2] of the FEL system for a far-infrared region from the wavelength of 20 μm to 80 μm or longer has been undertaken at Japan Atomic Energy Research Institute(JAERI), Tokai. The purpose of the present JAERI FEL program lies in constructing a very long pulse or quasi-continuous wave(cw) superconducting rf linac electron accelerator, and demonstrating a high-average power FEL in the far-infrared wavelength region. Because the wall losses and required rf power become minimal in the superconducting accelerator cavity, we may realize a quasi-cw and high-current rf linac driver, and hence a high-average power laser. Each major part of the program including future plans has been reported in other papers [3-8] in detail. Here, we report an outlook of the program including the present status and schedule.

Status of the JAERI FEL Facility

(1)Injector

The injector of the JAERI FEL consists of a thermionic cathode electron gun with a pulsing grid, a sub-harmonic buncher(SHB), and a buncher. The characteristics typically

obtained are as follows: an electron beam ranging from 85 to 140mA with 4ns bunch length was extracted from the gun at the accelerating voltage of 210-240kV. The beam was compressed to less than 70 ps at around the time focus point by the bunching system[1] in the injection beam line. Measured normalized emittance after the SHB was scattered around 10 to 20 π mmmrad.

(2) Superconducting RF Linac

The JAERI superconducting rf linac consists of two pre-accelerator modules of the single-cell cavity type and two main modules of the 5-cell cavity type. The resonant frequency of the cavities is 499.8MHz which is exactly the same with the buncher, and the sixth harmonic of SHB in the injector. Design values of the accelerating field strength and Q-value for the cavities are 5MV/m, and $2 \times 10^{+9}$, respectively. Since the beginning of 1993, we have observed very good cryogenic(stand-by loss<3.5W at 4.5K) and accelerating fields' performances(Eacc~7MV/m and Q~$2 \times 10^{+9}$) of four JAERI superconducting accelerator modules.

(3)Cryostat and Refrigerator

We have newly developed a multi-refrigerators system[5] integrated into the superconducting accelerator module cryostat to realize a independent, and highly-efficient system without any liquid coolant. Each accelerator module has own heat shield cooler and recondensor being equipped with refrigerators and compressors, independently. This modular structure of the module makes it possible to remove any single module for repairing, and to add more modules without warming other module.

In order to run the recondensor ecomonically, we introduced a new heat buffering material of ErHoNi magnetic compound instead of Pb, and successfully reduced the required electricity down to half. Cooling capacities of the 4K and 40K/80K refrigerators are about 12W at 4.5K and 40W/120W at 40K/80K, respectively.

(4)RF Power Source

One of the largest merits of a superconducting accelerating cavity is very low power loss, which makes it possible to use all-solid-state RF power amplifiers for all of the cavities[4]. All sets of the power supply have been ready to use at the experimental area since the middle of August 1992. Performance of the rf power supplies has been preliminarily measured to be better than 1% of amplitude and within 1 degree of phase stability at an rf power level of 50kW or more.

(5) Electron Beam Transport System

The energy of electron beams accelerated by the linac usually ranges from about 10 to 20 MeV. A conceptual design of the transport system was done by using the beam optics code TRACE-3D [9]. High current beams have to be fed to the undulator under isochronous and achromatic conditions for efficient lasing of FEL. Because of the large amount of charge density, space charge effects would become serious in a long transport line and a beam waist. Since the code could take into account partially space charge effects, the transport system has been investigated by using the code. In 1993, the optical resonators and beam transport system were already assembled, and installed in the accelerator vault.

(6)Experiments

Before an ending of the 1994 Japanese fiscal year, a beam test of the JAERI super-conducting rf linac FEL was successfully performed to get an electron beam of ten and several amperes of peak current after the main accelerator at around 15 MeV. Measured energy resolution of a pre-accelerated beam is about 3% of FWHM , and that of a fully-accelerated beam about 0.8% or less. Maximum transmission of the beam from the gun to the undulator is now obtained to be at around 100%. Since September 1994, we have tried several number of spontaneous and stimulated far-infrared (FIR) emission measurements. By utilizing Ge(Cu) and other detectors equipped with the Stanford-type fast current amplifier[10], very stable and large, and intermittently very large FIR signals were observed around 25 μm during the measurements.

References

1) M.Sawamura et. al. , Nucl. Instrum. Methods A318 (1992)127.

2) M.Ohkubo et. al. , Nucl. Instrum. Methods A296 (1990)270.

3)R. Kato, et al., in the Proceedings of Sixteenth International Free Electron Laser Conference, 1994, San Francisco, Nucl. Instrum. Methods A358 (1995)ABS 77.

4)M. Sawamura, et al., ibid.

5)N. Kikuzawa, et al., ibid.

6)R. Nagai, et al., ibid.

7)M.Sugimoto, et al., ibid.

8)K.R.Crandall, et al., TRACE 3-D Documentation, LA-1054-MS, UC-32 and UC-28, 1987.

9)K.W.Berrymann, Stanford University, private communication.

11.7 Commissioning of the Superconducting Booster

S. Takeuchi

By the end of March in 1994, we, the booster project group, had completed the superconducting booster for the tandem accelerator, gotten the first beams from it, and made additional improvements in frequency tuning and frequency stability of the resonators.

From April to November in 1994, we carried out acceleration tests with the heavy ion beams of $^{35}Cl^{10+}$, $^{35}Cl^{14+}$, $^{58}Ni^{20+}$, $^{107}Ag^{25+}$, $^{127}I^{27+}$ and $^{197}Au^{25+}$. From December, the booster has been out of use for the installation of a recoil mass separator in the target room. Meanwhile, we have been writing a summary of the development, construction and commissioning of the booster to publish it in a report of JAERI-Tech [1].

The beam acceleration tests were successfully done. The frequencies had been re-tuned well for all the resonators except one. The frequency stability against helium pressure instability had been improved 5 times and the resonators ran well with keeping their rf phases locked even at a big pressure change. The result of the beam acceleration tests is shown in the table 11.7.1. A few resonators were not used because of control circuit failures. The synchronous phases were set to the same value for all the resonators which gave a right phase space distribution in time and energy at the exit of the last accelerating resonator for a good debunching in a calculation

Table 11.7.1 Results of beam acceleration tests with the booster

Ions	Energy(MeV) initial	final	Current(nA) in	out	No. of resonators used	Total acceleration voltages(MV)	Synchronous phase (deg)
$^{35}Cl^{10+}$	164	291	130	38	38	16.6	-30
$^{35}Cl^{10+}$	164	351	130	40	37	24.6	-30
$^{35}Cl^{10+}$	164	351	-	-	37	24.6	-30
$^{35}Cl^{14+}$	164	446	80	16	38	27.6	-25
$^{58}Ni^{20+}$	190	628	80	30	38	28.2	-30
$^{58}Ni^{20+}$	190	606	33	10	37	27.6	-30
$^{58}Ni^{20+}$	190	658	170	100	37	27.7	-18
$^{107}Ag^{25+}$	231	798	45	15	37	27.6	-21
$^{127}I^{27+}$	225	812	20	4	38	28.3	-25
$^{127}I^{27+}$	225	880	100	23	38	30.2	-18
$^{197}Au^{25+}$	340	912	19	3	39	30.7	-22

of beam optics. Resonator phases of the control circuits were successfully set to the synchronous phases after a quick measurement of beam bunch phase shift as a function of resonator phase by using beam bunch phase detecting resonators which were normally conducting and put outside the cryostats and of which signals were processed by vector volt meters and a small work station.

The total acceleration voltages were the sum of the accelerating fields times acceleration length of 0.15 m for all the resonators. The fields of the resonators from no.1 to no.16 were 3 to 5 MV/m, which were lower than expected because of a severe degradation of the niobium resonator surface with niobium-hydride precipitated at about 120 K. The fields of the resonators from no.17 to no.40 were 5 to 6 MV/m, which were as high as expected because of much less degradation. The degradation can be released by precooling the resonators fast at the precipitation temperature arround 120 K. The last two acceleration tests for $^{127}I^{27+}$ and $^{197}Au^{25+}$ were done after a fast precooling at a rate of 1.5 times. The fields were increased by about 0.5 MV/m and the total acceleration voltages arrived at 30 MV which is the design goal for the total acceleration voltage.

The energy of beams during resonator phase setting was measured by a solid state detector with Rutherford scattering from Au foil. The final energy was measured by the beam analysing magnet. The largest energy gain factor of 3.8 was obtained for the case of $^{127}I^{27+}$. With respect to the beam current, the output current from the booster was mostly half as much as that expected from the design. It should be investigated in the next beam acceleration work.

The cryogenic system was shut down twice because of failures of an important heater in one of two cold boxes and a solenoid in one of two helium gas compressors. The refrigerators worked well with some parameter adjustments. We still had some problems with the helium distribution lines; the no. 5 linac unit had not enough liquid helium flow without opening the flow control valve much wider than others, the conductance of all the flow control valves were too large to precisely control the flow of liquid helium to the linac units, and the flow rate under a stable resonator operation is limited to half as much as those designed.

Installation of an experimental apparatus, a recoil mass separator, started just after the end of the beam tests in December, 1994. It should take about six months. The next ion beams from the booster will be provided to the appratus, then.

References

1) "Development and Construction of the JAERI Tandem-Booster", to be published in JAERI-Tech 95-034(written in Japanese)

Publication List
Proceedings/

S. Takeuchi, T. Ishii, M. Shibata and T. Yoshida
Acceleration Testing of JAERI Tandem Superconducting Booster
JAERI-Conf 94-003, Proc. of the 19th Linear Accelerator Meeting in Japan, July 20-22, 1994, Tokai, pp78-80

S. Takeuchi
Status of Beam Test of JAERI Tandem Superconducting Booster
Proc. of the 7th Tandem Accelerators and Their Associated Technology, June 28-29, 1994, Tokyo,
pp88-90

S. Takeuchi, M. Shibata, T. Ishii, H. Ikezoe, T. Yoshida
First Operating Experience with the Superconducting Heavy Ion Tandem-Booster Linac at JAERI
to be published Proc. of the 17th International Linac Conference, Aug.22-26,1994, Tsukuba

C. Kobayashi
Status of the Tandem Accelerator at JAERI Tokai
Proc. of the 7th □andem Accelerators and Their Associated Technology, June 28-29, 1994, Tokyo, pp30-32

Meeting/

Beam Acceleration Tests of JAERI Tandem Superconducting Booster
S. Takeuchi et al.
The 50th Meeting of the Physical Society of Japan, March 28, 1995, Yokohama

12. Facility Operation and Technique Development

Operations of two reactor engineering facilities and three accelerator engineering facilities were carried out as scheduled. They are Fast Critical Assembly (FCA), Heat Transfer and Liquid Flow Facility, Fusion Neutron Source (FNS), Tandem Accelerator and Van de Graaff Accelerator. Major activities of each facility of this fiscal year are summarized briefly below.

(1) The FCA was operated according to various purposes of experiments, and recorded the operation time of 596 hours. As for maintenance activities, besides annual and monthly inspections the wireless telegraphic control apparatus of the crane and transceiver were renewed. The monthly inspection and the physical inventory verification of nuclear fuel materials were carried out without problem by the safeguard authority.

(2) The Heat Transfer and Liquid Flow Facility was operated for various experiments such as visualization tests on flow mixing, two-phase fluid flow test, and ultra high heat flux test. Besides these operations, thermal-hydraulic test facilities, multi-dimensional fluid flow mock-up loop, and cylindrical core test facility were installed as scheduled.

(3) The FNS was operated as scheduled according to various requirements of experiments and recorded the operation time of 653 hours. Exhaust tritium gas was processed in safe by the tritium absorption processor (TAP). A turbo molecular pump at ground side was replaced with a magnetic-float-type one. As for technique developments, a new test target disk with micro-channels was tested for the flow rate.

(4) The Tandem Accelerator was operated as scheduled and recorded the operation time of 4436.9 hours. Beam test of the tandem booster has completed. 2MV Van de Graaff accelerator was operated as scheduled and recorded the operation time of 170 hours. These facilities are expected to be used widely by customers of various fields and to contribute greatly execution of their experiments.

(5) The Very High Temperature Critical Assembly (VHTRC) was not operated under the organization policy of this fiscal year. The annual inspection and fuel management were performed as scheduled the same as last year.

12.1 Operation Report of FCA

K. Satoh, K. Hayasaka, H. Sodeyama, K. Kurosawa, A. Ohno and H. Watanabe

Operation of Fast Critical Assembly (FCA) was carried out in accordance with the experimental schedule on the FCA XVII-1 and XVIII-1 assemblies. Operation of 99 times was carried out in 90 days. No scram was recorded during the operation. The total operation time was 596 hours and the integrated power was 4.6 kWh. A total number of 4,925 criticality operation has been recorded at the end of this fiscal year since the first achievement of criticality on the 29th of April 1967. For the safety regulation of operation, two days were devoted to the monthly inspection and about 10 weeks from June 1994 to the annual inspection. Routine maintenance activities were done during the inspections to provide maximum operation days for the experiments.

As for maintenance activities, since the radio wave law was revised on the 27th of January 1989, the wireless teiegraphic control apparatus of the crane in the reactor room and the transceiver were renewed. The electric power of transmission of the wireless telegraphic contorol apparatus of the crane was 10mW. Frequency band was 429MHz of frequency modulation. Consequently, Stability was more secured of wireless control. As for renewal of the transceiver, due to power up of the receiver, the noise was decline.

As for the physical protection (P/P), the management of the entrance and exit was done restrictively and the system was maintained properly. The constant-voltage constant-frequency power supply (CVCF) package of P/P control systems was renewed due to decrepitude.

In connection with safeguard, IAEA and NSB* carried out monthly inspection under the international treaty. The Physical Inventory Taking (PIT) of the fuels was performed from the 20th to the 24th of June by means of item counting, weighing and non-destructive assay. IAEA and NSB made the Physical Inventory Verification (PIV) from the 27th to the 29th of June. No anomaly was confirmed.

---

* NSB: Nuclear Safety Bureau

12.2 Operation Report of FNS

S. Tanaka, C. Kutsukake, Y. Abe, M. Seki, J. Kusano and H. Watanabe

Operation of the Fusion Neutronics Source(FNS) was carried out for a series of experiments including ones relating to ITER, as scheduled. The total operation time was 653 hours in this fiscal year. A new record on neutron generation of 1.2×10^{18} in 170 hours was marked in the operation for the heavy irradiation experiment using the rotating target tritium activity of which was nominally 29.6 TBq.

As for maintenance activities, the control circuit of the accelerator was inspected every four month. A sliding seal which was kept the vacuum of the rotating target was replaced with a new one. As electric discharge often happened to the high current(20mA) ion source for deterioration of isolation, the isolation bushing was renewed and recovered isolation performance. As 400kV DC power supply had voltage failure, its inner parts were inspected and repaired.

As for renewal activities, regulator system controling acceleration voltage was changed. A turbo molecule pump at ground side was replaced with a magnetic-float-type turbo molecule pump (maintenance free pump) to reduce tritium waste. The replacement of all vacuum pumps of ground side was finished.

Tritium Handling

Two small tritium targets with 370 GBq and two tritium targets with 24TBq were used for experiments at the 80° beam line and for heavy irradiation experiment at the 0° beam line, respectively. The Tritium Adsorption Processor(TAP) system processed a total amount of 2.8 TBq tritium in exhaust gas from the vacuum system of the accelerator. Ten rotating tritium targets and 48 small targets, total amount of 220.9TBq tritium were canned and transferred to the waste processing facility.

Development

A new test target disk with micro-channels was manufactured for the FNS future plan. In the flow test of the test disk, the flow rate was more than 15 l/min with water pressure of 20 kgf/cm^2. In parallel with the development of the target disk, development of a high speed rotating vacuum seal assembly with air bearings and differential pumping was also performed to get the highly cooling performance and maintenance-free.

12.3 Operation Report of Heat Transfer and Fluid Flow Test Facilities

T. Satoh, H. Watanabe, K. Nakajima, Y. Watanabe, M. Kimura and H. Watanabe

In FY-1994, operation and maintenance of Heat Transfer and Fluid Flow Test Facilities were carried out without any troubles as scheduled.

As for the maintenance of test facilities, annual inspections of the pressure vessels, the high pressure gas production system and the steam generator located at both of Large Scale Reflood Test Building and Chemical/Mechanical Engineering Building were carried out. As a result, those pressure vessel have passed the inspection by the Labor Standard Office without any problems.

As for the operation of test facilities, the following six tests were performed.

1)Test of Passive Safety Injection[1)]
2)Visualization Test on Flow mixing in Downcomer
3)Test with Two-Phase Flow Test Loop
4)Test with Ultra High Heat Flux Test Loop
5)Visualization Test on Steam condensation in a Water pool with NRG
6)Test with Multi-Dimensional Fluid Flow Mock-up Loop (Ⅱ)

As for the design and construction of test facilities, the following four facilities were newly constructed.

1)Thermal-hydraulic test facilities for JPSR
2)Plenum and horizontal-pipe loop for two-phase flow
3)Multi-Dimensional fluid flow mock-up loop (Ⅲ)
4)Cylindrical core test facility (Ⅱ)

Reference

1) Araya. F., et al : Study on concept of JAERI Passive Safety Reactor (JPSR), Spring Meeting of the Atomic Energy Society of Japan, D32, 1995

12.4 Tandem and Van de Graaff Accelerators Operation

Tandem accelerator operation group

Tandem Accelerator

The scheduled operation of the tandem accelerator for experiments was performed through the past one year containing two short periods for the scheduled maintenance. The accelerator ran with smoothly throughout the year. The accelerator running time was 4436.9 hours. The following are summary of the operation from April 1, 1994 to March 31, 1995.

1) Time distribution by terminal voltage

>16 MV	37 days	19.7 %	11–12 MV	1 5 days	8.0 %
15–16	78	41.5	10–11	8	4.3
14–15	28	14.9	9–10	3	1.6
13–14	11	5.8	8– 9	2	1.0
12–13	6	3.2	< 8	0	0.0

2) Time distribution by projectile

^{1}H	21 days	^{18}O	11 days	^{54}Fe	7 days
^{2}H	2	^{19}F	1	^{58}Ni	20
^{7}Li	6	^{27}Al	3	^{59}Co	3
^{11}B	6	^{28}Si	12	^{63}Cu	6
^{12}C	16	^{31}P	2	^{79}Br	1
^{13}C	3	^{32}S	12	^{108}Ag	3
^{14}N	0	^{35}Cl	13	^{127}I	13
^{16}O	16	^{52}Cr	3	^{197}Au	8

3) Time distribution by activity

Operation for research	188 days
Atomic and solid state physics	(28 days)
Radiation effects in materials	(22)
Nuclear chemistry	(28)
Nuclear physics	(74)
Fast neutron physics	(8)
Radiation chemistry	(1)
Detector development	(5)
Accelerator test	(22)
Voltage conditioning	1 1days

Operation training		6 days
Scheduled maintenance	(2 tank openings)	87 days
Unexpected repair	(1 tank opening)	5 days
Holidays and vacation		68 days

Beam test of the tandem booster has completed. The test was under going successfully. This item will be reported in other paragraphs.

The construction of the recoil mass spectrometer, special designed by JAERI and fabricated by Smitomo Heavy Industries, Ltd. has completed. The recoil mass spectrometer is main experimental apparatus of the tandem booster for nuclear physics research.

Van de Graaff Accelerator

The 2MV Van de Graaff accelerator was operated for the low energy ion experiments for solid state physics, atomic & molecular physics and material researches with the 170 hour beam time from April 1, 1994 to December 31, 1995. The following shows time distribution of the activities.

Solid state physics	16 days
Atomic & molecular physics	34 days
Material researches	19 days

13. Activities of Research Committee

The Department of Reactor Engineering works as secretariat of several research committees organized by JAERI. Members of committees are invited from senior experts in domestic institutions in the related field. Name and task of each committee are as follows;

Japanese Nuclear Data Committee

The committee is organized to promote evaluation of nuclear data and production of group constants. The committee takes a task of compiling the activities of the International Nuclear Data Committee and the Working Party on International Evaluation Cooperation under OECD/NEA/NSC. A symposium is held annually to discuss research activities on nuclear data.

Research Committee on Reactor Physics

The Committee is organized to discuss research activities on reactor core analysis method and neutronics of new concept reactors.

Atomic and Molecular Data Committee

The committee is organized to promote compilation and evaluation of atomic and molecular data for controlled fusion research. Three working groups are organized under the committee. Workshops on atomic and molecular data are held to discuss current problems relevant to fusion research.

Research Committee on Advanced Reactors

The committee is organized to review and discuss reactor concepts and fuel cycle with emphasis on Pu utilization and passive reactor safety.

Research Committee on Partitioning and Transmutation

The committee is organized to discuss research activities on partitioning and transmutation.

Research Committee on High Intensity Proton Accelerator

The committee was organized to promote research activities on high intensity proton accelerators. The first meeting was held February 1995

Committees on the International Conference on Physics of Reactors

The international conference on physics of reactors is planned to be held September 16-29 1996 at Mito city by the organization of JAERI. The organizing committee, the technical program sub-committee and the planning and management subcommittee were organized in FY 1994.

13.1 Activities of Japanese Nuclear Data Committee

Y. Kikuchi

The Japanese Nuclear Data Committee (JNDC) consists of three subcommittees, five standing groups, steering and counseling conunittees.

The Committee Meeting was held in July 1994 to discuss the nuclear data activity in the previous fiscal year and plans for the fiscal year 1994. Furthermore, discussion was made on several topics including the Gatlinburg Conference, the release and dissemination of JENDL-3.2 and the international activity on nuclear data.

The activities of subcommittees and standing groups are briefly summarized below.

Subcommittee on Nuclear Data

1) High Energy Nuclear Data Evaluation WG

JENDL High Energy Files are being made by this WG. The evaluation is made in two phases. In the phase-I, the data up to 50 MeV will be evaluated for neutron and proton induced reactions. Evaluation work of the phase-I is at the final stage for the neutron-induced reaction data of H, C, Cr, Fe, Ni, Be, N, O, Co, and proton-induced reaction data of C, Fe, Ni and Cu. The energy range will be extended up to a few GeV in the phase-II. Phase-II has already started for Si, Cr, Ni and Cu.

2) Covariance Data Evaluation WG

Methods of covariance matrix evaluation have been investigated, in particular the methods based on experimental data and on uncertainties of parameters used in theoretical calculations. A computer program KALMAN based on the uncertainties of parameters has been developed by Kawano et al. at Kyushu University. The covariance data will be provided for important reaction data of JENDL-3.2

3) Evaluation and Calculation System WG

Investigation on optical model parameters, level density parameters were made. A system for fission spectrum calculation was developed on the basis of two temperature Madland-Nix model. Integrated Nuclear data Evaluation System (INDES) is now being developed.

4) Fission Product Nuclear Data WG

Re-evaluation of nuclear data for about 60 fission products was finished and the results

were stored in JENDL-3.2. Benchmark calculation of the re-evaluated data has been made. It was confirmed that the FP nuclear data in JENDL-3.2 reproduce the integral experimental data within discrepancies of 15%.

5) Activation-Cross-Section Data WG

This WG has done evaluation, compilation and benchmark tests of JENDL Activation Cross Section File. The first version of Activation Cross Section File has been completed.

6) PKA Spectrum WG

A code system of ESPERANT for making PKA/KERMA files was modified. A PKA/KERMA file for 69 nuclei from F to Bi was constructed on the basis of JENDL Fusion File. This file will be used for testing of the data.

7) Charged Particle Nuclear Data WG

This WG is responsible to JENDL (α,n) Reaction File. No activity was made in 1994.

8) Photonuclear Data WG

Evaluation of photonuclear data for 48 nuclei has been made in the energy range below 140 MeV. The first version of JENDL Photonuclear Data file will have data for isotopes of H, C, N, O, Na, Mg, Al, Si, Ca, Ti, V, Cr, Mn, Fe, Co, Ni, Cu, Zn, Zr, Nb, Mo,Cs, Gd, Au, Ta, W, Pb, Bi and U. The compilation of the file will be completed in 1995.

Subcommittee on Reactor Constants

1) Reactor Integral Test WG

Benchmark test of JENDL-3.2 for fast and thermal reactors has been made. The cross section llibrary for use of SRAC, JOINT, MVP and VIM was created and distributed in the domestic user. Comparison between JENDL-3.2 and ENDF/B-VI will be performed in 1995.

2) Shielding Integral Test WG

Integral test of JENDL-3.2 with shielding benchmarks has been made for iron, sodium and oxygen. Comparison of gamma-ray production data of iron between JENDL-3.2 and FENDL-1 was also done.

3) Dosimetry Integral Test WG

Re-evaluation of dosimetry reaction cross section data in JENDL Dosimetry File is in progress.

4) Fusion Neutronics Integral Test WG

Integral test of JENDL-3.2 for fusion applications has been made for Li, Be, C, O, Al, Ti,

Mn, Cr, Fe, Co, Cu, Nb, W, Pb. Comparison between JENDL-3.2 and FENDL-1 was also done.

5) Standard Group Constants WG

No activities in the last year.

Subcommitte on Nuclear Fuel Cycle

The subcommittee on nuclear fuel cycle consists of two WGs. Generation of an ORIGEN-2/JNDC library based on JENDL-3.2 is in progress as a joint effort of the two WGs. Other activities are as follows:

1) Decay Heat Evaluation WG

Energy spectrum of the β-ray component of decay heat has been studied on the basis of Gross Theory of β-decay. Recent improvement of the theory was fully adopted and the calculated results agreed fairly well with the experiments in literatures.

2) WG on Evaluation of Nuclide Generation and Depletion

Experimental data on nuclide inventories in spent fuels were collected and compiled. The results were stored in SFCOMPO data management system, which had been developed for the present purpose.

Standing Groups

1) CINDA Group

Papers on neutron induced reaction data published in Japanese journals and reports are surveyed. The 104 entries were sent to the NEA Data Bank in the last one year.

2) ENSDF Group

The evaluation of nuclear structure data is performed for nuclei with mass numbers from 118 to 129. Re-evaluation of data for A=120 and 124 is in progress.

3) Group on Atomic, Molecular and Nuclear Data for Medical Use

Survey work has been done for the radiopharmaceutical data needed in the field of nuclear medicine.

4) JENDL Compilation Group

Compilation of JENDL-3.2 has been completed. Pointwise cross section files were made at 0 K and 300 K.

5) Editorial Group of "Nuclar Data News"

Three issues of "Nuclear Data News" which is a periodic informal journal in Japanese were published in a year.

13.2 Activities of the Research Committee on Reactor Physics

H. Yoshida, K. Tsuchihashi, H. Maekawa and S. Tanaka

The committee reviews research work related to reactor physics in Japan and supports the activities of Nuclear Science Committee (NSC) of OECD/NEA. It conducts the following three sub-committees. The sub-committee on reactor system discusses topics both of theory and experiments of fission reactors. The activities of sub-committee on fusion reactor involve neutronics and diagnostics of fusion reactors. The scope of sub-committee on shielding is mainly radiation shielding and protection of fission reactors and accelerators.

During the FY1994, the 64th meeting of Research Committee on Reactor Physics (RCRP) was held in June 1994. In the meeting, the following subjects under the topics of transmutation were discussed: 1) the research and development programs for transmutation in the world, 2) the concepts and characteristics of transmutation systems and 3) the present situation of integral experiments necessary to the transmutation system study. The meeting was also devoted to the distribution of the information discussed at the 5th meeting of NEA NSC held at OECD Head quarters, Paris FRANCE, May 25-27th, 1994. There were the status reports of two working parties on physics of plutonium recycling and on international evaluation cooperation of nuclear data. Brief summary was introduced on the specialists' meeting on Shielding Aspects of Accelerators, Targets and Irradiation Facilities which was held in Arlington, USA, April 24-28th, 1994.

The 40th meeting of Sub-committee on Reactor System was held in July 1993. Under the topic of physics issues of Pu, the 2nd meeting of the NEA/NSC Working Party on Physics of Plutonium Recycling (WPPR), the status of higher Pu nuclear data and core calculation methods for MOX fuel loaded LWRs, and the measurements and analyses of JUPITER and FCA experiments were presented. As the third issue in a series of introductions of reactor core design and core management software for commercial reactors, the system of Toshiba Corp. was introduced. The recent development was focused on an assembly analysis code TGBLA, a core neutronics-thermohydraulics code LOGOS and an expert system for core management CORES. The 41st meeting was held in March 1994. General features of DCA (Deuterium Critical Assembly) experiments and developed computer codes for ATR were presented together with the results of analysis of post-irradiated experiments in the Fugen reactor. As the fourth issue in a series of reactor core design and core management software for commercial reactors, the system of Toden Software was introduced. This system includes an assembly code CASMO, a 3-dimensional core neutronics-thermohydraulics coupled code SIMULATE, and core design support tools SIMLOAD, X-image and FINELOAD. Furthermore, the multiple reciprocity boundary element method to solve the neutron diffusion

equation was presented and the 3rd meeting of NEA/NSC WPPR were reported.

The Sub-committee on Fusion Reactor held the 42nd meeting in November 1994. The present status of ITER/EDA R&D on shielding experiments and related neutronics issues were presented. The results for the shielding experiments on SS316/Water bulk assembly were presented. It was pointed out that the reduction of background neutron at the rear side of assembly was essential to validate the experimental data in deep position in the assembly. Reports on 3rd International Symposium on Fusion Nuclear Technology held at UCLA (USA), IAEA/FENDL-AGM at Garching (Germany), and IAEA Specialists' Meeting on Activation Cross Section Measurement Technique at St. Petersburg (Russia) were given. Results for recent studies on data tests of JENDL-3.2 and FENDL-1 were presented. The 43rd meeting was held in March 1995 during the annual meeting of the Atomic Energy Society of Japan. Reports were given on the ITER/EDA T-218 Task Review Meeting and Technical meeting on IEA collaboration, held at Frascati (Italy). The ITER task sharing and working plan for '95 and '96 were discussed. The subcommittee discussed the procedure in response to the four working items identified in IEA collaboration. Continuous efforts on the FENDL/JENDL benchmark test were presented in the course of data validation for the IAEA-FENDL activity.

The 36th meeting of the Sub-committee on Shielding was held in July 1994. In the meeting, presented was the radiation shielding design of High Temperature Engineering Test Reactor (HTTR) which is under construction on the site of JAERI Oarai. Since no water is available as a shielding material in the core of HTTR, sophisticated shielding calculations are needed. The Monte Carlo calculations with MCNP code were made for the check of calculation accuracy of ANISN and DOT3.5 for neutron streaming. For a follow-up of the specialists' meeting on Shielding Aspects of Accelerators, Targets and Irradiation Facilities, the meetings of the working group were held to investigate shielding benchmark calculations and evaluation of attenuation length.

13.3 Activities of Atomic and Molecular Data Research Committee

T. Shirai

The Atomic and Molecular (A&M) Data Research Committee is organized to promote activities on A&M data for the research and development of controlled thermonuclear fusion. The committee consists of members from JAERI, universities and other research institutions. Three working groups concerning particle-material interaction, atomic collision and atomic structure are organized under the Research Committee.

In collaboration with the A&M Data Research Committee, compilation and evaluation work is continued for making the 4th edition of Japanese Evaluated Atomic and Molecular Data Library (JEAMDL-4) as a five-year project since 1992. The activities of these three working groups are briefly summarized below.

Particle-material interactions relevant to the particle-recycling in the plasma edge have been surveyed and reviewed for the carbon and high-Z materials. Domestic literatures published during the last year were surveyed to collect numerical data of particle-material interaction data.

Analytical least squares fits have been made to the recommended cross sections for ionization, charge production, electron loss, electron stripping, and electron detachment in collisions of H, H_2, He and Li atoms and ions with atoms and molecules as is presented in 1.18 of this report. A similar work is now in progress for dissociation and particle rearrangement collisions. In parallel, data compilation have been continued for recent experimental data on these collision processes in order to compare with the recommended data and to examine the validity of the analytical formulas used for extrapolation. A workshop was held on atomic and molecular processes and related data for gas divertors.

The updated version has been made of critically evaluated spectroscopic data on Ti through Cu, Kr and Mo, of particular interest to the fusion community. It will be submitted for publication in the J. Phys. Chem. Ref. Data. The next compilation is now undertaken for gallium which might be used as liquid divertor.

13.4 Activities of the Research Committee on Advanced Reactors

T. Tone, T. Osugi and T. Iwamura

The Research Committee on Advanced Reactors (RCAR) reviews and discusses broadly reactor concepts and fuel cycle with emphasis on Pu utilization and passive reactor safety. The RCAR and its three subcommittees comprise members from Japan Atomic Energy Research Institute (JAERI), universities, Power Reactor and Nuclear Fuel Development Corporation (PNC), and industries including utilities and reactor manufacturers.

The RCAR meeting is scheduled to be held once a year. At the meeting in March 1995, the RCAR reviewed activities of three subcommittees during the FY1994.

1. Subcommittee on Pu Utilization Reactors

Two meetings were held in this fiscal year. The third meeting of the subcommittee was held in June 1994. The topic discussed first was Pu cycle in fast reactors studied by the Power Reactor and Nuclear Fuel Development Corporation. To demonstrate effectiveness and flexibility of Pu and Minor Actinide utilization in fast reactors, three cores were presented and discussed; safety enhanced core (MOX and Nitride), Pu burning core (high Pu enrichment core), and Np cycle core. The second topic presented was concerning Pu utilization in the Advanced Thermal Reactor. The detailed design concept of the Demonstration ATR was also presented. In the third topic, the pyrochemical reprocessing for metal fuel based on the IFR process and the activities in the Central Research Institutes of Electric Power Industry were presented. The pyrochemical reprocessing for MOX fuel in Russia was introduced in the final topic.

The forth meeting of the subcommittee was held in December 1994. The current activities in JAERI for self-completed fuel cycle and once-through type Pu burner LWRs were reported. JAERI's activities for high level waste treatments were also presented, and newly developping ceramic was introduced as a promising candidate for solidification of high level wastes. The last topic of this meeting was concerning the safeguards system relating to Pu usage. It was pointed out that new safeguards technology or system would be required to meet the situation in wide-spread Pu utilization.

2. Subcommittee on Research and Development of Passive Safety Reactor

In this fiscal year, two meetings were held.In the third meeting in July 1994, concepts of the

system-integrated PWR (SPWR) and the advanced marine reactor (MRX) were presented. Active discussions were exchanged especially about the differences between the SPWR design and the loop-type passive safety reactor JPSR (JAERI Passive Safety Reactor) design which was presented in the previous fiscal year. The results and planning of thermal-hydraulic experimental activities concerning passive safety reactors were also explained.

In the fourth meeting in December 1994, the status of conceptual design of an integral-type test reactor was presented. The test reactor is designed to simulate the basic features of SPWR and MRX. However, it was clarified that there exists many problems to fulfil the prototype functions for these two reactors. The design of test reactor will be reviewed in FY 1995. The status of JAERI research activities concerning reactor engineering were explained. The presented research items were the development of advanced instrumentation and control systems, heat transfer and fluid flow experiments, and the development of reactor physics code and Intelligent Reactor Design System (IRDS). The major results of the ROSA-AP600 program were also presented.

It was agreed that the type of passive safety test reactor should not be fixed at present and opinions of other organizations such as industries and utilities should be considered to proceed to the test reactor project in JAERI.

3. Subcommittee on Improvement of Core Thermal-Hydraulic Analysis Codes

In this fiscal year, one meeting was held in July 1994. The attending organizations already agreed that bench-mark calculations to investigate the capability of various subchannel analysis codes should be performed in this subcommittee. The proposed bench-mark problems are as follows: (1) subchannel mixing between two channels simulating the single-phase mixing experiment by Hori et al. and the two-phase mixing experiment by Sato et al., (2) subchannel mixing among many channels simulating the Ispra 4 X 4 rod bundle experiment, (3) critical heat flux experiment simulating the JAERI 7-rod CHF experiments, (4) droplet entrainment and deposition simulating the low pressure air-water experiment by Cousin et al. and the high pressure steam-water experiment by Keeys et al.

In this fiscal year, the subchannel analysis results of problems (2) and (3) were presented by Mitsubishi Heavy Industries, Nuclear Fuel Corporation, and Toshiba Corporation. The results of problems (1) and (4) were already reported in the previous fiscal year. The reporting procedure of bench-mark calculations was discussed. In addition, the summary of the second international seminar on subchannel analysis held in November 1993 was reported by Prof. Ninokata.

13.5 Activities of the Research Committee on Partitioning and Transmutation

T. Mukaiyama, M. Kubota, T. Takizuka and T. Ogawa

The committee reviews and evaluates the research activities in JAERI related to partitioning and transmutation of long-lived nuclides. R&D of partitioning and transmutation is conducted under the OMEGA program of the Atomic Energy Commission of Japan.

The committee conducts three sub-committees. The sub-committee on partitioning and the sub-committee on transmutation discuss the topics on partitioning of high-level radioactive waste and transmutation of long-lived nuclides, respectively. These committees consist of JAERI staff and specialists relevant to the research fields outside JAERI. The program sub-committee consists of JAERI staff and discusses about how to better proceed and coordinate OMEGA R&D activities which extend across many departments of JAERI.

During the FY 1994, the 6th meeting of the Research Committee on Partitioning and Transmutation was held in January 1995. The outline of R&D activities and the recent attainments were overviewed. In December 1994, the 3rd OECD/NEA international information exchange meeting on partitioning and transmutation was held at Cadarache, France. This meeting is one of the best of this kind of meetings to exchange the recent information and knowledge in the field of partitioning and transmutation. Some details of the meeting were reported on the international, national programs, partitioning and transmutation system evaluation, partitioning technology development, transmutation system concepts, fuel technology, fuel irradiation experiments.

The 4th meeting of the Sub-Committee on Partitioning was held in February 1995. Topics of the meeting were R&D of partitioning, research activities on advanced reprocessing, electro-refining of nitride molten-salt. The overview of the session on partitioning and chemical separation at the 3rd OECD/NEA international information exchange meeting was reported.

The 4th meeting of the Sub-Committee on Transmutation was held in March 1995. The outline of transmutation system studies, nuclear data file compilation activity for OMEGA program and the study on nitride fuel cycle technology were reported and discussed. Dr. G. Ledergerber of Paul Scherrer Institute of Switzerland who was visiting JAERI under its invitation program presented the paper on proton irradiation of actinides as a part of the research on transmutation targets.

13.6 Activities of the Research Committee on High Intensity Proton Accelerator

M.Mizumoto, S.Tanaka, T.Takizuka, H. Terada and Y.Suzuki

The Research Committee on High Intensity Proton Accelerator has been organized to promote research activities for the high intensity proton accelerator. The committee consists of members from universities, national and industrial research institutions and JAERI. The first committee meeting was held on February 22, 1995. The outlines of the proposed research areas and user facilities based on the high intensity proton accelerator were presented to the committee in addition to the R&D results for the some accelerator components. Discussion was made to review the proposal, the scope of the activities and the national and international related activities.

The proposal and activities presented to the committee are briefly summarized as follows;

A high intensity proton accelerator has been proposed for many applications from basic researches to nuclear engineering. The proton accelerator proposal was originated for various engineering tests for accelerator-based nuclear waste transmutation as a part of the OMEGA Project (Options Making Extra Gains of Actinides and Fission Products). Though the energy-related research work is still an important part of the accelerator proposal, the emphases have been extended toward to the more basic side of the researches. Proposed research areas and facilities are OMEGA/Nuclear Energy Technology, Neutron Irradiation, Neutron Physics (Nuclear Data Measurement), Cold/Thermal Neutron Application (Intense Neutron Source), Meson/Muon Physics, Spallation Radio Isotope (RI) Beam Application and Medium Energy Experiment.

The study groups for proposed six user facilities had been set up voluntarily for each research area before the Research Committee was organized. The first workshop on Utilization of High Intensity Proton Accelerator was held at the Tokai Research Establishment in February 7-8, 1995 with more than 200 participants from various research fields including accelerator experts and nuclear physics and material science user groups from inside-JAERI, universities, governmental institutions and also industries.

13.7 Activities of Committees on the International Conference on Physics of Reactors

K. Tsuchihashi (secretariat of PHYSOR96)

The international conference on the Physics of Reactors (PHYSOR96) was named after PHYSOR90 held at Marseille in 1990. That is the second event held abroad in the series of the ANS reactor physics Topical Meetings held every two year. Since the organization of the conference was accepted by JAERI, the organizing committee was established by JAERI in the FY 1994. This committee is chaired by Dr. S. Matsuura: Vice-President of JAERI and members of the committee were invited from seniorstaff in the field of reactor physics of domestic universities and nuclear industries. This committee has the major responsibility for the conference, making the subcommittee member appointments, directing the preparation and presentation of the conference. The first meeting was held October 1994 and the preliminary plan prepared by secretariat for site, calendar, scale, budget, candidates of the international technical committee and of the international advisory committee were approved.

Under the organization committee, the technical program subcommittee chaired by Prof. Nishina Nagoya Univ. was established. This subcommittee works with the international technical program committee, in developing the technical scope and content of the conference. The first meeting was held February 1995 and the scope and preliminary technical topics were approved.

The planning and management subcommittee was also established to support the organizing committee and make the preparation in detail. The first meeting was held March 1995 and the preliminary budget, accommodation plan and schedule for preparation were approved.

The preliminary planning was submitted to National Program Committee of American Nuclear Society (ANS) November 1994 and approved. Major contents are as following;

Title	Breakthrough of Nuclear Energy by Reactor Physics
Sponsors	Atomic Energy Society of Japan (AESJ)
	Reactor Physics Division of AESJ,Reactor Physics Division of ANS
Co-operation	ANS, OECD/NEA, ENS(expected)
Organizer	JAERI
Co-organizer	PNC
Date of Conference	September 16-20, 1996
Location	Mito Plaza Hotel, Mito City Japan

Publication List

1. Nuclear Data, and Atomic and Molecular Data

1) Baba M., Ito N., Matsuyama I., Matsuyama S., Hirakawa N., Chiba S., Fukahori T., Mizumoto M., Hasegawa K. and Meigo S.: "Differential α-Production Cross Sections of Iron and Nickel for 4.3 to 14.1 MeV Neutrons""", J. Nucl. Sci. Technol., 31, 745 (1994).
2) S. Chiba and D.L. Smith: "Impacts of Data Transformations on the Least-Squares Solutions and Their Significance in Data Analysis and Evaluation""", J. Nucl. Sci. Technol., 31, 770 (1994).
3) Chiba S., Maruyama T., Niita K. and Iwamoto A.: "Applicability of the Quantum Molecular Dynamics to Nucleon-Nucleus Collisions", Proc. of Int. Conf. on Nuclear Data for Science and Technology, May 9-13, 1994, Gatlinburg, Tennessee, U.S.A., p.505 (1995)
4) Baba M., Ito N., Matsuyama I., Matsuyama S., Hirakawa N., Chiba S., Fukahori T., Mizumoto M., Hasegawa K. and Meigo S.: "Measurement of Double-Differential (n, α) Cross Sections of Fe, Ni, Cu and ^{50}Cr for 4.5 - 14.1 MeV Neutrons", ibid., p.941 (1995).
5) Fukahori T., Chiba S., Kawai M., Kikuchi Y. and Kishida N.: "Status of Nuclear Data Evaluations for JENDL High Energy File", ibid., p.765 (1995).
6) Watanabe Y., Aoto A., Kashimoto H., Chiba S., Fukahori T., Hasegawa K., Mizumoto M., Meigo S., Sugimoto M., Yamanouti Y., Koori N., Chadwick M.B. and Hodgson P.E.: "Measurement of Double Differential Charged-Particle Emission Cross Sections for Reactions Induced by 26 MeV Protons and FKK Model Analysis", ibid., p.308 (1995).
7) Watanabe Y., Koyama Y., Kashimoto H., Shinohara H., Harada M. and Chiba S.: "Calculation of Double Differential Particle Emission Cross Sections for Nucleon-Induced Reactions on ^{12}C and Carbon Kerma Factors Using a Monte Carlo Method", ibid., p.574 (1995).
8) Kawai M., Nakagawa T., Chiba S., Matsunobu H., Nakajima Y., Sugi T., Watanabe T. and Zukeran A.: "Revision of Fission Product Nuclear Data for JENDL-3.2", ibid., p.727 (1995).
9) Kawai M., Chiba S., Nakagawa T., Nakajima Y., Watanabe T., Zukeran A., Gruppelaar H., Hogenbirk A., Weigmann H., Meister A., Salvatores M., Dieze K., Wright R.Q. and Schenter R.E.: "NEANSC International Evaluation Cooperation SG10 Activities on Inelastic Scattering Cross Sections for Weakly Absorbing Fission Product Nuclides", ibid., p.795 (1995).

10) Vonach H., Chiba S. and Pashchenko A.B.: "Report on the IAEA Coordinated Research Program on Improvements of Measurements, Theoretical Calculations and Evaluations of Neutron Induced Helium Production Cross Sections": ibid., p.925 (1995).

11) Ishibashi K., Nakamoto T., Matsufuji N., Shigyo N., Maehata K., Wakuta Y., Watanabe Y., Takada H., Meigo S., Chiba S., Numajiri M., Nakamura T.: "Measurement of Neutron-Production Double-Differential Cross Sections for Incident Protons of 0.8, 1.5 and 3 GeV", ibid., p.347 (1995)."

12) Kikuchi Y.: "JENDL-3 Revision-2 JENDL-3.2", ibid., p.685 (1995).

13) Nakagawa T. and Kikuchi Y.: "JENDL Special Purpose Files", ibid., p.709 (1995).

14) Salvatores M., Gruppelaar H., Kikuchi Y., Roussin R. and Nordborg C.: "Status of NEANSC Working Party on International Evaluation Cooperation", ibid., p.3 (1995)."

15) Takano H., Akie H. and Kikuchi Y.: "Benchmark Tests of JENDL-3.2 for Thermal and Fast Reactors", ibid., p.809 (1995).

16) Chiba S., Takada H., Fukahori T., Maruyama T., Niita K. and Iwamoto A.: "The Quantum Molecular Dynamics Calculation of Nucleon-Nucleus Reactions", NEA/NSC Specialist Meeting on Intermediate Energy Nuclear Data, May 30 - June 1, 1994 (France), p.137 (1994).

17) Chiba S. and Smith D.L.: "Some Comments on Peelle's Pertinent Puzzle", JAERI-M 94-068, p.5 (1994).

18) Chiba S., Niita K., Maruyama T., Fukahori T., Takada H., and Iwamoto A.: "Analysis of the Nucleon-Nucleus Reactions by the Quantum Molecular Dynamics", Proc. the 1994 Symp. on Nuclear Data, November 17-18, 1994, JAERI-Conf 95-008, p.86 (1995).

19) Konshin V.A.: "Calculations of Nuclear Data for the Reactions of Neutrons and Protons with Heavy Nuclei at Energy from 1 MeV to 2 GeV", ibid., p.29 (1995).

20) Meigo S., Takada H., Chiba S., Nakamoto T., Ishibashi K., Matsufuji N., Maehata K., Shigyo N., Wakuta Y., Watanabe Y., Nakamura T. and Numajiri M.: "Measurements of Neutron Spectra from A Thick Lead Target Bombarded by 0.5 and 1.5 GeV Protons", ibid., p.213 (1995).

21) Nakagawa T., Shibata K., Chiba S. and Nakajima Y.: "Determination of Covariance Matrices for several Cross-section Data in JENDL-3", JAERI-Research 95-043 (1995) (in Japanese).

22) Konshin V.A.: "Consistent Calculations of Fast Neutron Induced Fission, (n,2n) and (n,3n) Cross Sections for 71 Isotopes of Th, Pa, U, Np, Pu, Am, Cm, Bk and Cf", JAERI-Research 95-010 (1995).

23) Tamura T.: "Nuclear Data Sheets for A= 122"", Nucl. Data Sheets, 71, 461 (1994).

24) Fukahori T. and Nakagawa T.: "A Code Guidance System for Integrated Nuclear Data Evaluation System on the Basis of Knowledge Engineering Technology", Proc. Specialists' Meeting on Application of Artificial Intelligence and Robotics to Nuclear Plants, May 30-June 1, 1994 Tokai, p.191(1994).

25) Shibata K. and Maekawa F.: "Gamma-Ray Production Data in JENDL-3.2", Proc. Specialists' Meeting in Measurement, Calculation and Evaluation of Photon Production Data", November 9-11, 1994 Bologna, NEA/NSC/DOC(95)1 p.317 (1995)."

26) Derrien H.: "R-Matrx Analysis of Neutron Effective Total Cross Section, Fission Cross Section and Capture Cross Section of 233U in the Energy Range from Thermal to 150eV", J. Nucl. Sci. Technol, 31, 379 (1994)."

27) Mengoni A., Maino G., Ventura A. and Nakajima Y.: "Algebraic and Geometric Approaches to the Collective Enhancement of Nuclear Level Densities", Proc. Int. Conf. on Perspectives for the Interacting Boson Model, June 13-17, 1994, Padova, Italy, p.421 (1994).

28) Ichihara A., Shirai T., and EichlerJ.: "Radiative Electron Capture in Relativistic Atomic Collisions", Phys. Rev., A49, 1875 (1994).

29) Shirai T., Nakagaki T., Okazaki K., SugarJ. and Wiese W.L.: "Spectral Data and Grotrian Diagrams for Highly Ionized Manganese, Mn VII through Mn XXV", J. Phys. Chem. Ref. Data, 23,179 (1994).

30) Mengoni A. and Shirai T.: "Mean Field for the Vibron Model: Dipole-Moment Function of Diatomic Molecules", Phys. Rev., A50, 863 (1994).

31) Ito R., Tabata T., Shirai T. and Phaneuf R.A.: "Analytic Cross Sections for Collisions of H, H_2, He and Li Atoms and Ions with Atoms and Molecules. II", JAERI-Data/Code 94-005 (1994)

32) Igarashi A., Toshima N. and Shirai T.: "Hyperspherical Coupled-Channel Calculation for Antihydrogen Formation in Antiproton-Positronium Collisions", J. Phys., B27, L497 (1994)

33) Igarashi A. and Shirai T.: "Ionization of Excited Hydrogen Atoms by Collisions with Bare Ions", Phys. Rev., A50, 4945 (1994)."

34) Igarashi A., Toshima N. and Shirai T.: "Muon Transfer and Elastic Scattering in t + d μ Collisions at Low Energies", Phys. Rev., A50, 4951(1994).

35) Ichihara A., Hayakawa S., Sataka M. and Shirai T.: "Cross Sections for Particle-Rearrangement in Ion-Molecule Collisions I. Hydrogen and Helium Species", JAERI-Data/Code 94-015 (1994).

36) Research Committee on Atomic and Molecular Data: "Report of the 1993 Workshop on Particle-Material Interactions for Fusion. March 8～9, 1994, Tokai Japan", JAERI- Conf 94-004 (1994) (in Japanese).

37) Stohlker Th., Geissel H., Irnich H., Kandler T., Kozhuharov C., Mokler P.H., Munzenberg G., Nickel F., Scheidenberger C., Suzuki T., Kucharski M., Warczak A., Rymuza P., Stachura Z., Kriessbach A., Dauvergne D., Dunford B., Eichler J., Ichihara A. and Shirai T.: "L-Subshell Resolved Photon Angular Distribution of Radiative Electron Capture into He-like Uranium", Phys. Rev. Lett., 73, 3520 (1994).

38) Stohlker Th., Kozhuharov C., Mokler P.H., Warczak A., Bosch. F., Geissel H., Moshammer R., Scheidenberger C., EichlerJ., Ichihara A., Shirai T., Stachura Z. and Rymuza P.: "Radiative Electron Capture Studied in Relativistic Heavy-Ion-Atom Collisions", Phys. Rev., A51, 2098 (1995).

39) Eichler J., Ichihara A. and Shirai T.: "Photon Angular Distributions from Radiative Electron Capture in Relativistic Atomic Collisions", Phys. Rev.,A51, 3027 (1995).

40) Maekawa F., Kosako K., Oyama Y.:" Verification of Gamma-Ray Data in JENDL-3. 1 Through Analysis of OKTAVIAN Experiment ", Proc. of Int. Conf. Nuclear Data for Science and Technology, Gatlinburg, USA,, 792-794 (1994)

41) Ikeda Y., et al.:" New Measurements of Activation Cross Section for the $^{63}Cu(n,2n)^{62}Cu$ and $^{65}Cu(n,2n)^{64}Cu$ Reactions at Energy Range for 1 3.3～14.9MeV ", ibid., pp.944-946 (1994)

42) Ikeda Y., et al.:" Measurements of Activation Cross Sections for the $^{187}Re(n,2n)^{186m}Re$ and $^{193}Ir(n,2n)^{92m2}Ir$ Reactions at 14 MeV Energy Region ", ibid., pp.1078-1080 (1994)

43) Kasugai Y., Ikeda Y., et al.:" Activation Cross Section Measurement of Reactions Producing Short-lived Nuclei at Neutroll Driven Induced Radioactivity and Nuclear Heating ", ibid., pp.935-940(1994)

44) Takao Y., Ikeda Y., et al.:" Cross Section Measulement of (n,x, α) Reactions for Al and Si around 14 MeV ", ibid., pp. 929-931 (1994)

45) Takano H., Akie H., Hasegawa A., et al.:"Benchmark Test of JENDL-3.2 for Thermal and Fast Reactors ", Int. Conf. on Nuclear Data for Sci. & Technol., May 9-13, 1994, Gatlinburg, TN, p809 (1994)

2. Theoretical Method and Code Development

1) Y. Nagaya and K. Kobayashi :"Solution of 1-D Multigroup Time-Dependent Diffusion Equations Using the Coupled Reactor Theory", annals of Nuclear Energy, vol. 22, p421 (1995)

2) T. Fujimura : "A Double Finite Element Method with Accurate Reflective Boundary Condition Treatment for Three-Dimensional Transport", Computer Physics Comm., vol.

82, plll (1994)

3) M. Sasaki, M. Nakagawa and T. Mori "An Application Study of Parallel Processing of the Particle Transport Simulation", Computer Assisted Mechanics and Engineering Science, vol. 1, pl77 (1994)
4) B.P. Kochurov : "An Advanced Method of Heterogeneous Reactor Theory", JAERI-Review 94-002 (1994)
5) T. Mori and M. Nakagawa : "MVP/GMVP: General Purpose Monte Carlo Codes for Neutron and Photon Transport Calculations based on Continuous Energy and Multigroup Methods", JAERI-Data/Code 94-007 (1994) (in Japanese)
6) T. Kugo, S. Fujii and M. Nakagawa : "Development of Core Thermal-Hydraulics Module for Intelligent Reactor Design System (IRDS) ", JAERI-Data/Code 94-001 (1994) (in Japanese)
7) M. Nakagawa and M. Akimoto : "Supercomputing in Nuclear Engineering", J. Inform. Proc. Soc. Japan, vol. 36, pl37 (1995) (in Japanese)
8) T. Kugo and M. Nakagawa :"Application to Reactor Design and Analysis " in "Research on Human Interface in Nuclear Power Engineering; The Present Status and Its Future Image ", J. At. Energy Soc. Jpn., vol. 37, p472 (1995) (in Japanese)

3. Reactor Physics Experiment and Analysis

1) Mukaiyama T., Kubota M., Ogawa T. and Wakabayashi T.:"Report on GLOBAL'93", J. At. Energy So. Japan Vol.36. pp325(1994)
2) Mukaiyama T.:"Status of TRU Transmutation Technology", Japan At. Industry Forum FBR Group Mtg., (April 1994)
3) Okajima S., Oigawa H., Andoh M. and Mukaiyama T.:"Doppler Effect Measurement up to 2000°C at FCA", Proc. of Int. Conf. on Nuclear Data for Science and Technology, Gatlinburg, USA, 1009-1011(1994)
4) Mukaiyama T.:"OMEGA Program and Status of Transmutation Study at JAERI", Japan-US Informal Mtg. on IAEA Safeguards (May 1994)
5) Mukaiyama T.:"Present Status of Transmutation Technology", Summer Seminar of Radioactive Waste Management Division of At. Energy Soc. Japan, (July 1994)
6) Mukaiyama T.:"Overview of plutonium usage technology", Strategic Studies on Nuclear Fuel, Inst. for Future Technology, (July 1994)
7) Mukaiyama T.:"Present Status of Transmutation Technology in the world", Summer Seminar of Reactor Physics Division of At. Energy Soc. Japan, (July 1994)

8) Okajima S., Oigawa H. and Mukaiyama T.:"Resonance Interaction Effect between Hot Sample and Cold Core in Analysis of Doppler Effect Measurement", J. Nucl. Sci. Technol. Vol.31,plO97(1994)

9) Mukaiyama T.:"Status of Partitioning and Transmutation R&D at JAERI", 16th JAIF-KAIF Seminar on Nuclear Industry, (October 1994)

10) Sakurai T., Nemoto T. and Iijima S.:"Measurement and Analyses of ^{238}U Capture to ^{239}Pu Fission Rate Ratio at Fast Critical Assembly", Proceedings of the 1994 Symposium on Nuclear data, JAERI-Conf. 95-008 (1995)

11) Mukaiyama T.:"OMEGA Program of JAERI", 3rd Symposium of Tokyo University Nuclear Research Center, (December 1994)

12) Mukaiyama T.:"Importance of Double Strata Fuel Cycle for Minor Actinide Transmutation", 3rd OECD/NEA International Information Exchange Mtg. on Partitining and transmutation of long-lived nuclides, (December 1994)

13) Oigawa H. and Iijima S.:"Experimental Study on Sodium Void Reactivity Worth in Mockup Cores of Metallic-fueled and MOX-fueled Fast Reactors Using FCA", JAERI-Research 95-007

14) Mukaiyama T.:"Status of Transmutaiton R&D", 42nd Mtg. of Nuclear System Association, (February 1995)

15) Mukaiyama T.:"Role of Partitioning and Transmutation as a technology of radioactive waste management", Mtg. on Condition of radioactive waste form Tokyo Institute of Technology, (February 1995)

16) Mukaiyama T.(editor):"Special Articles on "Research and Development of Transmutation of High Level Radioactive Waste", J. of At. Energy Soc. Japan, Vol.37, No.3, pp159(1995)

17) Mukaiyama T.(editor):"Present Status of Transmutaiton Research and Development", Report of At. Energy Soc. Japan(1994)

18) Osugi T., Nemoto T., Kurosawa K. and Sakurai T.:"Study of Activation Foil Technique for "Monju" Power Distribution Measurement (V)", JAERI-memo 07-068(1995)

19) Okajima S., Oigawa H., Andoh M. and Mukaiyama T.:"Experiments of High Temperature Doppler Effect for Fast Reactor in FCA Cores""", Japan-Russia Fast Reactor Specialist Meeting, (March 1995)

20) Mukaiyama T., Takizuka M., Mizumoto M. and Yoshida H.:"Partitioning and transmutation R&D program "OMEGA' and present status of the transmutaion study at JAERI", Proc. Technical Committee Mtg. on Safety and environmental aspects of partitioning and transmutation of actinides and fission products (IAEA-TECDOC-783), pp75(1995)

21) Mukaiyama T., Ogawa T. and Gunji Y.:"Minor actinide burner reactor and influence of

transmutation on fuel cycle facilities", ibid. pp115

22) Akino F., Takeuchi M. and Ono T.: "Measurement of Effective Delayed neutron Fraction of VHTRC-1 Core", J. Nucl. Sci. Technol., 31(8), 861(1994)."

23) Yasuda H., Yamane T. and Sasa T.: "VHTRC Temperature Coefficient Benchmark Problem", JAERI-Data/Code 94-013 (1994).

24) Yasuda H., Yamane T. and Akino F.: "A few Reactor Physics Experiments Related to the HTTR Safety at VHTRC", Proceedings of the Third JAERI Seminar on HTGR Technologies, Nov. 7-8, 1994, Tokai, JAERI-Conf 95-009,105 (1995)

25) H. Akie, H. Takano and K. Kaneko : "Analysis of Critical Experiment BFS-61 by Using the Continuous Energy Monte Carlo Code MVP and the JENDL-3.1 Nuclear Data", Int. Top. Mt. on Advanced Reactors Safety, Apr. 17-21, 1994, Pittsburgh, p544 (1994)

4. Advaneed Reactor Safety Design Studies

1) Iwamura T., Murao Y., Araya F. and Okumura K,: "A Concept and Safety Characteristics of JAERI Passive Safety Reactor (JPSR)"

2) Kunii K, Iwamura T. and Murao Y.: "Thermal Fluid Flow Analysis in Downcomer of JAERI Passive Safety Light Water Reactor (JPSR)", presented at presented at Int. Symp. on Grobal Environment and Nuclear Energy Systems, Susono-shi, Japan (Oct. 26, 1995)

3) Araya F., Iwamura T., Kunii K. and Murao Y.: "Thermal-hydraulic Analysis for Design of JAERI Passive Safety Reactor JPSR", presented at 72st JSME Spring Annual Meeting, Tokyo, Japan (March 29, 1995)

4) H. Akie, T. Muromura, H. Takano, et al. : "A New Fuel Material for Once-Through Weapons Plutonium Burning", Nucl. Technol.,vol. 107, pl82 (1994)

5) T. Muromura, N. Nitani, H. Akie, H. Takano, et al. "Once-Through Type Fuel for Plutonium from Nuclear Warheads and Their Burnup Characteristics", 2-nd Int. Seminar on Transmutation of Long-Lived Radio Active Waste and Conversion of Weapon-Grade Plutonium Based on Proton Accelerator, May 23-27, 1994, Moscow, Part I, pll7 (1995)

6) H. Takano, H. Akie, K. Nakamura, et al. : "A Design Study for Inherent Safety Core, Aseismicity and Heat Transport System in Lead-Cooled Nitride-Fuel Fast Reactor", Int. Top. Mt. on Advanced Reactors Safety, Apr. 17-21, 1994, Pittsburgh, p549 (1994)

5. Fusion Neutronics

1) Maekawa H.:"Shielding Research for Next Fusion Devices", Proc. of 8th Int. Conf. of

Radiation Shielding, Arlington, USA, pp.l5-24 (1994)

2) Oishi K., Ikeda Y.:"Reduction of Dose Rate from Concrete Shield in Fusion Facilities", ibid., pp.1031-1038 (1994)

3) Youssef M.Z., Oyama Y.:"Required Design Margins in Fusion Reactors to Compensate for Nuclear Data Uncertainties-A Global Approach to Define Safety Factors Based on Integral Experiments", Proc. of Int. Conf. Nuclear Data for Science and Technology, Gatlinburg, USA, pp 874-82 (1994)

4) Maekawa H., Kosako K., Oyama Y.:"A Review of Recent Fusion Neutronics Experiments", ibid., pp.866-873(1994)

5) Ikeda Y., Kumar A.:"Direct Nuclear Heating Measurements with a Micro-Calorimeter and KERMA Data Validation", ibid., pp.l93-200 (1994)

6) Kumar A., Ikeda Y.:" On Disagreement Between Measurement and Calculations of D-T Neutron Driven Induced Radioactivity ancl Nlclear Hearting", ibid., pp. 883-895 (1994)

7) Maekawa H., Oyama Y., Abdou M.A.:"A Summary of Benchmark Experiments for Simulation of Fusion Reactors using an Annlllar Blanket with a Line D-T Sorce", Proc. of 2nd Japan-China Symposium, Univ. of Tokyo, pp.235-246 (1994)

8) Oyama Y., Sekiyama K., Makeawa H.:"Spectrum Weighting Function Method for In-Situ Fast Neutron and Gamma-Ray Response Measurements in Fusion Integral Experiments", Proc. of ANS Topical Meeting on Technology of Fusion Energy, New Orleans, USA, Fusion Technol. 26 [3], pp.l09-1104 (1994)

9) Maekawa H., Maekawa F., Oyama Y., Konno C., Ikeda Y., et al.:"Tritium Production-Rate Measurements Techniques Developed at FNS/JAERI ", ibid., pp.1086-1091 (1994)

10) Oyama Y., Maekawa H.: "JAERI-USDOE Collaborative Program on Fusion Blanket Neutronics, " Journal of Japan Atomic Energy Society, 36[7], pp. 611-618 (1994)

11) Noda K., Ohno H., Sugimoto M., Kato Y., Matsuo H., Kikuchi T., Sawai T., Usui T., Oyama Y., Kondo T.:"Present Status of ESNIT Progrclm ", J. Nucl. Mat., 212-125, pp. 1649- 1654 (1994)

12) Verzilov Y., Maekawa F., Oyama Y. ancl Maekawa H.:"A New Method of Extracting Tritium Produced in Neutron-lrradiated Litium-Containing Pellets for Liquid Scintillation Counting ", JAERI-Research 94-042 (1994)

13) Konno C., Maekawa F., Oyama Y., Ikeda Y., Kosako K. and Maekawa H.:"Bulk Shielding Experiments of Large SS316 Assemblies Bombarded by D-T Neutrons Volume I: Experiment ", JAERI-Research 94-043 (1994)

14) Maekawa F., Konno C., Kosako K., Oyama Y., Ikeda Y., and Maekawa H.:"Bulk Shielding Experiments of Large SS316 Assemblies Bombarded by D-T Neltrons Volume II: Analysis",

JAERI-Research 94-044 (1994)

15) Konno C., Maekawa F., Oyama Y., Ikeda Y., Uno Y., Verzilov Y., Wada M., Maekawa H.:"Bulk Shielding Experiment on a large SS316/Water Assembly Bombarded by D-T Neutrons Volume II: Experiment ", JAERI-Research 9-017 (1995)

16) Maekawa F., Konno C., Wada M., Oyama Y., Ikeda Y., Uno Y., Verzilov Y., Maekawa H.:" Bulk Shielding Experiment on a large SS316/Water Assembly Bombarded by D-T Neutrons Volume II: Analysis ", JAERI-Research 95-018 (1995)

6. Radiation Shielding

1) Hasegawa A., Suzuki T., Tanaka S. and Nakashima H.: "Development of BERMUDA : A Radiation Transport Code System", Proc. 8th Lnt. Conf. Radiation Shielding, Arlington, USA, p.539 (1994).

2) Sakamoto Y., Nakashima H., Tanaka S., Nakane Y., et al.: " Shielding Experiments with Quasi-Monoenergetic Neutrons between 15 and 90 MeV at AVF Cyclotron, Facility TIARA", ibid., p.809 (1994).

3) Nakamura T., Uno Y., Nakashima H., Tanaka S., et al.: "Development of p-Li Quasi-Monoenergetic Neutron Field between 20 and 90 MeV for Cross Section and Shielding Experiments", ibid., p.264 (1994).

4) Nakao N., Nakamura T., Nakashima H., Tanaka S., Sakamoto Y., Nakane Y., et al.: "Spectrometry of Several Tens MeV Neutrons Penetrating Shields Using Organic Liquid Scintillator at 90 MeV AVF Cyclotron Facility, TIARA", ibid., p.272 (1994).

5) Harima Y., Hirayama H. and Sakamoto Y.: " Simplified Method of Gamma-Ray Skyshine Calculations", ibid., p.939 (1994).

6) Sakamoto Y., Sato O., Yoshizawa N., Furihata S. and Tanaka S.: "Evaluation of Fluence to Dose Equivalent Conversion Coefficients for High Energy Photons", ibid., p.1188 (1994).

7) Yamaji A. and Sakamoto Y.: "Accuracy of Shielding Design Values of Nuclear Ship MUTSU Based on Radiation Measurements on Board", ibid., p.1286 (1994).

8) Hayashi K., Sasamoto N., Nakashima H., Sakamoto Y., Tanaka S., et al.: "Accelerator Shielding Benchmark Analysis and Future Items to be Solved", Proc. Specialists' Meeting on Shielding Aspects of Accelerators, Targets and Irradiation Facilities, Arlington, USA, OECD Document p.135 (1995).

9) Tanaka S., Nakamura T., et al.: "Shielding Eperiments and Analysis at 90 MV AVF Cyclotron Facility TIARA", ibid., p.195 (1995).

10) Iwai S., Tanaka S., Sakamoto Y., et al.: "Evaluation of Effective Dose Irradiated by High Energy Radiation", ibid., p.305 (1995).

11) Nakashima H., Sakamoto Y., Tanaka S., Hasegawa A., Fukahori T., Nishida T., Sasamoto N., et al.: "Benchmark Problems for Intermediate and High Energy Accelerator Shielding", JAERI-Data/Code 94-012 (1994).

12) Sakamoto Y., Tanaka S., et al.: "Basic Physical Data Needed for Dose Evaluation", Proc. of the Workshop on Dosimetry for Extemal Radiations, Jan. 19-20, 1995, JAERI, Tokai, Japan, p48, JAERI-Data/Code 95-007 (1995).

13) Tanaka S.: "Summary of the Presentations and Proposed Issues", ibid., pl43 (1995).

14) Tanaka S.: "High Intensity Proton Accelerator and Its Application (Proton Engineering Center)", 2bd Specialists' Mt. on High Energy Nuclear Data, Jan. 26-27, 1995, JAERI, Tokai, Japan(1995).

15) Nariyama N., Tanaka S., Nakane Y., Nakashima H., et al.: " Absorbed Dose Measurements and Calculations in Phantoms for 1.5 to 50 keV Photons", Health Physics 68, No.2, 253-260 (1995).

7. Reactor and Nuclear Instrumentation

1) Sakasai K., Ara K., Ito H., Kishimoto M. and Katagiri M.: " Electric and Magnetic Characteristics of a Co-Fe-Si-B Based Amorphous Wire and its Application to a Multivibrator-type Magnetometer at Low Temperature." , Rev. Sci. Inst. Vol.65, No.5 (1994)

2) Yamada M. and Ara K.: "Development of Pt-Mo Alloy Thermocouple for Incore Temperature Measurement in HTGRs.", J. Nucl. Sci. & Technol., Vol.31, No.6 (1994)

3) Ara K., Katagiri M., Wakayama N. and Ogasawara T.: "Development of a Liquid Level Gauge based on Heated Differential Thermocouples", J. SICE, Vol. 33, No.8 , 700-707 (1994) (in Japanese)

4) Yamada M. and Ara K.: "High-themperature Performance Characteristics of Nicrosil/Nisil Thermocouples", J. SICE, Vol. 33, No. 12, 1070-1075 (1994) (in Japanese)

5) Katagiri M. and Ito H.: "Radiation Detector and Their Uses", KEK Proceeding 94-7, 1174 (1994)

8. Reactor Control, Dagnosis and Rabotics

1) Suzuki K.; "Reactor Control by H$^{\infty}$ Control", IEE Japan NE-94-9 pp.l3-22 (1994)

2) Suzuki K., Shimazaki J. and Watanabe K.: "Estimation of Time-varying Reactivity by the H∞ Optimal Linear Filter", NSE, Vol. 199, ppl28-138(1995)
3) Suzudo T. and Shinohara Y.: "Qualitative Analysis of Nonlinear Power Oscillation in NSRR", Ann. Nucl. Energy, Vol.21(5) (1994)
4) idem: "An Analytical Study of nonlinear Reactor Dynamics Based on Bifurcation Theory" with Reference to BWR Power Oscillation, J. Nucl. Sci. Technol. 31(5) (1994)
5) Suzudo T. :Analysis of Reactor Power Oscillation Based on Nonlinear Dynamic Theory, JAERI-Research 94-003 (1994)
6) Nabeshima K., Turkcan E. and Ciftcioglu O.: "Nuclear Power Plant Monitoring using Real-time Learning Neural Network " Proc. of Specialists' Meeting on Application of Artificial Intelligence and Robotics to Nuclear Plants, pp 313-322 (1994).
7) Konno H., Hayashi K. and Shinohara Y.: " Stochastic Center Manifold Dynamics of Limit Cycle Oscillation in Power Reactors and Measures of Nuclear Reactor Stability", Ann. Nucl. Energy, 21, pp.337-355, 1994.
8) Hayashi K., et al.: "Autoregressive Techniques for Acoustic Detection of In-Sodium Water Leaks - The Results of 1994 Benchmark Test on Detection of Sodium/Water Reaction-," Presented for Research Coordination Meeting on Acoustic Signal Processing for the Detection of Sodium Boiling or Sodium/Water Reaction in LMFBR, Kslpakkam, India, 1-3 November 1994.
9) Hayashi K., Shimazaki J., Nabeshima K., Shinohara Y., Inoue K. and Ochiai M. : "Reactor Dynamics Experiment of Nuclear Ship Mutsu Using Pseudo Random Signal (II), The Second Experiment", JAERI-Research 95-004 (In Japanese).
10) Hayashi K., Shimazaki J., Nabeshima K., Shinohara, Y., Inoue K. and Ochiai M.:"Reactor Dynamics Experiment of Nuclear Ship Mutsu Using Pseudo Random Signal (III), The Third Experiment", JAERI-Research 95-015 (In Japanese).
11) Ishikawa N., Fujii Y. and Shinohara Y.: "Improvement of Ultrasonic Aperture Imaging via Deconvolution Preprocessing", J.SICE, Vol. 30, No. 8, pp984-986 (1994)

9. Heat Transfer and Fluid Dynamics

1) Okazaki M.: "Analysis of Density Wave Instability in a Boiling Flow Using a Characteristic Method" , 31st National Heat Transfer Symposium of Japan, C141, Vol. Ⅰ, (1994) (in Japanese).
2) Akimoto H., Ikeda Y. and Kusano J.: "Analysis of Cooling Limit of Rotating Target for DT Neutron Source", 31st National Heat Transfer Symposium of Japan, C245, Vol. Ⅱ,

(1994) (in Japanese).

3) Ohnuki A., Akimoto H. and Murao Y.: "Analysis of Multi-dimensional Thermal-Hydraulic Behavior in a Core during the Reflood Phase of PWR-LOCA using the REFLA/TRAC Code", Proceedings of Int. Conf. on New Trends in Nuclear System Thermohydraulics, Vol. I , pp. 231-236, May 30th-June 2nd, Pisa, Italy (1994).
4) Okazaki M.: "Analysis of Density Wave Instability in a Boiling Flow Using a Characteristic Method", ASME Symposium on Transient Therrnal Hydraulics, Heat Transfer, Fluid-Structure Interaction, and Structual Dynamics, PVP-Vol. 270, pp. 65-73 (1994).
5) Sudo Y.: "Analytical Study on Mechanism of Counter-current Flow Limitation in Vertical Rectangler Channels", Transactions of JSME, B-Vol. 60 No. 574 (1994) (in Japanese).
6) Akimoto H., Abe Y., Ohnuki A. and Murao Y.: "Improvement of Pressure Drop Calculation Model in TRAC-PFI Code", JAERI-Data/Code 94-006 (1994) (in Japanese).
7) Ohnuki A., Akimoto H., Iguchi T. and Murao Y.: "Effect of Fuel Assembly Configuration and Fuel Rod Configuration on Thermal-hydraulic Behavior in Core during Reflood Phase of PWR-LOCA", JAERI-Research 94-012 (1994) (in Japanese).
8) Sudo Y.: "Analytical Study on Characteristics of Falling Water Limitation in Counter-current Two-phase Flow in Vertical Annular Channels", Transactions of JSME, B-Vol. 60 No. 576 (1994) (in Japanese).
9) Okubo T., Iguchi T. and Murao Y.: "Experimental Study on Difference in Reflood Core Heat Transfer among CCTF, FLECHT-SET and Predicted with FLECHT Correlation", J. Nucl. Sci. Technol., 31[8], pp. 839-849 (1994).
10) Ohnuki A., Akimoto H. and Murao Y.: "Applicability of REFLA/TRAC Code to a Small-Break LOCA of PWR", J. Nucl. Sci. Technol., 32[3], pp. 245-256 (1995)."
11) Iwamura T., Watanabe H. and Murao Y.: "Critical Heat Flux Experiments under Steady-state and Transient conditions and Visualization of CHF Phenomenon with Neutron Rediography", Nucl. Eng. and Design 149(1994)

10. Transmutation System and Partitioning-Transmutation Fuel Cycle

1) Takizuka T.: "Accelerator Based Transmutation of Radioactive Wastes," Proc. Accelerator-SOR Workshop, (Tokyo) (1994).
2) Takizuka T., Nishida T., Mizumoto M. and Yoshida H.: " Present Status of Accelerator Based Transmutation Research," Proc. 8th Journees SATURNE, LNS/Ph/94-12, p.109-113 (Saclay) (1994).
3) Mukaiyama T., Kubota M., Ogawa T., Wakabayashi T.: "Window on International

Conferences - GLOBAL'93 held in ANS- ," Jour. of the Atomic Energy Society of Japan, Vol.36, p.325 (1994).

4) Kondo Y., Takizuka T.: " Technology Assessment of Partitioning Process (1) Status of the Partitioning Technology," JAERI-M 94-067 (1994).
5) Mukaiyama T. :" Prospect on TRU Transmutation Technology," Japan Atomic Industrial Forum, Proc. Meeting of Atomic Power Reactor Research Group, (1994).
6) Takizuka T.: "Accelerator-Based Transmutation of Radioactive Wastes," Proc. Intense Proton Accelrator Workshop, (Tokai) (1994).
7) Takada H., Nakahara Y., Nishida T., Ishibashi K., Yoshizawa N.: " Microscopic Cross Section Calculations with NUCLEUS and HETC-3STTEP," Proc. NEA/NSC Specialist Meeting (Paris) (1994).
8) Nishida T., Takizuka T., Takada H., Sasa T., Meigo S., Mizumoto M., Katsuta H., Kato Y. and Yoshida H. :" Research on Accelerator-based Transmutation ," Proc. 19th Linear Accelerator Meeting, JAERI-Conf 94-003, p.66-68 (Tokai) (1994).
9) Mukaiyama T.: " Present Status on Transmutation Technology," Summer Seminor on Radioactive Waste, (Genkai) (1994).
10) Mukaiyama T.: "Present Status on Transmutation Resaerch in the world," 26th Summer Seminor on Reactor Physics, p.24-38, (Koyasan) (1994).
11) Nishida T.: " Transmutation Using Accelerator," 26th Summer Seminor on Reactor Physics, p.47-66, (Koyasan) (1994).
12) Takizuka T.: " Transmutation of Radioactive Waste," Text for International Nuclear Safety Seminor, (Tokai), JAERI-memo 06-269 (1994).
13) Yoshizawa N., Nishida T. and Takada H.: " Evaluation of High Energy Fission Models for High Energy Nuclear Reaction and Transport Codes, " Proc. Symp. on Nuclear Data, JAERI-Conf 95-008, p.221-224 (1994).
14) Sasa T., Takizuka T., Nishida T., Katsuta H. and Takahashi H.: " Conceptual Design Study of Accelerator-based Transmutation with Liquid TRU Alloy Target and Molten Salt Blanket," Proc. Inter. Symp. Global Enviro. Nucl. Energy System (Susono) (1994).
15) Mukaiyama T. :"Design Study on Minor Actinide Burner Reactor," Present Status of Transmutation Research and Development -BreakthroughPossibility in NuclearTechology-, JAES, p.21-28 (1994).
16) Nishida T. :"Accelerator-based Transmutation," Present Status of Transmutation Research and Development -Breakthrough Possibility in Nuclear Techology-, JAES, p.94-100 (1994).
17) Nishida T.: "Spallation Integral Experiment," Present Status of Transmutation Research and Development -Breakthrough Possibility in Nuclear Techology-, JAES, p. 162-166

(1994).

18) Takizuka T.: "International Trend on Accelerator-based Transmutation," Present Status of Transmutation Research and Development -Breakthrough Possibility in Nuclear Techology-, JAES, p.213-216 (1994).

19) MukaiyamaT.: "International Conference Report - IAEA Consultant Meeting, GLOBAL'93," Present Status of Transmutation Research and Development -Breakthrough Possibility in Nuclear Techology- JAES, p.232-236 (1994).

20) Mukaiyama T.: " Present Status of Transmutation Technology," Seminor on the Atomic Energy System (1995).

21) Mukaiyama T.: "Resaerch and Development of Transmutation of High Level Radioactive Waste - Introduction, What is transmutation ?, Summary -," Jour. of the Atomic Energy Society of Japan, Vol.37, No.3, p.159-162 (1995).

22) Takahashi H., Takizuka T.: "Resaerch and Development of Transmutation of High Level Radioactive Waste -Transmutation with Accelerator-, " Jour. of the Atomic Energy Society of Japan, Vol.37, No.3, p.167-171(1995).

23) Takizuka T.: "Resaerch and Development of Transmutation of High Level Radioactive Waste - R&D Activities at JAERI-," Jour. of the Atomic Energy Society of Japan, Vol.37, No.3, p.184-186 (1995).

24) Takizuka T. : " Present Status of Transmutation Research, -International Status-," Jour. of the Atomic Energy Society of Japan, Vol.37, No.3, p.191-192 (1995).

25) Baba M, Ito N., Matsuyama I., Matsuyama S., Hirakawa N., Chiba S., Fukahori T., Mizumoto M., Hasegawa K., Meigo S.: "Differential a-Production Cross Sections of Iron and Nickel for 4.3 to 14.1 MeV Neutrons", J. Nucl. Sci. and Technol. 31, 745, (1994).

26) Baba M., Kiyosumi T., Iwasaki T., Yoshioka M., Matsuyama S., Hirakawa N., Nakamura T., Tanaka Su., Tanaka R., Tanaka Sh., Nakashima H., Meigo S.: "Characterization and Application of 20-90 MeV 7Li(p,n) Neutron Source at TIARA", Proc. of Int. Conf. on Nucl. Data for Sci. and Technol., Gatlinburg, Tennessee, May 9-13, 1994, p90 (1994).

27) Watanabe, Y., Aoto A., Kashimoto H., Chiba S., Fukahori T., Hasegawa K., Mizumoto M., Meigo S., Sugimoto M., Yamanouti Y., Koori N., Chadwick M. B., Hodgson P.E.: "Measurement of Double Differential Charged-Particle Emission Cross Sections for Reactions Induced by 26 MeV Protons and FKK Model Analysis", ibid., p308.

28) Ishibashi K., Nakamoto T., Matsufuji N., Shigyo N., Maehata K., Wakuta Y., Watanabe Y., Takada H., Meigo S., Chiba S., Numajiri M., Nakamura T.: "Measurement of Neutron-Production Double Differential Cross Sections for Incident Protons of 0.8, 1.5 and 3.0 GeV", ibid., p347.

29) Chiba S., Fukahori T., Takada H., Maruyama T., Niita K., Iwamoto A.: "Applicability of the Quantum Molecular Dynamics to Nucleon-Nucleus Collisions", ibid., p505.

30) Ishibashi K., Yoshizawa N., Takada H., Nakahara Y.: " High Energy Transport Code HETC-3STEP Applicable to Incident Energies Below 100 MeV", ibid., p571.

31) Takada H., Nakahara Y., Nishida T., Ishibashi K., Yoshizawa N.: "Microscopic Cross Section Calculations with NUCLEUS and HETC-3STEP", Intermediate Energy Nuclear Data: Models and Codes, Proc. of A Specialists' Mtg., Issy-les-moulineaux, FRANCE May 30- June 1, 1994, OECD/NEA pl21, (1994).

32) Chiba S., Takada H., Fukahori T., Maruyama T., Niita K., Iwamoto A.: " The Quantum Molecular Dynamics Calculation of Nucleon-Nucleus Reactions" , ibid., pl37, (1994).

33) Chiba S., Niita K., Maruyama T., Fukahori T., Takada H., Iwamoto A.:" Analysis of the Nucleon-Nucleus Reactions by the Quantum Molecular Dynamics", Proc. of the 1994 Symposium on Nucl. Data, November 17-18, 1994, JAERI, Tokai, Japan, JAERI-Conf 95-008, p86, (1995).

34) Kiyosumi T., Baba M, Iwasaki T., Sanami T., Matsuyama S., Hirakawa N., Nakamura T., Tanaka Su., Nakashima H., Meigo S, Tanaka Sh.: "Measurement of C(n,z) Double Differential Cross Section at 40, 64 MeV", ibid., pl93.

35) Meigo S., Takada H., Chiba S., Nakamoto T., Ishibashi K., Matsufuji N., Shigyo N., Maehata K., Shigyo N., Wakuta Y., Watanabe Y., Nakamura T., Numajiri M.: "Measurement of Neutron Spectra from a Thick Lead Target Bombarded by 0.5 and 1.5 GeV Protons", ibid., p213.

36) Yoshizawa N., Nishida T., Takada H.: "Evaluation of High Energy Fission Models for High Energy Nuclear Reaction and Transport Codes", ibid., p221.

11. Accelerator Development

1) Kusano J., et al.: "R&D Works on JAERI BTA" Proc. 19th Linear Accelerator Meeting in Japan, Tokai, July 20-22,1994, JAERI-Conf. 94-003 p69

2) Kawai M., et al.: "Design of 100 kW Proton Beam Stopper for BTA in JAERI" Proc. 19th Linear Accelerator Meeting in Japan, Tokai, July 20-22, 1994, JAERI-Conf. 94-003 p301

3) Mizumoto M., et al.: "Accelerators for the Transmutation of Nuclear Wastes" Proc. 17th Int. Linac Conf., Tsukuba, Aug. 21-26,1994, p317

4) Hasegawa K., et al.: "First Beam Test of the JAERI 2 MeV RFQ for the BTA" Proc. 17th Int. Linac Conf., Tsukuba, Aug. 21-26,1994, pll3

5) Ito N., et al.: "Fabrication and tests of the DTL Hot Model in the R&D Works for the

BTA in JAERI" Proc. 17th Int. Linac Conf., Tsukuba, Aug. 21-26, 1994, p119

6) Oguri H., et al.: "A High Brightness Hydrogen Ion Source for the BTA at JAERI" Proc. 17th Int. Linac Conf., Tsukuba, Aug. 21-26,1994, p381

7) Oguri H., et al.: "Requirements for Ion Source Performance of ETA" Proc. Workshop on Ion Source Issues Relevant to a Pulsed Spallation Neutron Source, Oct. 24-26, Berkeley, USA,

8) Oguri H., et al.: "High Brightness Hydrogen Ion Source for the BTA" Proc. Workshop on Ion Source Issues Relevant to a Pulsed Spallation Neutron Source Berkeley, USA, Oct. 24-26

9) Sawamura M., Nagai R., Takao M., Minehara E.J., Kil;uzawa N., Kato R., Sugimoto M., Ohkubo M. and Suzuki Y.: "Rf power tests for JAERI FEL superconducting accelerator modules", Nucl. Instr. and Meth. A341 (1994) 391-393

10) Takao M., Sugimoto M., Sawamura M., Nagai R., Kato R., Minehala E.J., Ohkubo M. and Suzul;i Y.: "Recirculation scheme in the second phase of the JAERI FEL project, Nucl. lnstr. and Meth. A341 (1994) 394-39

11) Sugimoto M., Takao M., Sawamura ., Nagai R., Kato R., Kikuzawa N., Minehara E.J., Ohkubo M., Kawarasaki Y. and Suzuki Y.: "Progress of the IR FEL development at JAERI", Nucl. lnstr. and Meth. A341 (1994) ABS 41-ABS 42

12) Takeuchi S., Ishii T., Shibata M. and Yoshida T. :"Acceleration Testing of JAERI Tandem Superconducting Booster", JAERI-Conf 94-003, Proc. of the 19th Linear Accelerator Meeting in Japan, July 20-22, 1994, Tokai, pp78-80

13) Takeuchi S. : "Status of Beam Test of JAERI Tandem Superconducting Booster", Proc. of the 7th Tandem Accelerators and Their Associated Technology, June 28-29, 1994, Tokyo, pp88-90

14) Takeuchi S., Shibata M., Ishii T., Ikezoe H., Yoshida T.: "First Operating Experience with the Superconducting Heavy Ion Tandem-Booster Linac at JAERI", to be published Proc. of the 17th Intemational Linac Conference, Aug.22-26,1994, Tsukuba

12. Facility Operation and Technique Development

1) Kobayashi C.:"Status of the Tandem Accelerator at JAERI Tokai", Proc. of the 7th Tandem Accelerators and Their Associated Technology, June 28-29, 1994, Tokyo, pp30-32

2) S. Takeuchi et al.:"Beam Acceleration Tests of JAERI Tandem Superconducting Booster",The 50th Meeting of the Physical Society of Japan, March 28, 1995, Yokohama

Appendix I

Department of Reactor Engineering Organization Chart

March 1995

Department of Reactor Engineering

Director:	H.Yoshida
Deputy Director:	Y.Suzuki
	Y.Murao

T.Tone
H.Goto
H.Yoshida
S.Momiyama
H.Katsuta (2)

Administrative Services

T.Okabe (Administrative Manager)	
K.Shibata	A.Motoishi
M.Sato	Y.Tamura
M.Tsukakoshi	K.Shinozuka
D.Koyanagi	T.Naganawa

Reactor Engineering Facility Operation Division

Hideaki Watanabe (Head)			
A.Ohno	K.Nakajima	K.Kurosawa	M.Takeuchi
S.Fujisaki	K.Sato	Hironori Watanabe	
T.Kutsukake	S.Tanaka	T.Sato	T.Ono
Y.Watanabe	Y.Abe	K.Hayasaka	M.Seki
H.Sodeyama	S.Matsumoto(1)	I.Takahashi(1)	M.Yabuki(1)

Accelerators Division

C.Kobayashi (Head)			
S.Takeuchi	T.Yoshida	T.Shoji	I.Ohuchi
S.Kanda	K.Horie	Y.Tsukihashi	S.Abe
S.Hanashima	S.Kanazawa	N.Ishizaki	H.Tayama
Y.Kazumata(2)	Y.Sugiyama(3)	H.Ikezoe(3)	M.Ohshima(3
Y.Tomita(3)	M.Sataka(2)	Y.Nagame(4)	K.Ideno(3)
Y.Yamanouchi(3)	S.Ichikawa(4)	T.Ishii(3)	S.Hamada(3)

Nuclear Data Center

Y.Kikuchi (Head)			
Y.Nakajima	T.Shirai	Y.Nakagawa	J.Katakura
K.Shibata	T.Narita	S.Chiba	T.Fukahori
A.Ichihara	Y.Hayashi	M.Sataka(2)	H.Iimura(4)
Y.Kazumata(2)	H.Takano(11)		

Reactor System Labolatory

K.Tsuchihashi (Head)			
M.Nakagawa	Y.Asahi	T.Mori	T.Fujimura
T.Tsutsui	H.Akie	K.Okumura	T.Kugo
Y.Nagaya	H.Takano(11)		

Fast Reactor Physics Labolatory

T.Mukaiyama (Head)			
S.Iijima	T.Ohsugi	T.Nemoto	S.Okajima
K.Sakurai	H.Ohigawa	M.Andoh	T.Ogawa(5)

Thermal Reactor Physics Labolatory

H.Yasuda (Head)			
F.Akino	T.Yamane	H.Takada	S.Meigo

Sensing Technology Labolatory

K.Ara (Head)			
H.Yagi	M.Yamada	M.Haruyama	H.Yamagishi
H.Ito	M.Takase	J.Kaneko	M.Katagiri(3)
T.Kakuta(3)	K.Sakasai(3)	M.Kishimoto(3)	

Contorol & AI Labolatory

K.Suzuki (Head)			
S.Sasaki	H.Usui	K.Watanabe	Y.Fujii
K.Hayashi	T.Suzudo	K.Nabeshima	N.Ishikawa
J.Shimazaki(6)			

Shielding Labolatory

S.Tanaka (Head)			
Y.Sakamoto	H.Kotegawa	H.Nakashima	Y.Nakane
N.Sasamoto(7)			

Heart Transfer & Fruid Flow Labolatory

H.Akimoto (Head)		
T.Iguchi	M.Okazaki	A.Ohnuki

Fusion Neutronics Labolatory

H.Maekawa (Head)			
Y.Ikeda	Y.Ohyama	C.Konno	F.Maekawa
Y.Uno	M.Wada	Y.Seki(8)	T.Nishiya(9)

Passive Safety Reactor Systems Labolatory

T.Iwamura (Head)			
F.Araya	K.Kunii	H.Yoshida	T.Ishida(6)
J.Shimazaki(6)			

Transmutation System Labolatory

T.Takizuka (Head)			
T.Nishida	K.Takeuchi	T.Sasa	Y.Nakahara(3
Y.Kato(5)	S.Hamada(2)	K.Hayashi(5)	M.Akahori(5)
Y.Kondo(5)			

Accelerator Engineering Labolatory

M.Mizumoto (Head)			
J.Kusano	K.Hasegawa	Y.Kouchi	N.Ito
H.Oguri	Y.Okumura(8)	S.Moriyama(10)	

Free Electron Laser Labolatory

E.Minehara (Head)			
M.Ohkubo	M.Sugimoto	M.Sawamura	R.Nagai
N.Kikusawa			

Research Committees

Japanese Nuclear Data Committee
Research Committee on Reactor Physics
Atomic and Morecular Data Committee
Research Committee on Advanced Reactor
Research Committee on Partitionig and Transmutation
Research Committee on High Intensity Proton Accelerator
Committee on the Internatinal Conference on Physics of Reactors

(No.) : Original Organization of the Shared-Time Menbers

(1) Dept. of Engineering Services
(2) Dept. of Materials Science and Engineering
(3) Advanced Science Reseach Center
(4) Dept. of Radioisotopes
(5) Dept. of Chemistry and Fuel Reseach
(6) Office of Nuclear Ship Rescach and Development
(7) Dept. of Synchrotron Radiation Facility Project
(8) Dept. of Fusion Engineering Reseach
(9) Dept. of Fusion Plasma Research
(10) Dept. of Fusion Facilities
(11) Plutonium Rock-Like Fuel Integrated R&D Team

Appendix II Engineering Facilities related to the Department

CCTF: Cylindrical Core Test Facility

The CCTF is an experimental facility to study overall primary system response as well as the in-core behavior during the refil and reflood phase pf a large scale cold leg break LOCA.

FCA: Fast Critical Assembly

The FCA is a split-table type facility of horizontal matrix structure designed for studying nuclear characteristics of fast reactor. The construction of the FCA was started in 1965 and the first core went critical on 29th April, 1967. The main features of the facility are summarized as follows:

Type :	Split-table type of horizontal matrix structure
Size :	2.8 m ×2.8 m×1.3 m (each half assembly)
Fuel :	Enriched uranium and plutonium (Plate type)
Other material :	Sodium, stainless steel, aluminum, oxide (Al203), polystyrene etc. (Plate type)
Maximum power:	2 kW

Assembly name constructed: FCA-I FCA-XVII

Critical experiments using enriched uranium cores were made in 1960s for investigating basic characteristics of fast reactor cores. Mock-up experiments were extensively made in 1970s for the Fast Experimental Reactor JOYO and the Prototype Fast Breeder Reactor MONJU. In 1980s, the main subjects of experiments were the investigation of the core characteristics of an axially heterogeneous large fast breeder reactor and the core physics study on a high conversion light water reactor. Since 1989, the reactor physics experiments of metallic-fueled LMFBR have been carried out by using the FCA-XVI and XVII cores.

FNS: Fusion Neutronics Source

The FNS is an accelerator based D-T neutron source installed for the purpose of investigating the neutronics on the D-T fusion reactor blanket and shielding It provides following three functions to meet experimental requirements

1) High intensity DC point source

2) DC point source with wide variation of neutron yield rate

3) Pulsed neutron source

The D-T neutrons are generated via $^{3}T(d,n)^{4}He$ reaction There are two beam lines; one is so called

0° line for high current operation, and the other is so called 80° line for rather low current operation The major specifications of the FNS accelerator are shown in the following Table;

Items	0°	80°
• Beamcurrent	>20 mA	3 mA
• Beamsize	<15 mm	<15 mm
• Pulsewidth	--	2 ns
• Frequency	--	2 MHz
• Peakcurrent	--	40 mA
• Target assembly	Rotating	Stationary
(Water cooled)	(Water cooled, Air cooled)	
• Amount of ^{3}T	<37T Bq	370G Bq
• Neutron yield	4×10^{12}/s	5×10^{11}/s

The major experimental subjects are as follows:

1) Tritium production rate in the various blanket configurations
2) Nuclear heating rate in materials
3) Shielding performance for D-T neutrons in the various configurations
4) Induced effects on materials by D-T neutrons

HTTR: High Temperature engineering Test Reactor

JAERI is constructing the HTTR to carry out the necessary R&D for establishing and upgrading the HTGR (High Temperature Gas-cooled Reactor) technology basis, and to conduct various innovative basic researches on high-temperature technologies. The HTTR consists of a reactor core, a main cooling circuit, an auxiliary cooling circuit and related components. The size of active core is 2.3 m in diameter and 2.9 m high. The reactor pressure vessel of 13.2 m in height and 5.5 m in diameter contains the core, graphite reflectors, core support structures and core restraint mechanism.

Specification of HTTR

Thermal power	30 MW

Outlet coolant temperature	850℃/950℃
Inlet coolant temperature	395℃
Fuel	3～10wt% enriched UO2
	(coated particle fuel compact)
Fuel element type	Prismatic block (pin-in block)
Primary coolant	Helium gas, 4MPa
	Downward-flow in core
Pressure vessel	Steel
Number of main cooling loop	1
Heat removal	IHX(10MW) and PWC(30MW)
Containment type	Steel containment

VHTRC: Very High Temperature Reactor Critical assembly

The VHTRC is a low-enriched uranium fueled and, graphite moderated and reflected critical assembly. At VHTRC, reactor physics experiments have been carried out mainly for the verification of the neutronics design of the HTTR.

Main features of VHTRC

Type	Split table type of hexagonal prism
	(prismatic block structure)
Size	2.4 m across the flats and 2.4 m long
Fuel	2, 4 and 6 wt% enriched UO2
	Coated particle fuel compact
	Pin-in-block type
Moderator/reflector	Graphite
Core temperature	Room temperature to 210℃ by electric heaters
Maximum power	10 W
Auxiliary equipments	(1) Sample heating device (Up to 800℃)
	(2) Pulsed neutron source